

Preparation and Application of Cyclic Chiral Organoboron Compounds for the
Stereoselective Synthesis of Vacquinol-1 Analogs, and Trisubstituted Cyclobutylboronates

by

Rory McDonald

A thesis submitted in partial fulfillment of the requirements for the degree of

Master of Science

Department of Chemistry
University of Alberta

©Rory McDonald, 2019

Abstract

Boron is a versatile atom in synthetic organic and medicinal chemistry. The formation of a variety of carbon-carbon and carbon-heteroatom bonds, and the ability to act as a pharmacophore makes boron a powerful tool in drug discovery. An area of drug discovery that remains underexplored with boron is the application and preparation of cyclic chiral boronates to synthesize bioactive scaffolds of interest. The use of chiral boronates is particularly appealing for the preparation of privileged scaffolds, as a greater amount of synthetic diversity can be become available, which has important implications in drug repurposing, and discovering new biological activity with common molecular scaffolds. With such great potential, the chemistry and applications of chiral boronates warrant further study.

To study the application of cyclic boronates, a rapid library of analogs for vacquinol-1 (vac-1)—a preclinical candidate against glioblastoma multiforme (GBM)—was synthesized using racemic allylic piperidinyl boronates and quinoline aldehydes. This library was generated to try and find a more potent and efficient analog, as vac-1 has now been abandoned as a clinical candidate, largely due to its poor *in vivo* activity in mice transplanted with GBM tumours. For the preparation of chiral boronates, a variety of cyclobutenones were synthesized using an optimized route. This library of cyclobutenones were subjected to a catalytic enantioselective conjugate borylation reaction to examine the generality of the reaction and limitations of substrates. This project is particularly noteworthy, as it is one of the first successful examples of preparing tertiary trisubstituted cyclobutylboronates using conjugate borylation chemistry. Since these cyclobutylboronates are unknown, they represent a wonderful opportunity to discover potential drug candidates incorporating a polysubstituted cyclobutane motif.

Preface

The research conducted in Chapter 2 is a continuation of Samantha Kwok's master's thesis. Samantha synthesized, characterized, and tested all enantioenriched stereoisomers of vacquinol-1 **1**, and its dehydro analogs **27**. She was also successful in the preparation of enantioenriched *threo* isomers of the bromine vac-1 analog **18**, which became the lead compound of interest and ultimately led to the current SAR study to improve the drug candidate's potency. My contributions to the project were the successful synthesis, characterization, and testing of racemic *threo* vac-1 analogs **18-29**, **45**, **47-54**, **62**, and **75**. The *in vitro* testing of vac-1 analogs against U251 and A4-004 glioblastoma multiforme cell lines was conducted via a collaboration with Dr. Saket Jain and Dr. Roseline Godbout from the Department of Oncology at the University of Alberta.

The conjugate borylation reaction methodology outlined in Chapter 1 and Chapter 3 was developed and optimized by Michele Boghi and Helen Clement in collaboration with Jack C. Lee, Louise Bernier, William Farrell, Neal Sach, Matthew R. Reese, Jotham Coe, and Christopher J. Helal at Pfizer Inc. Michele optimized the first synthetic route towards cyclobutenone **7a**, and was successful in developing conjugate borylation conditions to access the racemic version of cyclobutylboronate **8a**. Jack and the other team members at Pfizer performed a high-throughput screen (HTS) to discover the optimal (*S,S*)-BDPP chiral ligand for an enantioselective conjugate borylation reaction, and gave us feedback throughout the project. Using the chiral ligand, Helen successfully optimized the enantioselective reaction on **7a** to acquire enantioenriched cyclobutylboronate **8a** in good isolated yield and high diastereoselectivity. She was also successful in obtaining a crystal structure to prove the stereochemistry of the cyclobutylboronate products and synthesized the corresponding cyclobutylboronates from cyclobutenones **7j**, and **9-15** for the substrate scope. My contributions to the project were the development of a new alkene migration reaction, which led to the preparation of cyclobutenones **1a**, and **7b-7j**. I also performed a preliminary substrate scope with the optimized conjugate borylation reaction, which led to cyclobutylboronates **2a**, **8b-8g**. We currently have an accepted manuscript in press for *Angewandte Chemie International Edition (ACIE)*.

Acknowledgements

I would first like to thank my supervisor Dr. Dennis Hall for giving me the opportunity to join his group and participate in these amazing projects. It's been three great years. Dennis has been an incredible mentor in all my academic studies and research. His amazing support, steady guidance, hands-on approach to running the group, and passion for synthetic organic and medicinal chemistry has been a true inspiration for me in this field. I would not be the chemist I am today without him.

A very gracious thank you to our analytical technician Ed Fu, for all his tenacious work with the HPLC purifications and chiral separations utilized in both my projects. I am forever grateful for your patience and amazing work. This research would not have been possible without the care and support of my fellow group members. I would like to thank Helen Clement. She has been a wonderful lab mentor to me throughout my entire degree, an amazing editor of my scientific writing, and an incredible partner to work with on our collaboration with Pfizer Inc. Helen is a fantastic scientist; one that I aspire to be like every day. I am also very thankful to Marco Palladino, Carl Estrada, Mohamad Estaitie, Jason Rygus, Hannah Hackney, Jasmine Bhangu and Hwee-Ting Ang for their endless encouragement, friendship, and support in the lab.

I also need to thank the incredible support staff within the department of chemistry. Namely, Wayne Moffat and Jennifer Jones whose data services and UV-Vis spectroscopy training was indispensable for my main project. Mark Miskolzie, who trained and helped me countless times in determining the best ways to acquire the relevant NMR data. The Mass Spectrometry lab, whose service was essential in elucidating a number of complex molecules in all my projects.

Lastly, I need to thank my partner Mary McInnes. Mary has always pushed me to be the best version of myself inside and outside of the lab. She has helped me through the many failures and low points of my research, and has never faltered in supporting my dream of becoming an organic chemist. I cannot express how lucky and grateful I am to have her with me at this time in my life.

Table of Contents

Chapter 1: The Utility of Organoboron Compounds in Modern Drug Discovery

1.1	The Importance of Drug Discovery, and the Growing Need for New Strategies in the Field.....	1
1.2	Polypharmacology and Drug Repurposing.....	5
1.3	Boron in the Medicinal Chemistry Toolbox.....	7
1.3.1	Boron as a Carboxylic Acid Bioisostere.....	8
1.3.2	Benzoxaboroles as Novel Heterocycles in Medicinal Chemistry.....	10
1.3.3	Accessing Privileged Scaffolds through Carbonyl Chemistry: β -Amino Alcohols.....	12
1.4	Applying Chiral Allylic Piperidinyl Boronates for the Stereoselective Synthesis of Mefloquine and Vacquinol-1.....	18
1.5	Accessing Privileged Scaffolds through Borylation: Chiral Polysubstituted Cyclobutanes.....	24
1.6	Cyclobutenone Synthesis, and the Preparation of Cyclobutylboronates through Copper-Catalyzed Conjugate Borylation.....	26
1.7	Thesis Objectives.....	29
1.8	References.....	30

Chapter 2: Application of Allylic Piperidinyl Chiral Boronates towards the Synthesis of Novel Vacquinol-1 Analogs, a Potential Drug Candidate for Glioblastoma Multiforme

2.1	Glioblastoma multiforme: Prevalence, Characteristics, Genetics, and Outlook.....	36
2.2	A High-Throughput Screen (HTS) with Beneficial Modifications: The Discovery of Vacquinol-1.....	38
2.3	Overview of Vacquinol-1.....	39
2.3.1	Stereoisomers, and Biological Activity of Vac-1.....	40
2.3.2	Non-stereoselective synthesis of Vacquinol-1 Analogs, and SAR.....	41
2.3.3	Stereoselective Synthesis of Vac-1.....	46
2.4	Methuosis: A Nonapoptotic Form of Cell Death Against GBM.....	48
2.5.	2 nd Generation Vac-1 Analogs: Bioisosteres, Dehydropiperidines, and Dehydroazepane.....	54
2.6.	Synthesis of Bioisosteric, and Dehydropiperidinyl Vac-1 Analogs.....	57
2.6.1	Synthesis of Remaining <i>Classical</i> , <i>Nonclassical</i> Bioisosteric, and Dehydroazepane Vac-1 Analogs.....	62
2.7	Biological Activity of Bioisosteric, Dehydropiperidinyl, and Dehydroazepanyl Vac-1 Analogs.....	65
2.8	The 3 rd Generation Vac-1 Analogs: Variable Size <i>para</i> Alkyl Substituents, Endocyclic Alkene Functionalization, and Scaffold Hopping.....	69

2.9	Synthesis of 3 rd Generation Vac-1 Analogs: Azepane Moiety and Indole Scaffold.....	72
2.10	Synthesis of 3 rd Generation Vac-1 Analogs: Endocyclic Alkene Functionalizations.....	75
2.11	Biological Activity of Azepanyl, Dehydropiperidinyl, Dehydro- <i>N</i> -Methyl Quinoliny, and Variable Alkyl Group Vac-1 Analogs.....	77
2.12	Summary and Future Work.....	81
2.13	Experimental Procedures.....	84
2.13.1	General Information.....	84
2.13.2	General Procedure for the Synthesis of Quinoline Carboxylic Acids.....	85
2.13.3	General Procedure for the Synthesis of Quinoline Aldehydes.....	91
2.13.4	General Procedure for the Synthesis of the Alkenyl Nonaflate.....	97
2.13.5	General Procedure for the Synthesis of Allylic Piperidinyl Boronate.....	98
2.13.6	General Procedure for the Synthesis of Racemic <i>t</i> -Boc Dehydro-Vacquinol-1 Analogs.....	99
2.13.7	General Procedure for Hydrogenation of Dehydro-Br-Vacquinol-1.....	106
2.13.8	General Procedures for Hydrogen Atom Transfer (HAT).....	106
2.13.9	General Procedure for Rosemund-von Braun Type Reaction.....	107
2.13.10	General Procedure for Suzuki-Miyaura Cross-Coupling.....	109

2.13.11	General Procedure for Sonogashira Cross-Coupling.....	110
2.13.12	General Procedure for the Synthesis of HCl Salt Vacquinol-1 Analogs.....	111
2.13.13	General Procedure for Simmons-Smith Reaction/N-Methylation.....	122
2.13.14	General Procedure for Fischer Indole Synthesis.....	123
2.13.15	General Procedure for Vilsmeier-Haack Formylation.....	123
2.14	References.....	124
Chapter 3: Preparation of Enantioenriched Trisubstituted Cyclobutylboronates by Asymmetric Conjugate Borylation of Cyclobutenones		
3.1	Conjugate Borylation.....	131
3.2	Conjugate Borylation of Cyclic Enones.....	134
3.3	Cyclobutanones and Cyclobutylboronates.....	136
3.4	Alkene Migration Optimization for α,β -Substituted Cyclobutenones.....	138
3.5	Synthesis of a Small Library of α,β -Substituted Cyclobutenones.....	143
3.6	Preliminary Substrate Scope of Conjugate Borylation.....	146
3.7	Summary and Future Work.....	149
3.8	Experimental Procedures.....	151

3.8.1	General Information.....	151
3.8.2	General Procedure for the Synthesis of α,β -Disubstituted Cyclobutenones.....	152
3.8.3	General Procedure for the Synthesis of Trisubstituted Cyclobutylboronates.....	157
3.8.4	General Procedure for the Reduction of (2 <i>S</i> ,3 <i>R</i>)-2-methyl-3-(4,4,5,5-tetramethyl- 1,3,2-dioxaborolan-2-yl)-3-(<i>p</i> -tolyl)cyclobutanone	163
3.9	References.....	164

Chapter 4: Conclusion and Outlook

4.1	Overview.....	168
4.2	Application of Allylic Piperidinyl Boronates for the Synthesis of Vac-1 analogs.....	168
4.3	Preparation of Cyclobutylboronates through Asymmetric Conjugate Borylation of Cyclobutenones.....	170
4.4	Bibliography.....	172
Appendix: Reproductions of Important NMR Spectra and Selected Chromatograms for Enantiomeric Excess Measurements.....		185

List of Figures

Figure 1-1: Some small molecule milestones in the treatment of disease, during the “golden age” of drug discovery.....	2
Figure 1-2: 2010 decline in innovation from the pharmaceutical industry.....	3
Figure 1-3: The collaborative drug discovery pipeline.....	5
Figure 1-4: Chemical approaches towards developing a multitarget drug.....	6
Figure 1-5: Boron’s open shell, and the reversibility of neutral and anionic forms of phenylboronic acid at physiological pH.....	7
Figure 1-6: (Top) Structure of bortezomib, the first successful boronic acid drug. (Bottom) an example of a hit (a) repurposed with a boronic acid (b) , with high <i>in vitro</i> activity against wild type (WT 1a and WT 1b), and mutated HCV (1b 316N) strains.....	9
Figure 1-7: Chemical properties of benzoxaboroles in aqueous media at physiological pH.....	10
Figure 1-8: Marketed drugs and a drug candidate featuring a benzoxaborole.....	11
Figure 1-9: Drug repurposing of vancomycin with a benzoxaborole scaffold.....	12
Figure 1-10: General structure of 1,2-amino alcohol scaffold and its appearance in natural products, drugs, and chiral catalysts.....	13
Figure 1-11: Synthetic methodologies to prepare 1,2-amino alcohols.....	14

Figure 1-12: Forms of allylic organoborons, and the differences between Type I and Type II transition states for allylic metal reagents.....	15
Figure 1-13: Structures of quinine, and mefloquine (top), and all stereoisomers of mefloquine (bottom).....	19
Figure 1-14: Biological activity of 2-phenyl and 2-(4-bromophenyl) analogs, where SKH-V-103 is a synthetic [R,R] Vac-1 isomer prepared by Kwok to use as a positive control in the assay.....	24
Figure 1-15: Pharmaceuticals containing a cyclobutyl motif, and common synthetic pathways to access polysubstituted cyclobutanes.....	26
Figure 2-1: Chemical structure of temozolomide and its active MTIC form.....	37
Figure 2-2: A comparison of early antimalarials that inspired the analog scaffolds of vacquinol-1 and mefloquine.....	39
Figure 2-3: Analogs of the vacquinol-1 scaffold towards other pharmaceutical applications.....	40
Figure 2-4: Biological activity of vac-1, and its four possible stereoisomers.....	41
Figure 2-5: Scaffold hopping analogs of vac-1.....	45
Figure 2-6: Biological activity of individual Vac-1 stereoisomers.....	47
Figure 2-7: Pathway of micropinocytosis.....	49
Figure 2-8: Endosomal trafficking.....	49

Figure 2-9: GBM cells undergoing methuosis.....	50
Figure 2-10: An early working model for MOMIPP induced methuosis.....	51
Figure 2-11: A hypothetical pathway of biological targets for vac-1 and MOMIPP leading to methuosis.....	52
Figure 2-12: Recently identified compounds capable of inducing methuosis in cancer.....	53
Figure 2-13: Biological activity of all vac-1 stereoisomers.....	54
Figure 2-14: Proposed <i>classical</i> and <i>nonclassical</i> bioisostere analogs of racemic <i>threo</i> Br-vac-1 18 , and racemic <i>threo</i> vac-1 22	55
Figure 2-15: Biological activity of dehydro-vac-1 stereoisomers.....	56
Figure 2-16: Dehydropiperidine and dehydroazepane racemic <i>threo</i> Vac-1 analogs.....	56
Figure 2-17: Proposed bioreduction of MTS to formazan.....	66
Figure 2-18: MTS assay results of dehydropiperidinyl, dehydroazepanyl, racemic vac-1 22 , and racemic variant of Kwok's lead compound 18 , where RMH-VI-103 is a positive control.....	67
Figure 2-19: MTS assay results of bioisosteric and carbamate vac-1 analogs, where RMH-VI-103 is a positive control.....	68
Figure 2-20: 3 rd Generation vac-1 analogs with alkyl groups of variable size, a saturated azepane moiety, and dehydropiperidinyl moiety on the lead analog 23	70
Figure 2-21: Retrosynthesis of vac-1 analogs with functionalized endocyclic alkenes, and indole scaffold.....	71

Figure 2-22: MTS assay results of dehydropiperidinyl analog 54 , azepanyl analog 53 against appropriate controls.....	78
Figure 2-23: MTS assay with various alkyl/aryl vac-1 analogs, and the dehydro- <i>N</i> -alkylated quinolinium derivative against positive control SKH-103.....	79
Figure 2-24: MTS assay using A4-004 patient derived neurospheres and lead alkyl vac-1 analogs, with SKH-103 serving as positive control.....	80
Figure 2-25: Potential functionalization of lead candidate 49 to improve biological activity.....	83
Figure 3-1: Stereospecific applications of organoboron compounds.....	132
Figure 3-2: ¹ H NMR of ethyl phenyl cyclobutenone regioisomers, as well as the proposed ring-opened and dimer byproducts.....	140
Figure 3-3: Unsuccessful substrates in the cyclobutenone synthetic route.....	145
Figure 3-4: ORTEP representation of Clement's cyclobutylboronate crystal structure revealing the stereochemistry of the major diastereomer after conjugate borylation.....	146
Figure 3-5: Proposed diastereofacial selectivity model for the conjugate borylation of cyclobutenones.....	147
Figure 3-6: Additional cyclobutenones to test the scope of the conjugate borylation.....	150
Figure 3-7: Examples of some synthetic applications of cyclobutylboronates utilizing the Bpin and ketone units.....	151

List of Schemes

Scheme 1-1: Matsuda and co-workers' borylation conditions (top), and optimized conditions for the Hall Group's enantioselective borylative migration reaction (bottom).....	17
Scheme 1-2: Applications of heterocyclic allylic boronates: (a) regioselective Suzuki-Miyaura cross-coupling, (b) thermal allylboration.....	18
Scheme 1-3: Synthesis of all stereoisomers of mefloquine.....	20
Scheme 1-4: Comparison of mefloquine to Vac-1 (top), and retrosynthesis of Vac-1 (bottom).....	22
Scheme 1-5: Synthetic route to cyclobutenones.....	27
Scheme 1-6: Racemic conjugate borylation for the stereoselective preparation of cyclobutylboronates.....	27
Scheme 1-7: Pfizer's chiral ligand HTS, with enantiomeric excess on the x-axis and product yield on the y-axis.....	28
Scheme 1-8: Optimized conjugate borylation conditions (top), and difficult cyclobutenones to synthesize using the current reaction methodology (bottom).....	29
Scheme 2-1: Non-stereoselective synthesis of vac-1 for a preliminary SAR study.....	42
Scheme 2-2: Stereoselective synthesis of vac-1.....	45
Scheme 2-3: Preparation of quinoline carboxylic acids (32), unsuccessful LAH reduction, and hypothetical explanation as to why (box).....	57
Scheme 2-4: Revised synthesis of quinoline aldehydes.....	58

Scheme 2-5: Potential chemoselectivity issues of nitrile and acetylene functionalities during hydrogenation.....	59
Scheme 2-6: Synthetic route to the racemic allylic piperidinyl boronate.....	59
Scheme 2-7: Synthesis of dehydro- <i>t</i> -Boc-vac-1 analogs, dehydro-vac-1 halogen analogs, and formation of HCl salts of 27-29	60
Scheme 2-8: Synthesis of some of the <i>classical</i> bioisosteric Vac-1 analogs.....	61
Scheme 2-9: Synthesis of Mn(dpm) ₃ , and HAT hydrogenation conditions to access the <i>t</i> -Boc vac-1 SMe and iodo analogs 41 and 42	63
Scheme 2-10: Synthesis of the functionalized nitrile and alkyne vac-1 intermediates 43 and 44-45	64
Scheme 2-11: Synthesis of the remaining bioisosteric (20 , 24-25) and dehydroazepane (26) analogs.....	65
Scheme 2-12: Synthesis of cyclopropyl vac-1 analogs 52 and 62	72
Scheme 2-13: Synthesis of azepanyl vac-1 analog 53	73
Scheme 2-14: Preparation of indole aldehyde 68 and attempted allylboration.....	74
Scheme 2-15: Attempted preparation of indole vac-1 analog.....	74
Scheme 2-16: Attempted dihydroxylation reactions on dehydro-vac-1 analog 54	75

Scheme 2-17: Attempted cyclopropanation, and accidental synthesis of alkylated quinolinium 75.....	76
Scheme 3-1: General conjugate borylation reaction.....	131
Scheme 3-2: Yun's optimal conditions for a catalytic enantioselective Cu(I) conjugate borylation.....	133
Scheme 3-3: Proposed catalytic cycle of Yun's Cu(I) conjugate borylation.....	133
Scheme 3-4: Asymmetric Cu-catalyzed conjugate borylation of cyclic enones with (R,S) Taniaphos.....	134
Scheme 3-5: Asymmetric Cu-catalyzed conjugate borylation of β -substituted cyclic enones with (R,S)-QuinoxP*.....	135
Scheme 3-6: Contemporary reactions to synthesize enantioenriched α/β substituted cyclobutanones.....	136
Scheme 3-7: Synthetic methods for the preparation of cyclobutylboronates.....	137
Scheme 3-8: Attempted preparation of ethyl phenyl α,β -substituted cyclobutenone 1	139
Scheme 3-9: Alternative approaches to alkene migration.....	141
Scheme 3-10: Scope of α,β -substituted cyclobutenones.....	144
Scheme 3-11: Preliminary substrate scope for the preparation of cyclobutylboronates by catalytic enantioselective conjugate borylation.....	148

List of Tables

Table 2-1: Preliminary SAR of vac-1, based on synthesized analogs, and hits from the NIH diversity set.....	45
Table 2-2: Summary of biological activity for lead vac-1 analogs 75 , 23 , and 49	82
Table 3-1: Summary of alkene migration conditions for ethyl phenyl α,β -substituted cyclobutenone 1	142

List of Abbreviations

Å	ångström
Ac	acetyl
AcOH	acetic acid
ANDA	Abbreviated New Drug Application
Apaf-1	apoptotic protease activating factor 1
API	active pharmaceutical ingredient
App	apparent (NMR)
Ar	aryl
BA	boronic acid
BBB	blood-brain barrier
BDE	bond dissociation energy
BDPP	(2 <i>S</i> ,4 <i>S</i>)-2,4-bis(diphenylphosphino)pentane
BNCT	boron-neutron capture therapy
B ₂ pin ₂	bis(pinacolato)diboron
Bz	benzyl
° C	degree Celsius
CF ₃	trifluoromethyl
CH ₃ CN	acetonitrile
CIE	clathrin-independent endocytosis
cm ⁻¹	wavenumbers
CME	clathrin-mediated endocytosis
CNS	central Nervous System
Crabtree's catalyst	(1,5-cyclooctadiene)(pyridine)(tricyclohexylphosphine)-Ir(I) PF ₆
CRO	contract research organization
CSC	cancer stem cells
d	doublet
dd	doublet of doublets
ddd	doublet of doublet of doublets

dt	doublet of triplets
DBU	1,8-diazabicyclo[5.4.0]undec-7-ene
DIPEA	diisopropylethylamine
DMAP	4-dimethylaminopyridine
DMF	dimethylformamide
DMP	Dess-Martin Periodinane
DMSO	dimethylsulfoxide
DPEPhos	bis[(2-diphenylphosphino)phenyl] ether
dpm	tris(dipivaloylmethanato
dppf	1,1'-ferrocenediyl-bis(diphenylphosphine)
EE	early endosome
EDCI	1-ethyl-3-(3-dimethylaminopropyl)carbodiimide
EGFR	epidermal growth factor receptor
Et	ethyl
Et ₂ O	diethyl ether
Equiv.	equivalents
FABPs	fatty acid binding protein
FCC	flash column chromatography
FDA	Food and Drug Administration
FG	functional group
GBM	glioblastoma multiforme
h	hours
HAT	hydrogen atom transfer
HBpin	pinacolborane
HCV	hepatitis C virus
hERG	human Ether-à-go-go-Related Gene
HOBt	hydroxybenzotriazole
HPLC	high performance liquid chromatography
HTS	high-throughput screen
Hz	hertz
IC ₅₀	half maximal inhibitory concentration

IGF-IR	insulin-like growth factor I receptor
<i>i</i> -Pr	isopropyl
IR	Infrared spectroscopy
<i>J</i>	coupling constant (in NMR spectrometry)
JNK	c-Jun N-terminal kinases
Josiphos	(R)-1-[(SP)-2-[Di(1-naphthyl)phosphino]ferrocenyl]ethyl-di-tert-butylphosphine
LA	Lewis acid
LAH	lithium aluminum hydride
LE	late endosome
LiOt-Bu	lithium <i>tert</i> butoxide
M	molar/molarity
m	multiplet
Mandyphos	(<i>R_p</i> , <i>R'_p</i>)-1,1'-Bis{bis[3,5-bis(trifluoromethyl)phenyl]phosphino}-2,2'-bis[(<i>S</i>)- α -(dimethylamino)benzyl]ferrocene
MAP	mitogen-activated protein
mCPBA	metachloroperbenzoic acid
Mdm2	murine double minute 2
Me	methyl
MeOH	methanol
MGMT	O ⁶ -methylguanine DNA methyltransferase
MHz	megahertz
MIC	minimum Inhibitory Concentration
Min	minutes
mL	milliliters
mol	moles
mmol	millimoles
mol. siev.	molecular sieves
MTIC	imidazole-4-carboxamide
MTS	[3-(4,5-dimethylthiazol-2-yl)-5-(3-carboxymethoxyphenyl)-2-(4-sulfophenyl)-2H-tetrazolium

NADH	nicotinamide adenine dinucleotide
NADPH	nicotinamide adenine dinucleotide phosphate
NaNH ₂	sodium amide
NaO <i>t</i> -Bu	sodium <i>tert</i> -butoxide
NCE	new chemical entity
NDA	New Drug Application
NfF	perfluorobutanesulfonyl fluoride
NIH	National Institutes of Health
NMO	4-methylmorpholine N-oxide
NMR	Nuclear Magnetic Resonance spectroscopy
NRTI	nucleoside reverse transcriptase inhibitors
OAc	acetoxy
OsO ₄	osmium tetroxide
PAIN	pan-assay interference
PEPPSI-IPr catalyst	[1,3-Bis(2,6-Diisopropylphenyl)imidazol-2-ylidene](3-chloropyridyl)palladium(II) dichloride
PES	phenazine ethosulfate
PF ₆	hexafluorophosphate
Ph	phenyl
PhNMe ₂	dimethylaniline
PIKFYVE	phosphoinositide kinase
PK	pharmacokinetic
POCl ₃	phosphoryl chloride
q	quartet
rt	room temperature
s	singlet
SAR	structure-activity relationship
sep	septet
sext	sextet
SHIP	inositol-5'-phosphatase
shRNA	short hairpin RNA

SMe	methyl thiol ether
SOCl ₂	thionyl chloride
SO ₂ Me	methyl sulfone
t	Triplet
TACE	TNF α converting enzyme
Taniaphos	R _P -1-Dicyclohexylphosphino-2-[(R)- α -(dimethylamino)-2-(dicyclohexylphosphino)benzyl]ferrocene
<i>t</i> -Boc	tert-Butyloxycarbonyl
<i>t</i> -Bu	<i>tert</i> -butyl
td	triplet of doublets
Tf	trifluoromethanesulfonyl
Tf ₂ O	trifluoromethanesulfonic anhydride
TFA	trifluoroacetic acid
THF	tetrahydrofuran
TMZ	temozolomide
Tr	trityl
TS	transition state
TNFR	tumour necrosis factor receptors
μ M	micromolar
Vac-1	vacuol-1
VT-NMR	variable-temperature nuclear magnetic resonance spectroscopy
Xantphos	4,5-bis(diphenylphosphino)-9,9-dimethylxanthene
Xphos	2-dicyclohexylphosphino-2',4',6'-triisopropylbiphenyl

Chapter 1: The Utility of Organoboron Compounds in Modern Drug Discovery

1.1 The Importance of Drug Discovery, and the Growing Need for New Strategies in the Field

Drug discovery is the process of finding new chemical entities (NCEs) to treat a disease through innovations in the fields of chemistry, biology, pharmacology, biochemistry, and biotechnology.¹ The inception of this multidisciplinary process can be traced back to prehistoric times and Chinese medicine practices, where the ingestion of plants or extracts thereof could induce a myriad of different medicinal effects on the subject, such as disease treatment, symptom alleviation, and psychoactive effects.¹ However, the more rational foundations of modern drug discovery come from the industrial era, and Paul Ehrlich's work with azo and phenothiazine dyes from 1872-1874.¹

Ehrlich's empirical observations on dye affinities for biological tissues led him to hypothesize the idea of *chemoreceptors*, and how such receptor cells on parasites, microorganisms, and cancer cells would be chemically unique from the chemoreceptors on healthy surrounding tissues when interacting with molecules.² Ehrlich then surmised that the chemoreceptors of harmful pathogens and/or cells could be selectively targeted with therapeutics, while leaving the healthy tissues unharmed.² This "magic bullet" theory was the first major step in the development of modern chemotherapy, and aided Ehrlich in the discovery of the arsenic chemotherapeutic drug Salvarsan—one of the first treatments for Syphilis.²⁻³ Ehrlich's crucial hypothesis would grow into modern receptor-ligand theory and the concept of pharmacophores. These concepts would deliver the basic conceptual ideas for drug discovery. However, it would take another 100 years for advances in animal modeling, X-ray crystallography, molecular modeling, high-throughput screening (HTS), and DNA recombination and transfection, to evolve drug discovery into the multifaceted juggernaut it is today.¹

There is no question about the profound effects drug discovery can have on the well-being of humanity. In 1935, Gerhard Domagk helped discover and distribute Prontosil, a red dye that would be the foundation for the *sulpha drugs* or sulphonamides, which were the first treatments for systemic bacterial infections.³⁻⁴ Domagk's discovery was an inspiration for the antibiotic

revolution, as isolation of large quantities of penicillin came to fruition in 1940.³ Only four years after penicillin became readily available, Albert Schatz isolated the aminoglycoside streptomycin from soil bacteria, which would inspire further exploration for antibiotics containing tetracyclines and β -lactams in the 1950-1960s, effectively bringing bacterial diseases under control for several decades.³ From this success in treating infections, several other milestones in medicine would result from drug discovery efforts: the psychoactive benzodiazepines, which revolutionized therapy in psychiatry; the statins, which reduced illness and mortality in heart disease; Nucleoside Reverse Transcriptase Inhibitors (NRTIs) for the treatment of HIV/AIDS; and lastly, the platins, taxanes, kinase inhibitors, and other agents that expanded the arsenal against cancer (Figure 1-1).^{1,5} This renaissance of small molecules helped pharmaceutical giants prosper, which rapidly expanded research and development into even more therapeutics that would change the face of modern medicine. Despite these breakthroughs in the “golden age” of drug discovery, from the 1950s to the present day, drug discovery innovations in pharma began to decline at a steady rate.^{6,9}

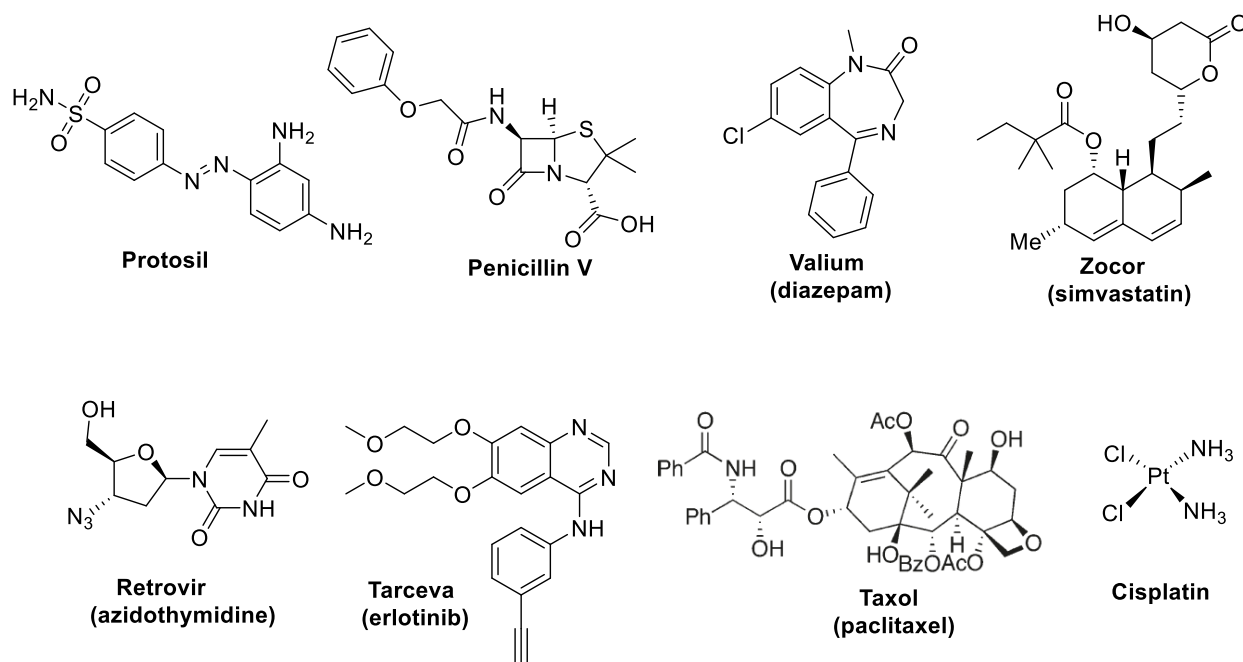


Figure 1-1: Some small molecule milestones in the treatment of disease, during the “golden age” of drug discovery.^{1,5}

Despite an annual spending of \$130 billion in pharmaceutical R&D in 2012, and a consistent rise in drug discovery investments, the annual number of NCEs approved by the FDA

was between 25-42 from the period of 2007 to 2012.⁷ With an average cost of over \$1 billion, a 30% failure rate in preclinical development, and a ~60% attrition rate of experimental drugs in phase II and phase III clinical trials, the likelihood of an NCE reaching the market is a dismal 4%.⁷⁻⁸ These alarming numbers in combination with “Eroom’s Law” (the tongue-and-cheek inverse of Moore’s Law), aptly summarize the downward trend in R&D efficiency of the pharmaceutical industry (Figure 1-2).⁹ Moore’s Law states that every two years the number of semiconductors in an integrated circuit will double.⁹ When applied to the pharmaceutical industry, the reverse of Moore’s Law is seen, where increased spending in the industry gives fewer drugs over time (hence the backwards moniker Eroom).

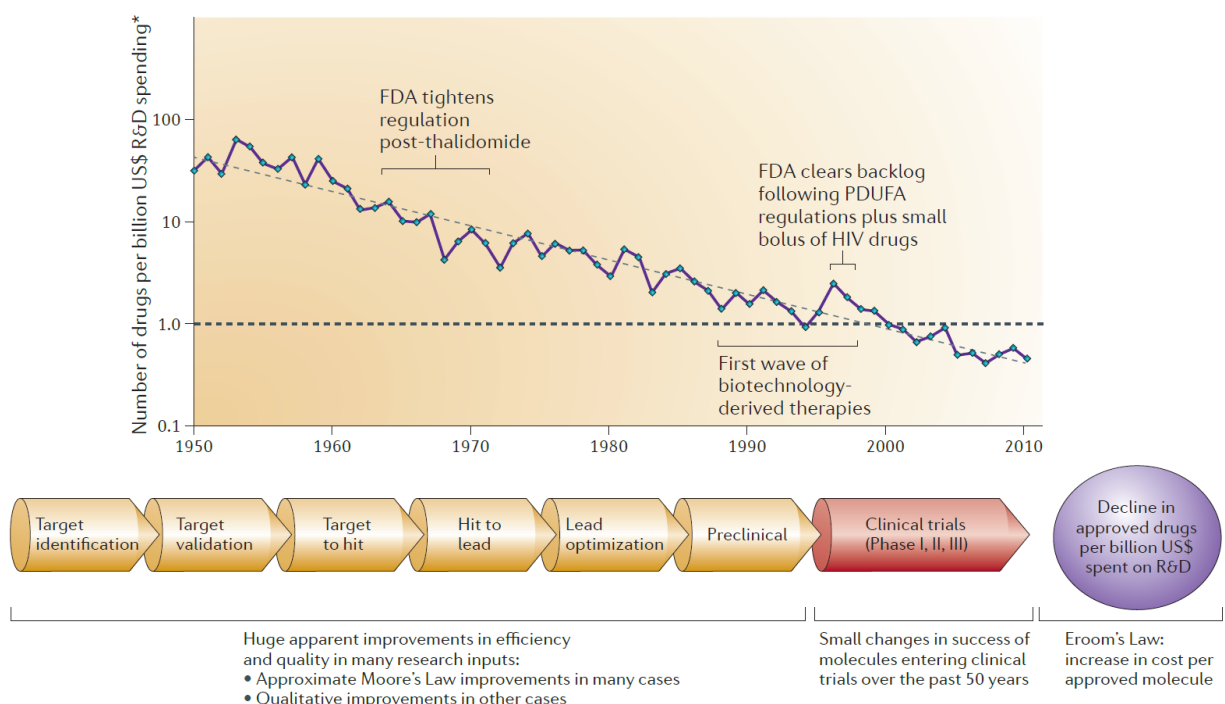


Figure 1-2: 2010 decline in innovation from the pharmaceutical industry, reproduced with permission by Springer Nature.⁹

This apparent innovation gap can largely be attributed to two economic factors: 1) generic drugs, and 2) the patent cliff, and two scientific factors: 1) clinical attrition, and 2) increasing complexity of disease targets.⁸⁻¹⁰

Generic drugs are medications that contain the same active pharmaceutical ingredient (API) as a brand-name drug, and mimics its dosage, safety profile, and general performance.¹⁰⁻¹¹

From their foundation to increase competition and lower drug prices, 80% of prescriptions are now generics, and the global generics industry is estimated to be \$385 billion dollars by 2016.¹⁰ This rising industry, coupled with a generic drug's power to compete with a brand-name drug four years after it hits the market with an Abbreviated New Drug Application (ANDA), has cost the pharmaceutical industries \$290 billion from 2012-2018.¹⁰ Directly tied to this competition is the patent cliff, which in its simplest form, is the expiration of major blockbuster drugs that have/can earn between \$1.0-4.5 billion in a year for a company.¹⁰ Blockbusters drugs that will no longer be patented, combined with the reality that the most recent FDA approved NCEs are orphan drugs or target disease niches, will limit the amount of return to cover the increasing cost of R&D, which paints a problematic future for drug discovery.¹⁰

Even if one can somehow avoid the economic pitfalls, there is still the problem of getting a drug from clinical trials to market. As alluded to above, drug candidates are abandoned due to a combined ~90% attrition rate from preclinical to phase III clinical trials.^{8,10} This attrition is influenced by increased FDA regulations and scrutiny during a New Drug Application (NDA), as well as drug efficacy, toxicology, clinical safety, and other factors.^{8,10} But, perhaps the most important dynamic towards drug failure is the biological target itself. The notion that one drug should only affect one biological target with high affinity is beginning to erode, as researchers are becoming increasingly aware that targets of interest for a disease are involved with many biological networks of genes, proteins, enzymes, and other active molecules.⁸⁻⁹ This biological system of redundancies can cause a single-target drug to lose its beneficial effects against a disease.⁸⁻⁹ But, not all hope is lost for all drug discovery endeavours!

The pharmaceutical industry is increasingly externalizing their innovation efforts via academic collaborations, biotech start-ups, and contract research organizations (CROs) to aid them in the drug discovery process; effectively altering the linear drug discovery pipeline that medicinal chemists are all too familiar with (Figure 1-3).⁷ This paradigm of pooling innovations and intellectual properties is clearly having a large impact, as academic-industrial collaborations are more likely to succeed at phase III trials and filing an NDA, compared to internal innovation efforts.¹² Two non-business strategies from a medicinal chemistry standpoint may also be able to help combat the negative holding pattern of the pharmaceutical industry and its drug discovery efforts (Section 1.2).

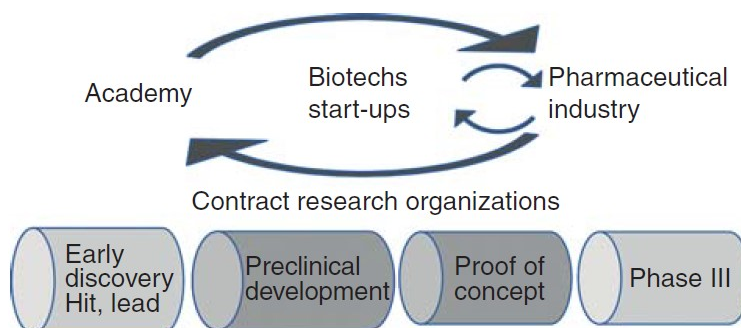


Figure 1-3: The collaborative drug discovery pipeline, reproduced with permission from Taylor & Francis.⁷

1.2 Polypharmacology and Drug Repurposing

Since many diseases employ several pathways and interactions with biological entities to promote pathogenesis, then it stands to reason that NCEs from drug discovery efforts should target all these different networks as well! This concept defines the evolving practice of polypharmacology.¹³ From a drug design standpoint, polypharmacology can encompass two possibilities: 1) multiple drugs binding to different targets, or 2) one drug binding to multiple targets in a biological network.¹³ Some small molecule drugs like paracetamol and metformin are known to follow the latter possibility, though these were largely serendipitous in discovery.¹⁴ However, more rational chemical approaches towards multitarget drugs have emerged since this strategy's growth in popularity, such as a) adding a chemical linker between two active pharmacophores, b) fusing two active drugs with separate targets together with a functional group, and c) merging pharmacophores together so that the biological activity of both is maintained, (Figure 1-4).¹⁴ The potential benefits of polypharmacology are enticing, such as reducing drug-drug interactions as treatment becomes less complex due to fewer single-target drugs being used, improving efficacy via synergistic effects of modulating multiple targets at once, and the economic benefit of designing one drug for multiple targets, compared with multiple specific drugs.¹⁴

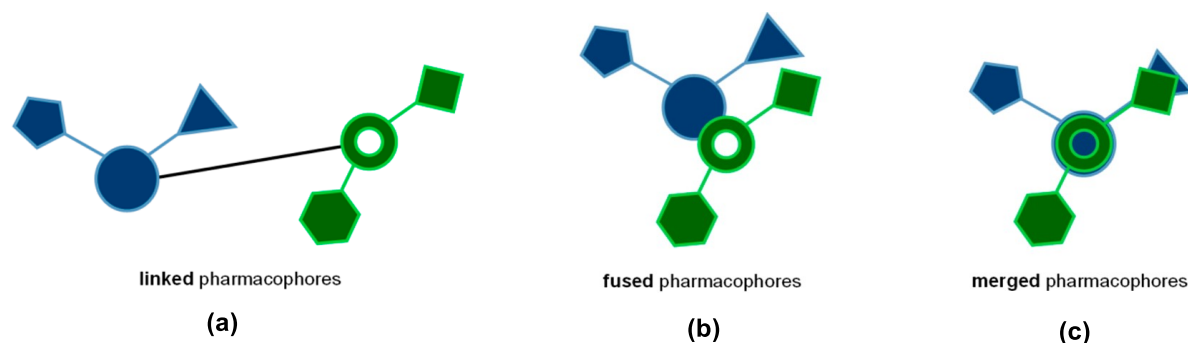


Figure 1-4: Chemical approaches towards developing a multitarget drug.¹⁴ Reprinted with permission from Proschak, E.; Stark, H.; Merk, D. *J. Med. Chem.* **2019**, *62*, 420-444. Copyright 2018, American Chemical Society.

A direct application of polypharmacology is the idea of drug repurposing, which is looking for new clinical applications or biological targets of existing drugs or NCEs that have failed to progress to market or are in clinical development.¹⁵ Drug repurposing can arise from a number of mechanisms.¹⁶ One such mechanism is serendipity, which is classically exemplified by Viagra (sildenafil), which was originally an angina treatment, but is now primarily used to correct erectile dysfunction based on empirical observations during clinical trials.¹⁶⁻¹⁷ Other options to repurpose a drug include data-driven approaches, or *in vitro* screening against new targets, which can be demonstrated by Gleevec (imatinib), originally a treatment for chronic myelogenous leukemia, it is now repurposed for treating systematic mastocytosis, and gastrointestinal stomal tumours.¹⁶ Lastly, there is the tactic of taking a known drug and systematically combining it with other drugs to produce an alternative effect, as shown by Topamax (topiramate) an epilepsy and migraine therapy, which can also be used for weight-loss in combination with phentermine.¹⁶ Repurposing approaches are growing in popularity in pharma. Indeed, 43% of leads from drug discovery programs arise from previously known compounds, and 30% of FDA approved drugs in the past few years were repurposed.^{16,18} However, another way to look at drug repurposing is by chemically modifying existing drugs or candidates that have failed to progress pass preclinical or clinical development, such that the biological activity is improved and/or acquires more favourable properties for interaction with one or more biological targets. To accomplish this strategy of drug design, there is also a need for developing new pharmacophores to incorporate into existing drug scaffolds to improve clinical significance, as there is consensus that the “low-hanging fruits” or common bioactive functional group (FGs) and/or single protein targets of these FGs have been

exhausted.^{18b} This lack of novel biological activity can stymie innovation, and drastically narrow the patent space for NCEs as a result. However, an emerging area of medicinal chemistry that can add a diverse exploitable pharmacophore, and repurpose drugs in new ways is by incorporating boron into bioactive molecules.

1.3 Boron in the Medicinal Chemistry Toolbox

With an atomic number of 5, boron has one less electron than carbon, which results in an empty *p* orbital within its neutral sp^2 configuration.¹⁹ As a result of this open shell, boron has strong Lewis acid character, and weaker BDE between B-O bonds (75 kJ/mol) compared to C-O bonds (355-380 kJ/mol).¹⁹ Some of the most stable boron compounds are boronic acids (BAs). BAs commonly have a pKa range of 8-9, have good hydrogen bonding potential (20-30 kJ/mol), and at physiological pH (~7.4), they can typically exist in equilibrium between a neutral sp^2 form, and the anionic tetrahedral sp^3 form via its reactive open shell.¹⁹ This dynamic is shown in Figure 1-5 with phenylboronic acid.¹⁹ With their air stability, low toxicity profile, and transient ability to exist in two different molecular geometries, a rich variety of pharmaceutical applications have been developed: carbohydrate sensors based on the BAs reversible binding to diols, they can polymerize and be used as drug delivery systems, hydrolytic enzyme inhibitors, and many other applications.¹⁹⁻²²

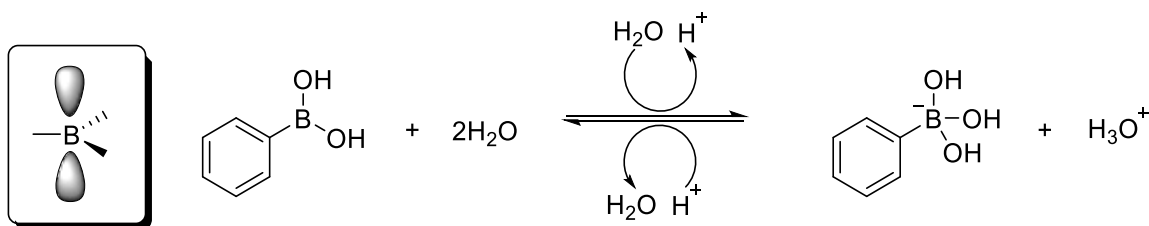


Figure 1-5: Boron's open shell, and the reversibility of neutral and anionic forms of phenylboronic acid at physiological pH.¹⁹

From the standpoint of drug repurposing, one can look at the boronic acid functional group as a carboxylic acid bioisostere to improve biological activity, and increase a drug's clinical significance. Boron is a valuable molecular editor of drug scaffolds via formation of boron

heterocycles, and its rich chemistry/synthetic utility can provide alternate synthetic routes to access privileged scaffolds, which can allow further diversification of existing drug classes.

1.3.1 Boron as a Carboxylic Acid Bioisostere

Bioisosterism can be broadly defined as replacing part(s) of the molecular structure of a drug candidate with substituents or functional groups that have similar shape/sizes and chemical properties that can either improve or attenuate biological activity.²³ This concept branches into two subsets termed *classical* and *nonclassical*, in which classical isosteres refer to groups that have roughly the same number of atoms, as well as similar steric and electronic factors as the portion of molecule to be replaced.²³ A common example of this isosterism would be a functional group replacement.²³ Nonclassical isosteres do not follow the physicochemical equivalencies of a classical isostere, but still manage to produce similar biological activity.²³ A technique that highlights this isosterism is the scaffold hop, where the core of a drug molecule is modified with a similar template to improve potency.²³ Based on the definitions above, boronic acids function as a classical bioisostere of the carboxylic acid functional group.²⁴

Carboxylic acid moieties are prolific functional groups in medicinal chemistry. They are part of the general structure of all amino acids, the fatty acids that make up biological membranes, as well as certain steroids.²⁴ Carboxylic acids can be desirable from a drug design standpoint, because they can lower lipophilicity of a molecule and improve aqueous solubility as a result of low pKa (~4.5), strong electrostatic interactions, and hydrogen bonding ability.²⁴ However, the location of the biological target has to be taken into account when working with carboxylic acid moieties, as the charged functionality under physiological conditions will be unlikely to cross the blood-brain barrier (BBB) or get to other central nervous system (CNS) destinations.²⁴ In addition, they can pose a threat from a pharmacokinetic (PK) standpoint, as they can be rapidly metabolized, which can lead to poor bioavailability or increased toxicity.²⁴

BAs are a potential solution to the flaws of carboxylic acids. The two hydroxy groups bound to the boron atom can readily hydrogen bond to acquire favourable interactions—similar to the carboxylic acid; the higher pKa (8-9) may help prevent fast metabolism and subsequent clearance.²⁴ However, there are risks of nonspecific interactions or loss of biological activity with this pharmacophore, due to deboronation, oxidation, or formation of boronate esters with other

biological targets or molecules.^{19a} In spite of this, use of the boronic acid pharmacophore led to the successful marketing of Velcade (bortezomib), a peptidylboronic acid proteasome inhibitor for multiple myeloma—a plasma cell cancer (Figure 1-6).^{19b} As well, the BA has been successful in repurposing hits into lead drug candidates. A recent example of this is seen by GlaxoSmithKline’s (GSK) efforts into developing new therapies against the hepatitis C virus (HCV).²⁵ They found that a BA pharmacophore in the *para* position of a phenyl moiety on a benzofuran scaffold was essential for enhanced *in vitro* potency against wildtype and mutated HCVs.²⁵ As well, the BA was upwards of 100X to 1000X more potent compared to a carboxylic acid FG—highlighting its power in drug repurposing as a potent carboxylic acid bioisostere (Figure 1-6).²⁵ After adding a fluoro group *ortho* to the BA to further improve its potency, the lead compound was advanced to clinical trials.²⁵ While the boronic acid is very promising as a pharmacophore and bioisostere for drug repurposing, another increasingly popular area is transforming the boronic acid into a benzoxaborole—a novel boron heterocycle.

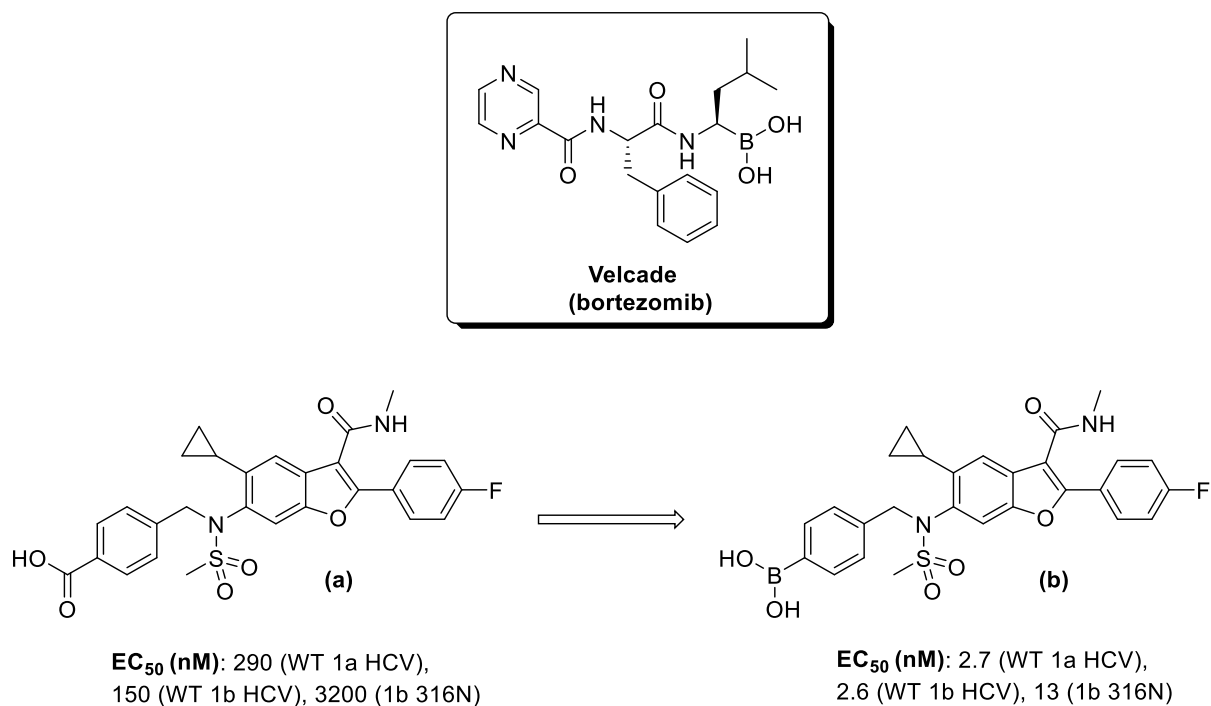


Figure 1-6: (Top) Structure of bortezomib, the first successful boronic acid drug. (Bottom) an example of a hit (a) repurposed with a boronic acid (b), with high *in vitro* activity against wild type (WT 1a and WT 1b), and mutated HCV (1b 316N) strains.^{19b,25}

1.3.2 Benzoxaboroles as Novel Heterocycles in Medicinal Chemistry

Benzoxaborole is a five-membered boronic acid hemiester embedded onto a phenyl ring, which is typically formed from an intramolecular dehydration reaction of 2-(hydroxymethyl)phenylboronic acid.²⁶ Benzoxaboroles were originally isolated in 1957 by Torsell, and were found to have good water solubility, as well as stability towards acidic and alkaline media.²⁷ These heterocycles are significantly more acidic ($pK_a \sim 7.4$) than BAs, which means that at physiological pH, there is an equal proportion of its neutral sp^2 form and its tetrahedral sp^3 anionic intermediate.²⁸ The large difference in acidity is due to the inherent ring strain of the five-membered ring.²⁸ This strain gives a shorter boron-oxygen bond, which is subsequently relieved when a hydroxide ion complexes the Lewis acidic boron atom.²⁸ There was some speculation as to whether the benzoxaborole could exist between an open and closed form in aqueous media. However, Hall and co-workers demonstrated through VT-NMR studies that five, six, and seven membered benzoxaboroles predominantly existed in the closed-form in aqueous-organic mixtures, likely due to the enthalpy of ring formation and the release of water, which is thermodynamically favourable (Figure 1-7).²⁷

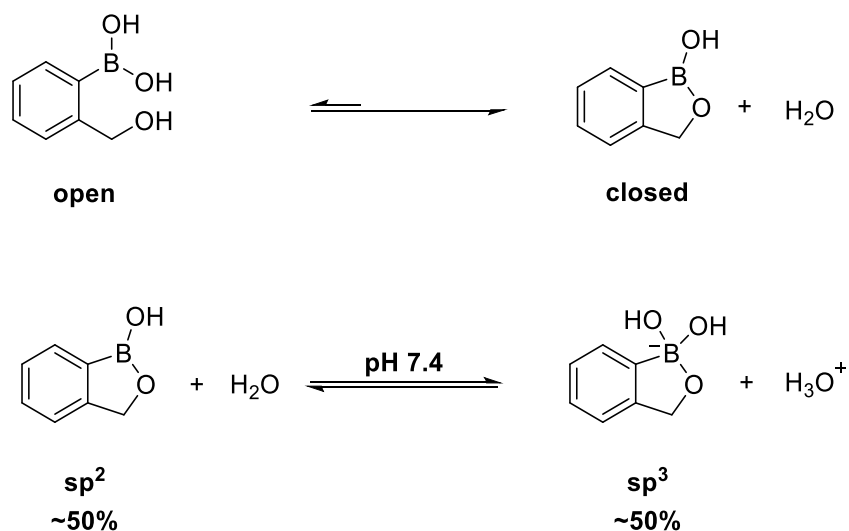


Figure 1-7: Chemical properties of benzoxaboroles in aqueous media at physiological pH.²⁷⁻²⁸

Despite their stability and intriguing properties, benzoxaboroles were largely ignored in drug discovery endeavours, until it was revealed that they were very efficient at binding to diols, forming so-called *spiro complexes*, which can inhibit the active sites of a variety of enzymes.^{28d} This binding affinity and further research into benzoxaboroles as a drug scaffold culminated in the marketing of two drugs: Kerydin (tavaborole), for the treatment of onychomycosis, and Eucrisa (crisaborole), as a topical treatment for dermatitis, as well as many experimental derivatives like SCYX-7158 for the treatment of human African trypanosomiasis or “sleeping sickness” (Figure 1-8).²⁷⁻²⁹ Based on market success, it is no surprise that drug discovery programs are attempting to repurpose the benzoxaborole scaffold to find additional biological targets or increased potency.

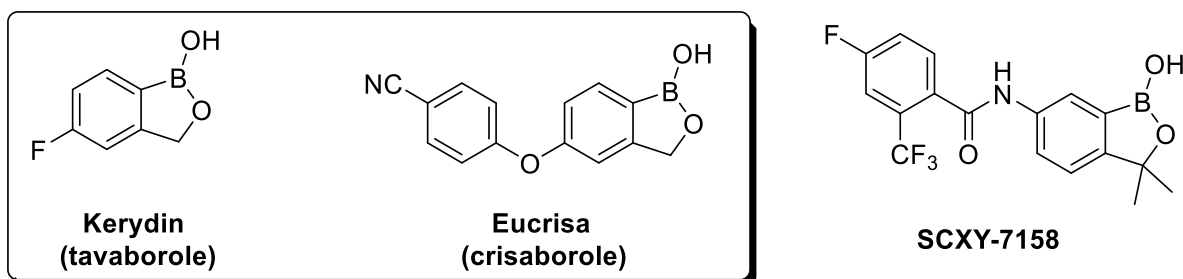


Figure 1-8: Marketed drugs and a drug candidate featuring a benzoxaborole.²⁷⁻²⁹

One example of this trend is the repurposing of the antibiotic vancomycin. The free carboxylic acid moiety on vancomycin was coupled with a chiral amino benzoxaborole to generate analog (c).^{28a} The repurposed vancomycin was shown to have a significant increase in the minimum inhibitory concentration (MIC) against *Staphylococcus* and *Enterococcus* strains of bacteria (Figure 1-9).^{28a} It is clear that both the characteristics of benzoxaboroles and boronic acids are beneficial for pharmaceuticals. However, another essential application of organoboron compounds are the use of its novel chemistry to access common drug scaffolds in innovative ways.

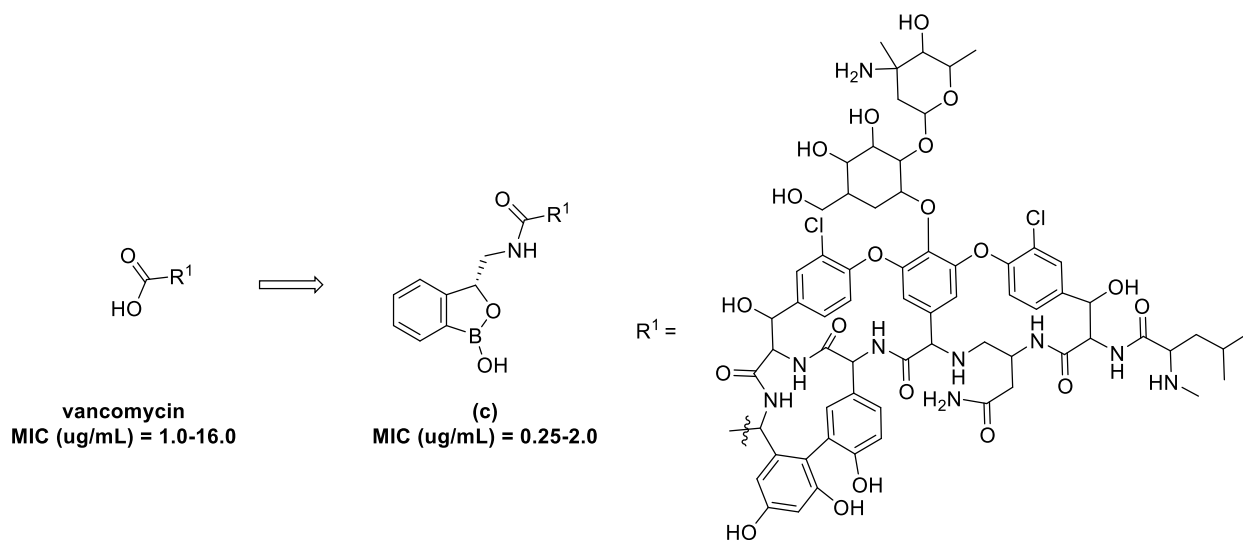


Figure 1-9: Drug repurposing of vancomycin with a benzoxaborole scaffold.^{28a}

1.3.3. Accessing Privileged Scaffolds through Carbonyl Chemistry: β -Amino Alcohols

The β -amino alcohol (also known as vicinal amino alcohol, or 1,2-amino alcohol) is a scaffold commonly encountered in natural and synthetic products.³⁰ Structurally, the scaffold can be acyclic with the free alcohol and amine, or the amine and/or hydroxyl portion can be acylated, alkylated or contained within rings.³⁰ The contiguous 1,2 linkage of the carbons containing the hydroxy and amine functional groups give the scaffold an inherent chirality and biological activity in many molecules—making it a sought after *privileged scaffold* in medicinal chemistry (Figure 1-10).³⁰ Examples of 1,2-amino alcohols can be seen in the amino acids serine and threonine, sphingosine, (a structural lipid involved in cell signaling), febrifugine, (an antimalarial), and the hormones epinephrine, and norepinephrine.^{30b,30e} This motif has broad pharmaceutical use, as 82 FDA approved drugs, and an additional 119 experimental drugs yet to be approved contain a β -amino alcohol.^{30a} Some pharmaceuticals with this prolific scaffold include Invirase (saquinavir), an HIV protease inhibitor, Ranexa (ranolazine) an antianginal medication, and Relenza (zanamivir) a drug used to treat influenza.^{30b,30e} Additional utility of the β -amino alcohols can be seen in organic synthesis, from Evans' oxazolidinone auxiliaries used for stereoselective aldol reactions, the chiral oxaborolidine ligands used in the Corey-Bakshi-Shibata (CBS) reaction to reduce carbonyls to generate enantioenriched alcohols, and organocatalysts like prolinol (Figure 1-10).^{30c,30e}

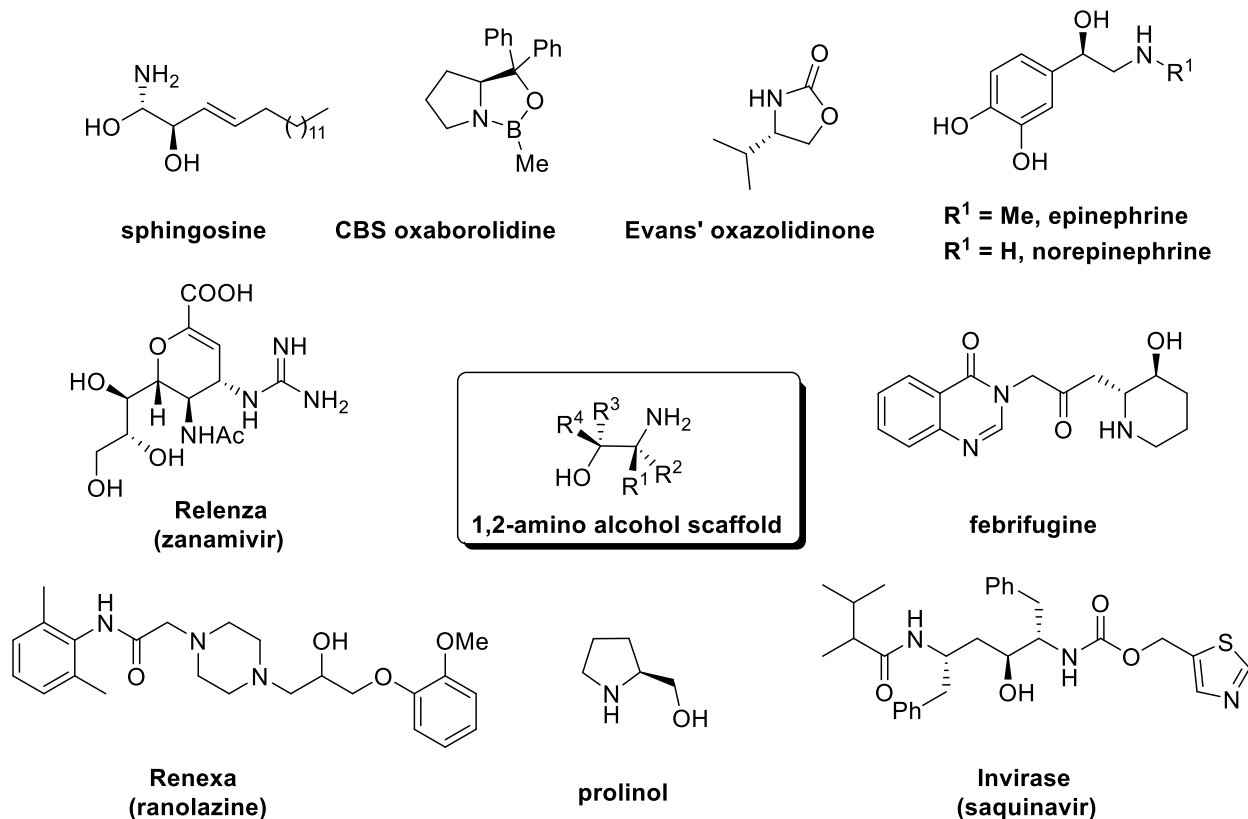


Figure 1-10: General structure of 1,2-amino alcohol scaffold and its appearance in natural products, drugs, and chiral catalysts.³⁰

Due to their ubiquity, several synthetic routes exist to prepare β -amino alcohols (Figure 1-11). Traditional routes of preparation would involve reduction of carbonyl, imino, or nitro groups, ring opening of epoxides or aziridines, or aminohydroxylation.³¹ More contemporary methods would include late stage C-H activation, and Ru-catalyzed reduction of α -amino nitriles.³¹ To access this motif with boron chemistry, a boronate ester can easily serve as a “masked” alcohol via oxidation, as such aminoboration or hydroboration on an alkene or enamine could yield the scaffold.³² In addition, addition of 1,1-diborylalkanes to an aldimine—followed by monoprotodeboronation, oxidation, and deprotection as required—could also readily access vicinal amino alcohols.³² Herein, the major focus of accessing β -amino alcohols will be on allylboration of aldehydes.

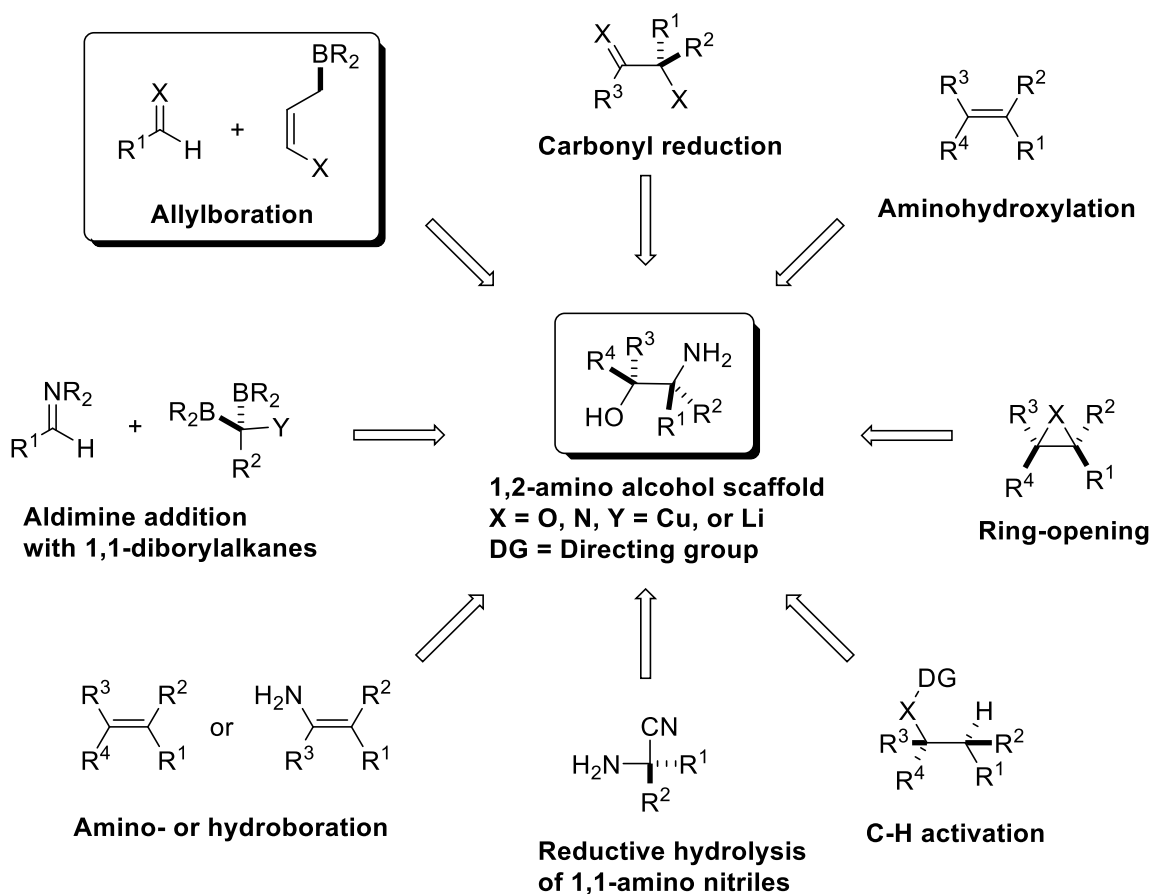


Figure 1-11: Synthetic methodologies to prepare 1,2-amino alcohols.³¹⁻³²

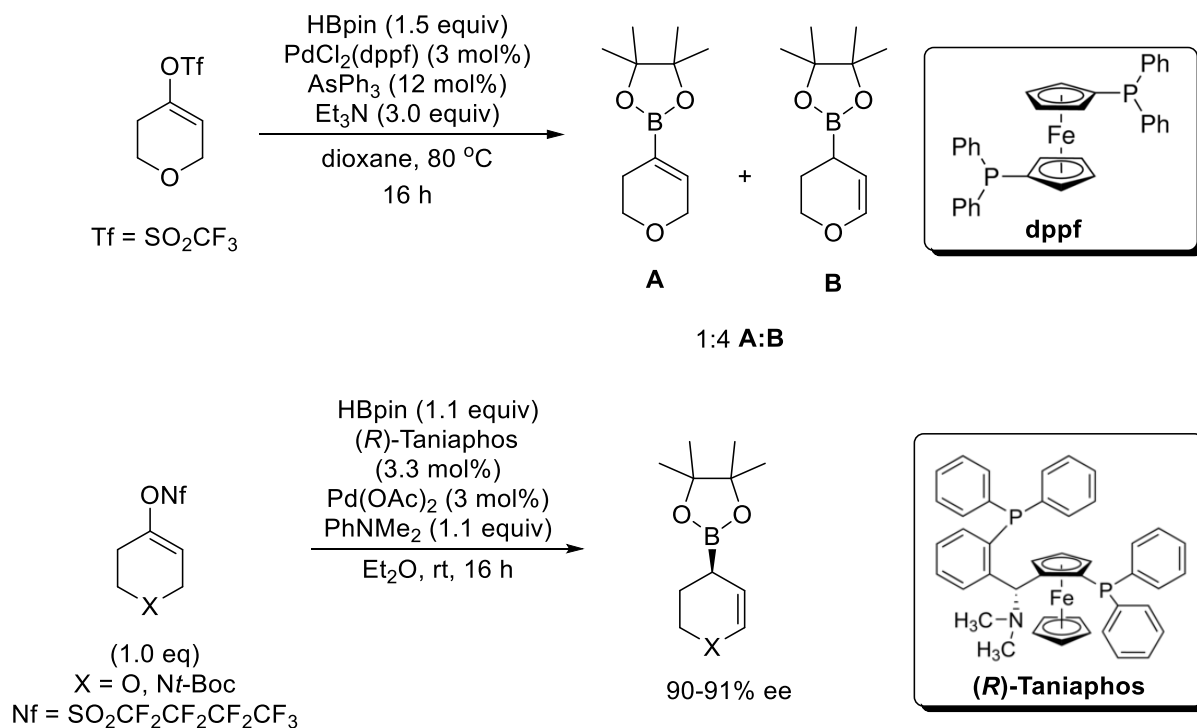
Carbonyl allylboration is an addition reaction between an allylic organoboron reagent and a carbonyl compound, most commonly an aldehyde or imine.³³ This nucleophilic allyl transfer to the carbonyl generates a homoallylic alcohol or amine via formation of a new C–C bond.³³ This new bond creates two stereogenic centres, as well as a residual allyl fragment which can be further functionalized as desired.^{19a,33} In general, the allylic organoboron reagent falls under two classes: 1) borane, or 2) boronate.^{19a,33} Boranes typically have two alkyl substituents bound to the boron atom, whereas boronates will have alkoxy substituents (Figure 1-12).³³ Allylic boranes are more reactive, but unlike boronates, they are unstable to air and moisture.^{19a,33}

The chirality of an allylic organoboron can exist in two forms: the first being as an auxiliary, where the chirality is contained on the alkyl groups of the borane/boronate, which is referred to as a *B-chiral* allylic boronate, and the second form where chirality is present on the α -

In addition, catalytic allylboration can also be performed to generate homoallylic alcohols in a highly diastereo- and enantioselective fashion.^{33b} Hall and co-workers optimized a catalytic allylboration sequence by forming a *C-chiral* allylic boronate via addition of a Grignard reagent to a vinyl boronate ester in the presence of a chiral phosphoramidite–Cu(I) complex.^{33b} This enantioenriched allylic boronate was then immediately reacted with the aldehyde in the presence of a suitable Lewis acid, like boron trifluoroetherate (BF₃ • Et₂O).^{33b} These one-pot conditions form the product in high ee and E/Z ratios, which is attributed towards a tighter Type I TS due to the Lewis acid coordination to an oxygen on the boron ester—creating more prominent steric interactions.^{33b}

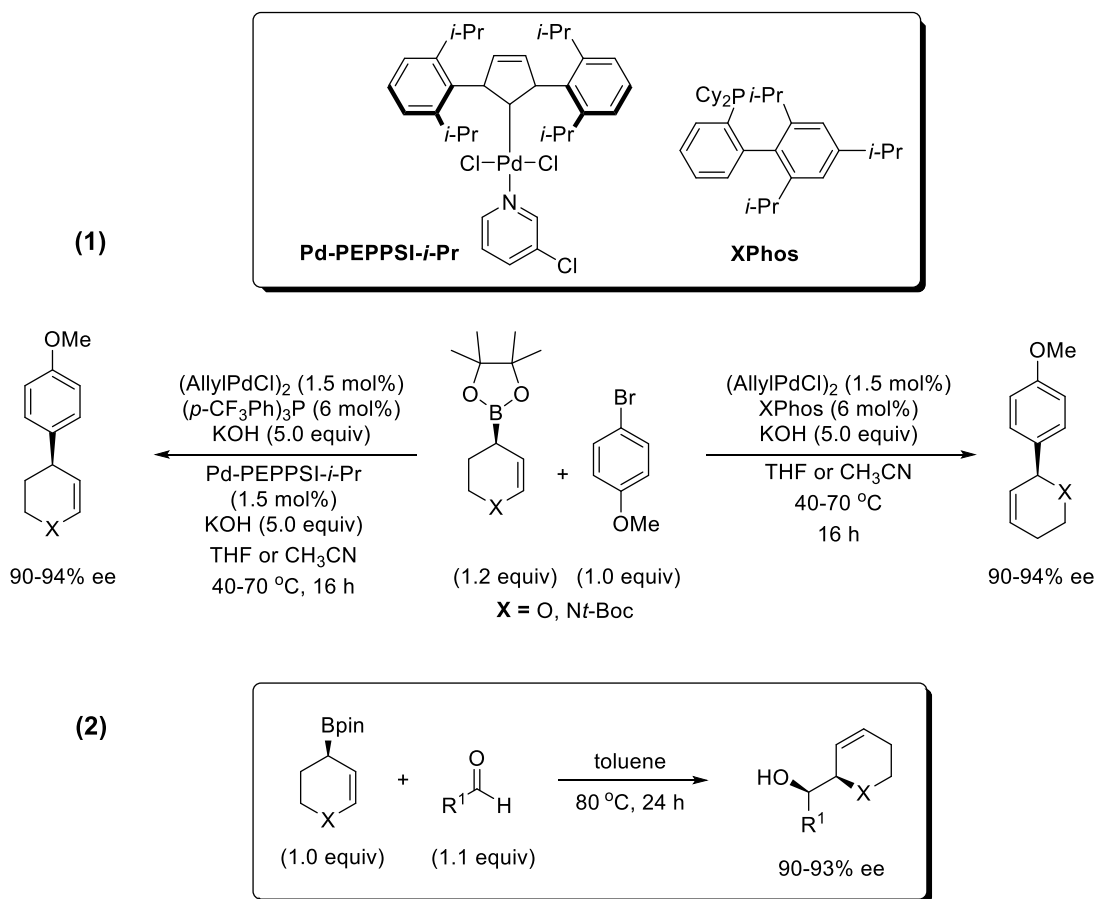
While the allylboration is highly stereoselective, it is difficult to produce an homoallylic alcohol with an amine γ -substituent, as allylic boronates with an amino group at the 2-position or “aminoallyl boronate” are quite rare, have limited reactivity and scope, and require several functional group manipulations for their preparation.³⁴ The Hall Group wanted to resolve this problem to access the 1,2-amino alcohol scaffold by developing a more facile method to prepare a 3-aminoallyl boronate. In this regard, an interesting opportunity emerged when Matsuda and co-workers reported a Pd-catalyzed borylation of cyclic alkenyl triflates to access the corresponding alkenyl boronate.³⁵ Their reaction was highly selective and robust on all substrates with the exception of a tetrahydropyranyl triflate, where unexpectedly, the allyl boronate product was formed preferentially over the alkenyl boronate (Scheme 1-1).³⁵

Inspired by this strange outcome, the Hall Group optimized the olefin isomerization on the tetrahydropyranyl triflate/nonaflate to access the allylic tetrahydropyranyl boronate under very mild conditions, and were successful in making the transformation enantioselective by using the chiral ligand, Taniaphos.³⁶ This borylative migration, which generates an enantioenriched cyclic chiral boronate, was further optimized and applied to the corresponding piperidinyl triflate/nonaflate to access an allylic piperidinyl boronate on gram scale with high enantioselectivity.³⁶ The application of the borylative migration to piperidines has considerable potential in medicinal chemistry programs, as the piperidine ring is a privileged scaffold that makes up a large portion of FDA approved drugs (Scheme 1-1).³⁶⁻³⁷



Scheme 1-1: Matsuda and co-workers' borylation conditions (top), and optimized conditions for the Hall Group's enantioselective borylative migration reaction (bottom).³⁵⁻³⁶

With a powerful methodology in hand, the Hall Group then wanted to examine some of the synthetic applications of the enantioenriched allylic tetrahydropyranyl and piperidinyll boronates. A major utility of boronate esters is employing the Suzuki-Miyaura cross-coupling to form new C–C bonds. While the reaction is very robust in forming sp²–sp² bonds, cross-coupling to form sp³–sp² bonds is challenging due to a slow transmetalation step, and the tendency to form side products via β-hydride elimination.³⁸ In addition, when the chiral boronate is allylic there is also the issue of regioselectivity, where steric or electronic effects can dictate whether the cross-coupling product will be at the α or γ carbon of the boronate ester.³⁸ However, the Hall Group was able to circumvent all of these selectivity issues by employing different ligands on a palladium metal catalyst to preferentially form the α or γ substituted products in high regioselectivity from the Suzuki-Miyaura reaction (Scheme 1-2).³⁸ This elegant cross-coupling methodology was then used in the preparation of the antidepressant drug Paxil (paroxetine).³⁸



Scheme 1-2: Applications of heterocyclic allylic boronates: **(a)** regioselective Suzuki-Miyaura cross-coupling, **(b)** thermal allylboration.^{36,38}

In addition, allylic piperidiny boronates can readily be used in thermal allylboration with a chosen aldehyde, which can generate the desired 1,2-amino alcohol scaffold (Scheme 1-2).³⁶ This is a particularly useful process, one that enables access to several α -hydroxyalkyl piperidine-based cinchona alkaloid scaffolds in high enantio- and diastereoselectivity.

1.4 Applying Chiral Allylic Piperidiny Boronates for the Stereoselective Synthesis of Mefloquine and Vacquinol-1

Cinchona alkaloids are natural products isolated from the bark of cinchona trees and have tremendous utility in organic chemistry and drug discovery.³⁹⁻⁴⁰ Perhaps some of the oldest drugs known, the cinchona alkaloids were the first treatments against malaria, an infectious disease

caused by the *plasmodium* group of microorganisms.³⁹⁻⁴⁰ A popular subset of these potent natural products are known as the 4-methanolquinolines, which get their group name by a quinoline ring linked to a saturated piperidine bicycle via a β -amino alcohol scaffold (Figure 1-13).³⁹⁻⁴⁰ The classical example of this class would be quinine.³⁹⁻⁴⁰ In addition to its antimalarial activity, quinine's natural optical purity is exploited extensively in organic synthesis as a chiral ligand, phase-transfer catalyst (PTC), and resolution agent for racemic molecules.³⁹⁻⁴⁰

In the 1960s to 1970s, quinine was used as a starting point to find new antimalarial drugs, as quinine-resistance began to emerge in malaria strains.⁴¹ One drug that arose from these efforts was mefloquine, a substituted quinoline ring where the β -amino alcohol is linked to a saturated piperidine ring instead of the complex bicyclic ring observed on quinine.⁴¹ With potent biological activity against the majority of malaria *plasmodiums*, mefloquine is an essential global medicine, however, it is known to have detrimental psychotropic effects, which is a result of one of the two possible *erythro* stereoisomers binding to the adenosine receptor in the CNS.⁴¹ Mefloquine exists on the market as Lariam, a racemic mixture of the *erythro* stereoisomers as acid salts, where the hydroxy and amine FGs of the 1,2-amino alcohol are *anti* to each other (Figure 1-13).⁴¹

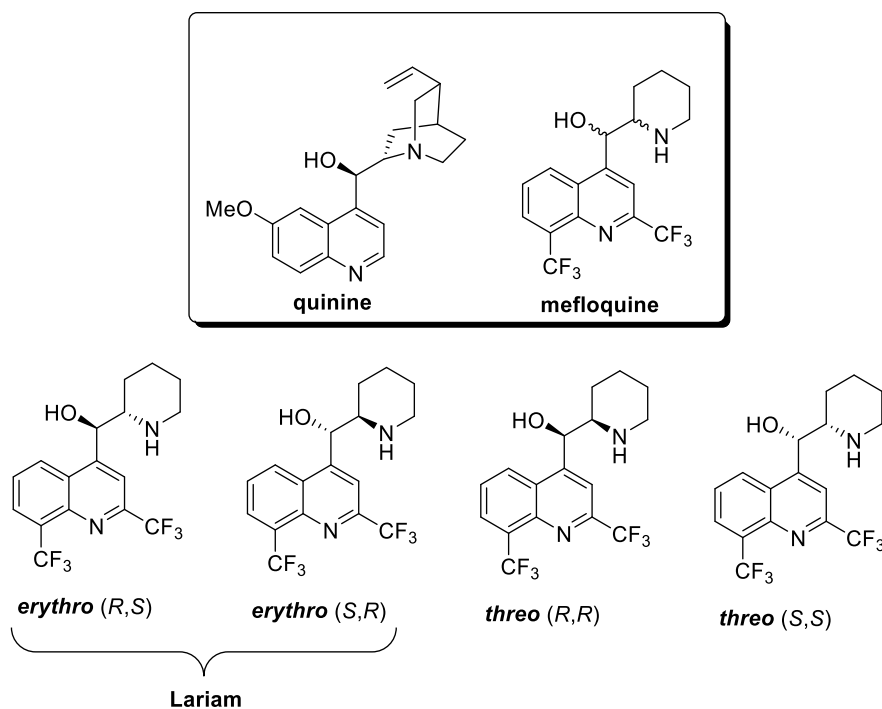
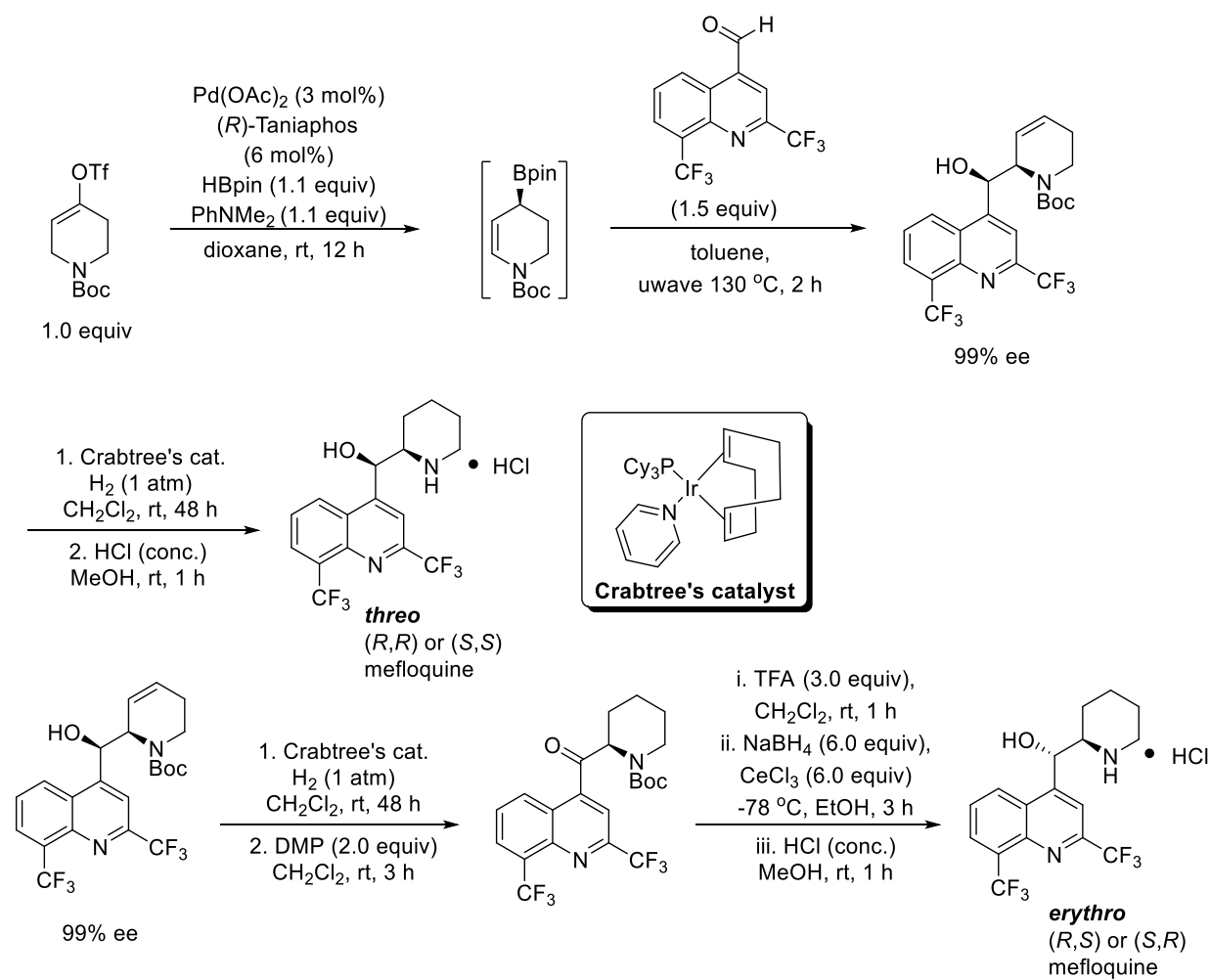


Figure 1-13: Structures of quinine, and mefloquine (top), and all stereoisomers of mefloquine (bottom).⁴¹

All stereoisomers of mefloquine have unique biological activity and half-life, however, the *threo* stereoisomers, where the hydroxy and amine FGs of the 1,2-amino alcohol are *syn* to each other, are not well known or readily accessible without HPLC separation.⁴¹ Due to these limitations to access all stereoisomers of mefloquine, Ding and Hall attempted to synthesize all individual stereoisomers of mefloquine using the above described allylic piperidinyl boronates, and assess their individual biological activities (Scheme 1-3).⁴¹

The synthesis of the *threo* stereoisomers of mefloquine by Ding and Hall began with a borylative migration on the *t*-Boc-protected piperidinyl triflate to obtain the desired allylic piperidinyl boronate, followed by an allylboration with the requisite bis-trifluoromethyl quinoline aldehyde to obtain the β -amino alcohol scaffold.⁴¹ From this dehydro-mefloquine intermediate, a hydroxyl-directed hydrogenation with Crabtree's catalyst, and *t*-Boc deprotection yields the *threo* isomers of mefloquine (Scheme 1-3).⁴¹



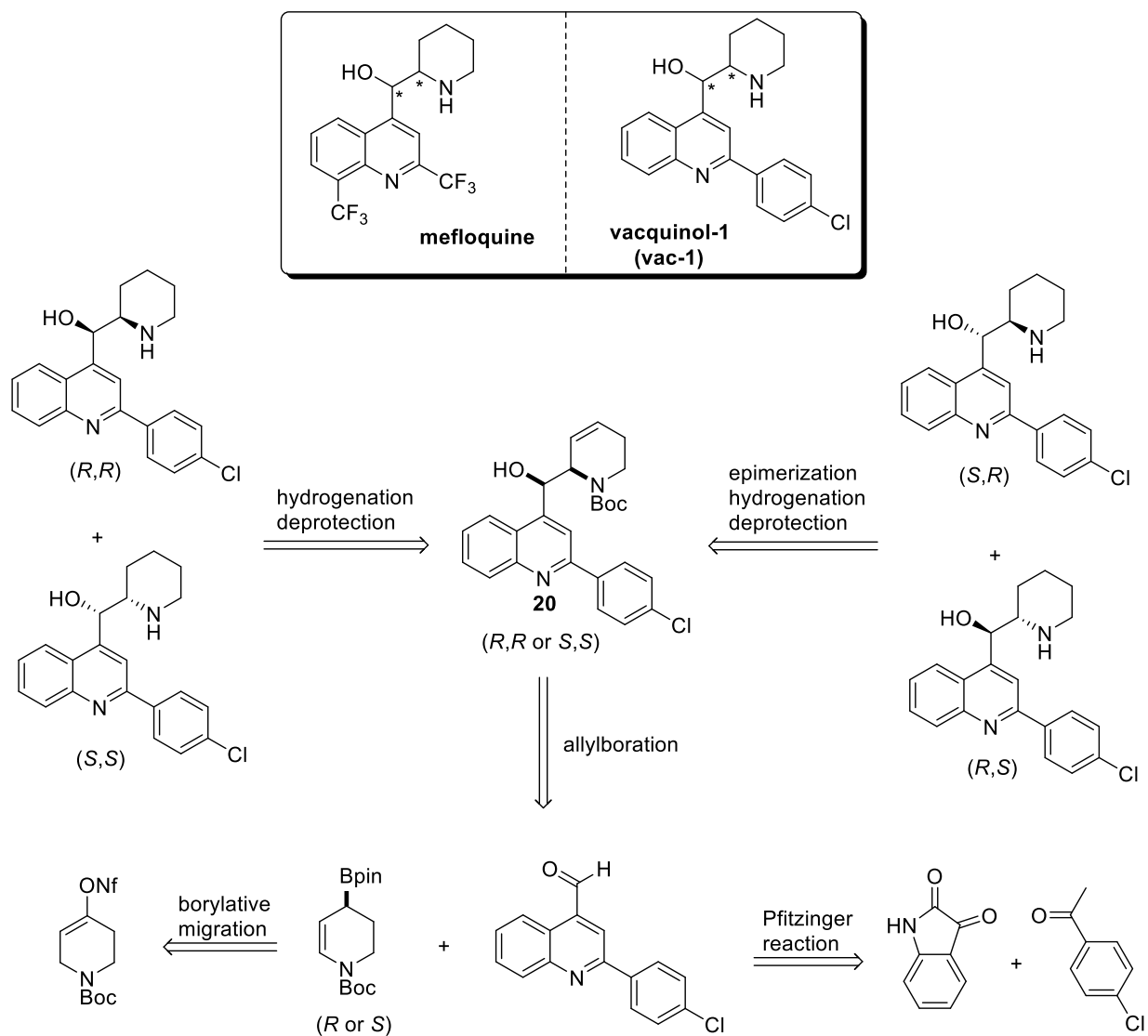
Scheme 1-3: Synthesis of all stereoisomers of mefloquine.⁴¹

To access the *erythro* isomers of mefloquine, the dehydro-mefloquine was hydrogenated and then oxidized with Dess-Martin Periodinane (DMP) to the β -amino ketone.⁴¹ *t*-Boc deprotection and an amine-directed Luche reduction effectively produces the *anti* amino alcohol in high diastereoselectivity via chelation control.⁴¹ Formation of the HCl salt yields mefloquine.⁴¹

With all stereoisomers in hand, as well as two *threo* dehydro-mefloquine analogs, they were tested against *Plasmodium falciparum*.⁴¹ The 3H-Hypoxanthine assay, which measures activity of drugs against *Plasmodium falciparum*, revealed that the (*S,S*) *threo* isomer of mefloquine in addition to its dehydro analog had greater biological activity than the *erythro* isomers used in Lariam!⁴¹ Ding and Hall's success in obtaining all stereoisomers of mefloquine illustrate the power of carbonyl allylboration in accessing the β -amino alcohol scaffold with a chiral allylic piperidinyl boronate.⁴¹ The facile synthesis of the more potent *threo* isomers and dehydro analogs highlight the methodology's ability to repurpose mefloquine, and potentially offers a solution towards the detrimental psychotropic effects observed in Lariam.⁴¹ This study could pave the way towards newer analogs with even greater potency or new activity against other *plasmodium* strains.⁴¹ Encouraged by the medicinal chemistry applications of the allylic piperidinyl boronate, the Hall Group looked to continue applying it to another target with the 1,2-amino alcohol scaffold: vacquinol-1 (vac-1), a drug candidate against glioblastoma multiform (GBM), an aggressive stage IV brain cancer.⁴²⁻⁴³

Vac-1 is a lead compound discovered by Ernfors and co-workers in 2014 through a phenotypic high-throughput screen (HTS) against GBM cells.⁴² With a promising IC₅₀ of 3.1 μ M, encouraging *in vivo* pharmacokinetics (PK), and a groundbreaking nonapoptotic mechanism of GBM cell death, they performed a SAR study on vac-1 and generated several analogs to try to increase potency.⁴² While they were successful in finding some analogs with lower IC₅₀ they did not display favourable PK or showed nonspecific cytotoxicity towards healthy cells.⁴² Thus, vac-1 was considered their lead compound.⁴² However, the synthetic route to vac-1 was a major issue. Vac-1 has a similar scaffold to mefloquine, and was also originally a quinine derivative synthesized as part of the antimalarial drug discovery programs in the 1960s to 1970s.⁴² Structurally, it is a quinoline ring with a 2-(4-chlorophenyl) moiety, and has a β -amino alcohol linked to a saturated piperidine (Scheme 1-4).⁴² The presence of two contiguous stereogenic centres can give rise to four possible stereoisomers (similar to mefloquine), and Ernfors and co-workers synthesized it as a statistical mixture of all isomers. The authors commented that three out

of four isomers were equipotent, but initially had no data to support this claim.⁴² Having access to all stereoisomers is a key factor in repurposing an existing drug, as certain stereoisomers may have less side effects and increased potency. Based on this postulate, Kwok and Hall began a project to synthesize and test all stereoisomers of vac-1 and its dehydro analogs via a borylative migration and allylboration sequence similar to that used for mefloquine.⁴³



Scheme 1-4: Comparison of mefloquine to vac-1 (top), and retrosynthesis of vac-1 (bottom).⁴³

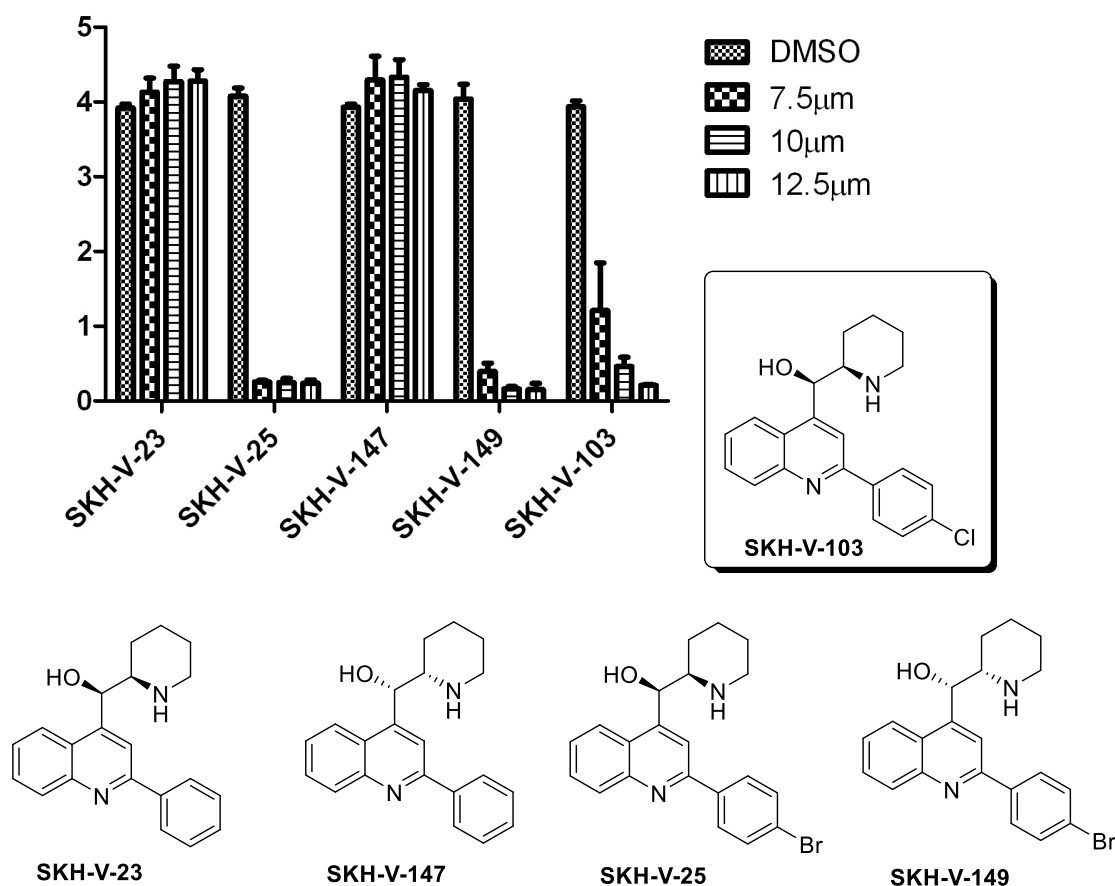
A retrosynthesis of vac-1 can break down the vicinal amino alcohol scaffold into the familiar allylic piperidiny boronate and a disubstituted quinoline aldehyde. The aldehyde can be

prepared via a Pfitzinger reaction, a condensation between an isatin and acetophenone to form a quinoline carboxylic acid.⁴³ The allylboration reaction will establish the dehydro-vac-1 analogs, which can then be hydrogenated and epimerized as necessary to access all stereoisomers of vac-1 and its dehydro analogs (Scheme 1-4).^{41,43} The synthesis of vac-1 proceeded smoothly via this methodology.⁴³

Kwok and Hall, in collaboration with Dr. Roseline Godbout and Dr. Saket Jain from the Department of Oncology from the University of Alberta, tested all stereoisomers of vac-1 and its dehydro analogs against U251 GBM cell lines using an *in vitro* colourimetric assay.⁴³ Surprisingly, Kwok noticed that all stereoisomers of vac-1 were similar in potency at concentrations of 50.0, 30.0, and 15.0 μM , which seemed to confirm Ernfors and co-workers unsubstantiated observation about the equipotency of their vac-1 stereoisomer mixtures.⁴³ Unfortunately, vac-1 deviated from the mefloquine studies in that the dehydro analogs had significantly reduced biological activity against the U251 GBM cells, compared to vac-1.⁴³ As such, the saturated piperidine was deemed to be an essential pharmacophore for the drug candidate.⁴³ Kwok subsequently synthesized a small library of analogs with a variable functional group in the *para* position of the 2-(4-chlorophenyl) moiety to see if this modification could improve the potency.⁴³ A methyl and methoxy group led to attenuated biological activity, as well as replacing the 2-(4-chlorophenyl) group with a 2-phenyl moiety.⁴³ On the other hand, replacing the Cl atom with a Br group slightly increased the activity at 12.5, 10.0 and 7.5 μM (Figure 1-14).⁴³

In parallel with the Hall Group's findings, Ernfors and co-workers later developed a new stereoselective synthesis of vac-1 to study the individual *erythro* and *threo* stereoisomers, as well as making a library of analogs with variable substituted aromatic systems in the 2 position of the quinoline ring.⁴⁴ Despite their intensive SAR analysis, they were unable to find a better analog compared to vac-1.⁴⁴ Later, they would retract a portion of their original claims regarding vac-1's *in vivo* potency and pharmacokinetics, as they were unable to replicate their initial *in vivo* studies showing that vac-1 prolonged the survival of mice with a transplanted GBM tumour.⁴² It is important to note that the poor *in vivo* potency of vac-1 was the only reason that the authors retracted their preliminary findings.⁴² The chemistry used to prepare vac-1, their SAR studies, and their tested biological activity of individual stereoisomers of vac-1 are still valid. This retraction did not deter the Hall Group. A more potent analog of vac-1 may demonstrate better *in vivo* activity and lead to prolonged survival of animals with transplanted GBM tumours, which could revive

this GBM drug candidate. By this reasoning, it was a perfect opportunity to repurpose vac-1 with cyclic chiral boronates by synthesizing a larger library of analogs to expand upon the Br-vac-1 analog.



increased metabolic stability, act as a rigidifying unit to increase binding affinities, and can exist with four possible stereogenic centres, a feature that can help a drug candidate “escape from flatland” and acquire more beneficial physicochemical properties.⁴⁶ As a result of these characteristics, cyclobutanes are becoming increasingly popular in drug discovery programs, which has led to marketed drugs and drug candidates featuring this privileged scaffold, such as carboplatin, (a chemotherapy medication), lobucavir, (an antiviral medication), SB-F1-26, (a fatty acid binding protein (FABPs) inhibitor to treat inflammation), and AEW541, (an inhibitor of the insulin-like growth factor I receptor (IGF-IR), which is implicated in cancer pathogenesis) (Figure 1-15).⁴⁷

Despite their biological prevalence and activity against a variety of diseases, there are limited synthetic methods to access chiral cyclobutanes. These few methodologies can be broken down into [2+2] cycloadditions, cyclization from acyclic substrates, or ring expansions of cyclopropanes (Figure 1-15).⁴⁸ Unfortunately, these routes can suffer from low yields, selectivity issues, as well as a limited number of ways to make the reactions enantioselective.⁴⁸ Another precursor to access cyclobutanes is the cyclobutenone.⁴⁸ Synthetic routes to prepare substituted cyclobutenones are also limited and tend to encompass [2+2] cycloadditions between alkynes, benzyne, and ketenes/keteniminium, intramolecular nucleophilic additions or cross-couplings, and 4π -electrocyclic ring closures.⁴⁹ However, if one is able to saturate the alkene on a cyclobutenone, the remaining ketone can allow for more structural elaboration and utility towards the four possible stereogenic centres on a cyclobutane ring. Asymmetric [2+2] cycloaddition methods to prepare cyclobutenones do exist, but stoichiometric and expensive chiral auxiliaries are required, making it less desirable.⁴⁸ Based on these limitations, the Hall Group in collaboration with Pfizer wanted to develop a new method of preparing enantioenriched cyclobutanes, which they envisioned achieving by generating a chiral cyclobutylboronate through an asymmetric conjugate borylation of cyclobutenone precursors (Figure 1-16). If successful, this new synthetic methodology from borylation chemistry could yield a new class of cyclobutanes which in turn could pave the way for new biological activity and future drug candidates—effectively repurposing this privileged scaffold with boron.

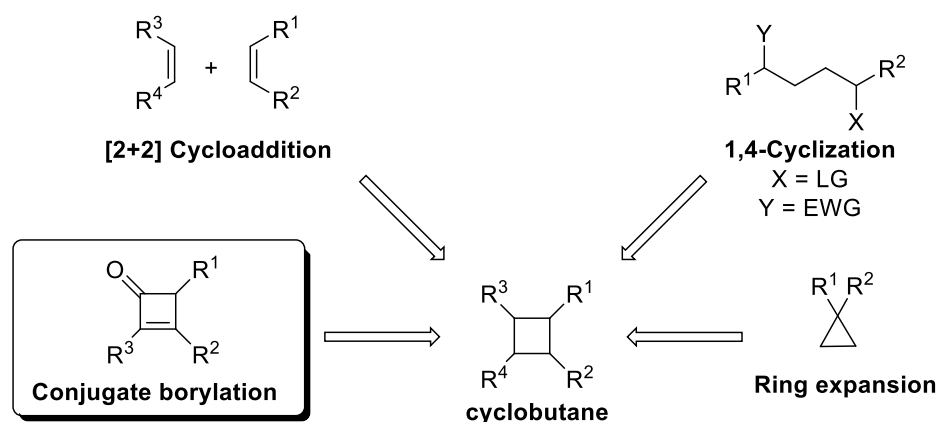
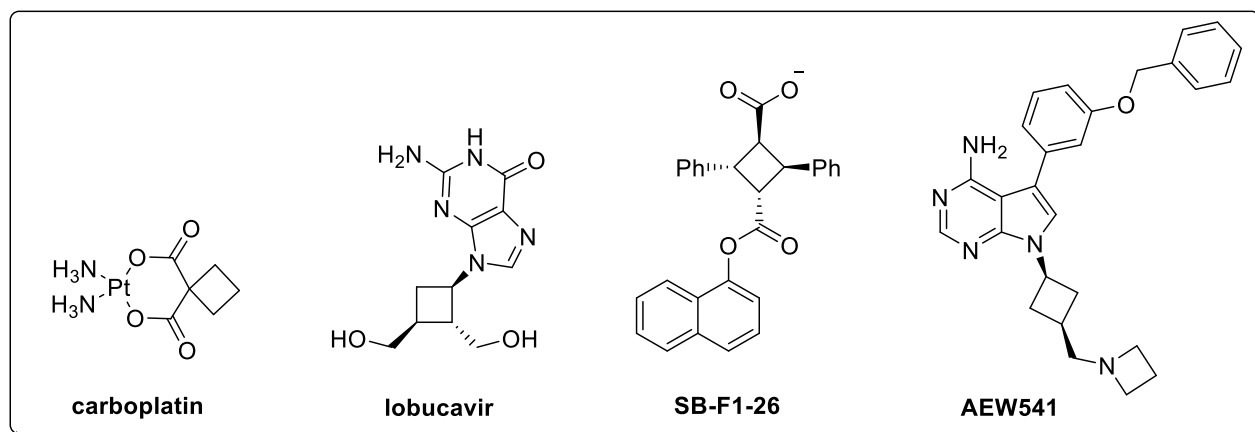
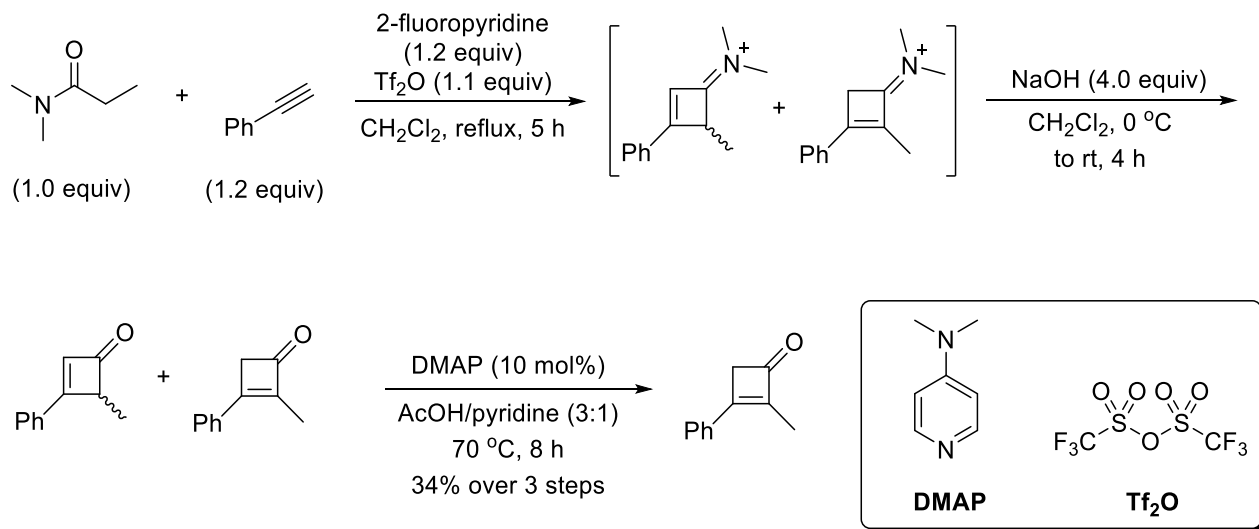


Figure 1-15: Pharmaceuticals containing a cyclobutyl motif, and common synthetic pathways to access polysubstituted cyclobutanes.⁴⁷⁻⁴⁹

1.6 Cyclobutenone Synthesis, and the Preparation of Cyclobutylboronates through Copper-Catalyzed Conjugate Borylation

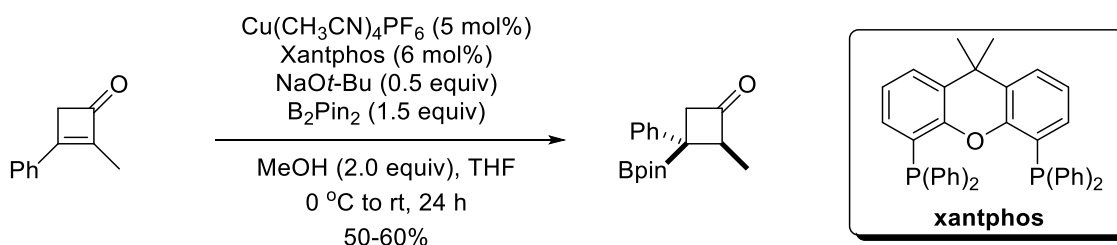
The initial work to develop a reliable synthesis of cyclobutenones was performed by Hall Group members Michele Boghi and Helen Clement in collaboration with Jack C. Lee, Louise Bernier, William Farrell, Neal Sach, Matthew R. Reese, Jotham Coe, and Christopher J. Helal at Pfizer. Boghi opted to employ a traditional [2+2] cycloaddition between an alkyne and a keteniminium generated *in situ* by reacting a tertiary amide with triflic anhydride, and a hindered pyridine base (Scheme 1-5).⁵⁰ The cyclobuteniminium salts were obtained as a regioisomeric mixture, and were then hydrolyzed to the corresponding cyclobutenone using optimized conditions based on work by Ghosez.⁵⁰ Boghi then managed to transform the regioisomeric products to the

more thermodynamically favourable cyclobutenone with a tetrasubstituted alkene by migrating the double bond under moderate acidic conditions, heat, and catalytic DMAP (Scheme 1-5).⁵¹



Scheme 1-5: Synthetic route to cyclobutenones.⁵⁰⁻⁵¹

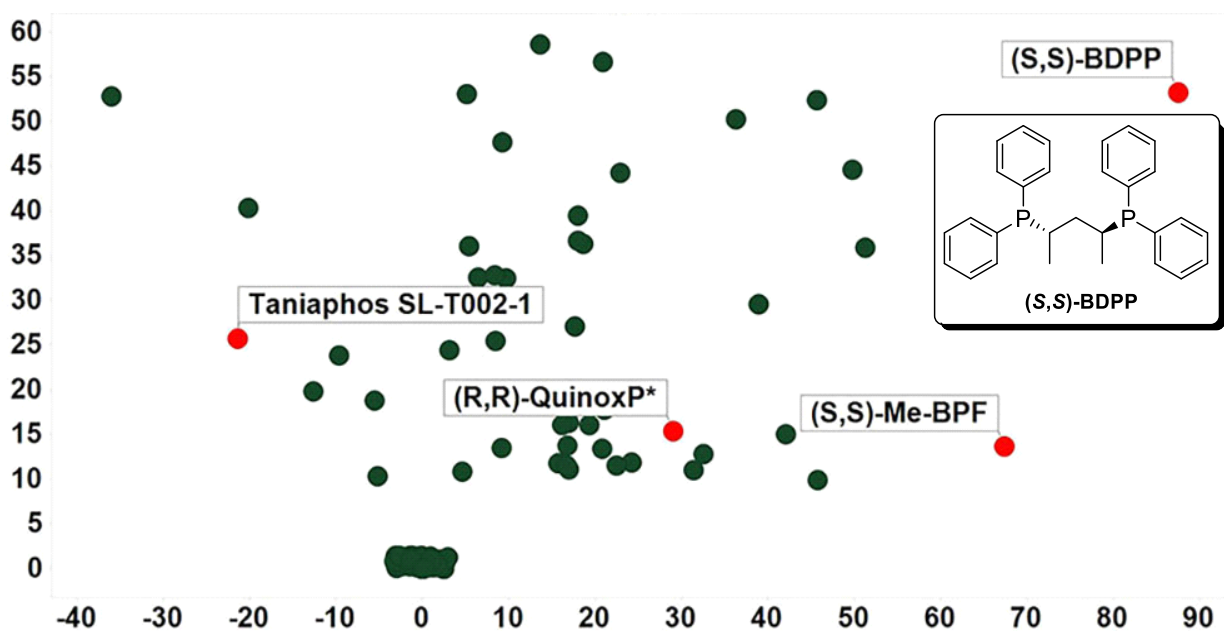
With the desired cyclobutenone regioisomer, Boghi and Clement then developed a racemic conjugate borylation reaction based off existing literature for the conjugate borylation of cyclopentenones (Scheme 1-6).⁵²



Scheme 1-6: Racemic conjugate borylation for the stereoselective preparation of cyclobutylboronates.⁵²

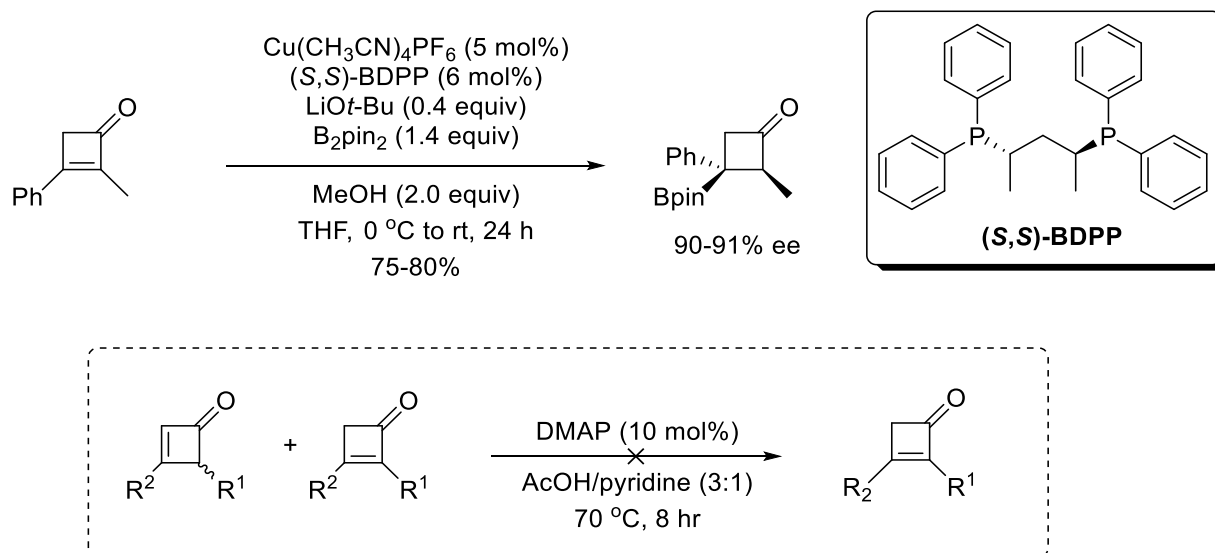
The team at Pfizer acquired the methyl phenyl disubstituted cyclobutenone, and conducted a HTS of 120 chiral ligands to substitute for xantphos in the racemic conjugate borylation conditions in attempts to make the reaction enantioselective. To everyone's delight, when the

(2*S*,4*S*)-2,4-bis(diphenylphosphino)pentane (BDPP) ligand was employed, the reaction gave 55% conversion to the cyclobutylboronate with an excellent 88% ee! (Scheme 1-7).



Scheme 1-7: Pfizer's chiral ligand HTS, with enantiomeric excess on the x-axis and product yield on the y-axis.

Upon further reaction optimization by Clement, it was possible to improve conversion such that the methyl phenyl cyclobutylboronate was obtained in an isolated yield of 75-80% with 90-91% ee (Scheme 1-8). However, there were limitations on an attempted substrate scope for the reaction. Larger alkyl/aryl substituents, and substituted phenyl rings in the α and β position of the cyclobutenone respectively, gave low yields and were difficult to purify after the alkene migration step in the synthetic route. As such, the cyclobutenone preparation needed to be optimized further in order to generate a diverse library of cyclobutylboronates to probe generalities and limitations of this powerful new reaction.



Scheme 1-8: Optimized conjugate borylation conditions (top), and difficult cyclobutenones to synthesize using the current reaction methodology (bottom).

1.7 Thesis Objectives

The application of chiral piperidinyl allylic boronates via allylboration, and the preparation of chiral cyclobutylboronates via conjugate borylation are extremely powerful in accessing privileged scaffolds of interest in medicinal chemistry. Since the methodologies to access these chiral boronates typically give uncommon functionality in the products, it represents the perfect opportunity to diversify and repurpose these scaffolds to improve biological activity and potentially find new targets for disease with these new medicinal compounds. As such, the major goal of this thesis will be to study the chemistry and applications of cyclic chiral boronates to further advance their incredible utility for the purpose of drug discovery and drug repurposing.

To showcase the applications of cyclic chiral boronates, novel analogs of vac-1 will be synthesized via allylboration of allylic piperidinyl boronates, which will be obtained from the catalytic enantioselective borylative migration methodology developed by the Hall Group (Scheme 1-1). The short-term goals of expanding the library of vac-1 analogs will be to increase potency using *in vitro* assays and surpass the biological activity of the Br-vac-1 analog—the strongest compound to date, previously shown by Kwok (Figure 1-14). If this endeavour is successful, then all stereoisomers of the best analog will be prepared and tested, in the hopes that the most powerful stereoisomer could progress to *in vivo* studies. A combination of bioisosteric

replacement, functionalization of the dehydro-piperidine, and scaffold hopping will be implemented on the vac-1 scaffold to accomplish these goals.

To further expand upon the tremendous utility of preparing cyclic chiral boronates to access the privileged cyclobutane scaffold, an optimization of the alkene migration conditions will be conducted to generate a more diverse library of cyclobutenones with improved yield and purity. A variety of transition metal catalyzed conditions will be attempted, as well as milder thermal conditions to migrate the alkene on the cyclobutenone product obtained from the [2+2] cycloaddition. If this first objective is met, then the new cyclobutenones will undergo conjugate borylation reactions to test the scope of this challenging reaction. Initially, the influence of steric and electronic factors will be explored by varying substitution on the phenyl ring, and the nature of the α -substituent on the model cyclobutenone (Scheme 1-7). If these substitutions turn out to be robust, then more challenging substrates will be attempted, such as aromatic heterocycles, or more complex FGs on the phenyl ring.

1.8 References

[1] Blass, B. E. *Basic Principles of Drug Discovery and Development*; Academic Press: San Diego, 2015.

[2] Drews, J. *Science* **2000**, *287*, 1960-1964.

[3] Patrick, G. L. *An Introduction to Medicinal Chemistry 5th Ed*; Oxford University Press: Oxford, 2013.

[4] Bosch, F.; Rosich, L. *Pharmacology* **2008**, *82*, 171-179.

[5] a) Calcaterra, N. E.; Barrow, J. C. *ACS Chem. Neurosci.* **2014**, *5*, 253-260. b) Collins, R.; et al. *Lancet*, **2016**, *388*, 2532-2561. c) Pazuki, G.; Vossoughi, M.; Taghikhani, V. *J. Chem. Eng. Data.* **2010**, *55*, 243-248. d) Browning, R. J.; Reardon, P. J. T.; Parhizkar, M.; Pedley, R. B.; Edirisinghe, M.; Knowles, J. C.; Stride, E. *ACS Nano* **2017**, *11*, 8560-8578. e) Wang, Y-F.; Shi, Q-W.; Dong,

M.; Kiyota, H.; Gu, Y-C.; Cong, B. *Chem. Rev.* **2011**, *111*, 7652-7709. f) Heffron, T. P. *J. Med. Chem.* **2016**, *59*, 10030-10066.

[6] Dugger, S. A.; Platt, A.; Goldstein, D. B. *Nat. Rev. Drug. Discov.* **2018**, *17*, 183-196.

[7] Tufféry, P. *Expert Opin. Drug Discov.* **2015**, *10*, 579-589.

[8] Morrow, J. K.; Tian, L.; Zhang, S. *Critical Reviews™ in Biomedical Engineering* **2010**, *38*, 143-156.

[9] a) Scannell, J. W.; Blanckley, A.; Boldon, H.; Warrinton, B. *Nat. Rev. Drug. Discov.* **2012**, *11*, 191-200. b) Moore, G. E. *Electronics.* **1965**, *38*(8), 1-4.

[10] Abou-Gharbia, M.; Childers, W. E. *J. Med. Chem.* **2014**, *57*, 5525-5553.

[11] U.S. Food & Drug Administration. Generic Drug Facts. <https://www.fda.gov/drugs/resourcesforyou/consumers/buyingusingmedicinesafely/genericdrugs/ucm167991.htm> (accessed March 14, 2019)

[12] Takebe, T.; Imai, R.; Ono, S. *Clin. Transl. Sci.* **2018**, *11*, 597-606.

[13] Bolognesi, M. L. *ACS Med. Chem. Lett.* **2019**, *10*, 273-275.

[14] Proschak, E.; Stark, H.; Merk, D. *J. Med. Chem.* **2019**, *62*, 420-444.

[15] Aubé, J. *ACS Med. Chem. Lett.* **2012**, *3*, 442-444.

[16] Polamreddy, P.; Gattu, N. *Drug Discov. Today* **2018**, *24*, 789-795.

[17] Pushpakom, S.; et al. *Nat. Rev. Drug. Discov.* **2019**, *18*, 41-58.

- [18] a) Brown, D. G.; Boström, J. *J. Med. Chem.* **2018**, *61*, 9442-9468. b) Valeur, E.; Jimonet, P. *J. Med. Chem.* **2018**, *61*, 9004-9029.
- [19] a) Hall, D. G. *Boronic Acids: Preparation and Applications in Organic Synthesis, Medicine, and Materials*, 1&2, 2nd Ed; Wiley-VCH Verlag & Co. KGaA: Weinheim, 2011. b) Ban, H. S.; Nakamura, H. *Chem. Rec.* **2015**, *15*, 616-635. c) Yang, W.; Gao, X.; Wang, B. *Med. Res. Rev.* **2003**, *23*, 346-368.
- [20] Leśnikowski, Z. *J. Expert Opin. Drug Discov.* **2016**, *11*, 569-578.
- [21] Brooks, W. L. A.; Sumerlin, B. S. *Chem. Rev.* **2016**, *116*, 1375-1397.
- [22] Whyte, G. F.; Vilar, R.; Woscholski, R. *J. Chem. Biol.* **2013**, *6*, 161-174.
- [23] a) Meanwell, N. A. *J. Med. Chem.* **2011**, *54*, 2529-2591. b) Seddon, M. P.; Cosgrove, D. A.; Gillet, V. J. *ChemMedChem* **2018**, *13*, 607-613.
- [24] Ballatore, C.; Huryn, D. M.; III, Smith, A. B. *ChemMedChem* **2013**, *8*, 385-395.
- [25] Maynard, A.; and et al. *J. Med. Chem.* **2014**, *57*, 1902-1913.
- [26] Yang, F.; Zhu, M.; Zhang, J.; Zhou, H. *Med. Chem. Commun.* **2018**, *9*, 201-211.
- [27] Vshyvenko, S.; Clapson, M. L.; Suzuki, I.; Hall, D. G. *ACS Med. Chem. Lett.* **2016**, *7*, 1097-1101.
- [28] a) Adamczyk-Woźniak, A.; Borys, K. M.; Sporzyński, A. *Chem. Rev.* **2015**, *115*, 5224-5247. b) Liu, C. T.; Tomsho, J. W.; Benkovic, S. J. *Bioorg. Med. Chem.* **2014**, *22*, 4462-4473. c) Baker, S. J.; Tomsho, J. W.; Benkovic, S. J. *Chem. Soc. Rev.* **2011**, *40*, 4279-4285. d) Dowlut, M.; Hall, D. G. *J. Am. Chem. Soc.* **2006**, *128*, 4226-4227.

- [29] Mereddy, G. R.; Chakradhar, A.; Rutkoski, R. M.; Jonnalagadda, S. C. *J. Organomet. Chem.* **2018**, *865*, 12-22.
- [30] a) Sehl, T.; Maugeri, Z.; Rother, D. *J. Mol. Catal. B. Enzym.* **2015**, *114*, 65-71. b) Karjalainen, O. K.; Koskinen, A. M. P. *Org. Biomol. Chem.* **2012**, *10*, 4311-4326. c) Burchak, O. N.; Py, S. *Tetrahedron.* **2009**, *65*, 7333-7356. d) Lee, H-S.; Kang, S. H. *Synlett.* **2004**, *10*, 1673-1685. e) Bergmeier, S. C. *Tetrahedron* **2000**, *56*, 2561-2576.
- [31] Calleja, P.; Ernst, M.; Hashmi, A. S. K.; Schaub, T. *Chem. Eur. J.* **2019**, 10.1002/chem.201900531.
- [32] Li, X.; Hall, D. G. *Angew. Chem. Int. Ed.* **2018**, *57*, 10304-10308.
- [33] a) Lachance, H.; Hall, D. G. *Org. React.* **2009**, *73*, 1-341. b) Hall, D. G.; Lee, J. C. H.; Ding, J. *Pure Appl. Chem.*, **2012**, *84*, 2263–2277.
- [34] a) Panda, S.; Coffin, A.; Nguyen, Q. N.; Tantillo, D. J.; Ready, J. M. *Angew. Chem. Int. Ed.* **2016**, *55*, 2205–2209. b) Hoffmann, R. W.; Brückner, D. *New. J. Chem.* **2001**, *25*, 369-373.
- [35] Murata, M.; Oyama, T.; Watanabe, S.; Masuda, Y. *Synthesis* **2000**, *6*, 778-780.
- [36] a) Kim, Y-R.; Hall, D. G. *Org. Biomol. Chem.* **2016**, *14*, 4739-4748. b) Lessard, S.; Peng, F.; Hall, D. G. *J. Am. Chem. Soc.* **2009**, *131*, 9612-9613.
- [37] Vitaku, E.; Smith, D. T.; Njardarson, J. T. *J. Med. Chem.* **2014**, *57*, 10257-10274.
- [38] Ding, J.; Rybak, T.; Hall, D. G. *Nat. Commun.* **2014**, *5*, 5474-5472.
- [39] Bräse, S. *Privileged Scaffolds in Medicinal Chemistry: Design, Synthesis, Evaluation*; The Royal Society of Chemistry: Cambridge, 2016.

- [40] Ramawat, K. G.; Mérillon, J. M. *Natural Products: Phytochemistry, Botany, and Metabolism of Alkaloids, Phenolics and Terpenes*; Springer-Verlag Berlin: Heidelberg, 2013.
- [41] Ding, J.; Hall, D. G. *Angew. Chem. Int. Ed.* **2013**, *52*, 8069-8073.
- [42] Kitambi, S. S.; et al. *Cell* **2014**, *157*, 313–328.
- [43] Kwok, S. Application and Substrate Scope Expansion of a Unique Borylative Migration Transformation. M.Sc. Thesis, The University of Alberta, 2016.
- [44] Hammarström, L. G. J.; et al. *J. Med. Chem.* **2016**, *59*, 8577-8592.
- [45] Dembitsky, V. M. *Phytomedicine* **2014**, *21*, 1559–1581.
- [46] a) Meanwell, N. A. *Chem. Res. Toxicol.* **2016**, *29*, 564–616. b) Hazelard, D.; Compain, P. *Org. Biomol. Chem.* **2017**, *15*, 3806–3827. c) Johnson, J. W.; et al. *J. Org. Chem.* **2008**, *73*, 6970–6982. d) Kuchar, M.; Mamat, C. *Molecules* **2015**, *20*, 16186-16220. e) Wroblewski, M. L.; et al. *Bioorg. Med. Chem. Lett.* **2006**, *16*, 3859–3863. f) Lovering, F.; Bikker, J.; Humblet, C. *J. Med. Chem.* **2009**, *52*, 6752–6756.
- [47] a) Oun, R.; Moussa, Y. E.; Wheate, N. J. *Dalton Trans.* **2018**, *47*, 6645-6653. b) Pager, V. V.; RajanBabu, T. V. *Science* **2018**, *361*, 68-72. c) Berger, W. T.; et al. *PLOS ONE*. **2012**, *7*, e50968. d) Slade, J.; et al. *Org. Process Res. Dev.* **2007**, *11*, 825-835.
- [48] a) Lee-Ruff, E. *Synthesis of Cyclobutanes. PATAI'S Chemistry of Functional Groups*, Rappoport, Z. (Ed.); John Wiley & Sons, Ltd: 2009, doi:10.1002/9780470682531.pat0322. b) Lee-Ruff, E.; Mladenova, G. *Chem. Rev.* **2003**, *103*, 1449-1484.
- [49] Chen, P-h.; Dong, G. *Chem. Eur. J.* **2016**, *22*, 18290-18315.

[50] a) Lumbroso, A.; Catak, S.; Sulzer-Mossé, S.; Mesmaeker, A. D. *Tetrahedron Lett.* **2015**, *56*, 2397–2401. b) Falmagne, J-B.; Escudero, J.; Taleb-Sahraoui, S.; Ghosez, L. *Angew. Chem. Int. Ed.* **1981**, *20*, 879–880.

[51] Danheiser, R. L.; Savariar, S. *Tetrahedron. Lett.* **1987**, *28*, 3299-3302.

[52] Fernández, E.; Whiting, A. *Synthesis and Application of Organoboron Compounds*; Springer International Publishing: Switzerland, 2015.

Chapter 2: Application of Allylic Piperidinyl Chiral Boronates towards the Synthesis of Novel Vacquinol-1 Analogs, a Potential Drug Candidate for Glioblastoma Multiforme

2.1 Glioblastoma multiforme: Prevalence, Characteristics, Genetics, and Outlook

Glioblastoma multiforme (GBM) is an extremely invasive, migratory brain cancer that affects between 2-3 adults per 100,000 in a given population.¹ This cancer is typically divided into two categories: primary and secondary.² Primary GBM is classified as a *de novo* tumour, which means it arises without any clinical or histological evidence prior to diagnosis, and makes up 90% of all cases.²⁻³ The remaining 10% of cases occur when a less threatening diffuse or anaplastic astrocytoma is upgraded into a more aggressive form; this is called a secondary GBM.²⁻³ Primary GBM is classified as a grade IV tumour. Grade IV tumours are fast growing, easily spreadable to many areas of the brain, and have the capacity to make new blood vessels via angiogenesis, which all contribute towards an indefinite aberrant growth.³⁻⁴ Depending on the astrocytoma, secondary GBM can range from a slower growing recurrent grade II tumour, or a lower malignancy less vascularized grade III tumour, both of which can upgrade to IV over time.²⁻⁴ Making up 15% of all primary intracranial tumours, GBM is an incredibly prolific, formidable cancer affecting society.⁵⁻⁶

Structurally, there are three main classifications of GBM: 1) small cell glioblastoma, 2) glioblastoma with oligodendrocomponent, and 3) glioneuronal tumor with neuropil-like islands.⁷ Each subtype of GBM is made from a combination of different glial cells, a plethora of histopathological characteristics, and unique patterns of gene expression.⁷⁻¹⁰ The gene expression of GBM alone can give rise to four more additional subtypes: proneural, neural, classical, and mesenchymal.⁷⁻¹⁰ The morphology of GBM can be made up of any combination of nuclear atypia, mitotic activity, vascular thrombosis, microvascular proliferation, and large areas of necrosis in the centre of the tumour or in nearby cells.^{3,11} These characteristics give the cancer a heterogeneity, and its “multiforme” namesake.¹²

Given the location, physical permutations, and genetic factors of GBM, this makes treatment extraordinarily difficult. The standard treatment for GBM is surgical resection, followed

by radiotherapy, and oral temozolomide (TMZ) chemotherapy.¹³ TMZ is a prodrug that forms the active imidazole-4-carboximide (MTIC) *in vivo*. MTIC damages GBM cells by alkylating the DNA, and promoting apoptosis (Figure 2-1). But, this series of treatments is limited, as one can only employ surgery if the tumour is localized in an area of the brain that is safe to operate on, and any GBM cells in a hypoxic (oxygen-lacking) environment are highly resistant to radiotherapy.³

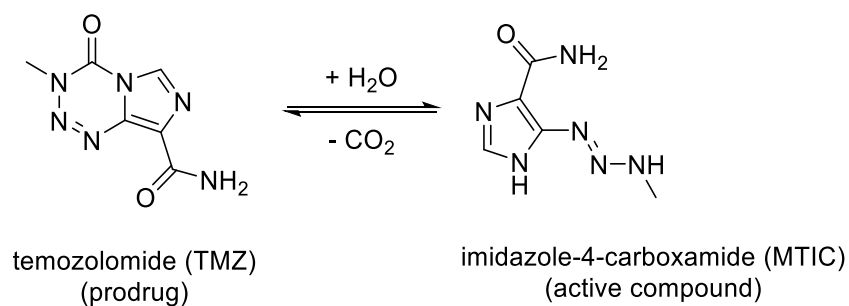


Figure 2-1: Chemical structure of temozolomide and its active MTIC form.¹³

TMZ is also rarely effective, as GBM has numerous biological mechanisms of resistance.¹³ One such mechanism are DNA repair pathways through the O⁶-methylguanine DNA methyltransferase (MGMT). Other methods of overcoming TMZ is through overexpression of oncogenes like epidermal growth factor receptor (EGFR), galectin-1, and murine double minute 2 (Mdm2). GBM can also mutate p53, which prevents its tumour suppression capabilities. Even if TMZ somehow gets through these biological redundancies, GBM still has another trick up its sleeve: a population of cancer stem cells (CSCs). CSCs are highly quiescent towards most treatments—typically lying dormant, and then once treatment has ended, they begin growing a new (and more resistant) population of GBM cancer cells. The fallibility of current treatments, combined with the tenacity of GBM gives a miserable prognosis for the disease. Patients typically only have a median survival rate of 14.6 months, and <10% of patients survive 5 years.¹⁴ Thus, new and more efficient treatments are desperately required for this terrifying brain cancer.

2.2 A High-Throughput Screen (HTS) with Beneficial Modifications: The Discovery of Vacquinol-1

In attempts to discover new treatments against GBM, Patrik Ernfors and co-workers performed a high-throughput screen (HTS) using 1,364 compounds from the National Institutes of Health (NIH) with the goal of bypassing resistance mechanisms in GBM.¹⁵ A traditional HTS typically uses between 100 to 1,000,000 compounds from in-house chemical libraries of pharmaceutical companies, or diversity sets from other organizations.¹⁶ These libraries are tested via an *in vitro* biological assay containing the biological target of interest—typically a receptor, enzyme, or cell line. This screening typically leads to a subset of compounds from the libraries that are weakly or strongly binding to the target of interest, and are termed *hits*. The hits of the screen will then undergo additional screening to maximize the potency against the target. Afterwards, lengthy cross-validation procedures of follow-up *in vitro* and *in vivo* assays are conducted.¹⁶⁻¹⁷ These rigorous tests help determine if any of the results were false positives, or have dangerous chemical scaffolds that can interfere with the assay efficacy—known as Pan-Assay Interference Compounds (PAINS).¹⁶⁻¹⁷ In addition, one also examines if the drug compounds effect other extant family members of the biological target, Cytochrome P450, transporters, or the hERG Channel, because these off-target effects can lead to toxicity, drug-drug interactions, or fatal heart arrhythmias respectively.¹⁶⁻¹⁷ If one is lucky, a group of hits from these rigorous follow-ups avoids all the pitfalls, and now optimization can begin to turn the hits into *leads*.¹⁸ Unfortunately, there are times where the compounds do not even make it past validation to develop a lead compound. In preparation for this reality, Ernfors and co-workers used alternative validation strategies to streamline their HTS, and avoid some of the common pitfalls.

Rather than focusing on a biological target, Ernfors and co-workers opted to target the phenotypes of GBM cells—specifically looking for cellular processes to exploit when treating the cells with the compounds during the HTS.^{15,19} In addition, the authors also used primary cultures derived from patients with GBM, rather than a serum-based GBM cell line, which are thought to not be as phenotypically or genotypically representative of the brain cancer.^{15,19-20} Employing this strategy against the more representative primary GBM cultures generated 234 hits. Instead of focusing on potency, they instead turned their attention towards toxicity, and followed up the hits by screening against seven more patient-derived GBM cultures, and counter-screening the hits

against healthy mouse embryonic stem cells, human fibroblasts, and an *in vivo* assay using a zebrafish GBM model.^{15,19} The culmination of this rigorous and elegant HTS led to the discovery of the GBM drug candidate vacquinol-1 (vac-1), a name partly derived from its quinoline and β -amino alcohol scaffolds, as seen in Chapter 1.

2.3 Overview of Vacquinol-1

While the use of vac-1 against GBM here is novel, its earlier discovery and pharmaceutical applications differed significantly. Vac-1 was originally synthesized as part of a series of exuberant investigations into more potent derivatives of the quinine and chloroquine antimalarials, in response to a worldwide rise in resistance from the 1950s and 1970s.²¹⁻²² This library of compounds employing the vac-1 scaffold would contribute towards the discovery and marketing of the antimalarial drug mefloquine, simply by replacing the 2-phenyl moiety with a CF_3 substituent, in addition to another CF_3 in position 8 of the quinoline ring (Figure 2-2).²²⁻²³

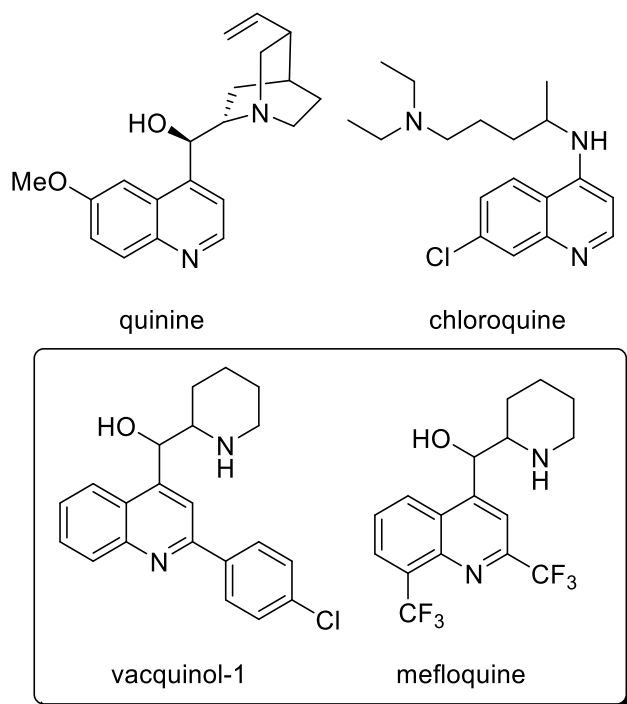


Figure 2-2: A comparison of early antimalarials that inspired the analog scaffolds of vacquinol-1 and mefloquine.²¹⁻²³

A few additional analogs to the vac-1 scaffold (Figure 2-3) have been synthesized and applied towards inhibitors of biofilm infections associated with *Vibrio cholerae*, a gram-negative bacteria that causes cholera, as well as inhibitors of inositol-5'-phosphatase 1 (SHIP1) and SHIP2, which are enzymes hypothesized to be proto-oncogenes.²⁴⁻²⁵ The incredible diversity of vac-1 scaffold's biological activity merits their investigation for the treatment of challenging targets like GBM

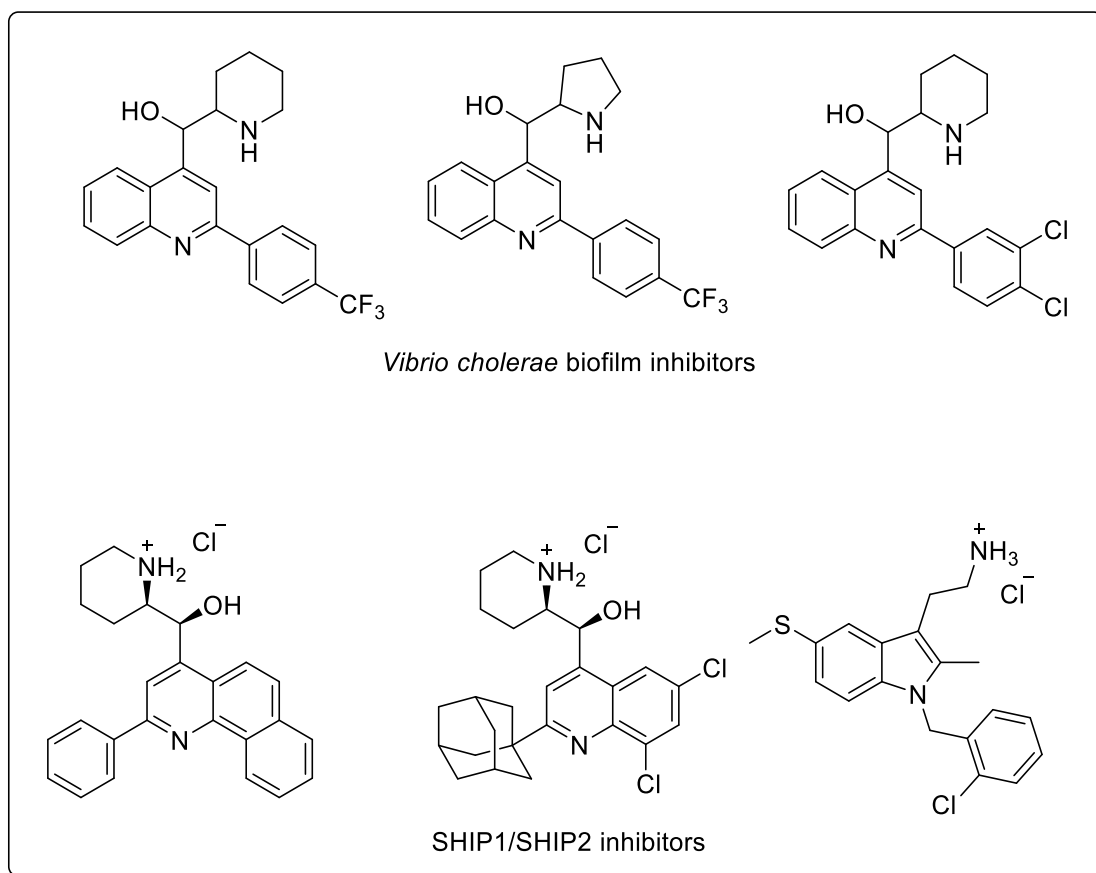


Figure 2-3: Analogs of the vacquinol-1 scaffold towards other pharmaceutical applications.²⁴⁻²⁵

2.3.1 Stereoisomers, and Biological Activity of Vac-1

Similar to mefloquine outlined in Chapter 1, vac-1 has two contiguous stereogenic centres within the β -amino alcohol, giving four potential stereoisomers (Figure 2-4).²⁶ These four stereoisomers can be divided into two groups: 1) *threo*, where the hydroxyl and amine functional groups are *syn*, and 2) *erythro*, where the hydroxyl and amine functional groups are *anti*.²⁶ After

its discovery from the HTS, Ernfors and co-workers determined the half maximal inhibitory concentration (IC_{50}) of vac-1 to be approximately 3.14 μM against GBM cells.¹⁵ It is important to note that this IC_{50} determination of vac-1 represents a statistical mixture of all possible stereoisomers.¹⁵

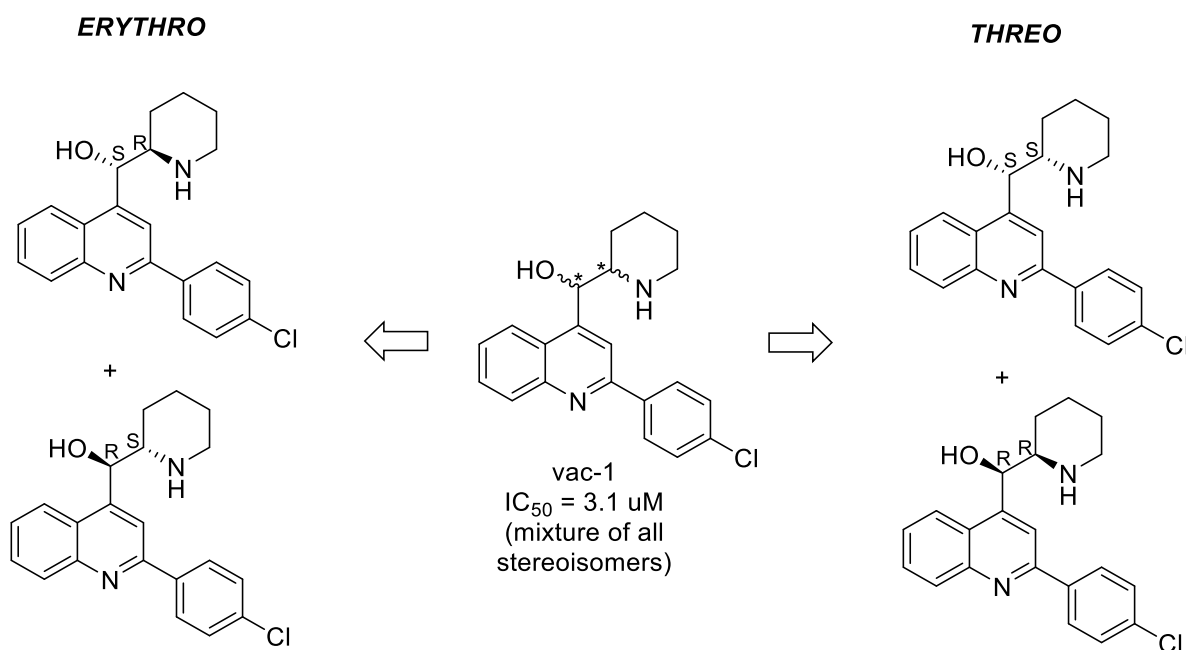


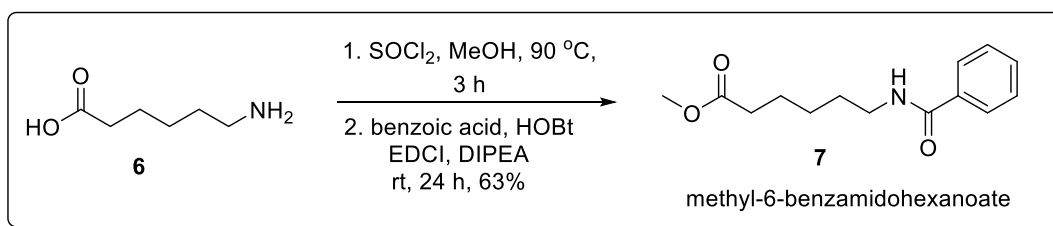
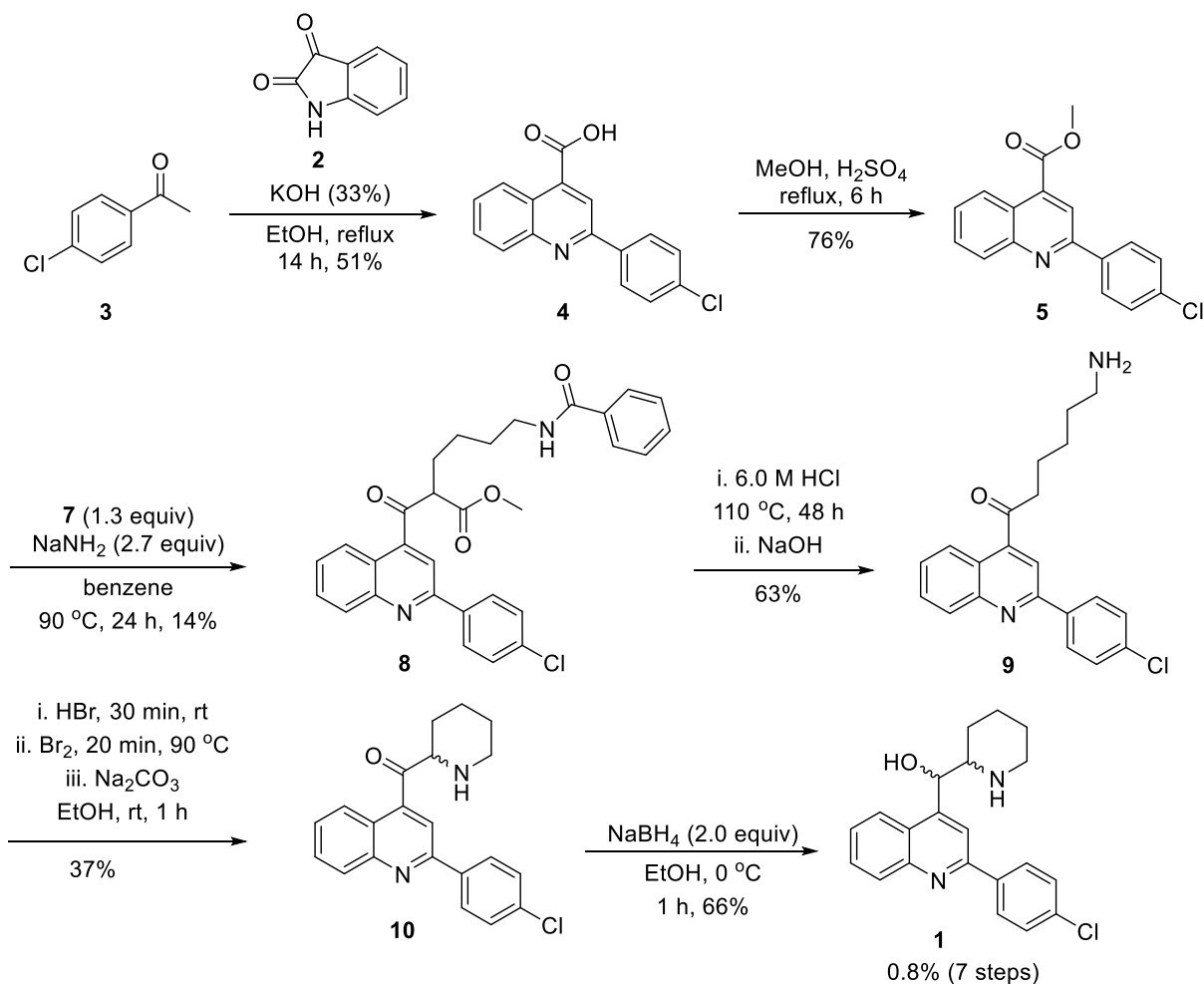
Figure 2-4: Biological activity of vac-1, and its four possible stereoisomers.^{15,26}

With the promising IC_{50} in hand, Ernfors and co-workers embarked on probing the structure-activity relationship (SAR) of vac-1 via a non-stereoselective synthesis to generate a library of analogs (Scheme 2-1).

2.3.2 Non-stereoselective synthesis of Vacquinol-1 Analogs, and SAR

The synthesis of vac-1 analogs begins with a Pfitzinger reaction on **2** and **3** to establish the 2,4-disubstituted quinoline scaffold.²⁷⁻²⁸ Intermediate **4** is then subjected to a Fischer esterification to obtain the methyl ester **5**, which undergoes a Claisen condensation with dicarbonyl **7** to form the tricarbonyl intermediate **8**.²⁷ A tandem saponification, decarboxylation, and Hofmann

rearrangement on **8**, gives ketone **9**.^{27,29} α -bromination and intramolecular displacement on **9** forms the 1,2-amino ketone **10**, and carbonyl reduction yields vac-1 (**1**) and related analogs.²⁷

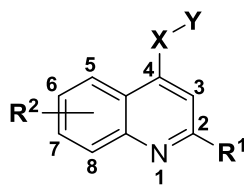


Scheme 2-1: Non-stereoselective synthesis of vac-1 for a preliminary SAR study.²

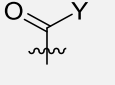
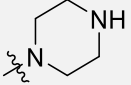
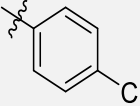
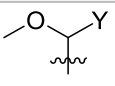
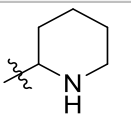
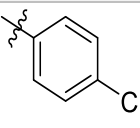
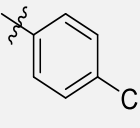
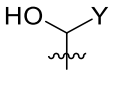
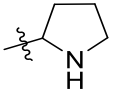
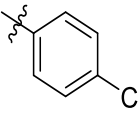
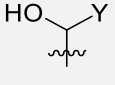
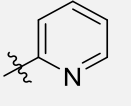
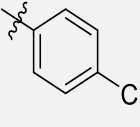
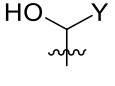
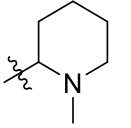
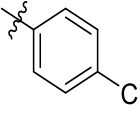
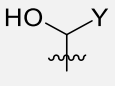
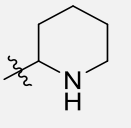
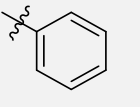
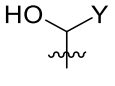
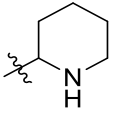
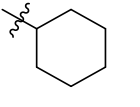
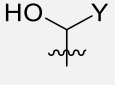
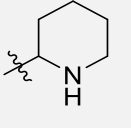
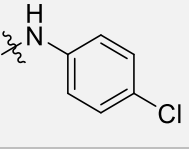
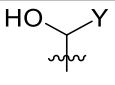
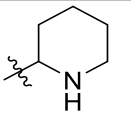
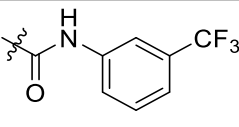
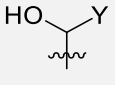
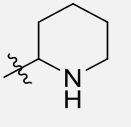
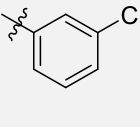
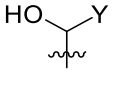
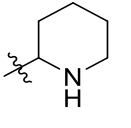
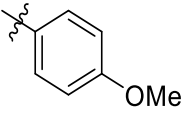
The SAR analysis of vac-1 and its analogs can roughly be broken down into four categories: 1) the hydroxyl group, 2) the piperidine ring, 3) quinoline substitutions, and 4) substitutions on or

modifications to the 2-(4-chlorophenyl) moiety (Table 2-1).^{15,27} It is important to note that the “NSC” designations for Table 2-1 are compounds from the NIH diversity set from the HTS, and that the “CBK” designations are analogs of vac-1 derived from Scheme 2-1.^{15,27}

In terms of the 1,2-amino alcohol pharmacophore, not much is tolerated. Changing the piperidine to a pyrrolidine, alkylating the amine, substituting to a pyridine, or eliminating the scaffold all reduce biological activity (entries 5-8). Switching to a ketone or amide moiety also eliminates potency (entries 2-3), although interestingly, a methyl ether instead of a hydroxy group is tolerated (entry 4). The 2-(4-chlorophenyl) moiety is also a fairly sensitive pharmacophore as entries 9-10, 14 hamper the biological activity. Interestingly, moving the chloride to the *meta* position, and changing to a 4-aminochlorobenzyl group, improve the IC₅₀ (entries 11, 13). Since two structural changes have occurred for entry 11, assessing the improvement in IC₅₀ is difficult. It is unclear whether the amine of the 4-aminochlorobenzyl group is the beneficial substituent, or if the methyl group on C6 of the quinoline is an example of a *magic methyl effect* contributing to increased potency.³⁰ Next, a 2-amido(3-trifluorophenyl) moiety completely loses activity, although this could be a result of the *meta* trifluoromethyl instead of a *para* chloride, or the trifluoromethyl group on C8 of the quinoline (entry 12). The last entries (15-17) all deal with substitutions on C6-C8 of the quinoline ring that lead to improved activity. The best compound of these entries is 15, a phenyl ring fused to C7-C8 of the quinoline.



Entry	X	Y	R ¹	R ²	IC ₅₀ (μM)
1(vac-1/NSC13316)				H (C3, C5-C8)	3.14 ± 1.23
2 (CBK277829)				H (C3, C5-C8)	> 50

3 (CBK277823)				H (C3, C5-C8)	> 50
4 (CBK277851)				H (C3, C5-C8)	3.62 ± 1.44
5 (CBK277855)		N/A		H (C3, C5-C8)	> 50
6 (CBK277828)				H (C3, C5-C8)	8.32 ± 1.36
7 (CBK277826)				H (C3, C5-C8)	> 50
8 (CBK277852)				H (C3, C5-C8)	> 25
9 (CBK277857)				H (C3, C5-C8)	> 25
10 (NSC13466)				H (C3, C5-C8)	12.7 ± 4.3
11 (NSC157571)				H (C3, C5, C7-C8) CH ₃ (C6)	0.71 ± 0.21
12 (NSC146028)				H (C3, C5, C6-C7) CF ₃ (C8)	> 50
13 (NSC14224)				H (C3, C5-C8)	2.13 ± 0.87
14 (NSC23925)				H (C3, C5-C8)	7.59 ± 2.65

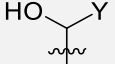
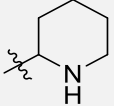
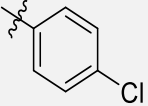
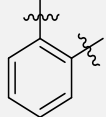
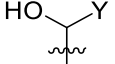
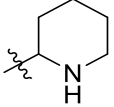
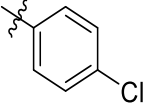
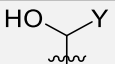
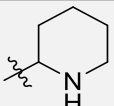
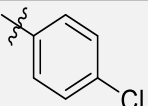
15 (NSC13480)				 (C7-C8) H (C3, C5-C6)	0.39 ± 0.12
16 (NSC305758)				Cl (C6, C8) H (C3, C5, C7)	1.10 ± 0.87
17 (NSC4377)				Cl (C8) H (C3, C5-C7)	1.03 ± 0.73

Table 2-1: Preliminary SAR of vac-1, based on synthesized analogs, and hits from the NIH diversity set.¹⁵

The last few alterations to vac-1 were scaffold hops. These changes proved to be fruitless, as the biological activity was lost completely in all cases (Figure 2-5). Based on the collective results of hit optimization, it is clear that the quinoline and 2-(4-chlorophenyl) scaffold unit are essential towards biological activity.

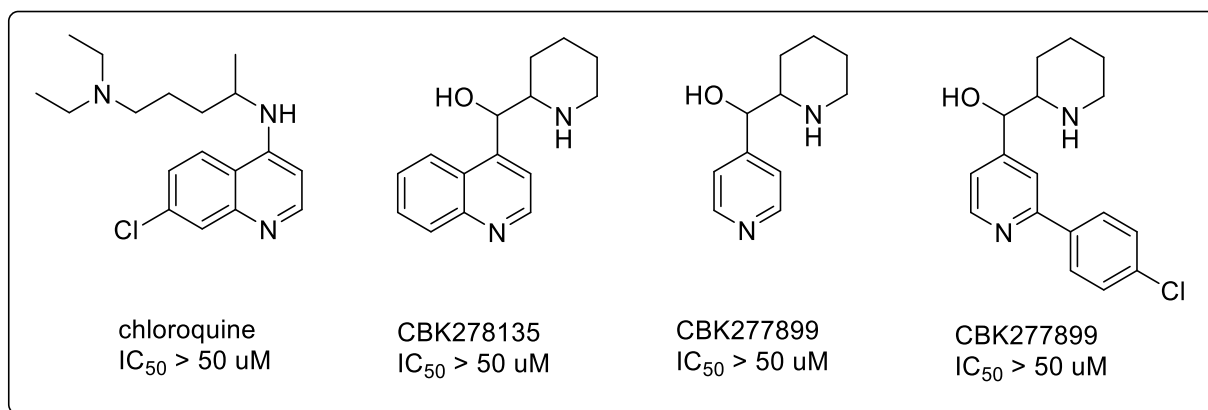


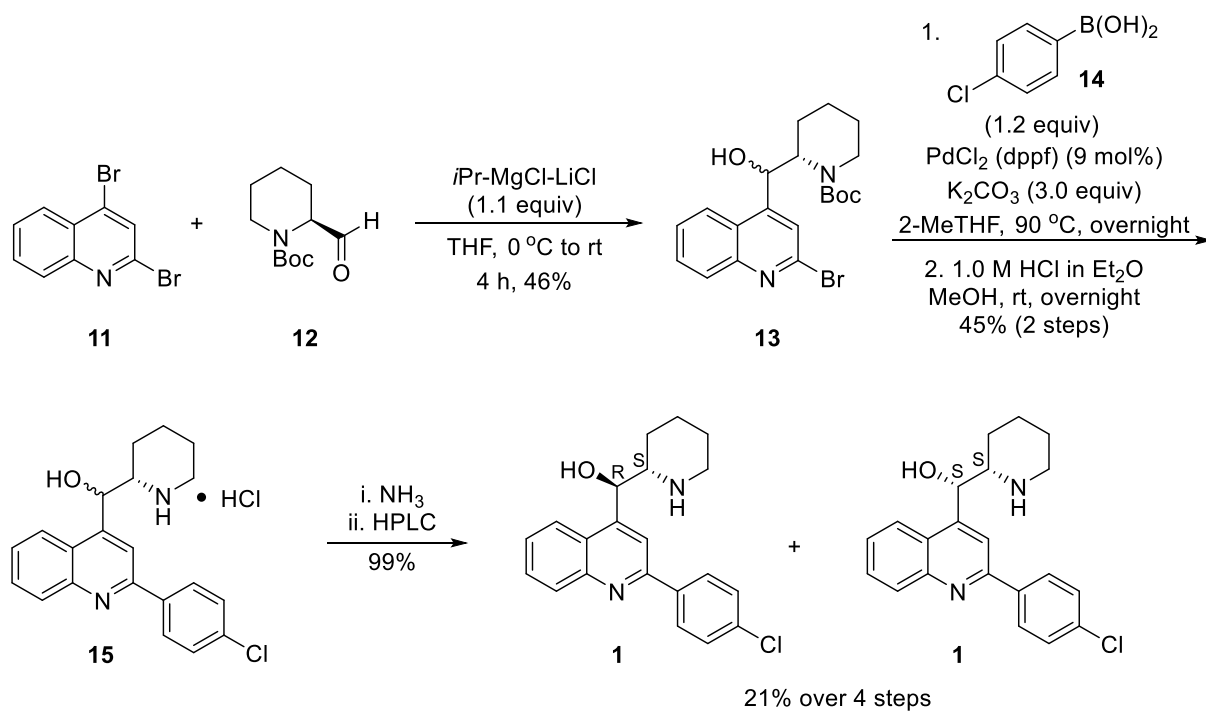
Figure 2-5: Scaffold hopping analogs of vac-1.¹⁵

Entries 11, 13, and 15-17 in Table 2-1 demonstrated greater potency compared to **1** *in vitro*, but were not selected for further optimization due to non-specific cytotoxicity effects, or because they were less effective at reducing GBM tumours for the *in vivo* zebrafish GBM models.¹⁵ Based

on this SAR study, the authors focused on optimizing **1** further by altering the 2(4-chlorophenyl) group, as well as developing a stereoselective synthesis to access all stereoisomers in order to determine if one isomer had more potency and efficiency *in vivo* compared to others.

2.3.3 Stereoselective Synthesis of Vac-1

In the early stages of hit-to-lead optimization, it is quite common to get a sense of potency, in relation to the SAR, by synthesizing chiral drug candidates as racemates or mixtures of diastereomers for testing with *in vitro* assays. Once one is ready to initiate clinical studies with the best drug candidate, it is imperative that all stereoisomers of the compound be assessed individually, because there is a plethora of literature that shows how enantioenriched chiral drugs are more likely to have higher biological activity, less toxicity and side-effects, higher FDA approval rates, and market success.³¹ As such, a stereoselective synthesis was developed by Ernfors and co-workers using an approach from the synthetic work of Linington and co-workers (Scheme 2-2).²⁵⁻²⁶



Scheme 2-2: Stereoselective synthesis of vac-1.²⁶

The synthesis commences with the commercially available 2,4-dibromoquinoline **11**, which is selectively activated on carbon four by a turbo Grignard reagent, which then undergoes a 1,2 addition onto *tert*-butyl 2-formylpiperidine-1-carboxylate **12** to establish the vicinal amino alcohol in one step, as a mixture of the (*R,S*) *erythro* and (*S,S*) *threo* isomers **13**.^{26,32} Suzuki-Miyaura cross-coupling of **13** with boronic acid **14**, followed by *tert*-butyloxycarbonyl (*t*-Boc) removal, basification, and HPLC separation yields the two enantioenriched *threo* and *erythro* isomers of **1**.²⁶ To acquire the other *erythro* (*S,R*) and *threo* (*R,R*) isomer, the chirality of **12** is simply switched, and synthesis according to Scheme 2-2 is followed with no additional alterations.²⁶ The 2nd-generation synthesis of **1** is much more streamlined and robust. However, HPLC or FCC purification is still required to isolate the individual *erythro* and *threo* isomers, which is a disadvantage. Regardless, with all isomers of **1** in hand, the authors went about testing them against GBM cell lines to assess potency *in vitro* (Figure 2-6).

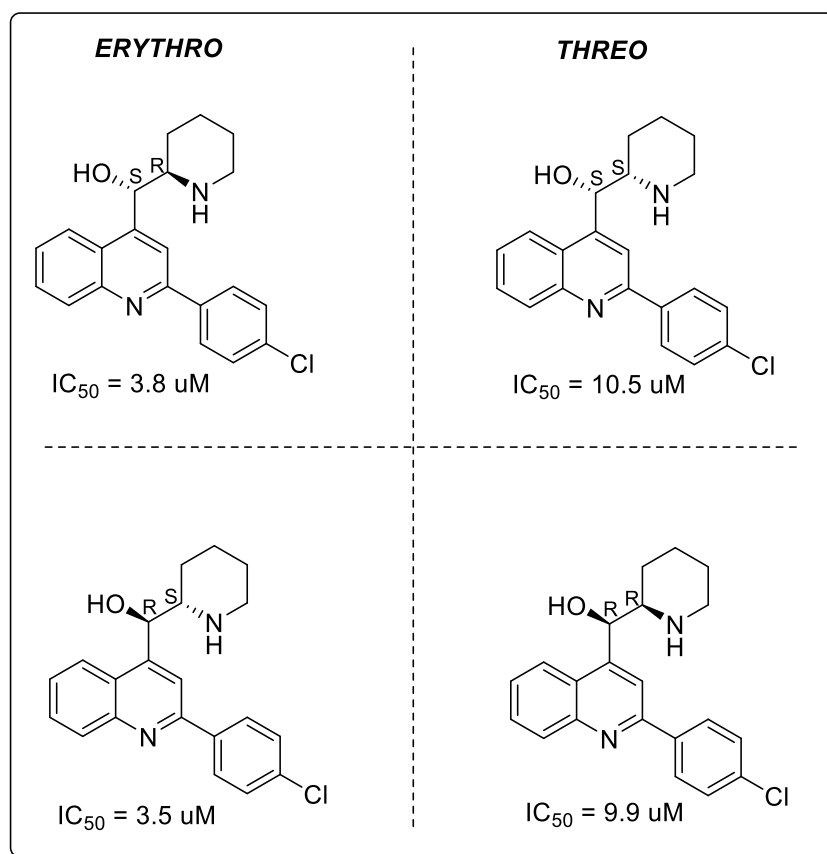


Figure 2-6: Biological activity of individual vac-1 stereoisomers.²⁶

The authors discovered that the *erythro* isomers afford a significant improvement in biological activity, compared to the *threo* isomers.²⁶ In addition, administering the *erythro* isomers of **1** to mice *in vivo* showed that the (*R,S*) enantiomer was superior in penetrating the Blood-Brain Barrier (BBB).²⁶ The improved penetration to the BBB is extremely advantageous, as it is a common problem with drug candidates against GBM not being able to reach the target cancer cells.³³ The effluxing of xenobiotics is largely attributed to carrier and transporter proteins within the BBB.³³ With the promising *in vivo* properties of the (*R,S*) enantiomer of **1**, the authors were able to synthesize it with 9:1 dr *erythro:threo*, simply by replacing the *t*-Boc group on **12** with a trityl (Tr) group, and continuing their synthesis as normal in an improved 59-63% overall yield in four steps.²⁶

The last series of studies featured the synthesis of analogs by replacing the 2-(4-chlorophenyl) scaffold with a variety of multisubstituted aryl rings, and other aromatic heterocycles, simply by changing the boronic acid **14** in the Suzuki-Miyaura reaction.²⁶ All analogs either displayed significantly reduced biological activity or no activity at all.²⁶ The biological activity and stereoisomers of vac-1 represent a wonderful opportunity for further optimization and development, and gives some hope towards an otherwise hopeless cancer. But, perhaps the most fascinating feature of this drug candidate is its unique biological mechanism against GBM, a process called methuosis.¹⁵

2.4 Methuosis: A Nonapoptotic Form of Cell Death Against GBM

Endocytosis encompasses a variety of biological pathways a cell uses to bring substances and/or fluid inside itself, which are then recycled back outside the cell or degraded within.³⁴ This cellular process can be divided into two main categories: 1) clathrin-mediated, and 2) clathrin-independent.³⁴ Clathrin-mediated endocytosis (CME), occurs when the molecular cargo binds to a pit on the cell coated in clathrin, a protein receptor that can recruit a series of other scaffolding proteins/molecules to facilitate formation of a vesicle for transport into the cell.³⁴ Clathrin-independent endocytosis (CIE), uses several biological mechanisms to form vesicles for transport into the cell; however, no clathrin is required to bind the cargo of interest, and initiate vesicle formation.³⁴ Methuosis is a disruptor of CIE: specifically, a subcategory of CIE called macropinocytosis, and its subsequent endosomal trafficking.³⁴⁻³⁵

Macropinocytosis begins when ruffles form on the exterior cell membrane in response to actin (a protein cytoskeletal microfilament) stimulation through a variety of growth factors.^{34c} These ruffles then elongate into actin extensions termed lamellipodia, which can then fold back in on themselves forming large vesicles, or macropinosome, that encapsulate extracellular fluid and any additional solutes and molecules, akin to the cell taking a large drink of water (Figure 2-7).^{34c}

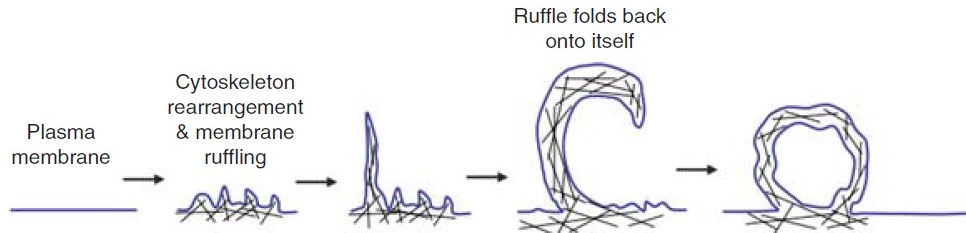


Figure 2-7: Pathway of macropinocytosis, reproduced with permission from John Wiley and Sons.^{34c}

Once formed, the macropinosome enters the cell where it shrinks, acquires a marker protein Rab5—a guanine-nucleotide protein or G protein, involved in membrane trafficking—and goes to an early endosome (EE), a membrane bound compartment from the Golgi Body that sorts vesicles (Figure 2-8).^{34c,36}

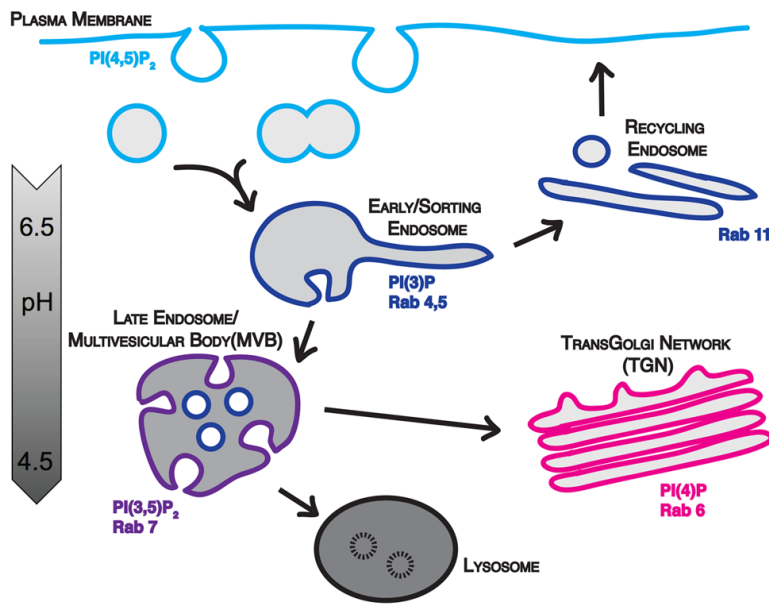


Figure 2-8: Endosomal trafficking, reproduced with permission from Springer Nature.^{34b}

At the EE, the macropinosome can be recycled outside the cell, or it can lose Rab5 to be replaced by its sibling Rab7, and become a late endosome (LE).^{34c,36} The LE lowers its pH, fuses with a lysosome, and the LE contents are eliminated via hydrolytic enzymes within the lysosome.^{34c,37} This sequence follows the typical endosomal trafficking pathways observed for CME and CIE.³⁴ When GBM cells are treated with vac-1, this traffic becomes disrupted, and the alternate process of methuosis commences.^{15,34-35}

Once vac-1 is present, the GBM cells will form macropinosomes rapidly; however, instead of traveling to an EE to be recycled or upgraded to an LE followed by lysosome annihilation, they accumulate and coalesce—forming larger and larger fluid-filled vacuoles.^{15,35} The rapid growth of vacuoles in tandem with an apparent disruption of endocytic traffic checks and balances, causes severe metabolic stress to the cell, and it will then undergo rupture in a necrotic-like cell death, also known as catastrophic vacuolization (Figure 2-9).^{15,35}

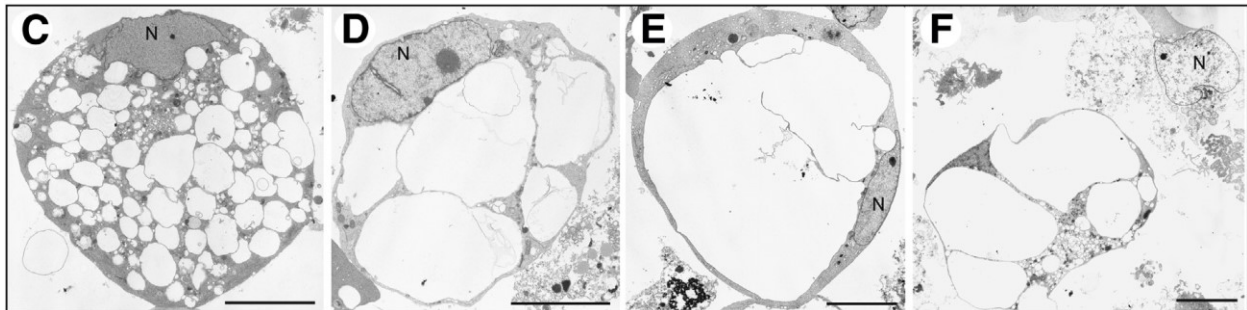


Figure 2-9: GBM cells undergoing methuosis, reproduced with permission from Elsevier via the Creative Commons Attribution-NonCommercial-No Derivatives License (CC BY NC ND), <https://creativecommons.org/licenses/by-nc-nd/4.0/>.³⁵

This method of cell death is nonapoptotic, in that it lacks the cellular morphology of chromatin condensation, dense cytoplasm, and plasma membrane blebbing.³⁸ As well, there is no activation of tumour necrosis factor receptors (TNFR), or the apoptotic protease activating factor 1 (Apaf-1), which are the hallmarks of the extrinsic and intrinsic apoptosis pathways.³⁸ Bypassing apoptosis has incredible therapeutic advantage, because the majority of resistance mechanisms in GBM and its progenitor CSCs are towards chemotherapy regimens that induce apoptosis via DNA alkylation (vide supra).^{15,35} The mechanism for how vac-1 disrupts endosomal traffic and what biological

targets it interacts with are still being investigated, but several key discoveries have arisen recently that implicate a number of kinases.

After the initial HTS and discovery of vac-1, Ernfors and co-workers used additional screening technology to try and elucidate a biological target influenced by vac-1.¹⁵ They targeted 5,043 different genes in GBM cells with a short hairpin RNA (shRNA) library.^{15,39} After incubating with the shRNA library, the authors dosed the GBM cells with vac-1, and then examined the cells that survived after being exposed to vac-1.^{15,39} They observed that GBM cells resistant to vac-1 induced methuosis had higher levels of shRNA viruses inhibiting MKK4, a mitogen-activated protein (MAP) kinase that phosphorylates serine, threonine, and tyrosine amino acid residues, and is implicated in the phosphorylation of the downstream c-Jun N-terminal kinases (JNK), another MAP kinase family member involved in a myriad of pathways in relation to stress stimuli.^{15,40} Knockdown of MKK4 in GBM cells completely prevented vac-1 induced methuosis, leading to the conclusion that MKK4 activity is required to exploit catastrophic vacuolization in GBM cells.¹⁵

Another methuosis-promoting compound is 3-(5-methoxy-2-methyl-1H-indol-3-yl)-1-(4-pyridinyl)-2-propene-1-one (MOMIPP), which was discovered by Maltese and co-workers, and seems to affect related biological targets of MKK4 in the endosomal trafficking pathways to facilitate catastrophic vacuolization in GBM.³⁵

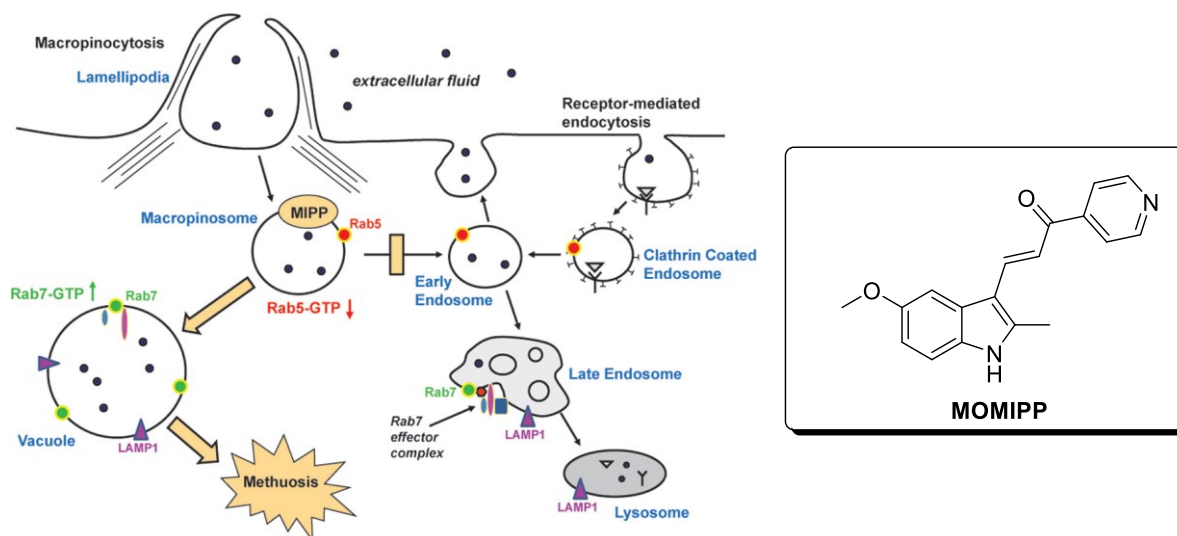


Figure 2-10: An early working model for MOMIPP induced methuosis, reproduced with permission from BioMed Central Ltd. Creative Commons Attribution-NonCommercial-No Derivatives License (CC BY NC ND), <https://creativecommons.org/licenses/by-nc-nd/4.0/>.³⁵

GBM cells treated with MOMIPP form macropinosomes, but deplete the concentrations of Rab5, which bypasses interactions with the EE, and instead rapidly incorporates Rab7 to form a LE.³⁵ After this point, the macropinosome-derived LE somehow evades fusion with lysosomes, allowing them to coalesce into the impervious vacuoles and initiate methuosis (Figure 2-10).³⁵

After proposing this early working methuosis model, it was quickly discovered by Cho and co-workers that MOMIPP inhibits the protein target PIKFYVE, a phosphoinositide kinase.⁴¹ Phosphoinositide kinases are regulators of lipids in membrane proteins, and are crucial in CME and CIE traffic pathways.⁴¹ In addition, Maltese and co-workers also discovered that MOMIPP is involved with MKK4 and the downstream JNK signaling pathway, where MOMIPP interferes with glucose uptake, and facilitates the JNK to phosphorylate the downstream B-cell lymphoma 2 (Bcl-2) family, which then promotes methuosis and nonapoptotic cell death.^{35d} It's possible that more cascades occur after interaction with Bcl-2, but none are known at this time. Based on the similar morphology and cell death of GBM cells treated with vac-1, it is possible that it follows a similar cascade to MOMIPP, especially since it requires MKK4 for methuosis to occur (Figure 2-11). However, it is unclear whether it interacts with PIKFYVE or directly activates MKK4 instead.

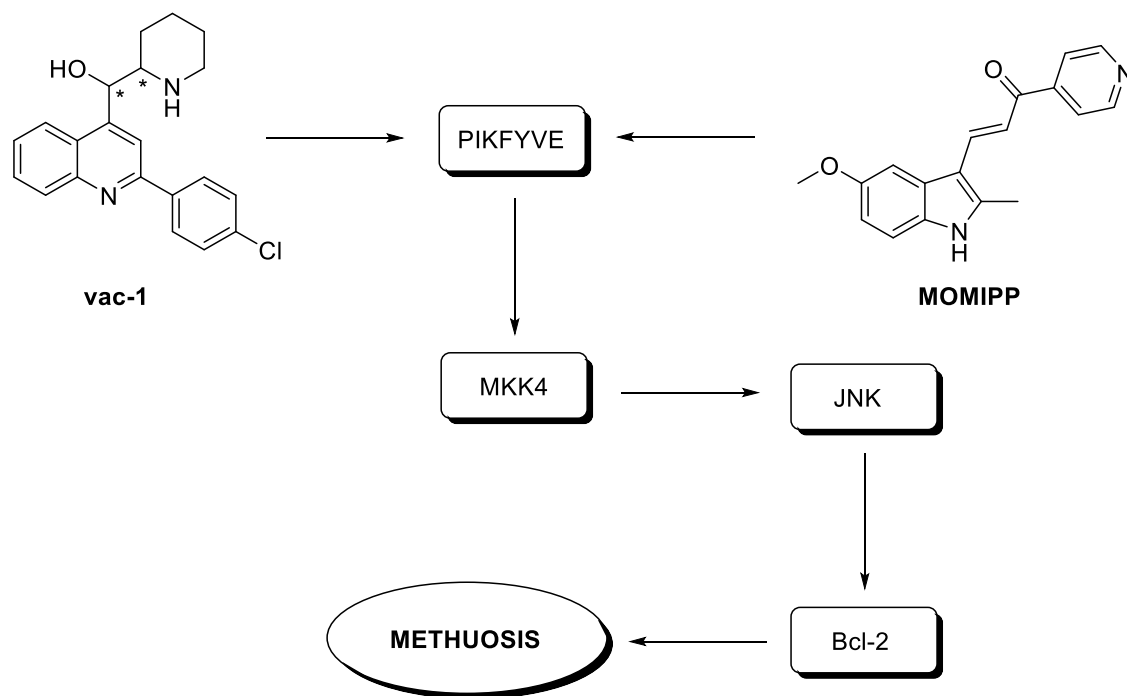


Figure 2-11: A hypothetical pathway of biological targets for vac-1 and MOMIPP leading to methuosis.

Since the recognition of methuosis as a nonapoptotic form of cell death emerged, along with a clearer understanding of the morphological characteristics that define it, additional compounds have begun to emerge that can initiate methuosis (Figure 2-12).⁴²

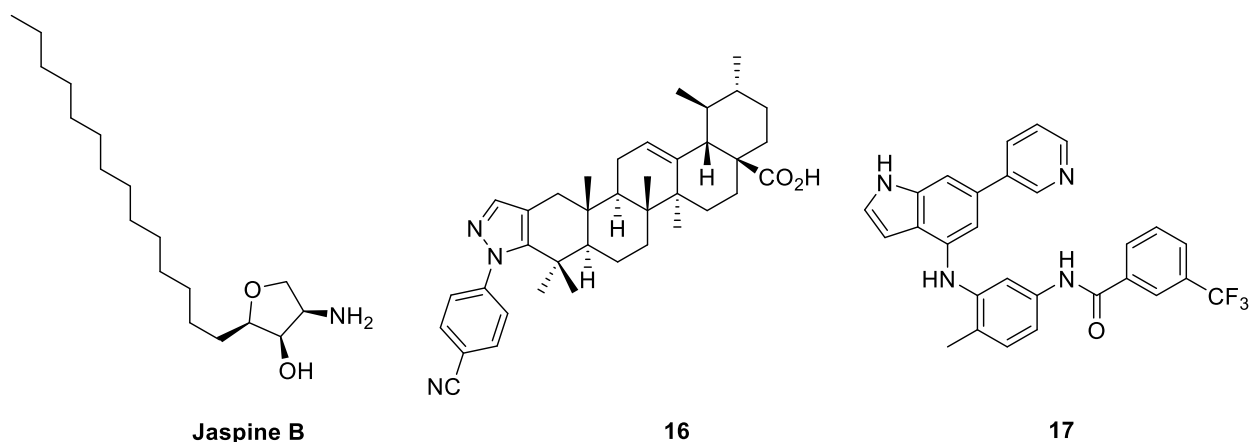


Figure 2-12: Recently identified compounds capable of inducing methuosis in cancer.⁴²

One such compound is a natural product called Jaspine B, which was found to cause methuosis when treating gastric cancer cells.⁴² The ursolic acid **16** and azaindole **17** were also capable of causing catastrophic vacuolization in a variety of cancer cell lines *in vitro*, with **17** also having activity *in vivo* as well.⁴² It would be very interesting to see if these methuosis promoters also interact with the same biological targets of vac-1 and MOMIPP.

The biological mechanism of methuosis is only starting to be understood. However, with the discovery of new molecules, and development of analogs of existing molecules that can induce this unique form of cell death, it represents an excellent way to undermine apoptosis resistance mechanisms in a variety of cancers. These drug discovery efforts will ideally give a clear sense of what molecular scaffolds and functionality are required to disrupt endosomal trafficking in cancer for medicinal chemistry endeavours in academia and industry. The novelty of this nonapoptotic cell death, and the future opportunity to study it was just another incentive for the Hall Group to repurpose vac-1 by designing more powerful analogs via their allylic piperidinyl boronate methodology.

2.5. 2nd Generation Vac-1 Analogs: Bioisosteres, Dehydropiperidines, and Dehydroazepane

As seen in Chapter 1, Kwok discovered that when the Cl atom in vac-1 was replaced with a Br atom there was a significant increase in biological activity against the U251 GBM cell lines.⁴³ From this finding, there was an interest in expanding the project by creating a larger library of vac-1 analogs to further increase *in vitro* potency. For ease of preparation, the analogs would be synthesized as *threo* racemates to avoid the extra synthetic steps for epimerization, and the relatively expensive Taniaphos ligand required for the catalytic enantioselective borylative migration.⁴³ The choice to use *threo* racemates was rationalized based on Kwok's observation that there was no significant difference in potency for the enantioenriched *threo* stereoisomers of vac-1 (Figure 2-13).⁴³

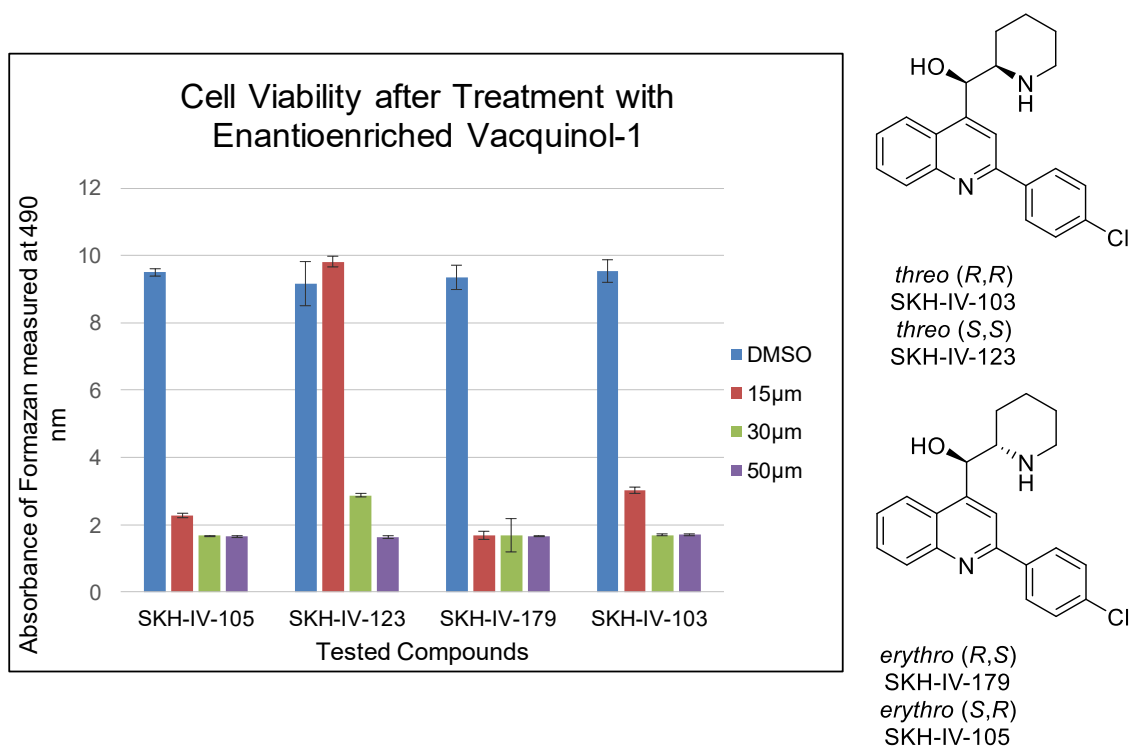


Figure 2-13: Biological activity of all vac-1 stereoisomers.⁴³

For the planned SAR analysis, the main strategy to generate new vac-1 analogs was bioisosteric replacement of the bromine atom (Figure 2-14).

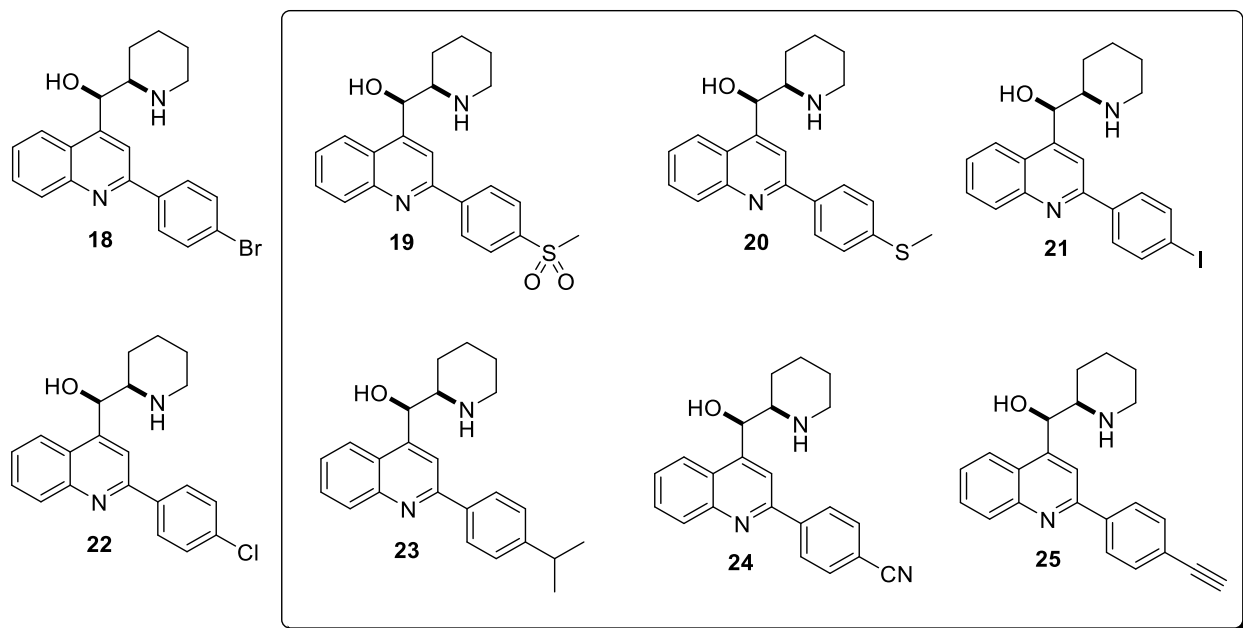


Figure 2-14: Proposed *classical* and *nonclassical* bioisostere analogs of racemic *threo* Br-vac-1 **18**, and racemic *threo* vac-1 **22**.

A combination of *classical* and *nonclassical* bioisosteric approaches was implemented to generate derivatives of the Br-vac-1 analog **18**. For the *classical* analogs, large alkyl substituents, polar groups, as well as functional groups of comparable molecular weight were primarily examined. The methyl sulfone moiety (SO₂Me) **19**, the isopropyl group (*i*-Pr) **23**, and the nitrile **24**, were chosen as they are well-documented bromine biososteres.¹⁶ From a *nonclassical* standpoint the methyl thiol ether (SMe) **20** and iodine atom **21** were also chosen to help determine if a larger heavier atom would create a more favourable binding interaction over the bromine, because this is a probable explanation for the improvement in potency when the Cl atom of vac-1 was replaced with a Br atom. The *nonclassical* acetylene **25** was chosen, because in certain instances, a terminal alkyne can sometimes mimic weak halogen interactions in the active site of a biological target.⁴⁴ In addition to the new analogs, **18**, and a synthetic *threo* racemate of vac-1 **22** would be tested to reaffirm Kwok's results that the Br-vac-1 analog led to improved biological activity over vac-1. Lastly, a series of racemic *threo* dehydro-vac-1 halogen analogs were prepared for testing. These analogs were made to reproduce Kwok's other major observation that the dehydro-vac-1 analogs were less active compared to vac-1 (Figure 2-15).⁴³

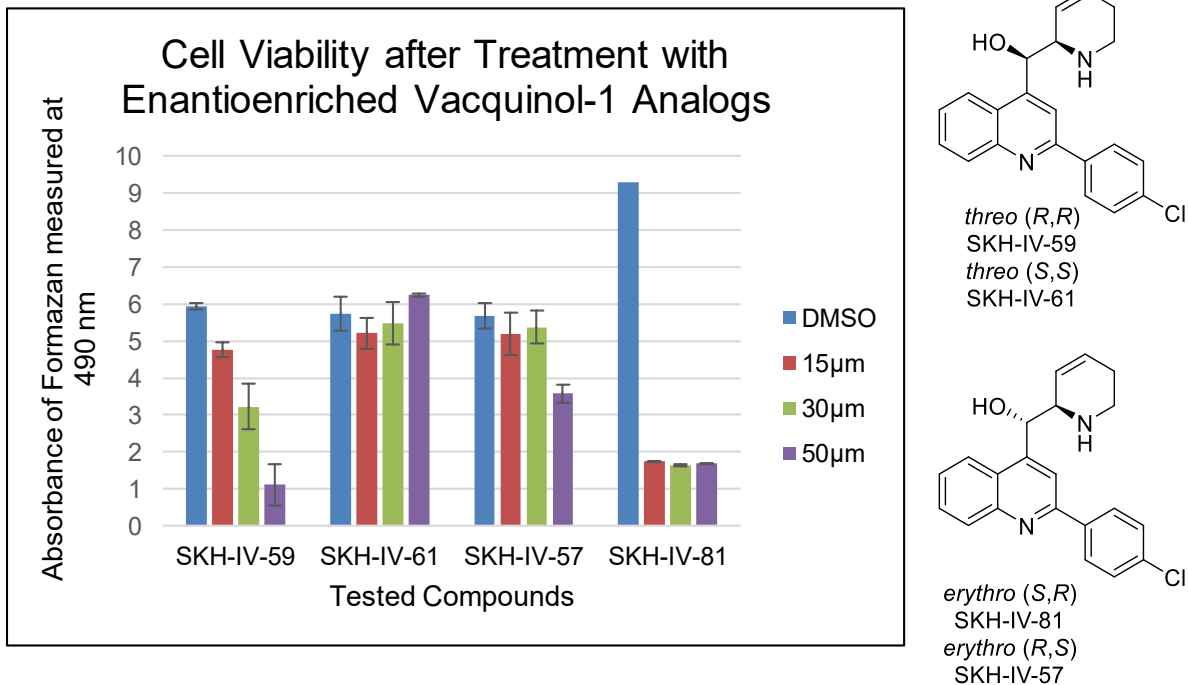


Figure 2-15: Biological activity of dehydro-vac-1 stereoisomers.⁴³

Later in the project, there was a desire to see if a dehydro-vac-1 analog with an azepane ring would improve activity, as Clement and Hall were recently able to apply the catalytic enantioselective borylative migration to include dehydroazepanes.⁴⁵ The structures of the dehydroazepane-vac-1 analog **26**, as well as the dehydro-vac-1 halogen analogs **27-29** are shown below (Figure 2-16).

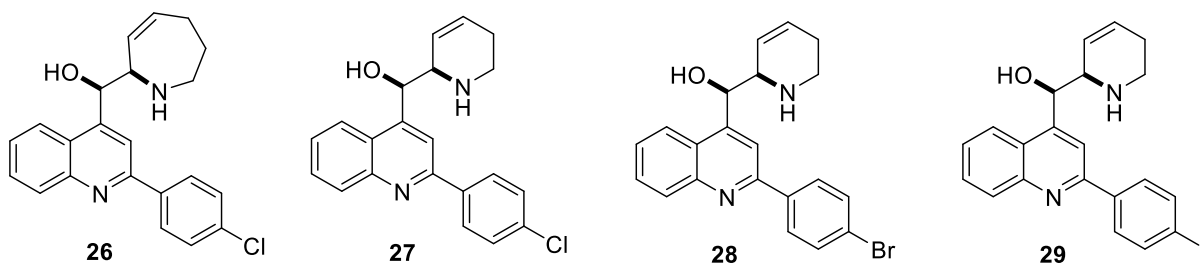
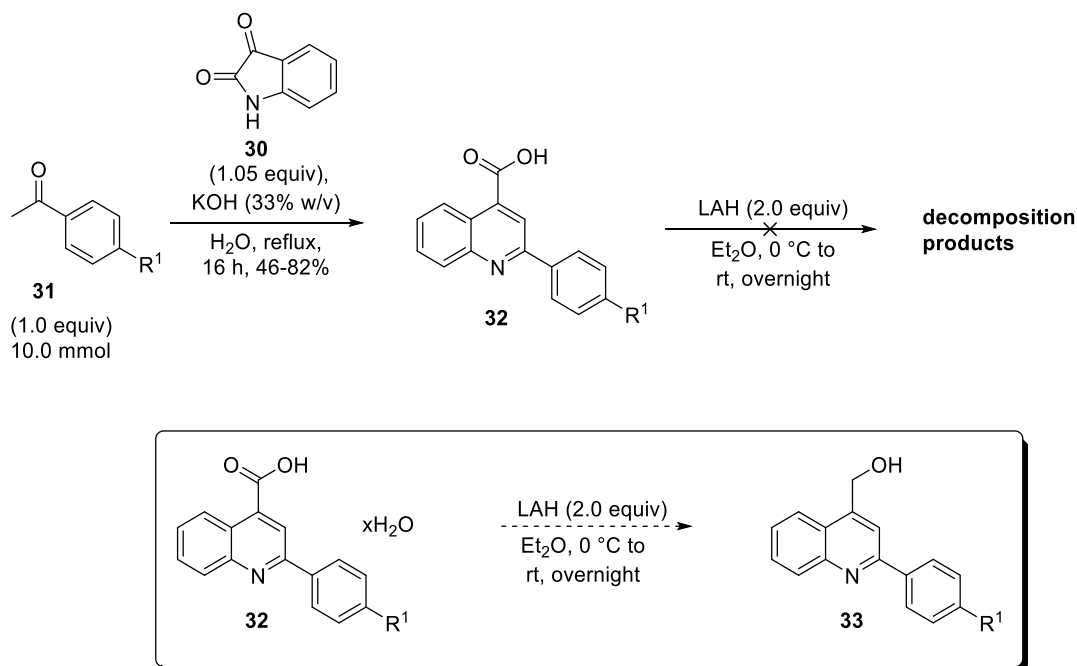


Figure 2-16: Dehydropiperidine and dehydroazepane racemic *threo* vac-1 analogs.^{43,45}

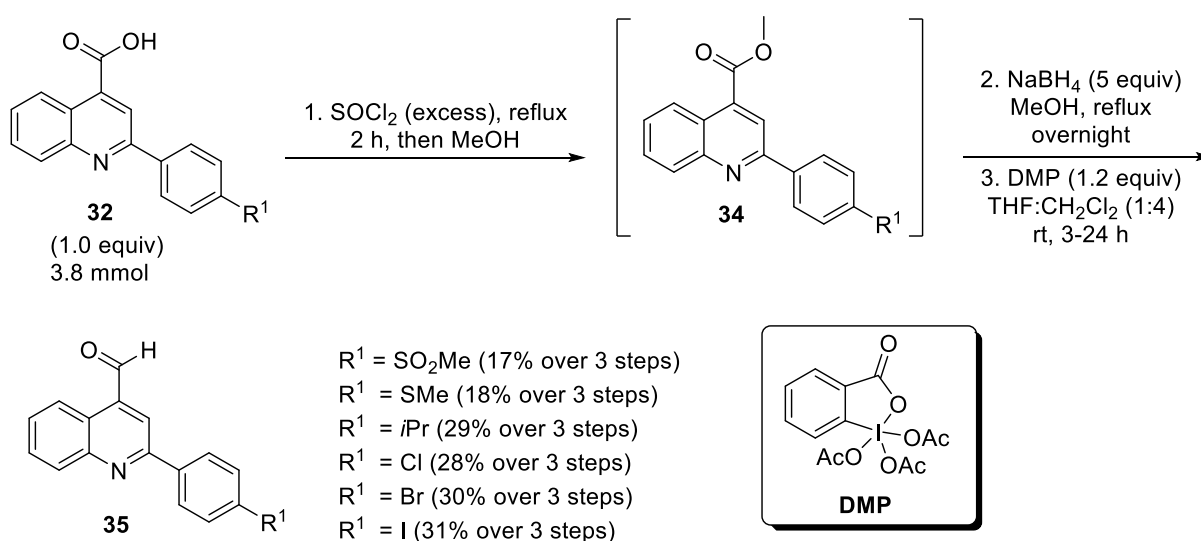
2.6. Synthesis of Bioisosteric, and Dehydropiperidinyl Vac-1 Analogs

Following the vac-1 retrosynthesis outlined in Chapter 1, the Pfitzinger reaction was successful in yielding the quinoline carboxylic acid **32** in good yields with the new *para* substituents after recrystallization and rigorously drying under vacuum to remove water (Scheme 2-3). However, problems arose in the preparation of the quinoline aldehyde. Initially, lithium aluminum hydride (LAH) was used to reduce the quinoline carboxylic acid based on Kwok and Hall's synthetic route.⁴³ However, this led to the decomposition of **32**, with only trace yields of the quinoline methanol **33**—possibly via overreduction of the quinoline ring.⁴⁶ A potential explanation could be that when **32** was synthesized by Kwok it existed in a hydrated form, as there was no report of recrystallization or high vacuum drying after the crude was obtained from the Pfitzinger reaction in their preparation of vac-1 analogs.⁴³ The water in the product may have suppressed the LAH from reducing the quinoline ring, as one or more equivalents of water would react with the LAH first—weakening its reducing power (Scheme 2-3).⁴⁷ Nonetheless, an alternative reduction sequence was attempted to try and resolve the inconsistencies.



Scheme 2-3: Preparation of quinoline carboxylic acids **32**, unsuccessful LAH reduction, and hypothetical explanation as to why.^{43,46-47}

The synthetic route from Yadav and co-workers to synthesize TNF α converting enzyme (TACE) inhibitors was adopted to prepare the quinoline aldehyde (Scheme 2-4).⁴⁸ To start, **32** was transformed into the acid chloride, and then reacted with methanol to get the methyl ester **34**. Sodium borohydride in refluxing MeOH facilitated the reduction. Although very clean, the reduction was often sluggish (as is typical with esters and NaBH₄), which left significant amounts of unreacted methyl ester **34**, which resulted in lower yields over the three steps. Oxidation with Dess-Martin Periodinane (DMP) gave the desired quinoline aldehydes **35** in low to modest yields over the three steps (Scheme 2-4).

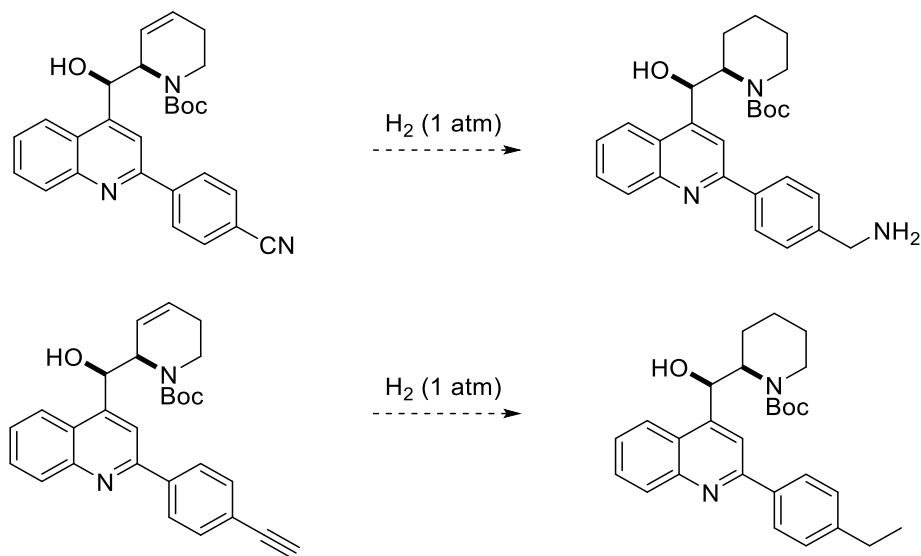


Scheme 2-4: Revised synthesis of quinoline aldehydes.⁴⁸

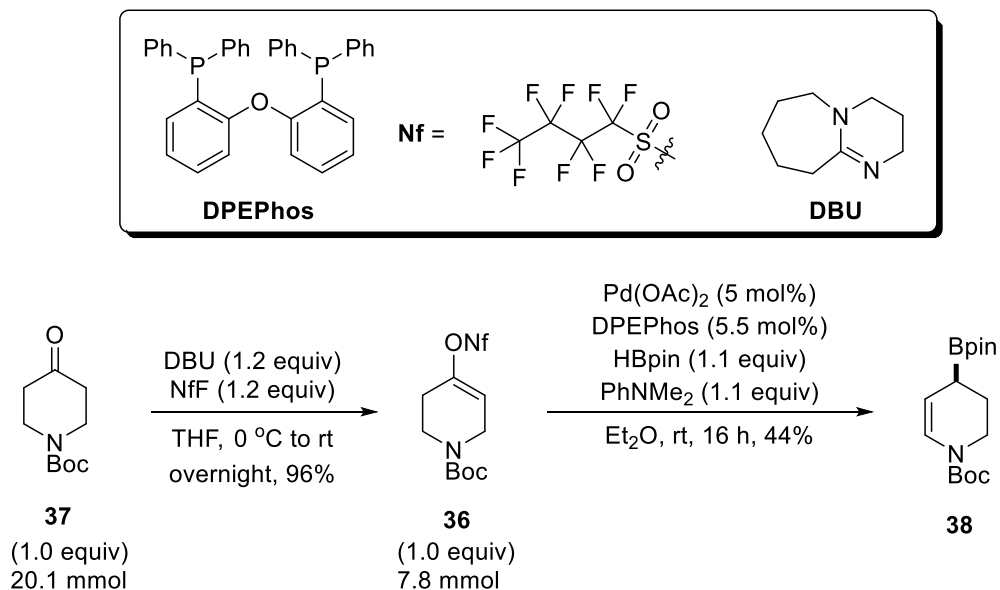
It should be noted that due to potential chemoselectivity issues encountered later in the synthesis, the alkynyl and cyano-substituted substrates were not prepared using this route. To access the saturated piperidine ring of vac-1, a hydrogenation has to be performed after the allylboration step (similar to the mefloquine synthesis). These conditions would likely also reduce the ethynyl group to ethyl, and the nitrile to the benzyl amine (Scheme 2-5). The substituents would be introduced at a later stage after the hydrogenation step, as such.

With aldehyde **35** in hand, the next step consisted in assembling the β -amino alcohol scaffold for vac-1 via an allylboration reaction. To set up this key reaction, the piperidinylnonaflate **36** was prepared by enolate trapping of the *N**t*-Boc piperidone **37** with nonafluorobutanesulfonyl fluoride (Scheme 2-6).⁴³ With gram scale quantities of **36** in hand, it was

then subjected to the optimized catalytic racemic borylative migration conditions from Kim and Hall,⁴⁹ which provided the racemic allylic piperidinyl boronate **38** in modest yield after flash column chromatography (FCC) (Scheme 2-6).

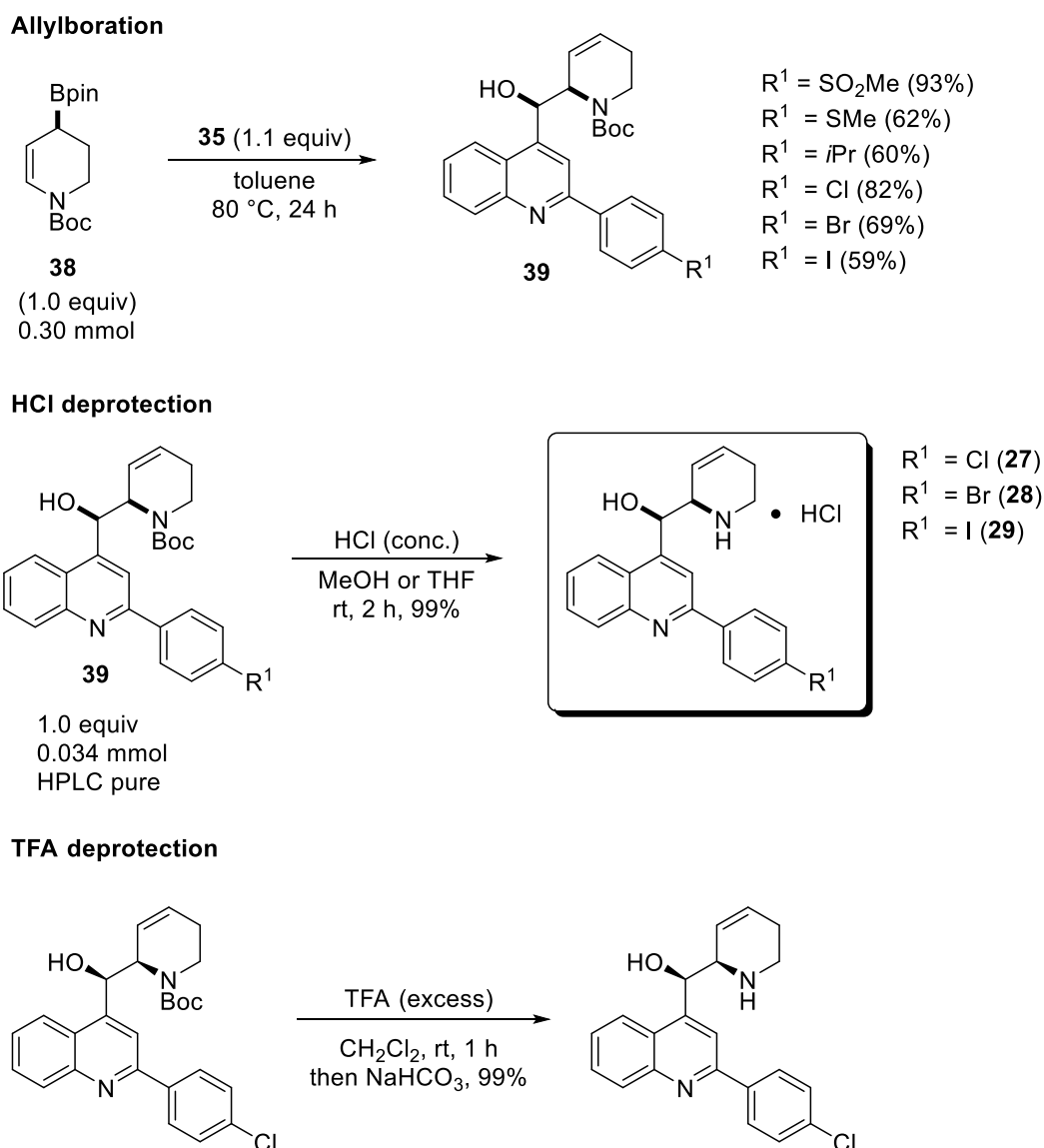


Scheme 2-5: Potential chemoselectivity issues of nitrile and acetylene functionalities during hydrogenation.



Scheme 2-6: Synthetic route to the racemic allylic piperidinyl boronate.⁴⁹

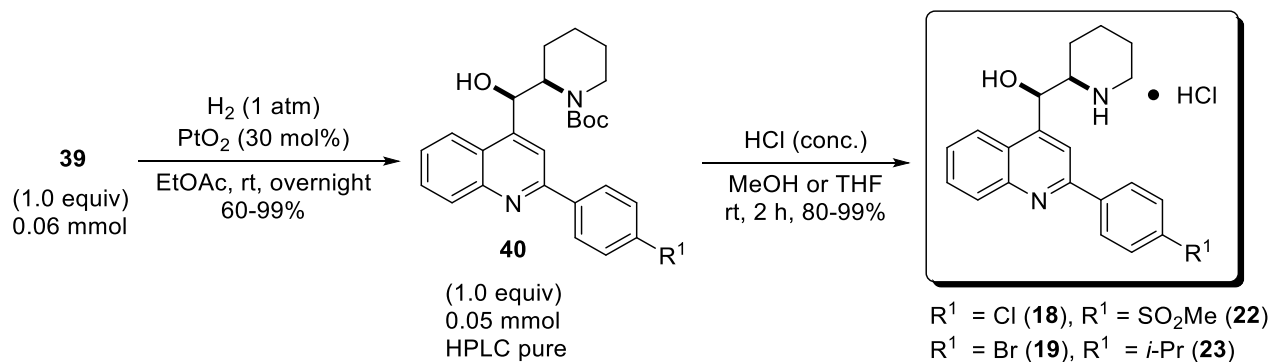
The key intermediates **35** and **38** were then subjected to a thermal allylboration, which established the dehydro-vac-1 scaffolds **39** in good yields (Scheme 2-7). After purifying the chloro, bromo, and iodo analogs of **39** by HPLC, the amine was deprotected with HCl to give the acid salts of **27-29** in quantitative yield. It is important to note that this deprotection is a variation from Kwok's original synthesis, where trifluoroacetic acid (TFA) was employed, and then basified to yield vac-1 and its analogs as the free base (Scheme 2-7).⁴³



Scheme 2-7: Synthesis of dehydro-*t*-Boc-vac-1 analogs, dehydro-vac-1 halogen analogs, and formation of HCl salts of **27-29**.⁴³

Initially, all the racemic *threo* vac-1 analogs were prepared as free bases—similar to Kwok.⁴³ However, upon testing with the *in vitro* colourimetric assay, none of them had any observed activity! It was only after transforming the analogs to HCl salts that the potency returned. A potential explanation for the lack of activity with the free base racemic *threo* vac-1 analogs is that as racemates they may be less water soluble compared to an enantioenriched stereoisomer, which could lead to inaccuracies in the serial dilutions required to get variable concentrations for the assay.⁵⁰ HCl salts are significantly more soluble in aqueous solutions, so it likely corrects for any reduced solubility the *threo* racemates may have.⁵⁰ From this point on, all analogs were prepared as HCl salts to minimize any issues with the assay, and get reproducible biological activity.

After acquiring the dehydro-vac-1 halogen analogs, the bioisosteric vac-1 analogs were tackled next. To accomplish this goal, hydrogenation of the endocyclic alkene in the piperidine ring had to be conducted. Crabtree's catalyst was unsuccessful on the vac-1 scaffold despite a variety of optimization attempts by Kwok.⁴³ After screening a variety of catalysts, Kwok was ultimately able to hydrogenate the endocyclic alkene with Adam's catalyst (PtO₂).⁴³ Therefore, the analogs of **39** were subjected to Kwok's optimized hydrogenation conditions (Scheme 2-8).



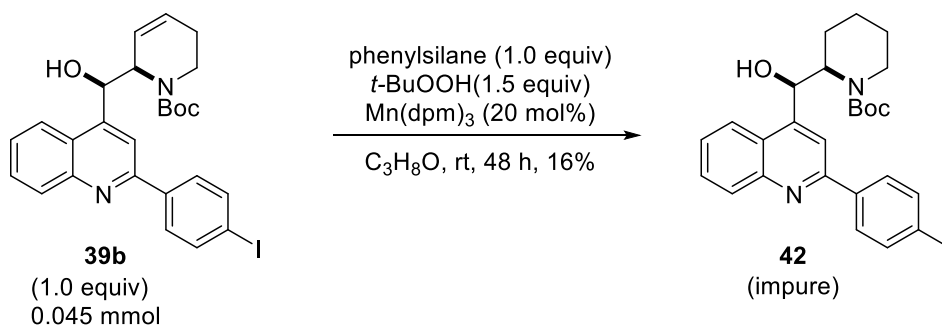
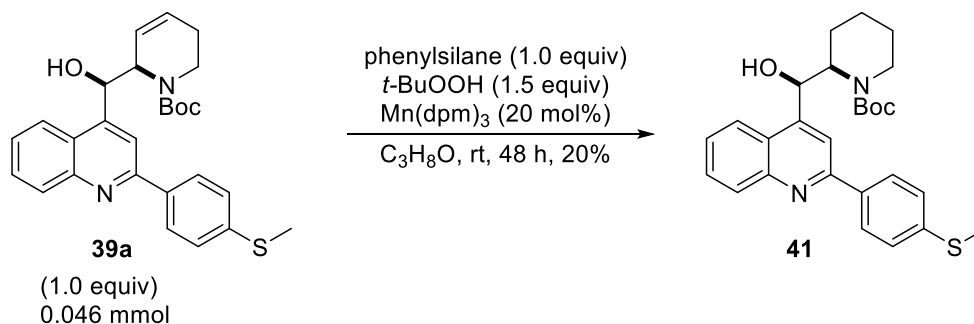
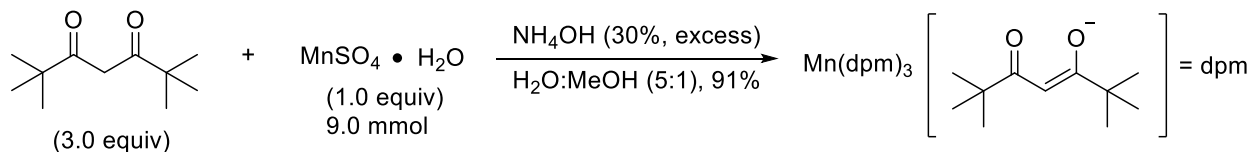
Scheme 2-8: Synthesis of some of the *classical* bioisosteric Vac-1 analogs.

The reaction proceeded smoothly, and gave the saturated *t*-Boc vac-1 analogs **40** with the Cl, Br, *i*-Pr, and SO₂Me groups in good to quantitative yields (Scheme 2-8). Unfortunately, the preparation of the saturated iodo and SMe analogs of **39** were unsuccessful. The hydrogenation conditions led to deiodination, and only starting material was recovered with the the MeS-substituted substrate—likely the result of the sulfur atom poisoning the PtO₂.⁵¹ As such, alternative

conditions would be required to saturate the endocyclic alkene on these analogs. The Cl, Br, *i*-Pr, and SO₂Me analogs of **40** were then purified by HPLC, and deprotected with HCl to obtain **18-19** and **22-23**.

2.6.1 Synthesis of Remaining *Classical, Nonclassical* Bioisosteric, and Dehydroazepane Vac-1 Analogs

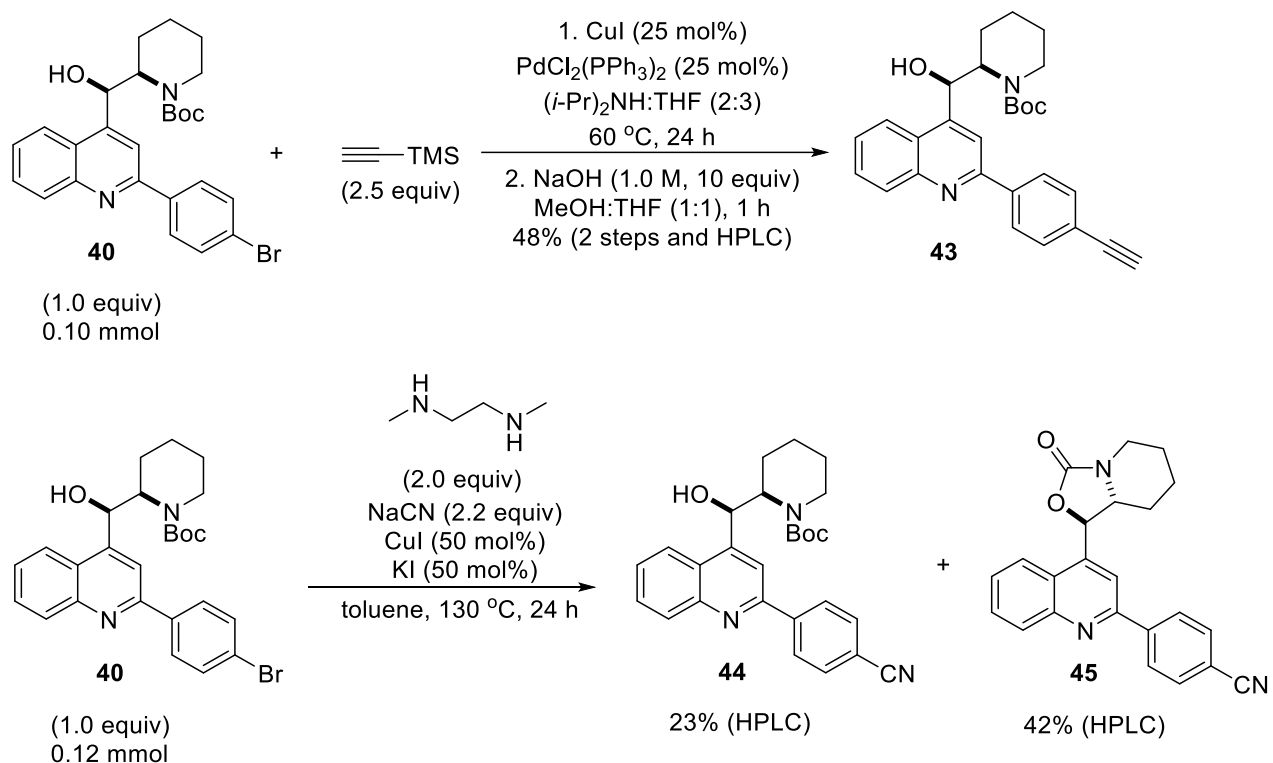
Since Adam's catalyst was unsuccessful on the iodo and SMe -substituted analogs, milder hydrogenation conditions were sought out with a catalyst that would be impervious to sulfur poisoning and one that would tolerate aryl iodides. A hydrogen atom transfer (HAT) reaction from Shenvi and co-workers was appealing, as they reported successful alkene reduction examples on aryl iodide and thiol ether-containing substrates respectively, with their novel manganese (Mn) catalyst.⁵² The Mn catalyst was readily prepared in near quantitative yield on multigram scale by reacting MnSO₄ • H₂O and dipivaloylmethane in the presence of excess aqueous ammonia hydroxide (NH₄OH) (Scheme 2-9).⁵² Using the Mn(dpm)₃ complex, the HAT was attempted on the SMe and iodo analog, following Shenvi and co-worker's optimized conditions.⁵² Gratifyingly, the HAT was successful in saturating the piperidine ring on the SMe analog **39a** to give product **41** in modest yield after HPLC purification. In contrast, the same conditions were less successful on the iodo substrate **39b**. Although the reaction did go to completion to give the desired product **42**, unfortunately it could not be purified effectively by HPLC, and so it was not advanced further with the other analogs. An indirect evaluation of the iodo group's potency could be performed by comparing dehydro analogs **27-29**. If the iodo group was the most powerful of these three analogs, then the HAT could be optimized to acquire the saturated iodo analog in higher yield and purity for future studies.



Scheme 2-9: Synthesis of Mn(dpm)_3 , and HAT hydrogenation conditions to access the *t*-Boc vac-1 SMe and iodo analogs **41** and **42**.⁵²

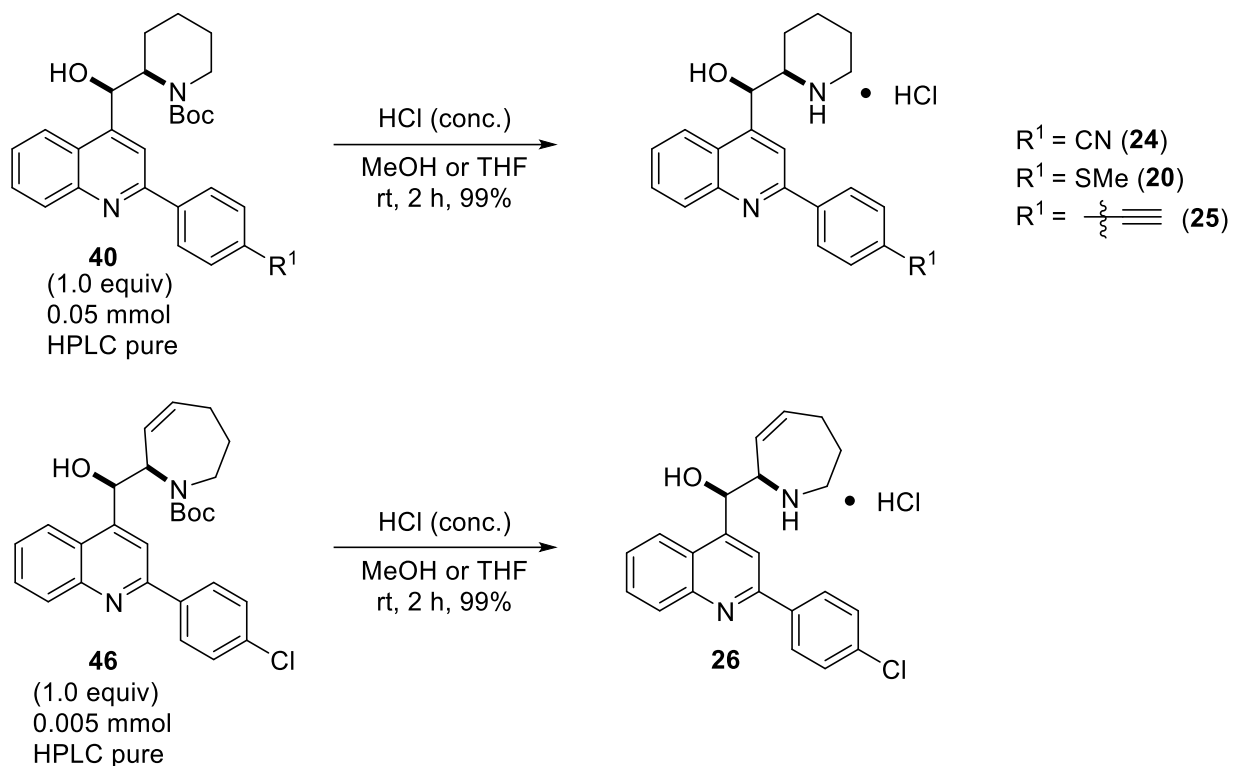
For the nitrile and alkyne analogs, we turned to cross-coupling chemistry. To acquire the ethynyl-substituted analog, the *t*-Boc protected Br-vac-1 scaffold **40** was subjected to a Sonogashira reaction with trimethylsilylacetylene, adapted from Jègou and Jenekhe (Scheme 2-10).⁵³ The alkynyl silane intermediate was then subjected to TMS hydrolysis, and purified by HPLC to give the desired terminal alkyne **43**. For the nitrile-substituted analog, intermediate **40** was used in a Rosemund-von Braun type reaction optimized from Buchwald and co-workers (Scheme 2-10).⁵⁴ The nitrile intermediate **44** was obtained in modest yields after HPLC purification, but the major product of the reaction was found to be a fused carbamate analog **45**—likely a result of *t*-Boc pyrolysis due to the high reaction temperature. Since **45** had never been made, it was purified by HPLC, and submitted for testing with the other analogs to determine if

biological activity is maintained when the 1,2-aminoalcohol unit are deprived of their hydrogen bond donor abilities



Scheme 2-10: Synthesis of the functionalized nitrile and alkyne vac-1 intermediates **43** and **44-45**.⁵³⁻⁵⁴

With the HPLC purified intermediates in hand, the remainder of the synthetic route required a simple HCl promoted deprotection as before to obtain **20**, and **24-25** (Scheme 2-11). My colleague Helen Clement kindly donated an HPLC purified racemic *t*-Boc protected dehydroazepane vac-1 analog **46**, which was also subjected to piperidine deprotection to obtain the desired expanded-ring analog **26** (Scheme 2-11). After acquiring all the 2nd generation *threo* racemic analogs of the Br-vac-1 testing against the U251 GBM cell line could be planned with the collaborators.



Scheme 2-11: Synthesis of the remaining bioisosteres **20**, **24-25** and dehydroazepane analog **26**.

2.7 Biological Activity of Bioisosteric, Dehydropiperidinyl, and Dehydroazepanyl Vac-1 Analogs

Once submitted to Dr. Saket Jain in the laboratory of Dr. Roseline Godbout, the potency of the new vac-1 analogs against the U251 GBM cells was determined using the CellTiter 96® Aqueous One Solution Cell Proliferation Assay (MTS).⁵⁵ The set-up of the colourimetric *in vitro* assay is as follows: GBM cells are incubated into a 96-well plate, and the cells are then dosed with the drug candidate of interest at variable concentrations, along with Owen's reagent [3-(4,5-dimethylthiazol-2-yl)-5-(3-carboxymethoxyphenyl)-2-(4-sulfophenyl)-2H-tetrazolium (MTS), and phenazine ethosulfate (PES), an electron coupling reagent (Figure 2-17).⁵⁵ When MTS and PES are exposed to living cells, they will succumb to bioreduction by dehydrogenase enzymes via the cellular redox cofactors nicotinamide adenine dinucleotide phosphate (NADPH), and nicotinamide adenine dinucleotide NADH; MTS will then form a coloured formazan product, which is soluble in cell tissue.⁵⁵

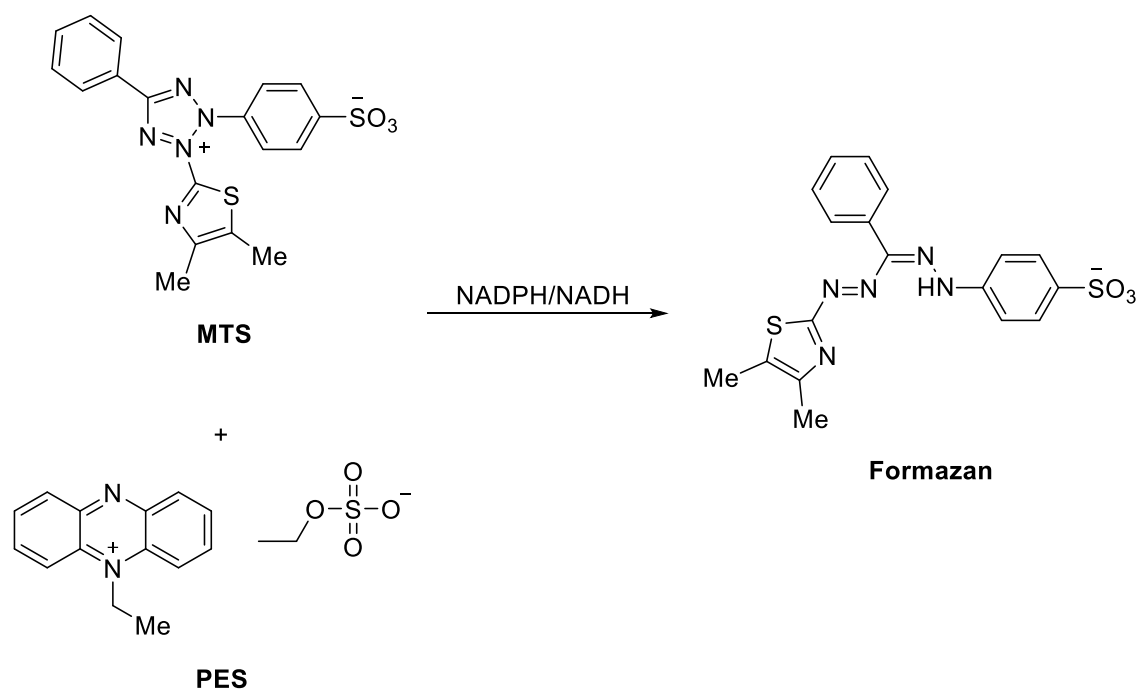


Figure 2-17: Proposed bioreduction of MTS to formazan.⁵⁵

This coloured solution can then be analyzed by UV-Vis spectrophotometry at 490 nm, and the measured absorbance at this wavelength is proportional to the number of viable cells in the well of the plate.⁵⁵ To ensure assay accuracy, DMSO is often run as a negative control, along with a positive control known to be active against the cells at a certain concentration, and the assay is typically run in triplicate and averaged, to minimize error and bias.⁵⁵

The first round of MTS assays compared compounds **18**, **22**, **26-29**, and **45** (Figure 2-14, Figure 2-16, and Scheme 2-10) at 10.0, 5.0, and 2.5 μM respectively, where compound RMH-VI-103 serves as a positive control of the enantioenriched *threo* (*R,R*) vac-1. This assay appeared to reproduce Kwok's observations in that the biological activity of **18** (RMH-VI-149) was greater than **22** (RMH-VI-173) at all tested concentrations with a cutoff at 5 μM (Figure 2-18). To further support Kwok's results, all the dehydropiperidinyll vac-1 analogs **27** (RMH-VI-195), **28** (RMH-VI-197), and **29** (RMH-VI-199) had significantly reduced potency compared to **18** and **22**. These results once again highlight how unfavourable an endocyclic alkene is on the piperidine moiety (Figure 2-18). In addition, analog **29** seemed to have worse biological activity compared to **28**,

which indicates that an iodide is not more beneficial than a bromide. The above plans to create a saturated iodo vac-1 analog were abandoned as such. An interesting result from this round of assays, was the dehydroazepane analog **26** (RMH-VI-189), which demonstrated is significant improvement in activity over the dehydropiperidine analog **27** (RMH-VI-195). This single comparison could indicate that a larger saturated nitrogen heterocycle is beneficial, and should be explored further in future studies.

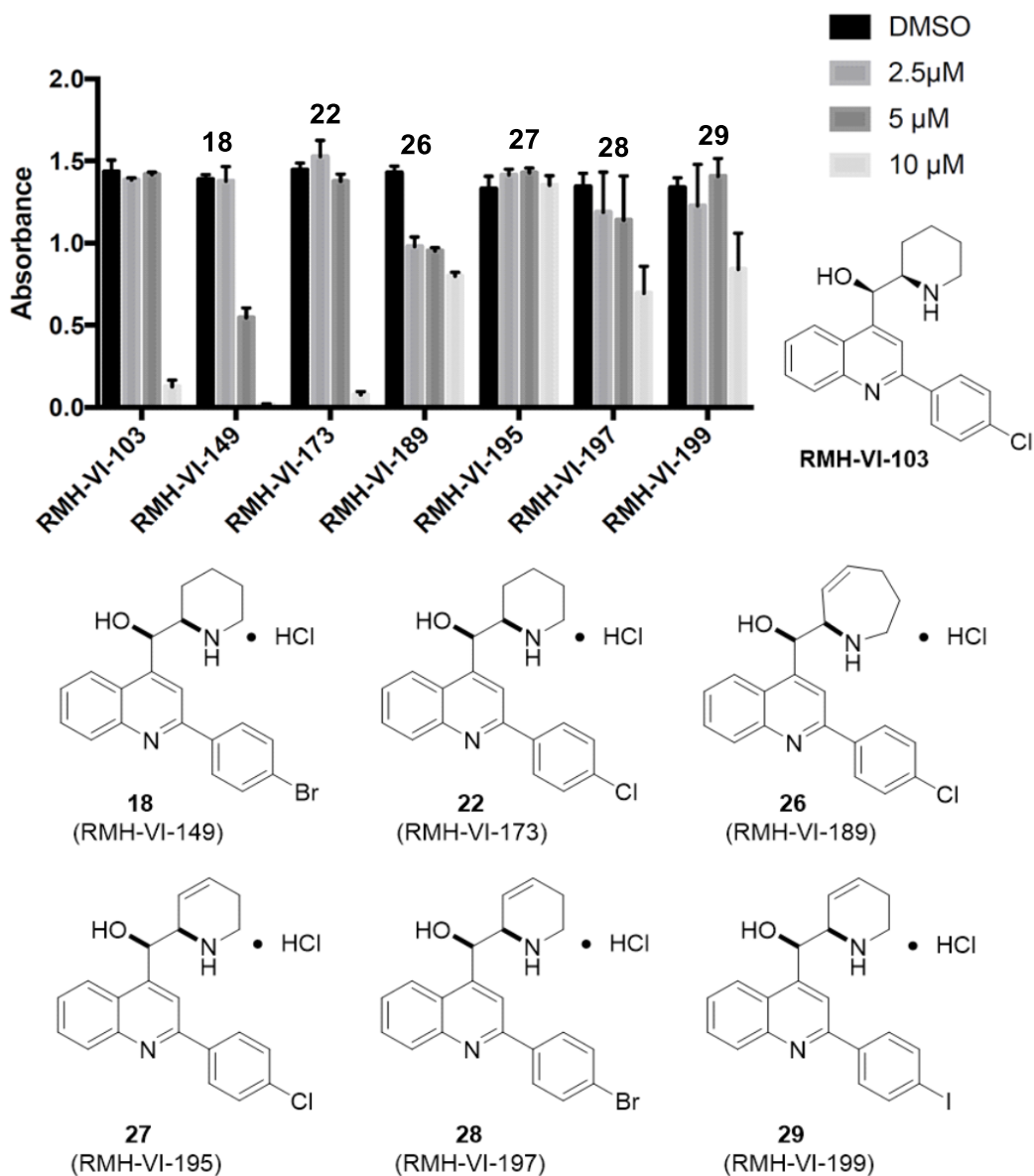


Figure 2-18: MTS assay results of dehydropiperidinyll, dehydroazepanyl, racemic vac-1 **22**, and racemic variant of Kwok's lead compound **18**, where RMH-VI-103 is a positive control.

The second MTS assay examined the new bromine bioisosteric vac-1 analogs **19** (RMH-VI-175), **20** (RMH-VI-187), **23** (RMH-VI-177), **24** (RMH-VI-191), **25** (RMH-VI-185), and carbamate analog **45** (RMH-VI-143) (Figure 2-19).

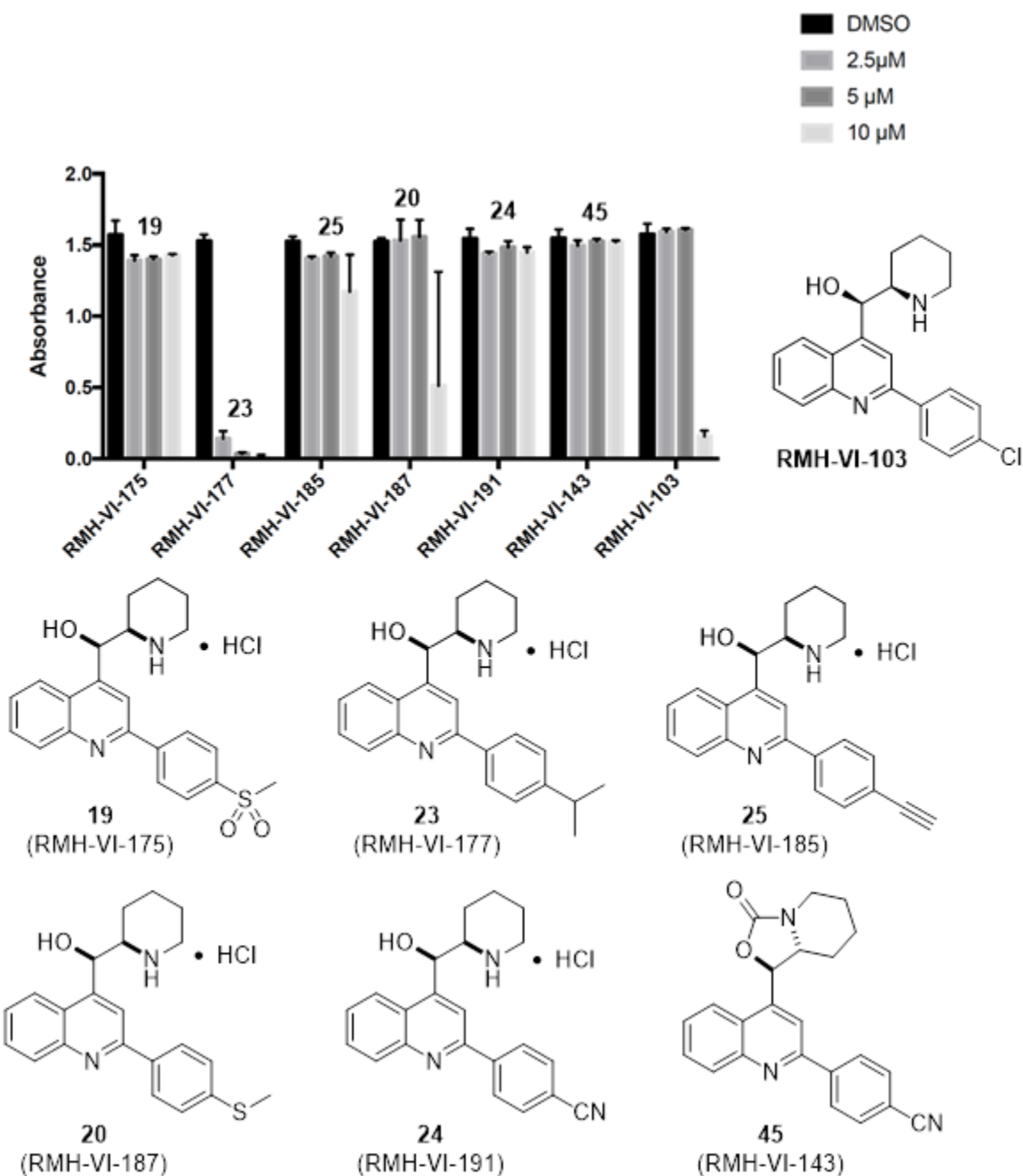


Figure 2-19: MTS assay results of bioisosteric and carbamate vac-1 analogs, where RMH-VI-103 is a positive control.

Using this preliminary evaluation, analogs **19-20**, and **24-25**, had either no activity, or there was no significant difference when compared to the positive control RMH-VI-103. The exception to the poor biological activity trend was **23**, which saw a massive increase in activity—even at the lowest concentration of 2.5 μM ! This new analog managed to surpass the 5 μM cap observed on **18**, and as such would become our new lead from this generation of vac-1 analogs. It would appear that when the 2-phenyl moiety has a *para* functional group that is greasy with steric bulk, and has the potential to undergo van der Waals interactions, it becomes an active pharmacophore against GBM cells. Polar functional groups or linear π systems do not have this favourable interaction, and should be avoided in any future optimization endeavours. Based on these exciting observations, a 3rd generation of vac-1 analogs would be synthesized to probe the 2-phenyl moiety further with variable sized alkyl substituents. These analogs would ideally help elucidate the optimal size and shape for the *para* alkyl substituent. Going beyond *para* substitution, functionalization of the endocyclic alkene on the piperidine, a saturated azepane vac-1 analog, and a scaffold hop would be attempted to try and increase biological activity even further.

2.8 The 3rd Generation Vac-1 Analogs: Variable Size *para* Alkyl Substituents, Endocyclic Alkene Functionalization, and Scaffold Hopping

To determine the ideal alkyl substituent in the *para* position of the 2-phenyl moiety, three factors were examined: 1) chain length, 2) steric bulk, and 3) flatness (Figure 2-20). Chain length and free rotation on an alkyl substituent led to analogs **47**, **48**, and **50**, to see if these properties on a linear substituent would more effectively interact with the biological targets. To further study the effects of steric bulk on the *para* substituent, and determine if an even larger substituent than the *i*-Pr group could improve potency, the *tert* butyl (*t*-Bu) analog **49** was the next logical choice. The *t*-Bu was appealing because it would likely prevent metabolic benzylic oxidation, which could be a possible pharmacokinetic (PK) issue for the *i*-Pr analog *in vivo*. Lastly, there was interest in determining whether a flatter and/or rigid alkyl substituent would lead to more favourable interactions, or whether the projecting globular methyl groups on the *i*-Pr were necessary for biological activity. These queries led to the consideration of analogs **51** and **52**.

Since there was an apparent increase in activity with a dehydroazepane moiety in comparison to a dehydropiperidine (Figure 2-18), we wanted to determine if a saturated azepane

was even more beneficial—this led us to analog **53** (Figure 2-20). Since **18** had a potency cap at 5 μM (Figure 2-19), we rationalized that if we were able to surpass this activity with **53** it would indicate that an azepane ring would be more beneficial than a piperidine ring on the β -amino alcohol moiety. Lastly, since there was such a drastic increase in biological activity with **23**, we decided to make a dehydro *i*-Pr vac-1 analog **54**, just to see if any decent biological activity could be obtained with an endocyclic alkene (and because their synthetic preparation is shorter).

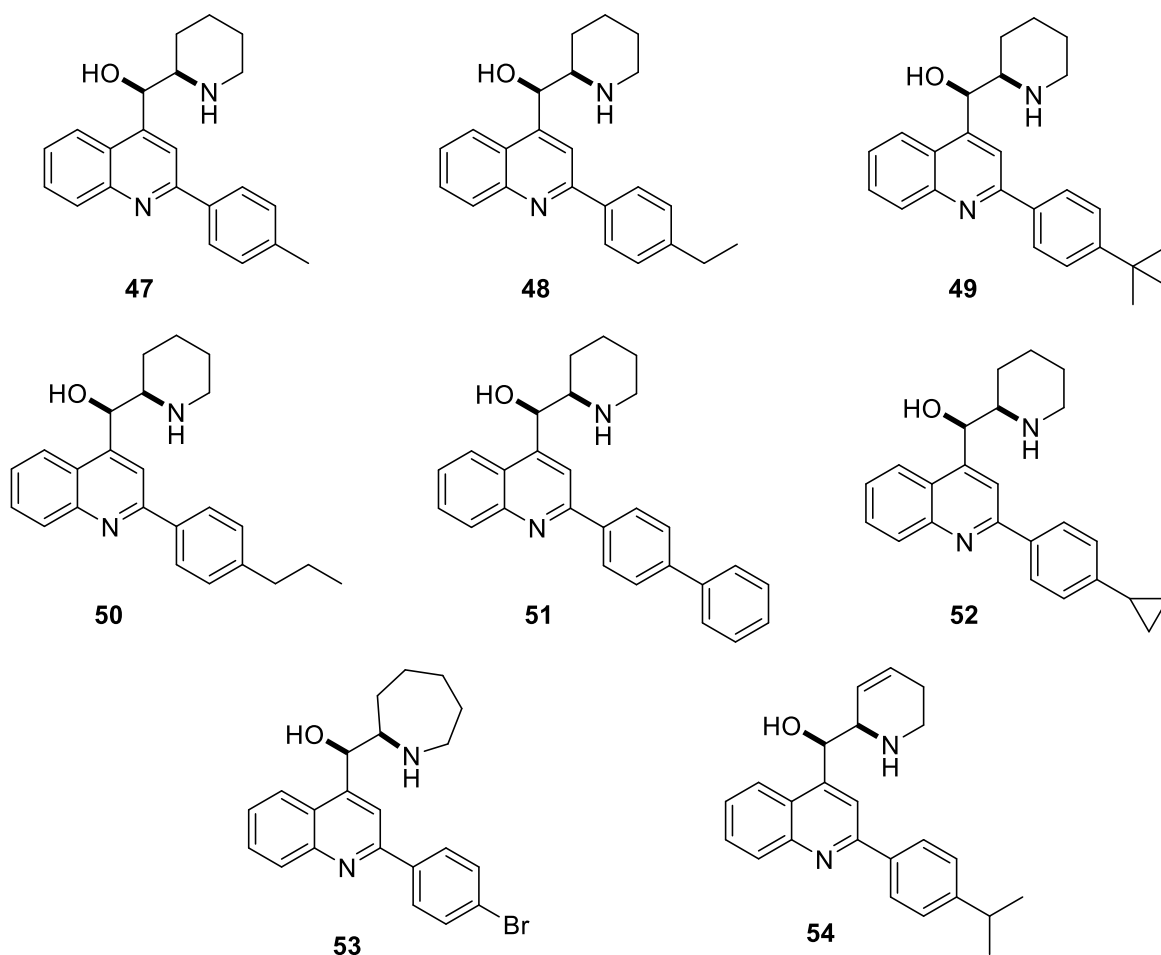


Figure 2-20: 3rd Generation vac-1 analogs with alkyl groups of variable size, a saturated azepane moiety, and dehydropiperidinyl moiety on the lead analog **23**.

Since the endocyclic alkene cannot be obtained by the stereoselective synthetic route of Ernfors and co-workers there was a desire to try and functionalize it (beyond hydrogenation) with polar or alkyl substituents. The functionalization strategies included a Simmons-Smith

cyclopropanation, and an Upjohn dihydroxylation on **54**, which would provide **55** and **56** respectively (Figure 2-21). With regards to scaffold hopping, Ernfors and co-workers showed that changing the quinoline scaffold to a pyridine or omitting the 2-(4-chlorophenyl) moiety eliminated biological activity (Figure 2-5). Based on these observations, a hop to a vac-1 indole scaffold **57** seemed desirable, as all the essential pharmacophores that are attached to the quinoline ring of vac-1 could be retained on the indole ring (Figure 2-21). This idea is particularly appealing as indoles are also known to promote methuosis, which can be seen with MOMIPP and the azaindole **17** (Figure 2-10 and Figure 2-12). Since the quinoline scaffold of vac-1 is assembled with acetophenones, preparing the indole was envisioned with an *i*-Pr acetophenone **58** and a hydrazine HCl salt **59** via a Fischer indole synthesis, then adding an aldehyde group via a Vilsmeier-Haack formylation, which could then be used for an allylboration with the allylic piperidinyl boronate (Figure 2-21)

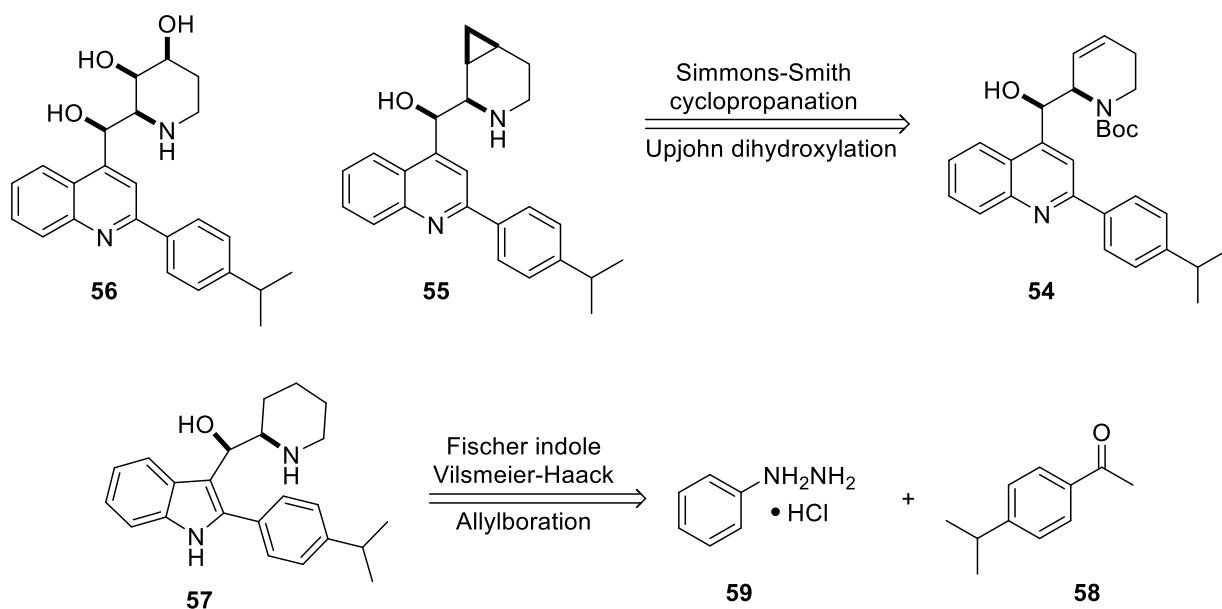
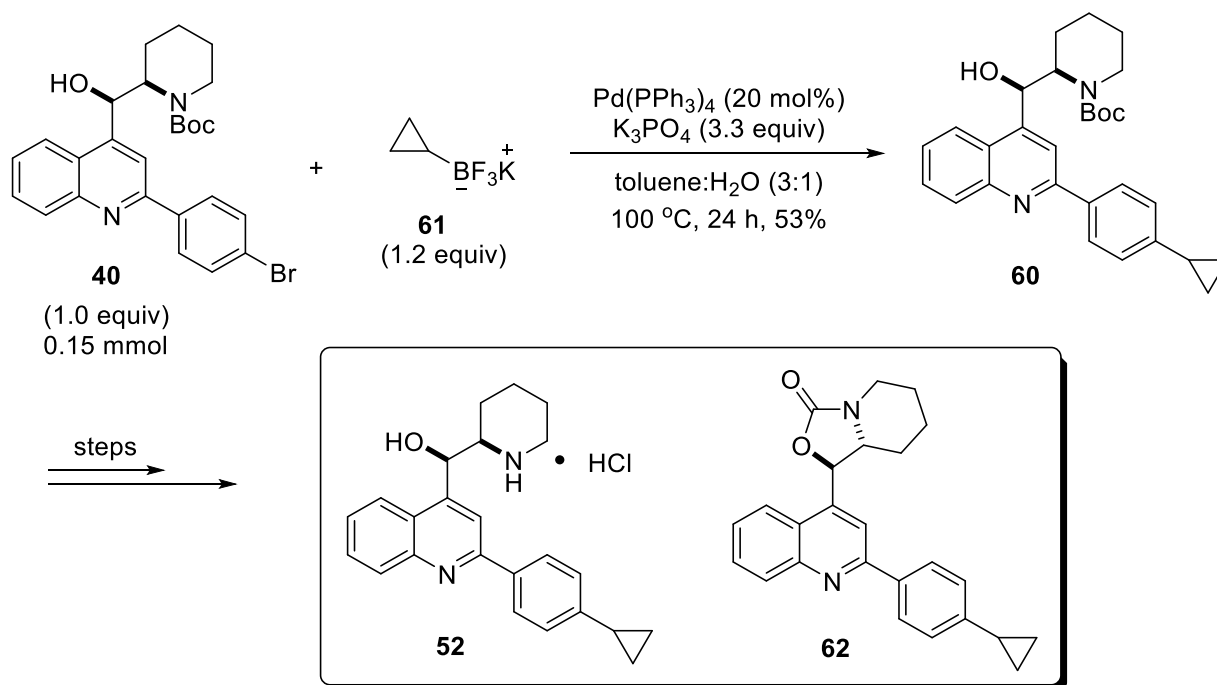


Figure 2-21: Retrosynthesis of vac-1 analogs with functionalized endocyclic alkenes, and indole scaffold.

2.9 Synthesis of 3rd Generation Vac-1 Analogs: Azepane Moiety and Indole Scaffold

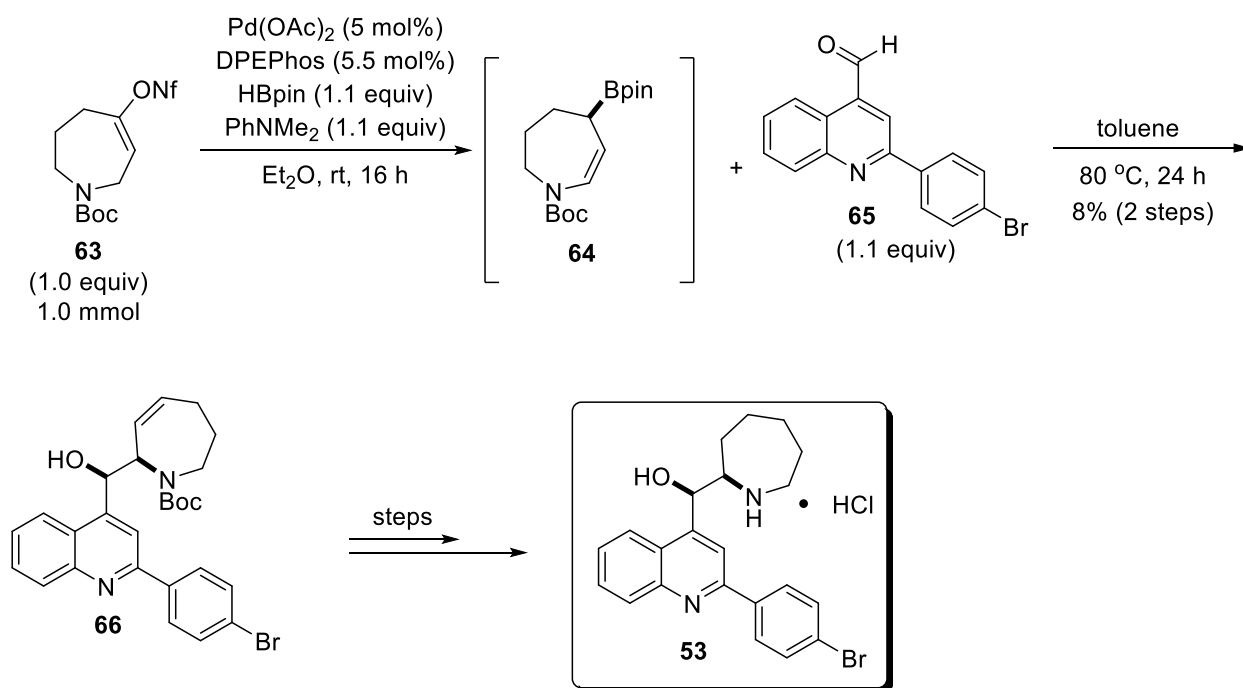
Analogs **47-51** and **54** were successfully prepared by varying the *para* substituent on the acetophenone, and then performing all the same synthetic transformations outlined in Section 2.6 for the 2nd generation vac-1 analogs. As such, these details will not be discussed here. Compounds, **52** and **53**, however, had to be prepared using alternative transformations. There was concern that a *para* cyclopropane in the benzylic position would not survive the reductive conditions of catalytic hydrogenation, so the endocyclic alkene would be saturated first, and then the cyclopropane group would be added with cross-coupling chemistry—similar to **24** and **25** (Section 2.6.1). The azepane analog **53** would be prepared using the racemic conditions developed by Clement and Hall.⁴⁵

Starting with **40**, the *para* cyclopropyl intermediate **60** was prepared via a Suzuki-Miyaura cross-coupling using potassium cyclopropyltrifluoroborate **61** following conditions developed by Deng and co-workers (Scheme 2-12).⁵⁶



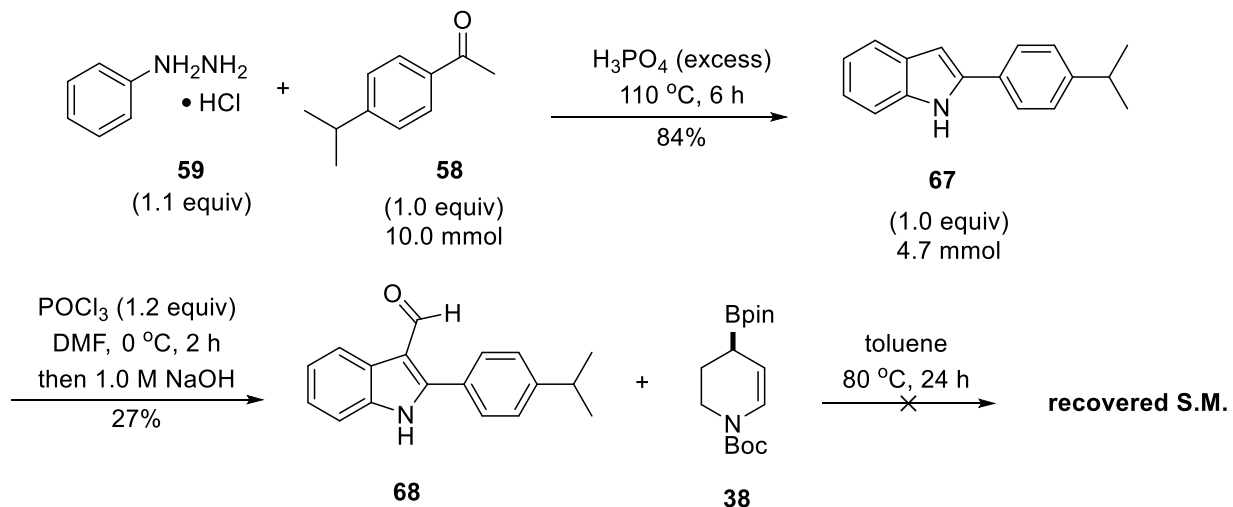
Scheme 2-12: Synthesis of cyclopropyl vac-1 analogs **52** and **62**.

Intermediate **60** was then purified by HPLC and subjected to HCl-promoted deprotection to get **52** (Section 2.6). It should be noted that a carbamate byproduct **62** formed from the Suzuki-Miyaura reaction, and this material was isolated and carried forward for testing. For azepane analog **53**, a racemic borylative migration of the *t*-Boc azepanyl nonaflate **63** formed the corresponding allylic azepanyl boronate **64**, which was reacted with quinoline aldehyde **65** to construct the dehydroazepane intermediate **66** (Scheme 2-13).⁴⁵ Hydrogenation, and deprotection steps would establish **53**.



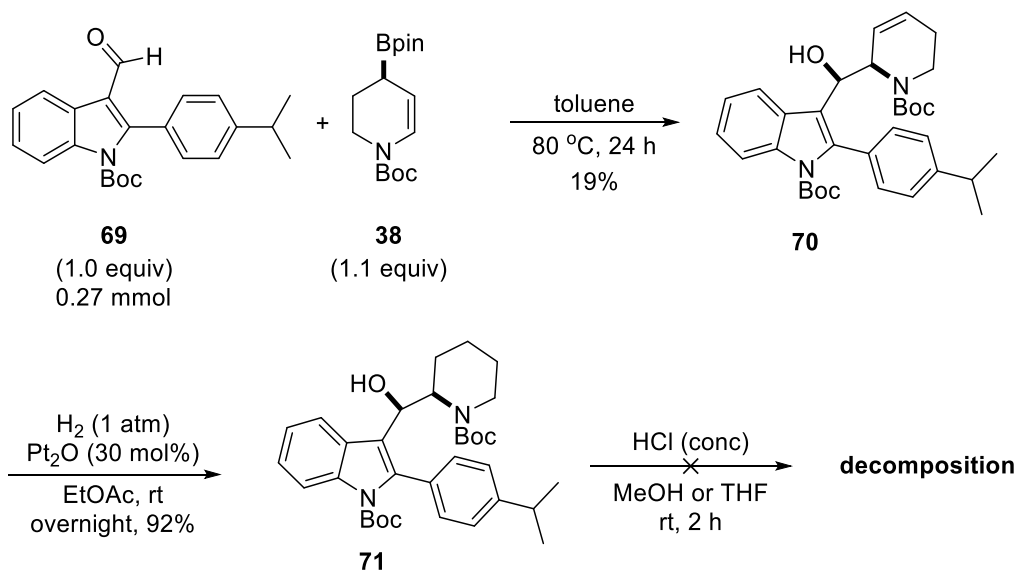
Scheme 2-13: Synthesis of azepanyl vac-1 analog **53**.

Synthesis of the vac-1 indole analog **57**, began with a Fischer indole reaction between **58** and **59**, under strongly acidic conditions, to establish the substituted indole **67** as a single regioisomer in good yield (Scheme 2-14). Vilsmeier-Haack formylation of **67** furnished the indole aldehyde **68** in modest yield.⁵⁷⁻⁵⁸



Scheme 2-14: Preparation of indole aldehyde **68** and attempted allylboration.

Several allylboration conditions were attempted on **68**, but only starting material was recovered. It was hypothesized that the free amine on the indole could be interfering with the reaction. Therefore, a *t*-Boc protected indole aldehyde **69** was synthesized, and subjected again to the thermal allylboration conditions with **38**, giving the dehydro-*vac*-1 *t*-Boc indole **70** in low yield (Scheme 2-15).

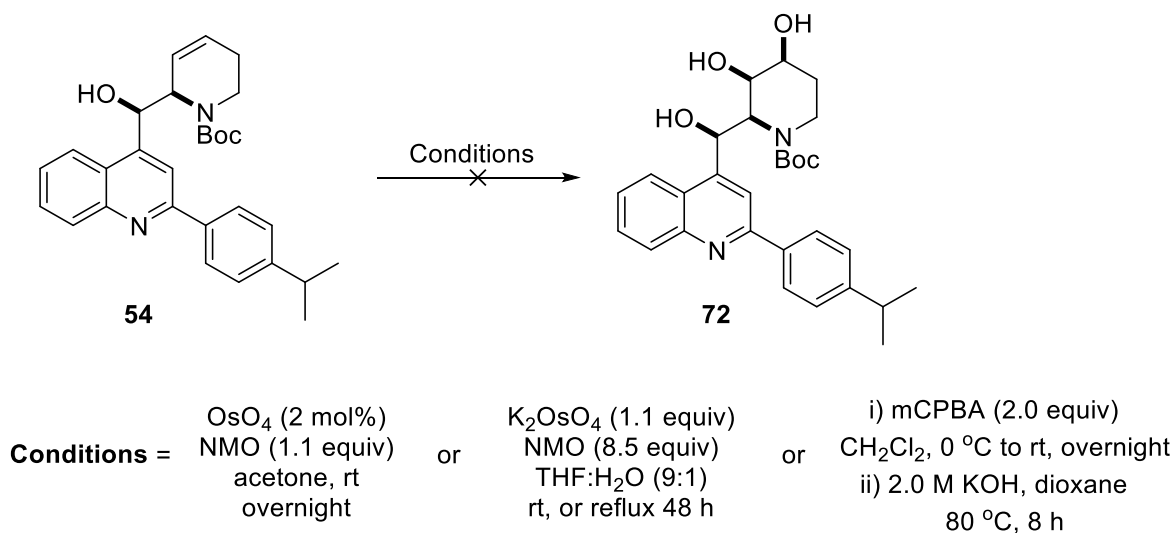


Scheme 2-15: Attempted preparation of indole *vac*-1 analog.

Hydrogenation of **70** gave the indole *t*-Boc vac-1 **71** in near quantitative yield. Unfortunately, when amine deprotection was attempted with HCl, the substrate completely decomposed. One theory towards this disappointing result is that in strongly acidic aqueous media, the indole ring can become protonated, and this could potentially lead to a variety of side reactions or decomposition.⁵⁹ Because time was limited at this point, the indole vac-1 analog was abandoned.

2.10 Synthesis of 3rd Generation Vac-1 Analogs: Endocyclic Alkene Functionalizations

The first attempts at functionalizing the endocyclic alkene were via the Upjohn dihydroxylation. The dehydro intermediate **54** was prepared according to methodologies outlined in Section 2.6, and was then subjected to the dihydroxylation conditions with a catalytic amount of osmium tetroxide (OsO₄) and stoichiometric oxidant 4-methylmorpholine N-oxide (NMO), to acquire the *t*-Boc dihydroxylated vac-1 intermediate **72** (Scheme 2-16).⁶⁰

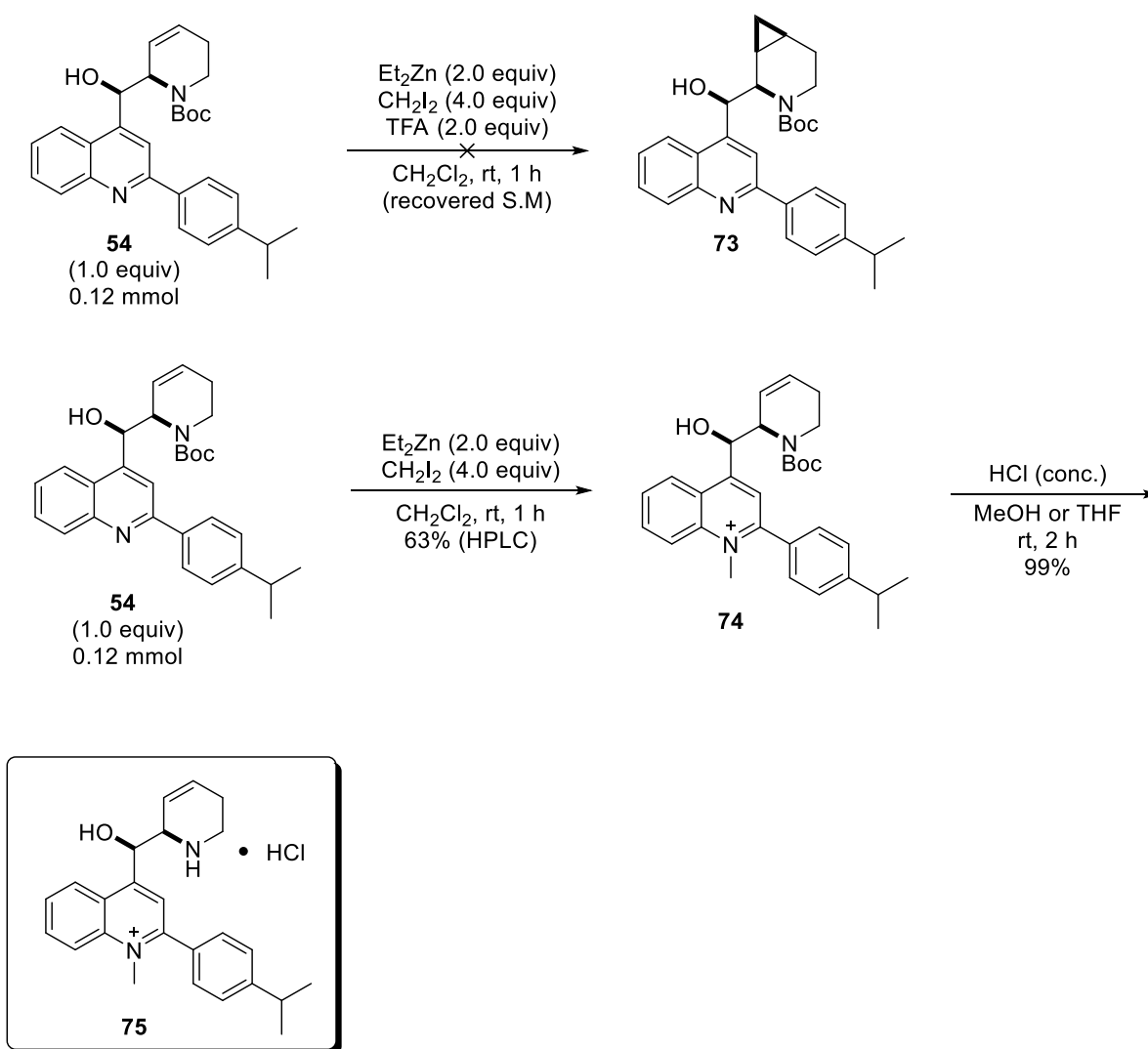


Scheme 2-16: Attempted dihydroxylation reactions on dehydro-vac-1 analog **54**.

Unfortunately, only trace amounts of the product were obtained after HPLC purification. Alternative conditions with the less volatile potassium salt of OsO₄ were attempted, but only starting material was observed despite using stoichiometric OsO₄.⁶⁰ Subjecting the reaction to reflux conditions led to decomposition. An attempt was made to epoxidize the alkene with *meta*-

chloroperbenzoic acid (mCPBA), and then to open it under strongly basic conditions, but this approach resulted in a complex mixture (Scheme 2-16).⁶⁰ Despite all these attempts, the endocyclic alkene remained very unreactive towards oxidation. As such no further dihydroxylation reactions were attempted at this time.

The next attempt at endocyclic alkene functionalization was the Simmons-Smith cyclopropanation using conditions from Davies and co-workers, where they were able to control which face the carbenoid attacked based on an allylic *t*-Boc amine, and the use or absence of TFA in the reaction (Scheme 2-17).⁶¹



Scheme 2-17: Attempted cyclopropanation, and accidental synthesis of alkylated quinolinium **75**.⁶¹

Since the amine in the dehydropiperidine is allylic to the alkene, it was thought that the facial selectivity of Davies and co-workers conditions would be applicable towards our own substrate. Thus, the dehydro intermediate **54** was subjected to both sets of conditions from Davies and co-workers, (in attempts to acquire intermediate **73**). The TFA promoted cyclopropanation returned starting material.⁶¹ On the other hand, the acid-free cyclopropanation gave full conversion to a new product; unfortunately, it was confirmed by NMR to be the dehydro-*N*-alkylated quinoline **74** (Scheme 2-17). While unsuccessful at functionalizing the endocyclic alkene, **74** had never before been observed, so it was purified by HPLC, deprotected, and the final analog **75** was submitted for testing to see if the basic quinoline nitrogen atom was a key pharmacophore.

2.11 Biological Activity of Azepanyl, Dehydropiperidinyl, Dehydro-*N*-Methyl Quinoliny, and Variable Alkyl Group Vac-1 Analogs

The first MTS assay explored the biological activity of the dehydropiperidinyl analog **54**, azepanyl analog **53**, and then compounds **18** and **23** (Figure 2-22). Unfortunately, analogs **53** and **54** had either no activity or had no significant difference against the positive control SKH 103. This indicated that the endocyclic alkene was not beneficial on the lead analog **23**, which was expected. Despite the promising activity on the dehydroazepane analog **26**, there was a lack of biological activity for azepane **53**. This disappointing result indicates that the saturated azepane ring system is not a beneficial pharmacophore. Perhaps the extra conformations of an azepane ring relative to a piperidine ring are not beneficial for binding to the biological target, and create more energetic penalties. A more erroneous result came with analogs **18** and **2**. When new samples of **18** (RMH-VI-149) and **23** (RMH-VI-177new) were tested, they had significantly reduced potency relative to the older sample of **23** (RMH-VI-177) used in prior assays. It is unlikely an issue with the assay itself, as the familiar positive control SKH 103 was active at 10 μ M. The new samples of **18** and **23** were examined by NMR, and HPLC, and there were no issues with decomposition or purity. Thus, the lack of potency likely points to an error in weighing the sample, and/or serial dilution miscalculation. Based on these conclusions, the remainder of the analogs were tested (Figure 2-23).

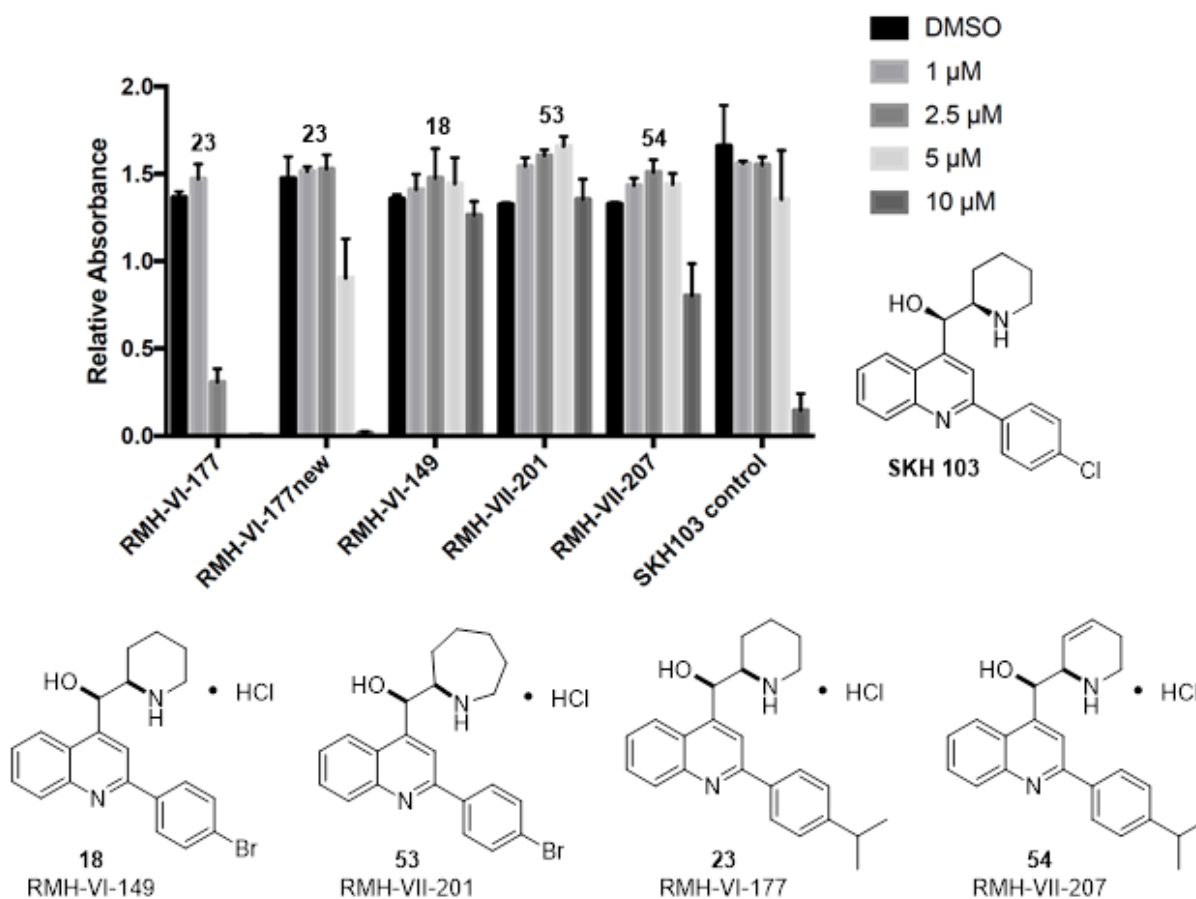


Figure 2-22: MTS assay results of dehydropiperidinyl analog **54**, azepanyl analog **53** against appropriate controls.

From this assay round there is a clear trend on which kind of *para* alkyl substituent is most beneficial for biological activity. Small alkyl groups like **47** (RMH-VIII-103) and **48** (RMH-VIII-105) either have no activity or are not more powerful than the lead. For longer chain alkyl substituents like **50** (RMH-VIII-119) there is significant activity at 10 μM and 5 μM, however, it is not nearly as powerful as the bulkier **49** (RMH-VIII-111), which has displays activity at 2.5 μM. In addition, flat rigid alkyl substituents like **52** (RMH-VIII-135) have significantly reduced potency relative to **49**, and the carbamate analog **62** (RMH-VIII-93) shows no effect—one again highlighting the importance of the free amine and hydroxy group on the 1,2-amino alcohol pharmacophore. Thus, to maximize the potency of the *para* substituent on the 2-phenyl moiety,

projecting methyl groups, greasiness, and globular steric bulk seem to be essential. While analog **51** (RMH-VIII-121) was not included in the above round of assays, it was later tested in a separate MTS assay, and had no activity at any concentrations (data not shown), which further supports the theory of large alkyl groups being necessary for activity.

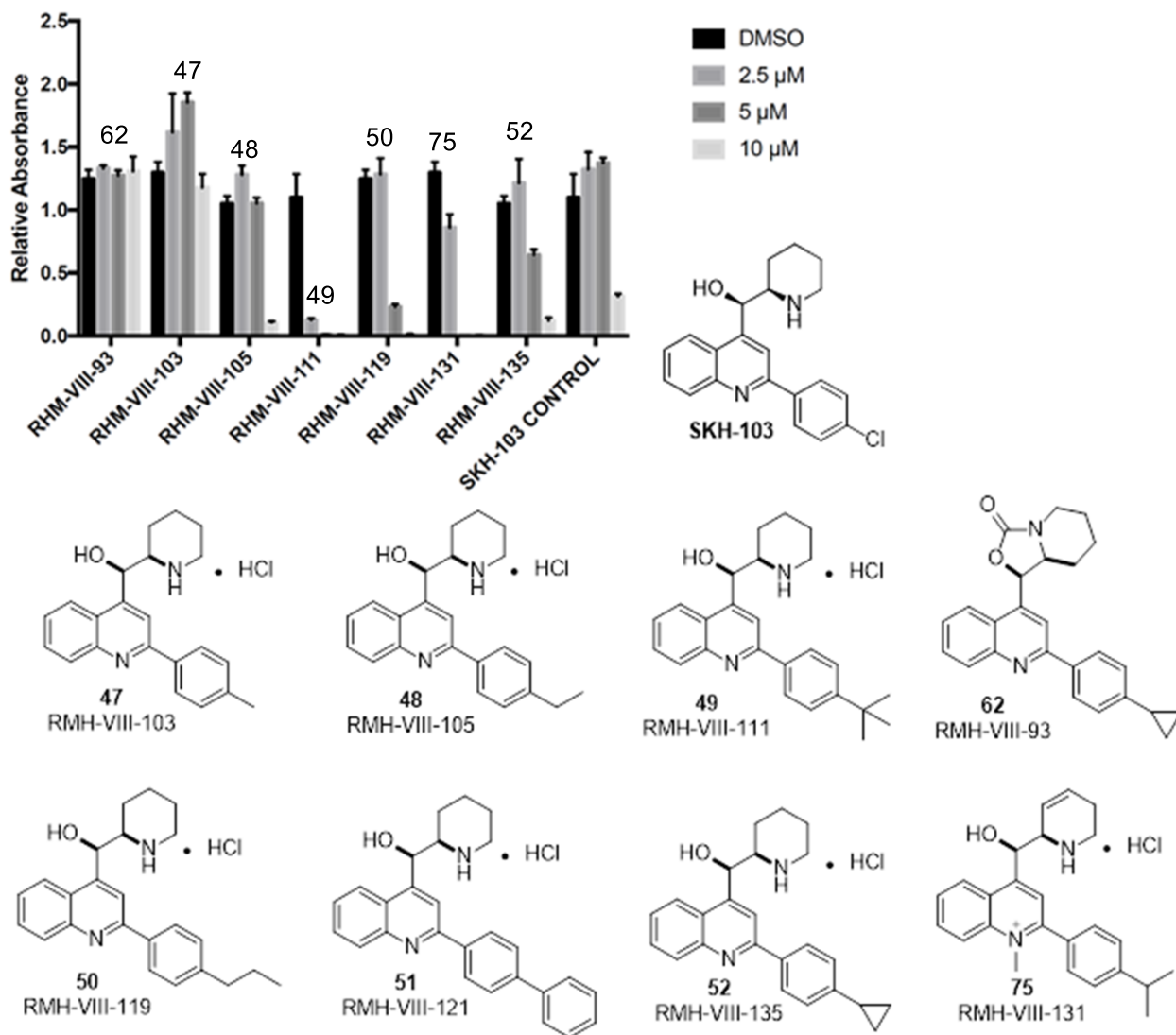


Figure 2-23: MTS assay with various alkyl/aryl vac-1 analogs, and the dehydro-*N*-alkylated quinolinium derivative against positive control SKH-103.

Another noteworthy result from this MTS assay was quinolinium **75** (RMH-VIII-131), which surprisingly, completely annihilated all GBM cells at 10 μM and 5 μM —despite having an endocyclic alkene in the piperidine moiety! To date, this is the most powerful dehydropiperidinyl vac-1 analog with comparable activity to **18**—the lead candidate at the start of this project. This result underscores the importance of a charged quinoline nitrogen as a pharmacophore, and should be explored in future endeavours to further optimize vac-1 analogs.

From the 2nd and 3rd generation of vac-1 analogs, the best results came from a *para* *i*-Pr and *t*-Bu substituent on the quinoline's 2-phenyl moiety. To test which lead candidate (**23** or **49**) was more powerful at treating GBM cells *in vitro*, Dr. Jain ran an MTS assay using A4-004 patient derived neurospheres (Figure 2-24).

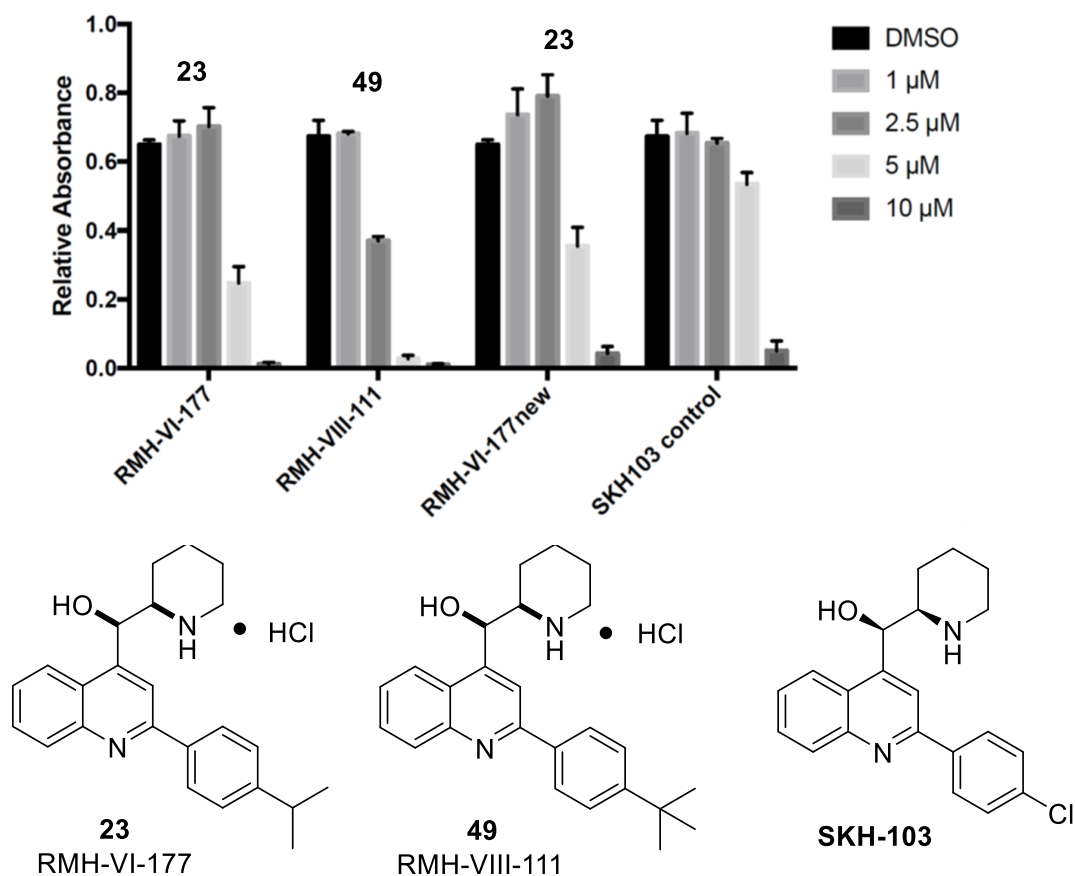


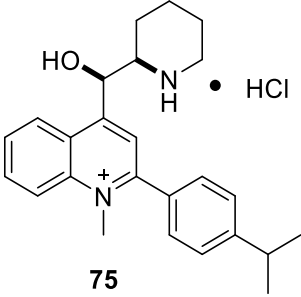
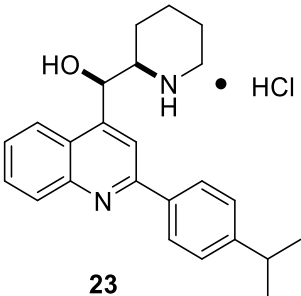
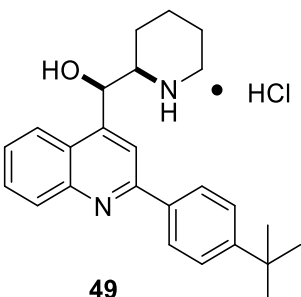
Figure 2-24: MTS assay using A4-004 patient derived neurospheres and lead alkyl vac-1 analogs, with SKH-103 serving as positive control.

Compound **49** was clearly the most potent analog against these aggressive GBM cells, with approximately 50% of GBM cells being destroyed at 2.5 μM . While **23** had good activity at 10 μM and 5 μM , it lost its efficacy at 2.5 μM . It should be noted that the new and old variants of RMH-VI-177 or **23**, which previously showed irregular activity (Figure 2-22), now had comparable activity in this assay, which supports the initially observed hypothesis that an error in weighting or serial dilutions likely resulted in the nonsensical biological activities.

2.12 Summary and Future Work

A set of 2nd generation of vac-1 analogs was prepared in attempts to optimize the lead candidate **18** discovered by Kwok and Hall. *Nonclassical* and *classical* bioisosteric replacement, as well as switching the piperidine moiety with a dehydro-azepane, was employed to generate this new library. The most beneficial substitution that increased potency was a *para i*-Pr group on the 2-phenyl moiety giving the next lead compound **23**, polar functional groups, π -systems, or larger atoms provided no improvements in activity. Dehydro-azepane showed a slight increase in potency, but ultimately was not beneficial when saturated. Compound **23** spawned a 3rd generation of vac-1 analogs looking primarily at larger alkyl groups, while also attempting to functionalize the endocyclic alkene and exploring scaffold hopping to a disubstituted indole. The endocyclic alkene was inert towards oxidation conditions, and carbenoid chemistry, which prevented the development of new analogs. The indole scaffold was successfully synthesized and could undergo allylboration when the amine was protected; however, its instability towards strong acids prevented a final access to the new analog. Of the various alkyl groups on the new vac-1 analogs, the best results came from globular groups that were sterically encumbered with projecting methyl substituents. Smaller alkyl substituents, or linear alkyl chains had either no activity or were less potent than the *i*-Pr-substituted analog **23**. A *N*-methyl quinolinium analog **75**, (which was accidentally synthesized) had surprisingly good potency despite having a dehydro-piperidine moiety. This analog suggests that the nitrogen atom in the quinoline ring is a promising pharmacophore to optimize. Lastly, a head-to-head comparison of compound **23** to its *t*-Bu sibling **49** using patient-derived GBM cells revealed that compound **49** is more active at 2.5 μM compared to compound **23**. Thus, analog **49** became the new lead candidate of all the new vac-1 analogs

synthesized to date, and future studies will continue to further optimize. The best three vac-1 analogs are summarized below.

Analogs	% Inhibition GBM Cells (10 μ M)	% Inhibition GBM Cells (5 μ M)	% Inhibition GBM Cells (2.5 μ M)
 <p>75</p>	95% ¹	95% ¹	0% ¹
 <p>23</p>	95% ²	33% ²	0% ²
 <p>49</p>	95% ²	90% ²	50% ²

¹ GBM cells derived from serum-based U251 cell lines

² GBM neurospheres derived from patient cell lines

Table 2-2: Summary of biological activity for lead vac-1 analogs **75**, **23**, and **49**.

For future studies, an IC_{50} of lead **49** in Table 2-2 should be obtained and tested against a series of other GBM cell lines to get a sense of its ability as a drug candidate, and to determine if it is a worthwhile compound for *in vivo* studies to acquire its pharmacokinetic and physicochemical properties. In terms of future optimization, all four stereoisomers of main lead **49** should be synthesized and tested with the MTS assay. Ernfors and co-workers revealed that the *erythro* isomers of vac-1 were significantly more active, compared to the *threo* congeners. There is the chance that compound **49** will be even more potent when an enantioenriched *erythro* isomer is tested (Figure 2-25).²⁶ Another avenue to explore would be replacing the *t*-Bu group with an even larger alkyl substituent, like an adamantyl group (analog **76**).

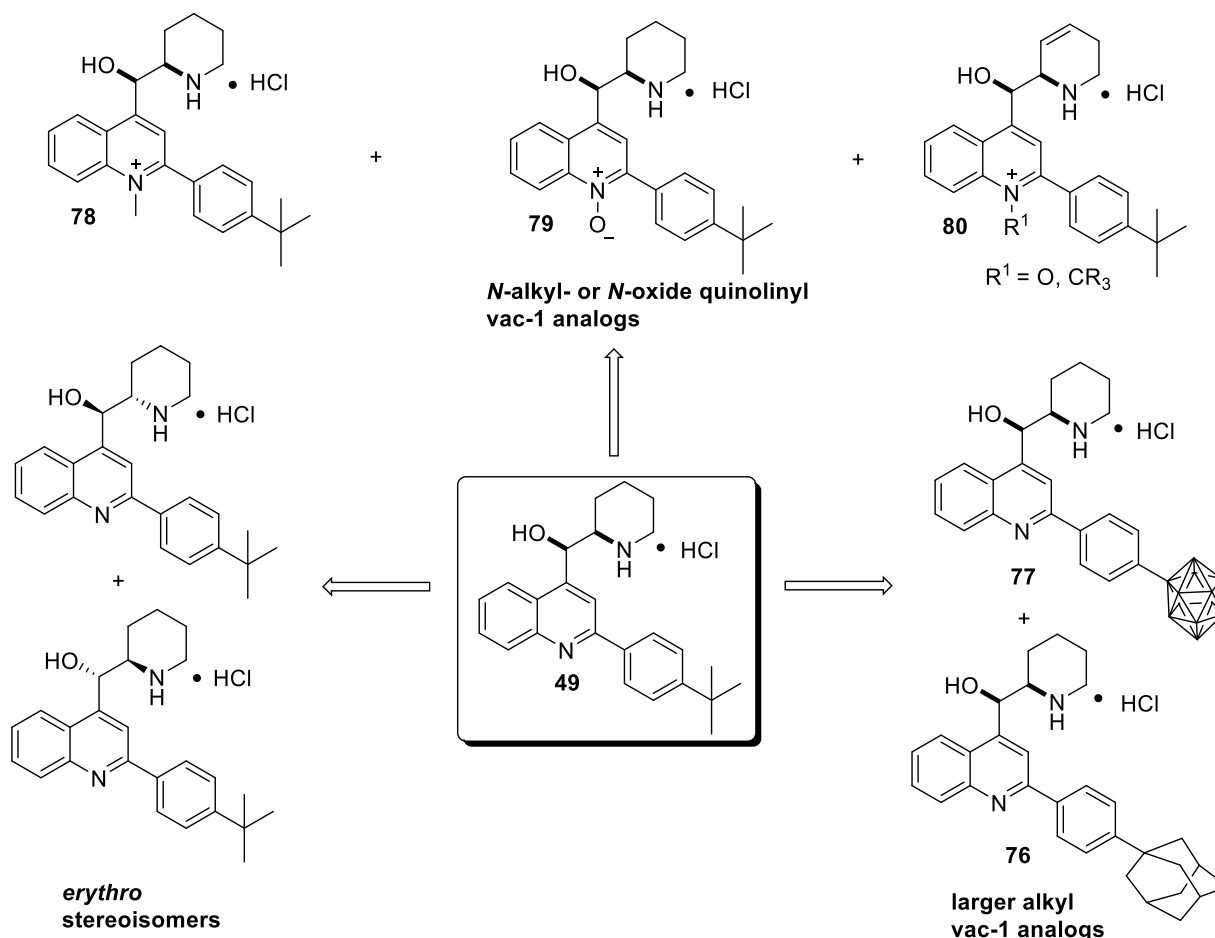


Figure 2-25: Potential functionalization of lead candidate **49** to improve biological activity.

Another functional group of comparable size to an adamantyl group would be a boron cluster (analog **77**). This is a particularly appealing group, as it has been shown that boron clusters have high *in vitro* uptake in GBM cells, and it opens up the therapeutic window of boron-neutron capture therapy (BNCT) to treat GBM, along with the nonapoptotic cell death induced by methuosis—creating a potential polypharmacological agent.⁶³ Since there was such an improvement in potency for *N*-methyl quinolinium **75**, alkylating the quinoline or forming a *N*-quinolinyl oxide should be attempted on **49** to give analogs **78** and **79**. This approach is also appealing, because if the nitrogen is functionalized, it may then be possible to cyclopropanate the endocyclic alkene, or the alkene could remain intact to give analog **80**. If functionalizing the endocyclic alkene to a diol is to be attempted again, a more powerful reagent could be employed, such as potassium permanganate (KMnO₄), or perhaps a Prévost reaction could give the desired product. Lastly, if the *vac*-1 indole analogs are to be attempted again, a more powerful EWG protecting group should be used on the indole amine, like a trifluoroacetamide, which could facilitate a more efficient allylboration. Another option could be a Lewis acid catalyzed allylboration. If successful, then a weaker acid should be used for *t*-Boc removal, like TFA, as this will likely keep the indole intact and give the final product.

2.13 Experimental Procedures

2.13.1 General Information

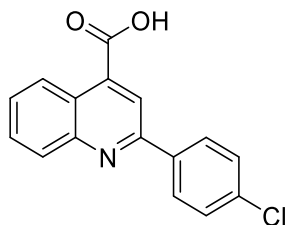
Unless otherwise indicated, all reactions were performed under a nitrogen atmosphere using glassware that was washed thoroughly with water and acetone and flame-dried *in vacuo* prior to use. Toluene, dimethylformamide, tetrahydrofuran, and dichloromethane were used directly from a MBraun Solvent Purification System. Diethyl ether was distilled over sodium/benzophenone ketyl in a solvent still. *N,N*-Dimethylaniline, *N,N'*-dimethylethylenediamine, diisopropylamine, diiodomethane, phosphoryl chloride, and thionyl chloride were purchased from Sigma Aldrich, and distilled prior to use. Trimethylsilyl acetylene (reagent grade, 98%), 1,8-Diazabicyclo[5.4.0]undec-7-ene (reagent grade, 98%), phenyl silane (reagent grade, 97%), *tert*-butyl hydroperoxide solution (5.5 M in nonane), diethyl zinc (1.0 M in hexanes), 1-boc-piperidone (reagent grade, 98%), and perfluorobutanesulfonyl fluoride (reagent

grade, 96%); Adam's Catalyst (reagent grade, >99%) palladium (II) acetate (reagent grade, >99%), DPEPhos (reagent grade, >97%), were respectively purchased from Sigma Aldrich, Combi-Blocks Inc. and Strem Chemical Inc.; and used without further purification. Pinacolborane (reagent grade, >97%) was purchased from Oakwood Chemicals and used without further purification. Thin layer chromatography (TLC) was performed on Merck Silica Gel 60 F254 plates, and visualized with UV light, KMnO₄, and PMA stain. Flash chromatography was performed on ultra-pure silica gel 230-400 mesh. Nuclear magnetic resonance (NMR) spectra were recorded on Agilent/Varian INOVA-400, INOVA-500, INOVA-600, or INOVA-700 MHz instruments. ¹H NMR data are presented as follows: chemical shift in ppm downfield from tetramethylsilane (multiplicity, coupling constant, integration). High resolution mass spectra were recorded by the University of Alberta Mass Spectrometry Services Laboratory using either electron impact (EI) ion source with double focusing sector analyzer (Kratos Analytical MS-50G), or electrospray (ESI) ion source with orthogonal acceleration TOF analyzer (Agilent Technologies 6220 oaTOF). Infrared spectra (performed on a Nicolet Magna-IR 750 instrument equipped with a Nic-Plan microscope) were recorded by the University of Alberta Analytical and Instrumentation Laboratory. Biological activity of vac-1 analogs were determined by CellTiter 96® Aqueous One Solution Cell Proliferation Assay (MTS), using U251 or patient derived neurosphere GBM cells. The *t*-Boc protected vac-1 analogs were purified on an HPLC Agilent instrument using a SB-C18 column, (250mm, 5µm) with the following instrument conditions and eluent: 0.6mL/min, 40 °C M.P.A: 0.1% acetic acid/formic acid/TFA in H₂O M.P.B: 0.1% acetic acid/formic acid/TFA in acetonitrile.

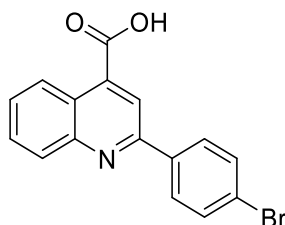
2.13.2 General Procedure for the Synthesis of Quinoline Carboxylic Acids

Potassium hydroxide (10.0 g) and distilled water (15.0 mL) were added to a 100 mL round bottom flask with a stir bar. The reagents were stirred until a clear solution formed, then isatin **30** (1.60 g, 10.6 mmol, 1.05 equiv) was added, forming a clear dark red solution. *Para* substituted acetophenone **31** (1.50 g, 10.1 mmol, 1.00 equiv) was added in one portion to the solution, followed by 95% ethanol (15.0 mL). A condenser was equipped to the round bottom flask, the reaction heated to 110 °C, and stirred overnight. The reaction was cooled to rt, and poured into a 250 mL Erlenmeyer flask. The opaque yellow solution was then acidified to pH 0-1 with concentrated hydrochloric acid, and the free carboxylic acid **32** precipitated out of solution. The

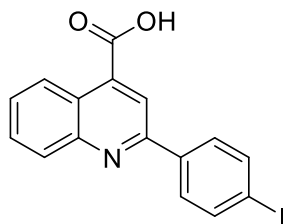
crude acid was collected by vacuum filtration, and washed with water (50.0 mL) and ethyl acetate (50.0 mL). The acid was then recrystallized with methanol and water, and dried on the rotovap and high vacuum to remove any residual water.



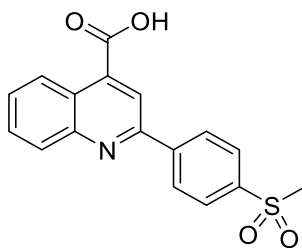
2-(4-chlorophenyl)-4-quinolinecarboxylic acid (32a): Yellow solid (80% yield). $^1\text{H NMR}$ (500 MHz, DMSO- d_6) δ 8.63 (app d, $J = 8.0$ Hz, 1H), 8.45 (s, 1H), 8.31 (app d, $J = 9.0$ Hz, 2H), 8.14 (app d, $J = 8.0$ Hz, 1H), 7.84 (ddd, $J = 8.0$ Hz, 7.0 Hz, 1.0 Hz, 1H), 7.69 (ddd, $J = 8.0$ Hz, 7.0 Hz, 1.0 Hz, 1H), 7.60 (app d, $J = 9.0$ Hz, 2H); $^{13}\text{C NMR}$ (125 MHz, DMSO- d_6) δ 167.5, 154.5, 148.3, 137.8, 136.6, 134.9, 130.3, 129.7, 128.9, 127.9, 125.4, 123.5, 118.9; **IR** (solid, cm^{-1}): 3097, 2507, 1979, 1704, 1594, 1552, 1512, 1497, 1282, 1095, 1011; **HRMS** (ESI) for $(\text{M}-\text{H})^-$ $\text{C}_{16}\text{H}_9\text{ClNO}_2$: calcd. 282.0327; found 282.0320.



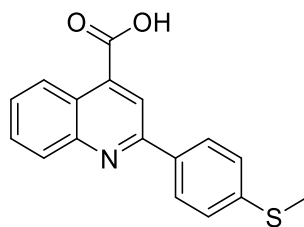
2-(4-bromophenyl)-4-quinolinecarboxylic acid (32b): Yellow solid (58% yield). $^1\text{H NMR}$ (500 MHz, DMSO- d_6) δ 8.63 (app d, $J = 8.0$ Hz, 1H), 8.45 (s, 1H), 8.24 (app d, $J = 8.5$ Hz, 2H), 8.14 (app d, $J = 8.0$ Hz, 1H), 7.84 (ddd, $J = 8.5$ Hz, 7.5 Hz, 1.0 Hz, 1H), 7.74 (app d, $J = 8.5$ Hz, 2H), 7.70 (ddd, $J = 8.0$ Hz, 7.5 Hz, 1.0 Hz, 1H); $^{13}\text{C NMR}$ (125 MHz, DMSO- d_6) δ 167.5, 154.6, 148.3, 137.8, 136.9, 131.9, 130.3, 129.7, 129.2, 127.9, 125.4, 123.7, 123.5, 118.9; **IR** (solid, cm^{-1}): 3092, 2482, 1951, 1708, 1590, 1401, 1247, 1077, 1007; **HRMS** (ESI) for $(\text{M}-\text{H})^-$ $\text{C}_{16}\text{H}_9\text{BrNO}_2$: calcd. 325.9822; found 325.9819.



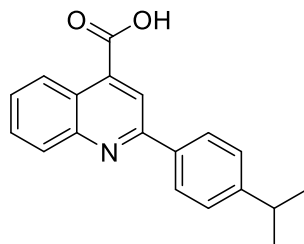
2-(4-iodophenyl)-4-quinolinecarboxylic acid (32c): Brown solid (46% yield). $^1\text{H NMR}$ (500 MHz, DMSO- d_6) δ 8.61 (app d, $J = 8.0$ Hz, 1H), 8.43 (s, 1H), 8.14 (app d, $J = 8.0$ Hz, 1H), 8.07 (dt, $J = 9.0$ Hz, 2.0 Hz, 2H), 7.91 (dt, $J = 9.0$ Hz, 2.0 Hz, 2H), 7.83 (ddd, $J = 8.0$ Hz, 6.5 Hz, 1.5 Hz, 1H), 7.69 (ddd, $J = 8.0$ Hz, 6.5 Hz, 1.0 Hz, 1H); $^{13}\text{C NMR}$ (125 MHz, DMSO- d_6) δ 167.5, 154.8, 148.2, 137.8, 137.3, 130.3, 129.7, 129.1, 127.9, 125.4, 123.5, 118.8, 97.3; **IR** (solid, cm^{-1}): 3271, 2509, 1983, 1725, 1634, 1493, 1369, 1198, 1005; **HRMS** (ESI) for $(\text{M}-\text{H})^-$ $\text{C}_{16}\text{H}_9\text{INO}_2$: calcd. 373.9683; found 373.9682.



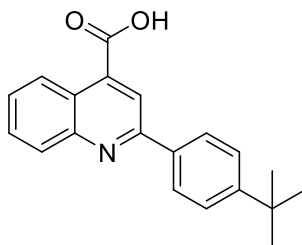
2-[4-(methylsulfonyl)phenyl]-4-quinolinecarboxylic acid (32d): Yellow solid (57% yield). $^1\text{H NMR}$ (400 MHz, DMSO- d_6) δ 8.68 (app d, $J = 7.6$ Hz, 1H), 8.57 (app d, $J = 8.4$ Hz, 2H), 8.56 (s, 1H), 8.23 (app d, $J = 7.6$ Hz, 1H), 8.13 (app d, $J = 8.4$ Hz, 2H), 7.91 (ddd, $J = 7.6$ Hz, 5.6 Hz, 1.6 Hz, 1H), 7.77 (ddd, $J = 7.6$ Hz, 5.6 Hz, 1.6 Hz, 1H), 3.31 (s, 3H); $^{13}\text{C NMR}$ (125 MHz, DMSO- d_6) δ 167.4, 154.1, 148.3, 142.4, 141.7, 138.0, 130.5, 129.9, 128.5, 128.1, 127.6, 127.3, 125.4, 123.8, 119.4, 43.5; **IR** (solid, cm^{-1}): 3394, 3067, 2647, 1909, 1715, 1633, 1597, 1299, 1146; **HRMS** (ESI) for $(\text{M}-\text{H})^-$ $\text{C}_{17}\text{H}_{12}\text{NO}_4\text{S}$: calcd. 326.0493; found 326.0488.



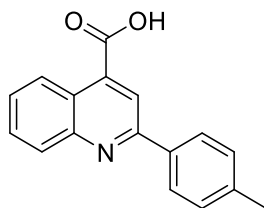
2-[4-(methylsulfonyl)phenyl]-4-quinolinecarboxylic acid (32e): Orange-red solid (82% yield). **¹H NMR** (500 MHz, DMSO-*d*₆) δ 8.60 (app d, *J* = 8.5 Hz, 1H), 8.42 (s, 1H), 8.23 (dt, *J* = 8.5 Hz, 2.5 Hz, 2H), 8.15 (app d, *J* = 8.5 Hz, 1H), 7.83 (ddd, *J* = 8.5 Hz, 6.5 Hz, 1.0 Hz, 1H), 7.67 (ddd, *J* = 8.5 Hz, 6.5 Hz, 1.0 Hz, 1H), 7.41 (dt, *J* = 8.5 Hz, 2.5 Hz, 2H), 2.53 (s, 3H); **¹³C NMR** (125 MHz, DMSO-*d*₆) δ 167.4, 155.1, 147.8, 141.3, 138.0, 133.7, 130.4, 129.2, 127.7, 125.8, 125.4, 123.3, 118.9, 14.2; **IR** (solid, cm⁻¹): 3382, 2920, 2660, 2548, 1982, 1719, 1634, 1597, 1500, 1411, 1303, 1201, 1099; **HRMS** (ESI) for (M-H)⁻ C₁₇H₁₂NO₂S: calcd. 295.0594; found 295.0591.



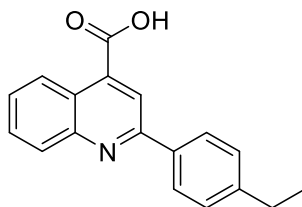
2-(4-isopropylphenyl)-4-quinolinecarboxylic acid (32f): Yellow solid (78% yield). **¹H NMR** (500 MHz, DMSO-*d*₆) δ 8.61 (app d, *J* = 8.5 Hz, 1H), 8.41 (s, 1H), 8.19 (dt, *J* = 8.5 Hz, 2.0 Hz, 2H), 8.16 (app d, *J* = 8.5 Hz, 1H), 7.83 (ddd, *J* = 8.5 Hz, 7.0 Hz, 1.5 Hz, 1H), 7.68 (ddd, *J* = 8.5 Hz, 7.0 Hz, 1.5 Hz, 1H), 7.42 (dt, *J* = 8.5 Hz, 2.0 Hz, 2H), 2.95 (sep, *J* = 7.0 Hz, 1H), 1.23 (d, *J* = 7.0 Hz, 6H); **¹³C NMR** (125 MHz, DMSO-*d*₆) δ 167.4, 155.7, 150.7, 147.8, 138.0, 135.1, 130.4, 129.1, 127.7, 127.4, 126.9, 125.4, 123.3, 119.1, 33.3, 23.7; **IR** (solid, cm⁻¹): 3058, 2955, 2922, 2870, 1922, 1698, 1642, 1612, 1589, 1546, 1281, 1232; **HRMS** (ESI) for (M-H)⁻ C₁₉H₁₆NO₂: calcd. 290.1187; found 290.1189.



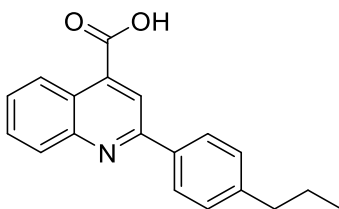
2-(4-*tert*-butylphenyl)-4-quinolinecarboxylic acid (32g): Yellow solid (72% yield). $^1\text{H NMR}$ (500 MHz, DMSO- d_6) δ 8.63 (app d, $J = 8.5$ Hz, 1H), 8.42 (s, 1H), 8.20 (app dt, $J = 8.5$ Hz, 2.0 Hz, 2H), 8.14 (d, $J = 8.5$ Hz, 1H), 7.83 (ddd, $J = 8.5$ Hz, 7.0 Hz, 1.5 Hz, 1H), 7.68 (ddd, $J = 8.5$ Hz, 7.0 Hz, 1.5 Hz, 1H), 7.56 (app dt, $J = 8.5$ Hz, 2.0 Hz, 2H), 1.33 (s, 9H); $^{13}\text{C NMR}$ (125 MHz, DMSO- d_6) δ 167.7, 155.7, 152.6, 148.4, 138.2, 135.2, 130.0, 129.6, 127.4, 126.9, 125.7, 125.5, 123.4, 118.7, 34.5, 31.0; **IR** (solid, cm^{-1}): 3349, 3082, 2962, 2903, 2869, 1699, 1656, 1594, 1419, 1366, 1231, 1112; **HRMS** (ESI) for $(\text{M}-\text{H})^-$ $\text{C}_{20}\text{H}_{20}\text{NO}_2$: calcd. 306.1494; found 306.1489.



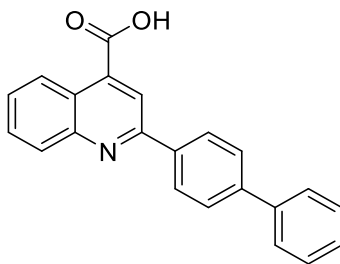
2-(4-methylphenyl)-4-quinolinecarboxylic acid (32h): Light brown crystals (33% yield). $^1\text{H NMR}$ (600 MHz, DMSO- d_6) δ 8.63 (app d, $J = 8.4$ Hz, 1H), 8.42 (s, 1H), 8.19 (app d, $J = 8.4$ Hz, 2H), 8.13 (app d, $J = 8.4$ Hz, 1H), 7.83 (ddd, $J = 8.4$ Hz, 6.6 Hz, 1.2 Hz, 1H), 7.67 (ddd, $J = 8.4$ Hz, 6.6 Hz, 1.2 Hz, 1H), 7.36 (app d, $J = 8.4$ Hz, 2H), 2.38 (s, 3H); $^{13}\text{C NMR}$ (125 MHz, DMSO- d_6) δ 167.6, 155.7, 148.4, 139.7, 137.5, 135.1, 130.1, 129.6, 129.5, 127.5, 127.1, 125.3, 123.3, 118.9, 20.9; **IR** (solid, cm^{-1}): 3066, 2919, 2511, 1933, 1713, 1602, 1548, 1230, 1194; **HRMS** (ESI) for $(\text{M}-\text{H})^-$ $\text{C}_{17}\text{H}_{12}\text{NO}_2$: calcd. 262.0874; found 262.0870.



2-(4-ethylphenyl)-4-quinolinecarboxylic acid (32i): Light brown solid (64% yield). $^1\text{H NMR}$ (500 MHz, DMSO- d_6) δ 8.61 (app d, $J = 8.0$ Hz, 1H), 8.41 (s, 1H), 8.19 (app d, $J = 8.5$ Hz, 2H), 8.12 (app d, $J = 8.0$ Hz, 1H), 7.81 (ddd, $J = 8.5$ Hz, 7.0 Hz, 1.5 Hz, 1H), 7.66 (ddd, $J = 8.5$ Hz, 7.0 Hz, 1.5 Hz, 1H), 7.38 (app d, $J = 8.5$ Hz, 2H), 2.66 (q, $J = 7.5$ Hz, 2H), 1.21 (d, $J = 7.5$ Hz, 3H); $^{13}\text{C NMR}$ (125 MHz, DMSO- d_6) δ 167.6, 155.7, 148.3, 145.9, 137.5, 135.4, 130.1, 129.6, 128.4, 128.3, 127.5, 127.2, 125.3, 123.3, 118.9, 26.6, 15.4; **IR** (solid, cm^{-1}): 3064, 2969, 2932, 2619, 1908, 1719, 1632, 1608, 1511, 1478, 1311, 1245; **HRMS** (ESI) for $(\text{M}-\text{H})^-$ $\text{C}_{18}\text{H}_{14}\text{NO}_2$: calcd. 276.1030; found 276.1033.



2-(4-propylphenyl)-4-quinolinecarboxylic acid (32j): Beige solid (80% yield). $^1\text{H NMR}$ (600 MHz, DMSO- d_6) δ 8.63 (app d, $J = 7.8$ Hz, 1H), 8.42 (s, 1H), 8.20 (app d, $J = 7.8$ Hz, 2H), 8.14 (app d, $J = 7.8$ Hz, 1H), 7.83 (ddd, $J = 8.4$ Hz, 7.2 Hz, 1.2 Hz, 1H), 7.68 (ddd, $J = 8.4$ Hz, 7.3 Hz, 1.2 Hz, 1H), 7.38 (app d, $J = 7.8$ Hz, 2H), 2.64 (t, $J = 7.2$ Hz, 2H), 1.64 (sext, $J = 7.2$ Hz, 2H), 0.92 (t, $J = 7.2$ Hz, 3H); $^{13}\text{C NMR}$ (125 MHz, DMSO- d_6) δ 167.6, 155.8, 148.4, 144.3, 137.6, 135.4, 130.1, 129.6, 128.9, 127.5, 127.0, 125.3, 123.3, 118.9, 37.0, 23.9, 13.6; **IR** (solid, cm^{-1}): 3032, 2959, 2930, 2870, 1713, 1611, 1592, 1375, 1340, 1233, 1194; **HRMS** (ESI) for $(\text{M}-\text{H})^-$ $\text{C}_{19}\text{H}_{16}\text{NO}_2$: calcd. 290.1187; found 290.1188.

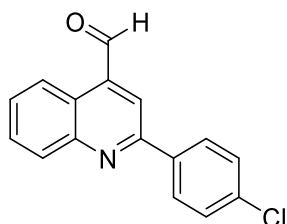


2-(4-biphenyl)-4-quinolinecarboxylic acid (32k): Bright yellow solid (80% yield). $^1\text{H NMR}$ (500 MHz, DMSO- d_6) δ 8.64 (app d, $J = 8.5$ Hz, 1H), 8.50 (s, 1H), 8.39 (app d, $J = 8.5$ Hz, 2H), 8.17 (app d, $J = 8.5$ Hz, 1H), 7.86 (m, 3H), 7.76 (app d, $J = 8.0$ Hz, 2H), 7.69 (ddd, $J = 8.5$ Hz, 7.0 Hz, 1.5 Hz, 1H), 7.50 (app t, $J = 7.5$ Hz, 2H), 7.40 (app t, $J = 7.5$ Hz, 1H); $^{13}\text{C NMR}$ (125 MHz, DMSO- d_6) δ 167.6, 155.3, 148.4, 141.5, 139.3, 137.6, 136.8, 130.2, 129.7, 129.0, 127.9, 127.8, 127.2, 126.7, 125.4, 123.4, 119.0; **IR** (solid, cm^{-1}): 3067, 3032, 1717, 1606, 1412, 1373, 1326, 1249, 1203; **HRMS** (ESI) for $(\text{M}-\text{H})^-$ $\text{C}_{22}\text{H}_{16}\text{NO}_2$: calcd. 326.1176; found 326.1173.

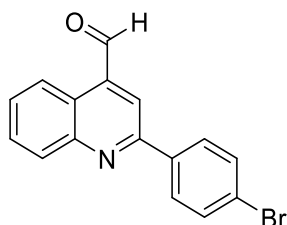
2.13.3 General Procedure for the Synthesis of Quinoline Aldehydes

To a flame-dried 100 mL round bottom flask with stir bar was added quinoline carboxylic acid **32** (1.25 g, 3.80 mmol, 1.00 equiv), and thionyl chloride (10.0 mL). A condenser with a drying tube calcium chloride trap was equipped to the round bottom flask, and the reaction stirred, forming a yellow slurry. The reaction heated to 95 °C, and was stirred for 2 h forming a clear orange solution. The mixture was concentrated *in vacuo* giving the crude acid chloride intermediate as a yellow solid. Methanol (20.0 mL) was added to the round bottom flask with stirring to form the methyl ester **34**. Sodium borohydride (0.719 g, 19.0 mmol, 5.00 equiv) was then added slowly in portions to the solution of **34**. A condenser was equipped to the round bottom flask, the reaction heated to 75 °C, and stirred overnight. The reaction cooled to rt, and was quenched with saturated ammonium chloride (20.0 mL) and water (20.0 mL), which precipitated out the quinoline alcohol, or a mixture of the alcohol and **34**. The crude solid was collected by vacuum filtration, triturated with 1 M sodium hydroxide (50.0 mL) and water (50.0 mL), and dried on high vacuum. Without further purification, the crude alcohol intermediate and Dess-Martin Periodinane (2.42 g, 5.70 mmol, 1.50 equiv) were added to another flame-dried 100 mL round bottom flask with stir bar, and the flask was evacuated and backfilled with nitrogen for three cycles.

A 1:4 mixture of tetrahydrofuran to dichloromethane (40.0 mL) was added to the round bottom flask, and the reaction stirred at rt, forming a dark red-brown solution. The reaction was monitored by TLC until the alcohol fully converted to the quinoline aldehyde **35** (3 h to 24 h). The reaction was quenched with 1 M sodium hydroxide (40.0 mL), and stirred until two distinct layers formed. The aqueous layer was separated and extracted with dichloromethane (3×50.0 mL), and the combined organic layers were washed with brine (150 ml), dried with sodium sulfate, filtered, and concentrated *in vacuo* giving a crude oil. If **34** was not present in the crude, then the oil was recrystallized with acetonitrile and water to give **35**. If **34** was present, then flash chromatography (1:11 ethyl acetate:hexanes) was used to isolate **35**.

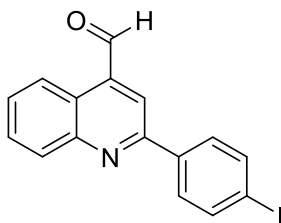


2-(4-chlorophenyl)-4-quinolinecarbaldehyde (35a): Fluffy yellow crystals (28% yield over three steps). $^1\text{H NMR}$ (500 MHz, DMSO- d_6) δ 10.55 (s, 1H) 8.93 (app d, $J = 8.0$ Hz, 1H), 8.70 (s, 1H), 8.28 (dt, $J = 9.0$ Hz, 2.0 Hz, 2H), 8.18 (app d, $J = 8.0$ Hz, 1H), 7.87 (ddd, $J = 8.0, 7.0$ Hz, 1.5 Hz, 2H), 7.76 (ddd, $J = 8.0$ Hz, 7.0 Hz, 1.5 Hz, 1H), 7.64 (dt, $J = 9.0$ Hz, 2.0 Hz, 2H); $^{13}\text{C NMR}$ (125 MHz, DMSO- d_6) δ 194.7, 155.3, 148.4, 137.9, 136.4, 135.1, 130.6, 129.7, 129.1, 128.9, 124.2, 124.1, 122.4.

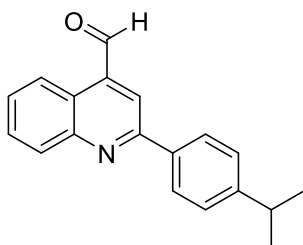


2-(4-bromophenyl)-4-quinolinecarbaldehyde (35b/65): Yellow solid (30% yield over three steps). $^1\text{H NMR}$ (500 MHz, DMSO- d_6) δ 10.54 (s, 1H) 8.93 (dd, $J = 8.5$ Hz, 0.5 Hz, 1H), 8.70 (s, 1H), 8.28 (dt, $J = 8.5$ Hz, 2.0 Hz, 2H), 8.18 (dd, $J = 8.5$ Hz, 0.5 Hz, 1H), 7.87 (ddd, $J = 8.5, 6.5$

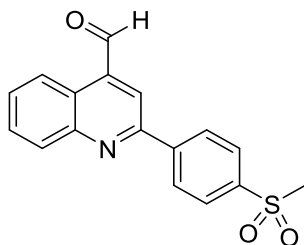
Hz, 1.5 Hz, 2H), 7.80 – 7.75 (m, 3H); ^{13}C NMR (125 MHz, DMSO- d_6) δ 194.7, 155.3, 148.4, 137.9, 136.8, 132.0, 130.6, 129.7, 129.1, 129.0, 124.2, 124.1, 124.0, 122.4.



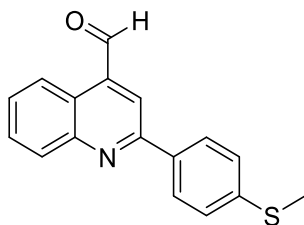
2-(4-iodophenyl)-4-quinolinecarbaldehyde (35c): Brown solid (31% yield over three steps). ^1H NMR (400 MHz, DMSO- d_6) δ 10.55 (s, 1H) 8.94 (dd, $J = 8.4$ Hz, 0.8 Hz, 1H), 8.70 (s, 1H), 8.18 (dd, $J = 8.4$ Hz, 0.8 Hz, 1H), 8.13 (dt, $J = 8.8$ Hz, 2.4 Hz, 2H), 7.96 (dt, $J = 8.8$ Hz, 2.4 Hz, 2H), 7.87 (ddd, $J = 8.4$ Hz, 7.2 Hz, 1.2 Hz, 1H), 7.79 (ddd, $J = 8.4$ Hz, 7.2 Hz, 1.2 Hz, 1H); ^{13}C NMR (125 MHz, DMSO- d_6) δ 194.7, 155.6, 148.4, 137.9, 137.8, 137.1, 130.5, 129.7, 129.1, 124.2, 124.0, 122.4, 97.6.



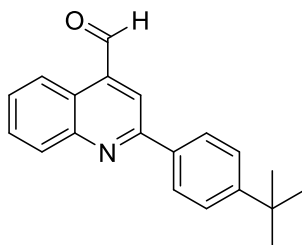
2-(4-isopropylphenyl)-4-quinolinecarbaldehyde (35d): Orange solid (29% yield over three steps). ^1H NMR (500 MHz, CDCl_3) δ 10.57 (s, 1H) 8.97 (ddd, $J = 8.5$ Hz, 1.5 Hz, 0.5 Hz, 1H), 8.24 (m, 2H), 8.15 (dt, $J = 8.5$ Hz, 2.0 Hz, 2H), 7.79 (ddd, $J = 8.5$ Hz, 7.0 Hz, 1.5 Hz, 1H), 7.67 (ddd, $J = 8.5$ Hz, 7.0 Hz, 1.5 Hz, 1H), 7.41 (dt, $J = 8.5$ Hz, 2.0 Hz, 2H), 3.00 (sep, $J = 7.0$ Hz, 1H), 1.31 (d, $J = 7.0$ Hz); ^{13}C NMR (125 MHz, CDCl_3) δ 193.1, 157.4, 151.2, 149.5, 137.6, 136.1, 130.3, 130.2, 128.7, 127.4, 127.2, 124.2, 124.1, 122.8, 34.1, 23.9; IR (cast film, CH_2Cl_2 , cm^{-1}): 3064, 2960, 2744, 1919, 1705, 1596, 1394, 1055; HRMS (ESI) for $(\text{M}+\text{H})^+$ $\text{C}_{19}\text{H}_{18}\text{NO}$: calcd. 276.1383; found 276.1394.



2-[4-(methylsulfonyl)phenyl]-4-quinolinecarbaldehyde (35e): White solid (17% yield over three steps). $^1\text{H NMR}$ (700 MHz, DMSO- d_6) δ 10.61 (s, 1H) 8.99 (app d, $J = 7.7$ Hz, 1H), 8.82 (s, 1H), 8.60 (app d, $J = 8.4$ Hz, 2H), 8.25 (app d, $J = 7.7$ Hz, 1H), 8.16 (app d, $J = 8.4$ Hz, 2H), 7.93 (ddd, $J = 7.7$ Hz, 7.0 Hz, 1.4 Hz, 1H), 7.83 (ddd, $J = 7.7$ Hz, 7.0 Hz, 1.4 Hz, 1H), 3.17 (s, 3H); $^{13}\text{C NMR}$ (125 MHz, DMSO- d_6) δ 194.5, 154.8, 148.5, 142.2, 141.9, 138.1, 130.7, 129.9, 129.6, 128.0, 127.7, 124.4, 124.3, 122.8, 43.5.

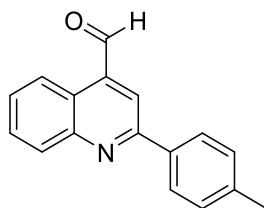


2-[4-(methylsulfanyl)phenyl]-4-quinolinecarbaldehyde (35f): Yellow solid (18% yield over three steps). $^1\text{H NMR}$ (500 MHz, DMSO- d_6) δ 10.55 (s, 1H) 8.93 (dd, $J = 8.5$ Hz, 0.5 Hz, 1H), 8.68 (s, 1H), 8.29 (dt, $J = 8.5$ Hz, 2.0 Hz, 2H), 8.15 (dd, $J = 8.5$ Hz, 0.5 Hz, 1H), 7.85 (ddd, $J = 8.5$ Hz, 7.0 Hz, 1.5 Hz, 1H), 7.73 (ddd, $J = 8.5$ Hz, 7.0 Hz, 1.5 Hz, 1H), 7.45 (dt, $J = 8.5$ Hz, 2.0 Hz, 2H), 2.55 (s, 3H); $^{13}\text{C NMR}$ (125 MHz, DMSO- d_6) δ 194.8, 155.9, 148.5, 141.4, 137.7, 133.9, 130.4, 129.6, 128.6, 127.5, 125.8, 124.8, 124.2, 122.2, 14.2; **HRMS** (ESI) for $(\text{M}+\text{H})^+$ $\text{C}_{17}\text{H}_{14}\text{NOS}$: calcd. 280.0791; found 280.0792.



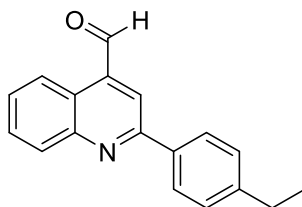
2-(4-*tert*-butylphenyl)-4-quinolinecarbaldehyde (35g): Beige solid (43% yield over three steps).

¹H NMR (700 MHz, DMSO-*d*₆) δ 10.59 (s, 1H) 8.96 (app d, *J* = 8.4 Hz, 1H), 8.69 (s, 1H), 8.27 (app d, *J* = 8.4 Hz, 2H), 8.19 (app d, *J* = 8.4 Hz, 1H), 7.88 (app t, *J* = 7.0 Hz, 1H), 7.77 (app t, *J* = 7.0 Hz, 1H), 7.62 (app d, *J* = 8.4 Hz, 2H), 1.35 (s, 9H); **¹³C NMR** (175 MHz, DMSO-*d*₆) δ 194.9, 156.5, 153.0, 148.5, 137.7, 135.0, 130.4, 129.6, 128.7, 127.0, 125.8, 124.3, 124.2, 122.2, 34.6, 31.0.

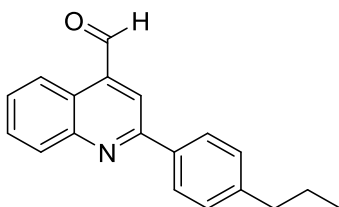


2-(4-methylphenyl)-4-quinolinecarbaldehyde (35h): Yellow solid (14% yield over three steps).

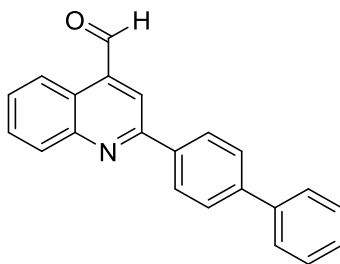
¹H NMR (400 MHz, DMSO-*d*₆) δ 10.59 (s, 1H), 8.97 (app d, *J* = 8.4 Hz, 1H), 8.73 (s, 1H), 8.28 (app d, *J* = 8.4 Hz, 2H), 8.20 (app d, *J* = 8.4 Hz 1H), 7.89 (ddd, *J* = 8.4 Hz, 6.8 Hz, 1.2 Hz, 1H), 7.77 (ddd, *J* = 8.4 Hz, 6.8 Hz, 1.2 Hz, 1H), 7.43 (app d, *J* = 8.4 Hz, 2H), 2.43 (s, 3H); **¹³C NMR** (125 MHz, DMSO-*d*₆) δ 194.9, 156.4, 148.5, 140.0, 137.7, 134.9, 130.4, 129.6, 129.5, 128.7, 127.1, 124.4, 124.2, 122.2, 20.9; **IR** (cast film, CH₂Cl₂, cm⁻¹): 3062, 2920, 2738, 1704, 1596, 1335, 1054; **HRMS** (EI) for (m/z) C₁₇H₁₃NO: calcd. 247.0997; found 247.0994.



2-(4-ethylphenyl)-4-quinolinecarbaldehyde (35i): Yellow crystals (61% yield over three steps). **¹H NMR** (500 MHz, DMSO-*d*₆) δ 10.55 (s, 1H), 8.93 (app d, *J* = 8.5 Hz, 1H), 8.68 (s, 1H), 8.25 (app d, *J* = 8.5 Hz, 2H), 8.16 (app d, *J* = 8.5 Hz 1H), 7.85 (ddd, *J* = 8.5 Hz, 7.5 Hz, 1.0 Hz, 1H), 7.73 (ddd, *J* = 8.5 Hz, 7.5 Hz, 1.0 Hz, 1H), 7.42 (app d, *J* = 8.5 Hz, 2H), 2.69 (q, *J* = 7.5 Hz, 2H), 1.22 (d, *J* = 7.5 Hz, 3H); **¹³C NMR** (125 MHz, DMSO-*d*₆) δ 194.9, 156.5, 148.5, 146.2, 137.7, 135.2, 130.4, 129.6, 128.7, 128.4, 127.2, 127.2, 124.4, 124.2, 122.2, 28.0, 15.4; **IR** (cast film, CHCl₃, cm⁻¹): 3062, 2965, 2932, 2873, 2747, 1704, 1596, 1336, 1056; **HRMS** (ESI) for (M+H)⁺ C₁₈H₁₆NO: calcd. 262.1226; found 262.1225.



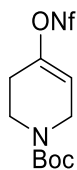
2-(4-propylphenyl)-4-quinolinecarbaldehyde (35j): Off-white solid (29% yield over three steps). **¹H NMR** (700 MHz, DMSO-*d*₆) δ 10.58 (s, 1H), 8.96 (dd, *J* = 8.4 Hz, 0.7 Hz 1H), 8.71 (s, 1H), 8.28 (app d, *J* = 8.4 Hz, 2H), 8.19 (dd, *J* = 8.4 Hz, 0.7 Hz, 1H), 7.88 (ddd, *J* = 8.4 Hz, 7.0 Hz, 1.4 Hz, 1H), 7.75 (ddd, *J* = 8.4 Hz, 7.0 Hz, 1.4 Hz, 1H), 7.42 (app d, *J* = 8.4 Hz, 2H), 2.66 (t, *J* = 7.7 Hz, 2H), 1.66 (sext, *J* = 7.7 Hz, 2H), 0.94 (t, *J* = 7.7 Hz, 3H); **¹³C NMR** (175 MHz, DMSO-*d*₆) δ 194.9, 156.5, 148.5, 144.6, 137.7, 135.2, 130.4, 129.6, 129.0, 128.7, 127.1, 124.4, 124.2, 122.2, 37.0, 23.9, 13.6.



2-(4-biphenyl)-4-quinolinecarbaldehyde (35h): Yellow crystals (27% yield over three steps). $^1\text{H NMR}$ (500 MHz, DMSO- d_6) δ 10.58 (s, 1H), 8.95 (app d, $J = 8.0$ Hz, 1H), 8.77 (s, 1H), 8.44 (app d, $J = 8.5$ Hz, 2H), 8.20 (app d, $J = 8.0$ Hz, 1H), 7.89 (m, 3H), 7.76 (m, 3H), 7.50 (app t, $J = 7.5$ Hz, 2H), 7.41 (app t, $J = 7.5$ Hz, 1H); $^{13}\text{C NMR}$ (125 MHz, DMSO- d_6) δ 194.9, 156.0, 148.5, 141.7, 139.2, 137.8, 136.6, 130.5, 129.7, 129.0, 128.9, 127.9, 127.7, 127.2, 126.2, 124.4, 124.2, 122.3; **IR** (cast film, CH_2Cl_2 cm^{-1}): 3059, 3032, 2853, 2745, 1944, 1704, 1594, 1488, 1336, 1054; **HRMS** (EI) for (m/z) $\text{C}_{22}\text{H}_{15}\text{NO}$: calcd. 309.1154; found 309.1153.

2.13.4 General Procedure for the Synthesis of the Alkenyl Nonaflate

To a flame-dried 100 mL round bottom flask with stir bar was added 1-boc-4-piperidone (4.00 g, 20.1 mmol, 1.00 equiv), and the flask was evacuated and backfilled with nitrogen for three cycles. Tetrahydrofuran (40.0 mL) was added, and the mixture stirred while cooling to 0 °C, forming a clear solution. 1,8-Diazabicyclo[5.4.0]undec-7-ene (3.60 mL, 24.1 mmol, 1.20 equiv) was added dropwise to the reaction, forming a pale yellow solution. Nonafluorobutanesulfonyl fluoride (4.20 mL, 24.1 mmol, 1.2 equiv) was added dropwise via syringe, and the reaction stirred overnight warming to rt. The reaction was quenched with water (40.0 mL), and the layers were separated. The aqueous layer was extracted with ethyl acetate (3×50.0 mL), and the organic layers were combined, washed with brine (100 mL), dried with sodium sulfate, filtered and concentrated *in vacuo*. The crude oil was purified by flash chromatography (3:17 diethyl ether: hexanes).

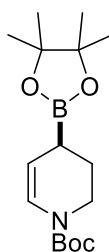


tert-butyl 4-(nonafluorobutylsulfonyloxy)-5,6-dihydropyridine-1(2H)-carboxylate (36):

Clear oil (96% yield). Spectral data matched that previously reported.^{43,49}

2.13.5 General Procedure for the Synthesis of Allylic Piperidinyl Boronate

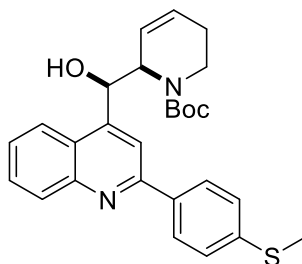
To a flame-dried 50 mL round bottom flask with stir bar was added palladium acetate (87.1 mg, 0.388 mmol, 0.0500 equiv), and DPEPhos (230 mg, 0.427 mmol, 0.0550 equiv), and the flask was evacuated and backfilled with nitrogen for three cycles. Diethyl ether (20.0 mL) was added to the flask, and the catalysts stirred for 30 min at rt forming a bright yellow solution. Diisopropylamine (1.50 mL, 8.54 mmol, 1.10 equiv) and pinacolborane (1.30 mL, 8.53 mmol, 1.10 equiv) were added sequentially, forming a brown-black solution. Alkenyl piperidinyl nonaflate **36** (3.76 g, 7.76 mmol, 1.00 equiv) in diethyl ether (3.00 mL) was added dropwise to the mixture, and the reaction stirred overnight at rt. The reaction was filtered through a silica plug with diethyl ether (200 mL), and concentrated *in vacuo*. The crude oil was purified by flash chromatography (1:3 diethyl ether:pentanes).



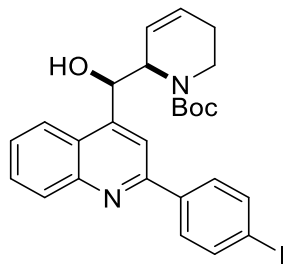
tert-butyl 4-(4,4,5,5-tetramethyl-1,3,2-dioxaborolan-2-yl)-3,4-dihydropyridine-1(2H)-carboxylate (38): Clear oil (50% yield). Spectral data matched that previously reported.^{43,49}

2.13.6 General Procedure for the Synthesis of Racemic *t*-Boc Dehydro-Vacquinol-1 Analogs

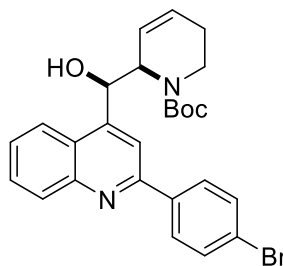
To a flame-dried 15 mL sealed tube with stir bar was added quinoline aldehyde **35** (65.3 mg, 0.240 mmol, 1.10 equiv), allylic piperidinyl boronate **38** (68.0 mg, 0.220 mmol, 1.00 equiv), and toluene (1.00 mL). The tube was sealed, heated to 80 °C, and stirred for 24 h. The reaction was cooled to rt, and quenched with water (0.300 mL). The solution was concentrated *in vacuo*, and the crude oil purified by flash chromatography (1:9 to 1:4 gradient of ethyl acetate:hexanes).



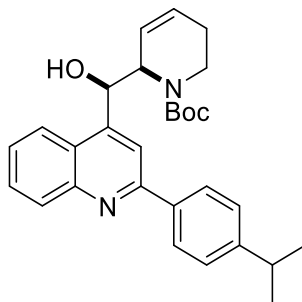
1(2H)-pyridinecarboxylic acid, 2-[[2-(4-methylsulfanylphenyl)-4-quinolinyl]hydroxymethyl]-5,6-dihydro-, 1,1-dimethylethyl ester (39a): Yellow foam (62% yield). ¹H NMR (500 MHz, CD₃OD) rotamers are present: δ 8.19-7.94 (m, 5H), 7.74 (m, 1H), 7.57 (m, 1H), 7.41 (m, 2H), 6.10-5.75 (m, 3H), 4.09 (dd, *J* = 13.0 Hz, 6.0 Hz, 1H), 3.79 (dd, *J* = 13.0 Hz, 6.0 Hz, 1H), 3.38 (td, *J* = 12.0 Hz, 4.0 Hz, 1H), 2.53 (s, 3H), 2.12-1.94 (m, 2H), 1.78 (m, 1H), 1.32 (s, 9H); ¹³C NMR (125 MHz, CD₃OD) rotamers are present: δ 159.2, 158.5, 156.4, 151.8, 151.1, 150.6, 149.2, 138.8, 138.5, 130.7, 130.6, 130.3, 130.2, 129.9, 129.2, 129.0, 127.9, 127.5, 127.3, 127.0, 126.8, 126.7, 125.6, 124.4, 124.1, 119.2, 119.0, 81.1, 80.8, 72.2, 70.7, 57.8, 39.7, 39.3, 35.3, 30.7, 28.6, 28.2, 27.9, 25.7, 25.4, 24.3; IR (cast film, CH₂Cl₂ cm⁻¹): 3424, 2971, 1692, 1419, 1337, 1164; HRMS (ESI) for (M+H)⁺ C₂₇H₃₁N₂O₃S: calcd. 463.2050; found 463.2050.



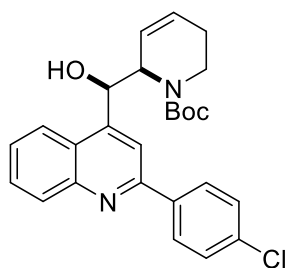
1(2*H*)-pyridinecarboxylic acid, 2-[[2-(4-iodophenyl)-4-quinolinyl]hydroxymethyl]-5,6-dihydro-, 1,1-dimethylethyl ester (39b): White foam (59% yield). $^1\text{H NMR}$ (500 MHz, CD_3OD) rotamers are present: δ 8.24-8.11 (m, 2H), 8.05 (s, 1H), 7.92 (m, 2H), 7.86-7.75 (m, 3H), 7.62 (m, 1H), 6.13-5.78 (m, 3H), 4.12 (m, 1H), 3.83 (dd, $J = 13.2$ Hz, 5.6 Hz, 1H), 3.39 (td, $J = 12.0$ Hz, 4.0 Hz, 1H), 2.17-1.95 (m, 2H), 1.34 (s, 9H); $^{13}\text{C NMR}$ (125 MHz, CDCl_3) rotamers are present: δ 148.5, 139.1, 137.9, 130.6, 129.5, 129.3, 128.0, 126.4, 126.4, 125.5, 124.1, 123.4, 122.8, 116.9, 95.9, 72.6, 58.4, 57.0, 38.5, 28.4, 27.9, 25.3, 24.7; **IR** (cast film, CH_2Cl_2 cm^{-1}): 3433, 2967, 1730, 1455, 1326, 1155; **HRMS** (ESI) for $(\text{M}+\text{H})^+$ $\text{C}_{26}\text{H}_{28}\text{IN}_2\text{O}_3$: calcd. 543.1139; found 543.1136.



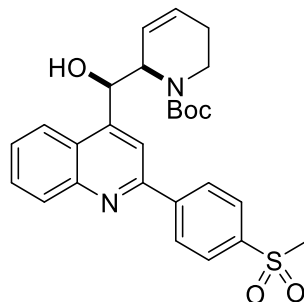
1(2*H*)-pyridinecarboxylic acid, 2-[[2-(4-bromophenyl)-4-quinolinyl]hydroxymethyl]-5,6-dihydro-, 1,1-dimethylethyl ester (39c): White foam (69% yield). Spectral data matched that previously reported.⁴³



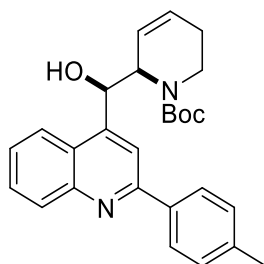
1(2*H*)-pyridinecarboxylic acid, 2-[[2-(4-isopropylphenyl)-4-quinolinyl]hydroxymethyl]-5,6-dihydro-, 1,1-dimethylethyl ester (39d): White foam (60% yield). ¹H NMR (500 MHz, CD₃OD) rotamers are present: δ 8.22-7.94 (m, 5H), 7.76 (m, 1H), 7.58 (m, 1H), 7.40 (m, 2H), 6.10-5.77 (m, 3H), 4.11 (dd, *J* = 13.0 Hz, 6.0 Hz, 1H), 3.79 (m, 1H), 3.38 (td, *J* = 12.5 Hz, 4.0 Hz, 1H), 3.00 (sep, *J* = 7.0 Hz, 1H), 2.14-1.96 (m, 2H), 1.81 (m, 1H), 1.31 (m, 12H); ¹³C NMR (125 MHz, CD₃OD) rotamers are present: δ 158.44, 157.78, 156.61, 156.43, 151.18, 150.86, 149.24, 146.60, 142.56, 142.03, 137.45, 137.16, 132.94, 131.12, 130.75, 130.45, 130.21, 129.21, 129.14, 128.95, 127.58, 127.41, 127.24, 127.05, 126.73, 125.65, 124.44, 124.16, 118.76, 118.67, 81.14, 80.84, 72.20, 70.71, 66.90, 57.83, 39.76, 39.29, 36.43, 28.64, 28.20, 27.88, 25.68, 25.36, 15.44, 15.24; IR (cast film, CH₂Cl₂ cm⁻¹): 3425, 2977, 1687, 1475, 1366, 1168; HRMS (ESI) for (M+H)⁺ C₂₉H₃₅N₂O₃: calcd. 459.2642.1139; found 459.2641.



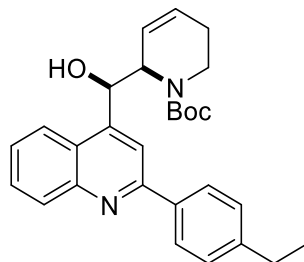
1(2*H*)-pyridinecarboxylic acid, 2-[[2-(4-chlorophenyl)-4-quinolinyl]hydroxymethyl]-5,6-dihydro-, 1,1-dimethylethyl ester (39e): White foam (82% yield). Spectral data matched that previously reported.⁴³



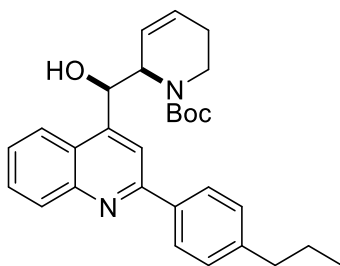
1(2*H*)-pyridinecarboxylic acid, 2-[[2-(4-methylsulfonylphenyl)-4-quinolinyl]hydroxymethyl]-5,6-dihydro-, 1,1-dimethylethyl ester (39f): Clear oil (93% yield). $^1\text{H NMR}$ (500 MHz, CD_3OD) rotamers are present: δ 8.41-8.11 (m, 7H), 7.78 (m, 1H), 7.63 (m, 1H), 6.11-5.80 (m, 3H), 4.10 (m, 1H), 3.80 (dd, $J = 13.5$ Hz, 6.0 Hz, 1H), 3.38 (td, $J = 12.5$ Hz, 4.5 Hz, 1H), 3.18 (s, 3H), 2.13-1.96 (m, 2H), 1.81 (m, 1H), 1.18 (s, 9H); $^{13}\text{C NMR}$ (125 MHz, CD_3OD) rotamers are present: δ 156.67, 156.40, 151.73, 149.41, 146.16, 142.63, 131.14, 131.02, 129.70, 129.60, 129.32, 128.99, 128.38, 127.15, 126.70, 124.24, 118.70, 80.81, 75.84, 72.19, 61.53, 57.85, 44.37, 39.78, 39.36, 28.63, 27.83, 25.67, 25.35, 25.03, 20.85, 14.46; **IR** (solid, cm^{-1}): 3452, 2975, 1684, 1455, 1335, 1150; **HRMS** (ESI) for $(\text{M}+\text{H})^+$ $\text{C}_{27}\text{H}_{31}\text{N}_2\text{O}_5\text{S}$: calcd. 495.1948; found 495.1948.



1(2*H*)-pyridinecarboxylic acid, 2-[[2-(4-methylphenyl)-4-quinolinyl]hydroxymethyl]-5,6-dihydro-, 1,1-dimethylethyl ester (39g): White foam (61% yield). Spectral data matched that previously reported.⁴³

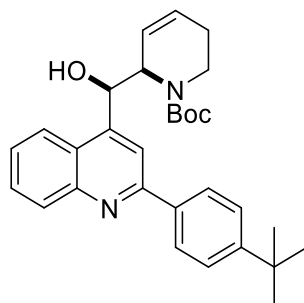


1(2*H*)-pyridinecarboxylic acid, 2-[[2-(4-ethylphenyl)-4-quinolinyl]hydroxymethyl]-5,6-dihydro-, 1,1-dimethylethyl ester (39h): White foam (53% yield). $^1\text{H NMR}$ (500 MHz, CD_3OD) rotamers are present: δ 8.20-7.94 (m, 5H), 7.75 (m, 1H), 7.63 (m, 1H), 7.59 (m, 1H), 7.39 (m, 1H), 6.10-5.77 (m, 3H), 4.10 (m, 1H), 3.80 (dd, $J = 13.5$ Hz, 5.5 Hz, 1H), 3.37 (td, $J = 12.5$ Hz, 4.0 Hz, 1H), 2.73 (q, $J = 7.5$ Hz, 2H), 2.11-1.95 (m, 2H), 1.79 (m, 1H), 1.34 (s, 9H), 1.29 (t, $J = 7.5$ Hz, 3H); $^{13}\text{C NMR}$ (125 MHz, CD_3OD) rotamers are present: δ 159.21, 158.55, 156.63, 156.44, 151.09, 150.66, 149.25, 147.30, 138.64, 138.40, 130.70, 130.59, 130.45, 130.25, 129.41, 129.24, 128.98, 128.90, 127.55, 127.35, 127.04, 126.77, 126.71, 125.64, 124.45, 124.16, 119.15, 119.03, 81.15, 80.85, 72.21, 70.69, 61.55, 57.84, 39.75, 39.31, 29.70, 28.66, 27.90, 25.69, 25.38, 20.87, 16.08, 14.48; **IR** (cast film, CH_2Cl_2 cm^{-1}): 3400, 2969, 1682, 1421, 1366, 1169; **HRMS** (ESI) for $(\text{M}+\text{H})^+$ $\text{C}_{28}\text{H}_{33}\text{N}_2\text{O}_3$: calcd. 445.2486; found 445.2482.

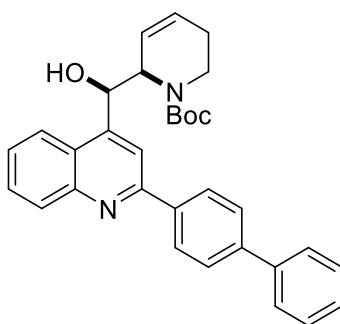


1(2*H*)-pyridinecarboxylic acid, 2-[[2-(4-propylphenyl)-4-quinolinyl]hydroxymethyl]-5,6-dihydro-, 1,1-dimethylethyl ester (39i): White foam (59% yield). $^1\text{H NMR}$ (700 MHz, CDCl_3) rotamers are present: δ 8.17 (d, $J = 8.4$ Hz, 1H), 8.10-7.89 (m, 4H), 7.68 (app t, $J = 6.3$ Hz 1H), 7.46 (app t, $J = 6.3$ Hz, 1H), 7.30 (d, $J = 7.7$ Hz 2H), 5.99-5.48 (m, 3H), 4.94 (m, 1H), 4.43-4.04 (m, 1H), 2.65 (t, $J = 7.7$ Hz, 1H), 2.05 (m, 2H), 1.69 (sext, $J = 7.7$ Hz, 2H), 1.55 (s, 9H), 0.964 (t, $J = 7.7$ Hz, 3H); $^{13}\text{C NMR}$ (175 MHz, CDCl_3) rotamers are present: δ 157.22, 157.19, 148.45, 144.14, 137.05, 130.38, 129.15, 128.92, 127.69, 127.46, 125.88, 125.03, 124.54, 124.20, 123.35,

117.38, 80.94, 80.12, 72.55, 60.36, 58.19, 56.92, 38.39, 37.83, 37.33, 36.62, 29.67, 28.42, 27.88, 24.71, 24.47, 21.02, 14.17, 13.77; **IR** (cast film, CH₂Cl₂ cm⁻¹): 3402, 2964, 1687, 1421, 1366, 1169; **HRMS** (ESI) for (M+H)⁺ C₂₉H₃₅N₂O₃: calcd. 459.2642; found 459.2642.

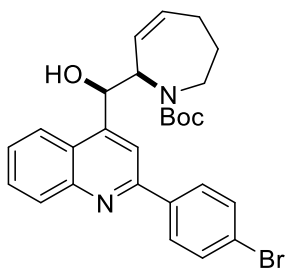


1(2H)-pyridinecarboxylic acid, 2-[[2-(4-tert-butylphenyl)-4-quinolinyl]hydroxymethyl]-5,6-dihydro-, 1,1-dimethylethyl ester (39j): White foam (52% yield). **¹H NMR** (700 MHz, CDCl₃) rotamers are present: δ 8.19-7.94 (m, 5H), 7.69 (t, *J* = 7.7 Hz, 1H), 7.53 (d, *J* = 8.4 Hz, 2H), 7.48 (app t, *J* = 7.4 Hz, 1H), 6.01-5.46 (m, 3H), 5.09-4.85 (m, 1H), 4.38-4.10 (m, 1H), 2.95 (m, 1H), 2.21-1.96 (m, 2H), 1.51 (s, 9H), 1.37 (s, 9H); **¹³C NMR** (175 MHz, CDCl₃) rotamers are present: δ 157.30, 157.05, 152.50, 148.55, 136.86, 130.45, 129.14, 127.69, 127.30, 125.90, 125.74, 125.31, 124.20, 123.40, 117.45, 80.98, 80.21, 72.82, 60.36, 58.22, 56.98, 38.38, 37.34, 34.72, 31.28, 28.42, 28.02, 27.90, 24.72, 24.34, 21.02, 14.18; **IR** (cast film, CH₂Cl₂ cm⁻¹): 3416, 2966, 1682, 1420, 1366, 1169; **HRMS** (ESI) for (M+H)⁺ C₃₀H₃₇N₂O₃: calcd. 473.2799; found 473.2798.

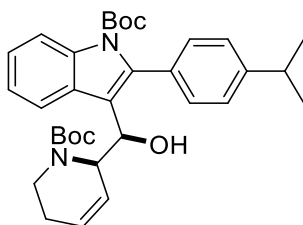


1(2H)-pyridinecarboxylic acid, 2-[[2-(biphenyl)-4-quinolinyl]hydroxymethyl]-5,6-dihydro-, 1,1-dimethylethyl ester (39k): White foam (55% yield). **¹H NMR** (700 MHz, CDCl₃) rotamers are present: δ 8.27-8.08 (m, 5H), 7.75-7.67 (m, 5H), 7.51-7.46 (m, 3H), 7.37 (app t, *J* = 7.7 Hz, 1H), 6.03-5.55 (m, 3H), 5.10-4.86 (m, 1H), 4.44-4.08 (m, 1H), 2.99 (m, 1H), 2.19-1.96 (m, 2H),

1.51 (s, 9H); ^{13}C NMR (175 MHz, CDCl_3) rotamers are present: δ 156.6, 148.5, 142.1, 140.6, 130.5, 129.3, 128.8, 128.0, 127.8, 127.5, 127.5, 127.1, 126.1, 124.2, 123.4, 117.3, 81.0, 77.2, 77.0, 76.8, 72.6, 60.4, 58.3, 38.4, 28.4, 28.0, 27.9, 24.7, 21.0, 14.2; IR (cast film, CH_2Cl_2 cm^{-1}): 3409, 2967, 2837, 1683, 1419, 1366, 1168; HRMS (ESI) for $(\text{M}+\text{H})^+$ $\text{C}_{32}\text{H}_{33}\text{N}_2\text{O}_3$: calcd. 493.2486; found 493.2488.



2,3,4,7-tetrahydro-1H-azepine, 2-[[2-(4-bromophenyl)-4-quinolinyl]hydroxymethyl]-5,6-dihydro-, 1,1-dimethylethyl ester (66): Clear oil in 8% yield. ^1H NMR (500 MHz, CDCl_3) rotamers are present: δ 8.15 (m, 1H), 8.11-8.04 (m, 2H), 7.99-7.95 (m, 2H), 7.78-7.67 (m, 3H), 7.59 (m, 1H), 5.89-5.65 (m, 3H), 5.25-5.11 (m, 1H), 3.85-3.72 (m, 1H), 3.45 (m, 1H), 3.25 (m, 1H), 2.18-1.80 (m, 2H), 1.63-1.43 (m, 1H), 1.26 (s, 9H); ^{13}C NMR (125 MHz, CDCl_3) rotamers are present: δ 157.66, 157.59, 157.06, 156.70, 151.49, 151.29, 149.26, 140.22, 139.98, 133.07, 130.82, 130.76, 130.72, 130.59, 130.52, 130.48, 130.44, 130.34, 129.12, 127.92, 127.68, 127.03, 126.74, 124.94, 124.45, 124.12, 118.59, 118.30, 80.95, 80.64, 73.41, 71.41, 62.64, 62.48, 44.04, 43.91, 28.62, 27.82, 26.55, 25.92, 24.29, 24.12; IR (direct deposit, cm^{-1}): 3066, 2932, 1948, 1633, 1415, 1341, 1072; HRMS (ESI) for $(\text{M}+\text{H})^+$ $\text{C}_{27}\text{H}_{30}\text{BrN}_2\text{O}_3$: calcd. 509.1434; found 509.1436.

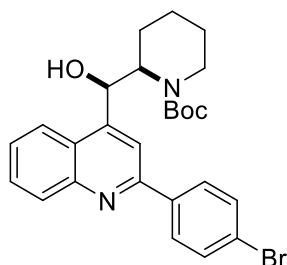


1,1-dimethylethyl ester,-1-indole-3-methanol, [1(2H)-Pyridinecarboxylic acid]-2-(4-isopropylphenyl)hydroxymethyl]-5,6-dihydro-, 1,1-dimethylethyl ester (70): Clear oil in 18% yield. ^1H NMR (500 MHz, CDCl_3) rotamers are present: δ 8.44-8.09 (m, 2H), 7.44 (m, 6H), 5.97-

4.81 (m, 3H), 4.29 (m, 1H), 3.10 (m, 1H), 2.46-2.02 (m, 2H), 1.75-1.31 (m, 27H); **IR** (direct deposit, cm^{-1}): 3066, 2932, 1948, 1633, 1415, 1341, 1072; **HRMS** (ESI) for $(\text{M}+\text{Na})^+$ $\text{C}_{33}\text{H}_{42}\text{N}_2\text{O}_5$: calcd. 569.2986; found 569.2980.

2.13.7 General Procedure for Hydrogenation of Dehydro-Br-Vacquinol-1 (**39c**)

To a flame-dried 10 mL pear flask with stir bar was added **39c** (20.0 mg, 0.0440 mmol, 1.00 equiv), and Adam's catalyst (3.00 mg, 0.0130 mmol, 0.300 equiv). The flask was evacuated and backfilled with nitrogen for three cycles. Ethyl acetate (1.5 mL) was added to the flask via syringe, and the reagents stirred at rt for 5 min, forming a clear solution. The solution was purged with a hydrogen balloon (1 atm) for 5 min, forming a dark black solution. The balloon was then moved into the flask's headspace, and the reaction stirred overnight at rt. The solution was filtered through a silica plug with ethyl acetate (150 mL), then concentrated *in vacuo* to get the *t*-Boc Br-vacquinol-1 analog **40**, which was purified by HPLC using the general conditions in 2.13.1.

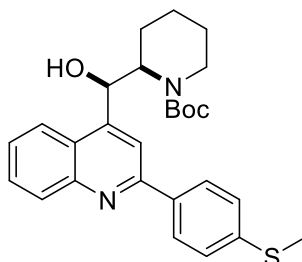


1-piperidinecarboxylic acid, 2-[[2-(4-chlorophenyl)-4-quinolinyl]hydroxymethyl]-, 1,1-dimethylethyl ester (40**):** Clear oil (98% yield). Spectral data matched that previously reported.⁴³

2.13.8 General Procedures for Hydrogen Atom Transfer (HAT)

To a flame-dried 5 mL pear flask with stir bar under argon was added dehydro-methylthiol vac-1 intermediate **39a** (32.3 mg, 0.0650 mmol, 1.00 equiv), isopropyl alcohol (1.10 mL), and the mixture stirred forming a clear solution. Phenylsilane (40.0 μL , 0.324 mmol, 5.00 equiv), and *tert*-butyl hydrogen peroxide (5.5 M, 60.0 μL , 0.324 mmol, 5.00 equiv), were added sequentially, and the solution was degassed with argon for 10 min. Shenvi Hydrogenation Catalyst (40.5 mg, 0.0650

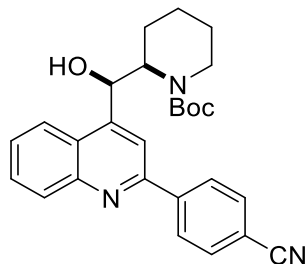
mmol, 1.00 equiv), was added in one portion with stirring, forming a dark green solution. The reaction was left overnight at rt. The reaction was concentrated *in vacuo* and purified by HPLC using the general conditions in 2.13.1.



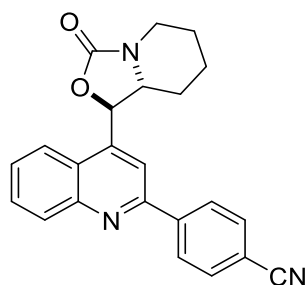
1-piperidinecarboxylic acid, 2-[[2-(4-methylsulfanyl)-4-quinolinyl]hydroxymethyl]-, 1,1-dimethylethyl ester (41): Yellow foam (20% yield). $^1\text{H NMR}$ (500 MHz, CDCl_3) rotamers are present: δ 8.29-7.94 (m, 5H), 7.71 (t, $J = 7.5$ Hz, 1H), 7.53 (t, $J = 7.5$ Hz, 1H), 7.37 (d, $J = 8.5$ Hz, 2H), 5.63 (bs, 1H), 4.76 (bs, 1H), 4.11 (m, 1H), 3.13 (bs, 1H), 2.54 (s, 3H), 1.84-0.860 (m, 16H); $^{13}\text{C NMR}$ (125 MHz, CDCl_3) rotamers are present: δ 156.4, 136.1, 130.7, 129.5, 127.8, 126.4, 126.2, 77.3, 77.2, 77.0, 76.8, 31.9, 29.7, 29.4, 28.5, 24.9, 22.7, 19.9, 15.57, 14.13; **IR** (cast film, CH_2Cl_2 , cm^{-1}): 3415, 2925, 1687, 1494, 1365, 1161; **HRMS** (ESI) for $(\text{M}+\text{H})^+$ $\text{C}_{28}\text{H}_{33}\text{N}_2\text{O}_3\text{S}$: calcd. 465.2206; found 465.2194.

2.13.9 General Procedure for Rosemund-von Braun Type Reaction

To a flame-dried 15 mL sealed tube was added sodium cyanide (17.1 mg, 0.266 mmol, 2.20 equiv), copper iodide (19.2 mg, 0.0610 mmol, 0.500 equiv), and potassium iodide (17.2 mg, 0.0610 mmol, 0.500 equiv). The tube was evacuated and backfilled with argon for three cycles. Toluene (1.00 mL) was added to the tube with stirring to form a white slurry. *N,N*-dimethylethylenediamine (0.100 mL, 0.242 mmol, 2.00 equiv), and Br-vac-1 intermediate **40** (60.2 mg, 0.121 mmol, 1.00 equiv) in toluene (3.00 mL) were added sequentially forming a dark green solution. The tube was sealed and heated to 130 °C for 24 h. The reaction was cooled, filtered through a silica plug with ethyl acetate (200 mL), and concentrated *in vacuo*. The crude residue was purified by HPLC using the general conditions in 2.13.1.



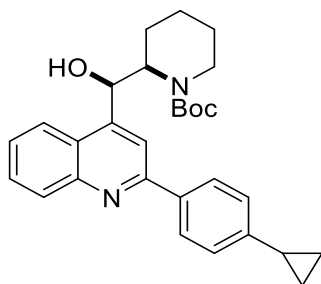
1-piperidinecarboxylic acid, 2-[[2-(4-nitrilephenyl)-4-quinolinyl]hydroxymethyl]-, 1,1-dimethylethyl ester (44): Yellow foam (23% yield). $^1\text{H NMR}$ (400 MHz, tetrahydrofuran- d_8) rotamers are present: δ 8.46 (m, 2H), 8.32-8.08 (m, 3H), 7.96-7.86 (m, 2H), 7.74 (m, 1H), 7.61-7.44 (m, 1H), 6.09-5.68 (m, 2H), 5.18-4.68 (m, 1H), 4.19 (m, 1H), 3.22 (m, 1H), 2.13-1.18 (m, 15H); $^{13}\text{C NMR}$ (125 MHz, tetrahydrofuran- d_8) rotamers are present: δ 156.4, 136.1, 130.7, 129.5, 127.8, 126.4, 126.2, 77.3, 77.2, 77.0, 76.8, 31.9, 29.7, 29.4, 28.5, 24.9, 22.7, 19.9, 15.57, 14.1; **IR** (cast film, CH_2Cl_2 , cm^{-1}): 3397, 3063, 2928, 2228, 1685, 1418, 1306, 1162; **HRMS** (ESI) for $(\text{M}+\text{H})^+$ $\text{C}_{27}\text{H}_{30}\text{N}_3\text{O}_3$: calcd. 444.2282; found 444.2284.



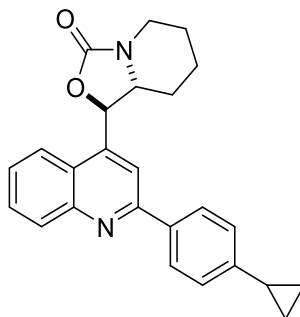
3H-oxazolo[3,4-a]pyridin-3-one, 1-[2-(4-nitrilephenyl)-4-quinolinyl]-1,5,6,8a-tetrahydro- (45): White foam (42% yield). $^1\text{H NMR}$ (500 MHz, CDCl_3) δ 8.33 (d, $J = 6.5$ Hz, 2H), 8.27 (d, $J = 8.5$ Hz, 1H), 8.04 (s, 1H), 7.81 (m, 4H), 7.65 (t, $J = 11.5$ Hz, 1H), 5.86 (d, 5.5 Hz, 1H), 3.99 (dd, 13.0 Hz, 4.5 Hz, 1H), 3.56 (ddd, $J = 11.5$ Hz, 5.0 Hz, 4.5 Hz, 1H), 2.85 (td, $J = 13.0$ Hz, 3.5 Hz, 1H), 2.24 (m, 1H), 2.06 (m, 1H), 1.76 (m, 2H), 1.59 (qt, $J = 13.0$ Hz, 4.0 Hz, 1H), 1.42 (qt, $J = 13.0$ Hz, 4.0 Hz, 1H); $^{13}\text{C NMR}$ (125 MHz, CDCl_3) δ 156.2, 155.1, 148.5, 145.0, 143.1, 132.6, 131.3, 130.2, 128.2, 127.7, 124.0, 121.8, 118.7, 114.4, 113.1, 68.0, 62.1, 41.9, 30.9, 29.7, 25.6, 24.2, 22.9; **IR** (cast film, CH_2Cl_2 , cm^{-1}): 3061, 2941, 2227, 1759, 1445, 1329, 1063; **HRMS** (ESI) for $(\text{M}+\text{H})^+$ $\text{C}_{23}\text{H}_{19}\text{N}_3\text{O}_2$: calcd. 370.1550; found 370.1550.

2.13.10 General Procedure for Suzuki-Miyaura Cross-Coupling

To a 15 mL sealed tube was added potassium cyclopropyltrifluoroborate (32.0 mg, 0.185 mmol, 1.20 equiv), palladium-tetrakis(triphenylphosphine) (10.4 mg, 0.00900 mmol, 0.0600 equiv), and potassium phosphate (126 mg, 0.508 mmol, 3.30 equiv). The tube was evacuated and backfilled with argon for three cycles. Br-vac-1 intermediate **40** (89.5 mg, 0.170 mmol, 1.00 equiv) and toluene:water (3:1, 0.800 mL) were added to the tube sequentially. The tube was sealed, heated to 100 °C, and stirred 20 h. The reaction was cooled to rt, filtered through a silica plug with ethyl acetate (200 mL), and concentrated *in vacuo*. The product was purified by HPLC using the general conditions in 2.13.1.



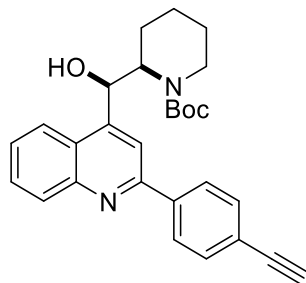
1-piperidinecarboxylic acid, 2-[[2-(4-cyclopropylphenyl)-4-quinolinyl]hydroxymethyl]-, 1,1-dimethylethyl ester (60): White foam (53% yield). $^1\text{H NMR}$ (400 MHz, CD_3OD) rotamers are present: δ 8.35-7.94 (m, 4H), 7.74 (m, 1H), 7.62-7.47 (m, 2H), 7.23 (d, $J = 8.4$ Hz, 2H), 5.72 (bs, 1H), 4.83-4.59 (m, 1H), 4.09 (m, 1H), 3.38 (m, 1H), 2.14-1.96 (m, 2H), 1.73-1.28 (m, 8H), 1.04 (m, 9H), 0.770 (m, 2H); $^{13}\text{C NMR}$ (175 MHz, CD_3OD) rotamers are present: δ 173.0, 157.4, 149.5, 147.5, 130.8, 130.7, 130.6, 130.4, 129.9, 128.9, 128.9, 127.5, 127.3, 127.0, 125.0, 119.1, 80.6, 73.3, 61.5, 56.1, 41.1, 37.6, 30.6, 28.3, 26.3, 25.6, 21.0, 20.8, 16.1, 14.4, 10.1; **IR** (cast film, CH_2Cl_2 , cm^{-1}): 3392, 2934, 1686, 1474, 1308, 1161; **HRMS** (ESI) for $(\text{M}+\text{H})^+$ $\text{C}_{29}\text{H}_{35}\text{N}_2\text{O}_3$: calcd. 459.2642; found 459.2642.



3H-oxazolo[3,4-a]pyridin-3-one, 1-[2-(4-cyclopropylphenyl)-4-quinolinyl]-1,5,6,8a-tetrahydro- (62): White foam (4% yield). **¹H NMR** (500 MHz, CDCl₃) δ 8.17 (m, 1H), 8.02 (m, 3H), 7.82 (m, 1H), 7.67 (m, 1H), 7.57-7.47 (m, 1H), 7.25 (d, *J* = 8.4 Hz, 2H), 6.05 (dd, 8.4 Hz, 5.6 Hz, 1H), 3.86 (m, 1H), 3.73 (m, 1H), 2.92 (m, 1H), 2.22-2.14 (m, 1H), 2.07-1.93 (m, 1H), 1.80-1.45 (m, 6H), 1.04 (m, 2H), 0.780 (m, 2H); **¹³C NMR** (125 MHz, CDCl₃) δ 158.8, 158.5, 149.7, 147.9, 146.3, 137.4, 131.3, 130.9, 130.0, 128.7, 128.6, 128.1, 127.0, 123.8, 116.2, 115.9, 79.0, 63.3, 42.8, 31.5, 30.7, 30.6, 25.4, 23.6, 16.1, 10.2; **IR** (cast film, CH₂Cl₂, cm⁻¹): 3054, 2926, 1760, 1423, 1351, 1063; **HRMS** (ESI) for (M+H)⁺ C₂₅H₂₅N₂O₂: calcd. 385.1911; found 385.1921.

2.13.11 General Procedure for Sonogashira Cross-Coupling

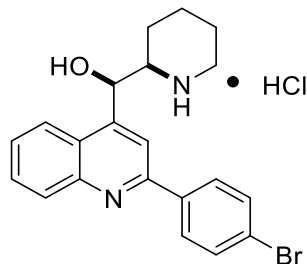
To a flame-dried 15 mL pressure tube with stir bar under argon was added Br-vac-1 analog **40** (52.0 mg, 0.105 mmol, 1.00 equiv), diisopropylamine (0.900 mL), and tetrahydrofuran (1.30 mL). The solution was degassed with argon for 1 h. Trimethylsilylacetylene (0.100 mL, 0.263 mmol, 2.50 equiv), palladium(II)bis(triphenylphosphine) dichloride (26.4 mg, 0.0260 mmol, 0.250 equiv), and copper iodide (10.8 mg, 0.0260 mmol, 0.250 equiv), were added sequentially, and the reaction heated to 60 °C and was stirred for 24 h, forming a black solution. The reaction was cooled to rt, filtered through a silica plug with ethyl acetate (200 mL), and concentrated *in vacuo*. The crude product was dissolved in methanol (1.00 mL) and tetrahydrofuran (1.00 mL) and 1 M sodium hydroxide (11.0 mL, 1.05 mmol, 10.0 equiv) was added to the solution with stirring for 1 h at rt. The reaction was concentrated *in vacuo* and purified by HPLC using the general conditions in 2.13.1.



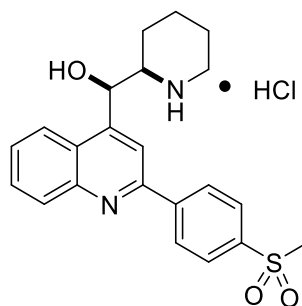
1-piperidinecarboxylic acid, 2-[[2-(4-ethynylphenyl)-4-quinolinyl]hydroxymethyl]-, 1,1-dimethylethyl ester (43): White foam (48% yield over two steps). $^1\text{H NMR}$ (500 MHz, CDCl_3) rotamers are present: δ 8.30-7.80 (m, 4H), 7.73-7.54 (m, 5H), 5.26 (bs, 1H), 4.73 (bs, 1H), 4.06 (m, 1H), 3.73 (m, 1H), 3.15 (m, 1H), 1.84-1.46 (m, 16H); $^{13}\text{C NMR}$ (125 MHz, CDCl_3) rotamers are present: δ 156.0, 148.8, 139.6, 132.6, 130.8, 129.6, 127.4, 126.6, 125.5, 123.1, 117.4, 83.5, 80.6, 78.6, 70.35, 68.0, 56.6, 40.9, 31.9, 30.1, 29.7, 29.4, 28.4, 25.6, 24.9, 22.7, 19.9, 14.1; **IR** (cast film, CH_2Cl_2 , cm^{-1}): 3390, 2927, 2107, 1683, 1419, 1365, 1161; **HRMS** (ESI) for $(\text{M}+\text{H})^+$ $\text{C}_{28}\text{H}_{31}\text{N}_2\text{O}_3$: calcd. 443.2329; found 443.2323.

2.13.12 General Procedure for the Synthesis of HCl Salt Vacquinol-1 Analogs

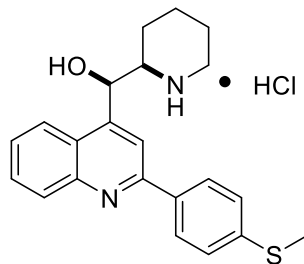
The dehydro *t*-Boc vac-1 analogs were hydrogenated following the general conditions outlined in 2.14.7 to obtain any desired saturated analogs. All dehydro and saturated *t*-Boc vac-1 analogs were then purified by HPLC using the standard conditions in 2.13.1. The purified analogs in methanol (1.00 mL) were added to a sample vial with stir bar under air. Concentrated hydrochloric acid (5-6 drops) was added dropwise to the solution with stirring at rt. The reaction was stirred for 1-2 h, forming a pale yellow solution. The solvent was evaporated *in vacuo* giving the pure HCl salts that could be further purified by trituration with dichloromethane (1.00 mL), ethyl acetate (1.00 mL), hexanes (1.00 mL), and diethyl ether (1.00 mL). Quantitative yields are reported as 99%.



4-quinolinemethanol, 2-(4-bromophenyl)- α -2-piperidinyl-, hydrochloride (18): White solid (99% yield). $^1\text{H NMR}$ (500 MHz, CD_3OD) δ 8.60 (d, $J = 9.5$ Hz, 1H), 8.53 (s, 1H), 8.45 (d, $J = 9.5$ Hz, 1H), 8.22 (app t, $J = 8.5$ Hz, 1H), 8.12 (dt, $J = 11.0$ Hz, 3.0 Hz, 2H), 8.04 (app t, $J = 8.5$ Hz, 1H), 7.95 (dt, $J = 11.0$ Hz, 3.0 Hz, 2H), 5.77 (d, $J = 7.5$ Hz, 1H), 3.67 (m, 1H), 3.40 (d, $J = 16.0$ Hz, 1H), 2.94 (td, $J = 16.0$ Hz, 4.0 Hz, 1H), 1.95-1.47 (m, 6H); $^{13}\text{C NMR}$ (125 MHz, CD_3OD) δ 158.9, 155.6, 140.9, 136.0, 134.2, 132.3, 132.1, 131.2, 129.2, 126.9, 126.0, 123.5, 121.4, 71.0, 62.3, 46.3, 27.2, 23.3, 22.8; **IR** (solid, cm^{-1}): 3290, 3064, 2934, 1597, 1446, 1350, 1168; **HRMS** (ESI) for $(\text{M})^+$ $\text{C}_{21}\text{H}_{22}\text{ClN}_2\text{O}$: calcd. 397.0910; found 397.0906.

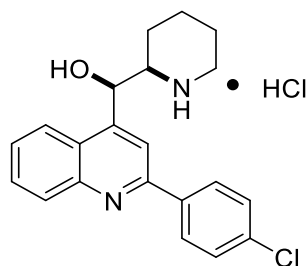


4-quinolinemethanol, 2-(4-methylsulfonylphenyl)- α -2-piperidinyl-, hydrochloride (19): White solid (80% yield). $^1\text{H NMR}$ (500 MHz, CD_3OD) δ 8.58 (d, $J = 8.5$ Hz, 1H), 8.57 (s, 1H), 8.46 (d, $J = 8.5$ Hz, 1H), 8.41 (d, $J = 8.0$ Hz, 2H), 8.29 (d, $J = 8.0$ Hz, 2H), 8.21 (t, $J = 7.5$ Hz, 1H), 8.04 (t, $J = 7.5$ Hz, 1H), 5.71 (d, $J = 6.0$ Hz, 1H), 3.64 (m, 1H), 3.39 (d, $J = 12.5$ Hz, 1H), 3.24 (s, 3H), 2.95 (t, $J = 12.5$ Hz, 1H), 1.94-1.50 (m, 6H); $^{13}\text{C NMR}$ (125 MHz, CD_3OD) δ 159.1, 154.9, 145.7, 141.3, 138.4, 136.1, 131.6, 131.5, 129.6, 127.3, 126.0, 123.9, 121.8, 71.0, 62.4, 46.3, 44.1, 27.3, 24.2, 23.3, 22.8; **IR** (solid, cm^{-1}): 3517-3243, 2942, 1634, 1502, 1259, 1099; **HRMS** (ESI) for $(\text{M})^+$ $\text{C}_{22}\text{H}_{25}\text{N}_2\text{O}_3\text{S}$: calcd. 397.1580; found 397.1578.



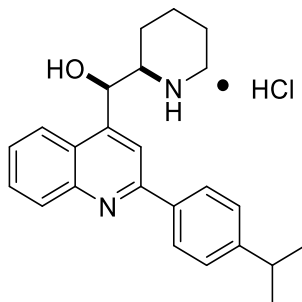
4-quinolinemethanol, 2-(4-methylsulfanylphenyl)- α -2-piperidinyl-, hydrochloride (20):

Green solid (99% yield). $^1\text{H NMR}$ (500 MHz, CD_3OD) δ 8.53 (d, $J = 8.5$ Hz, 1H), 8.50 (s, 1H), 8.41 (d, $J = 8.5$ Hz, 1H), 8.16 (t, $J = 7.5$ Hz, 1H), 8.10 (d, $J = 8.5$ Hz, 2H), 7.98 (t, $J = 7.5$ Hz, 1H) 7.58 (d, $J = 8.5$ Hz, 2H), 5.71 (d, $J = 6.0$ Hz, 1H) 3.63 (m, 1H), 3.39 (d, $J = 12.5$ Hz, 1H), 2.95 (t, $J = 12.5$ Hz, 1H), 2.61 (s, 3H), 1.90-1.45 (m, 6H); $^{13}\text{C NMR}$ (125 MHz, CD_3OD) δ 158.6, 156.0, 145.1, 135.9, 130.9, 130.6, 127.2, 126.0, 121.1, 71.1, 62.3, 46.3, 27.2, 23.3, 22.8, 14.6; **IR** (solid, cm^{-1}): 3232, 2930, 1634, 1420, 1349, 1102; **HRMS** (ESI) for $(\text{M})^+$ $\text{C}_{22}\text{H}_{25}\text{N}_2\text{OS}$: calcd. 365.1682; found 365.1680.

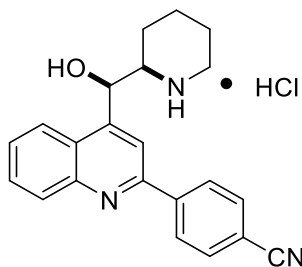


4-quinolinemethanol, 2-(4-chlorophenyl)- α -2-piperidinyl-, hydrochloride (22):

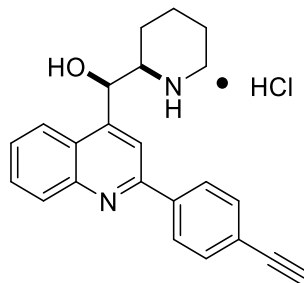
White solid (99% yield). $^1\text{H NMR}$ (500 MHz, CD_3OD) δ 8.58 (d, $J = 8.5$ Hz, 1H), 8.51 (s, 1H), 8.43 (d, $J = 8.5$ Hz, 1H), 8.18 (m, 3H), 8.07 (t, $J = 7.0$ Hz, 1H), 7.77 (dt, $J = 8.5$ Hz, 2.5 Hz, 2H) 5.75 (d, $J = 6.0$ Hz, 1H), 3.64 (ddd, $J = 8.5$ Hz, 6.5 Hz, 3.5 Hz, 1H), 3.39 (d, $J = 13$ Hz, 1H), 2.94 (td, $J = 13.0$ Hz, 3.0 Hz, 1H), 1.92-1.46 (m, 6H); $^{13}\text{C NMR}$ (125 MHz, CD_3OD) δ 159.2, 155.5, 140.8, 140.7, 136.1, 132.1, 131.7, 131.3, 131.2, 126.9, 126.0, 123.3, 121.5, 71.0, 62.3, 46.3, 27.2, 24.2, 23.3, 22.8; **IR** (solid, cm^{-1}): 3241, 3028, 2933, 1633, 1451, 1349, 1114; **HRMS** (ESI) for $(\text{M})^+$ $\text{C}_{21}\text{H}_{22}\text{ClN}_2\text{O}$: calcd. 353.1415; found 353.1412.



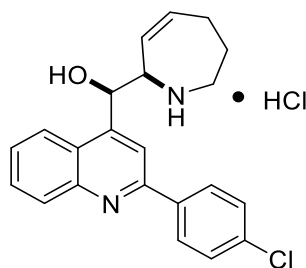
4-quinolinemethanol, 2-(4-isopropylphenyl)- α -2-piperidinyl-, hydrochloride (23): White solid (99% yield). $^1\text{H NMR}$ (500 MHz, CD_3OD) δ 8.59 (d, $J = 8.5$ Hz, 1H), 8.54 (s, 1H), 8.45 (d, $J = 8.5$ Hz, 1H), 8.20 (t, $J = 7.5$ Hz, 1H), 8.13 (d, $J = 8.0$ Hz, 2H), 8.01 (t, $J = 7.5$ Hz, 1H) 7.65 (d, $J = 8.0$ Hz, 2H), 5.77 (d, $J = 6.0$ Hz, 1H), 3.65 (m, 1H), 3.39 (d, $J = 12.5$ Hz, 1H), 3.09 (sep, $J = 7.0$ Hz, 1H), 2.95 (t, $J = 13.5$ Hz, 1H), 1.94-1.70 (m, 6H), 1.33 (d, $J = 7.0$ Hz, 6H); $^{13}\text{C NMR}$ (125 MHz, CD_3OD) δ 159.5, 156.8, 156.4, 139.9, 136.2, 131.2, 130.8, 129.9, 129.2, 126.6, 126.2, 122.5, 121.6, 71.0, 62.3, 46.3, 35.6, 27.2, 24.2, 24.0, 23.2, 22.8; **IR** (solid, cm^{-1}): 3290, 3064, 2934, 1597, 1446, 1350, 1168; **HRMS** (ESI) for $(\text{M})^+$ $\text{C}_{24}\text{H}_{29}\text{N}_2\text{O}$: calcd. 361.2274; found 361.2274.



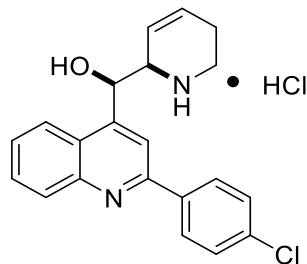
4-quinolinemethanol, 2-(4-nitrilephenyl)- α -2-piperidinyl-, hydrochloride (24): Yellow solid (99% yield). $^1\text{H NMR}$ (500 MHz, CD_3OD) δ 8.57 (d, $J = 8.5$ Hz, 1H), 8.53 (s, 1H), 8.45 (d, $J = 8.5$ Hz, 1H), 8.34 (d, $J = 8.5$ Hz, 2H), 8.19 (t, $J = 7.5$ Hz, 1H), 8.08 (d, $J = 8.5$ Hz, 2H) 8.02 (t, $J = 7.5$ Hz, 1H), 5.77 (d, $J = 6.0$ Hz, 1H) 3.64 (m, 1H), 3.41 (d, $J = 13.0$ Hz, 1H), 2.94 (t, $J = 13.5$ Hz, 1H), 1.92-1.46 (m, 6H); $^{13}\text{C NMR}$ (125 MHz, CD_3OD) δ 158.7, 154.8, 141.6, 135.9, 134.4, 131.4, 131.2, 127.2, 125.9, 124.2, 121.6, 118.7, 117.1, 71.8, 62.4, 46.3, 27.3, 23.3, 22.8; **IR** (solid, cm^{-1}): 3218, 3039, 2960, 2231, 1634, 1458, 1261, 1093; **HRMS** (ESI) for $(\text{M})^+$ $\text{C}_{22}\text{H}_{22}\text{N}_3\text{O}$: calcd. 344.1757; found 344.1756.



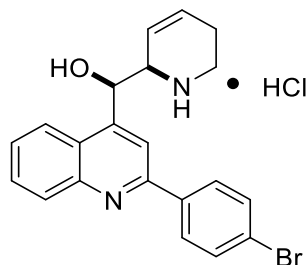
4-quinolinemethanol, 2-(4-ethynylphenyl)- α -2-piperidinyl-, hydrochloride (25): Yellow solid (99% yield). $^1\text{H NMR}$ (500 MHz, CD_3OD) δ 8.59 (d, $J = 8.5$ Hz, 1H), 8.55 (s, 1H), 8.45 (d, $J = 8.5$ Hz, 1H), 8.21 (t, $J = 7.5$ Hz, 1H), 8.17 (d, $J = 8.0$ Hz, 2H), 8.03 (t, $J = 7.5$ Hz, 1H) 7.82 (d, $J = 8.0$ Hz, 2H), 5.77 (d, $J = 5.5$ Hz, 1H), 3.90 (s, 1H), 3.64 (m, 1H), 3.39 (d, $J = 13.0$ Hz, 1H), 2.95 (t, $J = 10.5$ Hz, 1H), 1.94-1.47 (m, 6H); $^{13}\text{C NMR}$ (125 MHz, CD_3OD) δ 159.7, 155.5, 140.3, 136.3, 134.3, 132.6, 131.4, 130.7, 128.9, 127.0, 126.1, 122.9, 121.7, 83.4, 83.1, 71.0, 62.3, 46.3, 27.2, 23.2, 22.8; **IR** (solid, cm^{-1}): 3208, 3039, 2937, 2102, 1633, 1453, 1348, 1112; **HRMS** (ESI) for $(\text{M})^+$ $\text{C}_{23}\text{H}_{23}\text{N}_2\text{O}$: calcd. 343.1805; found 343.1803.



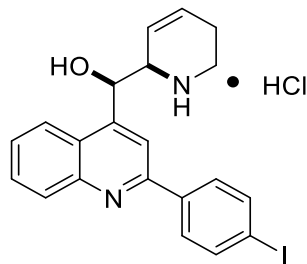
2-(4-chlorophenyl)-2,3,4,7-tetrahydro-1H-azepine-4-quinolinemethanol, hydrochloride (26): Off-white solid (99% yield). $^1\text{H NMR}$ (500 MHz, CD_3OD) δ 8.59-8.29 (m, 3H), 8.19-7.91 (m, 4H), 7.79-7.69 (m, 2H), 6.12-5.80 (m, 2H), 5.31 (m, 1H), 4.63 (bs, 1H), 3.71-3.65 (m, 4H), 2.45 (bs, 1H), 2.01-1.79 (m, 4H); **IR** (solid, cm^{-1}) 3221, 3053, 2925, 1635, 1419, 1097; **HRMS** (ESI) for $(\text{M})^+$ $\text{C}_{22}\text{H}_{22}\text{ClN}_2\text{O}$: calcd. 365.1415; found 365.1412.



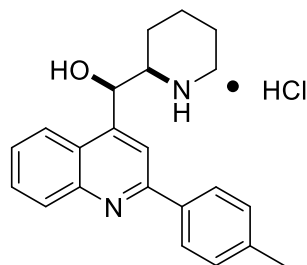
2-(4-chlorophenyl)-2-5,6-dihydropyridinyl-4-quinolinemethanol, hydrochloride (27): Off-white solid (99% yield). $^1\text{H NMR}$ (500 MHz, CD_3OD) δ 8.58 (m, 2H), 8.45 (d, $J = 8.5$ Hz, 1H), 8.20 (m, 3H), 8.02 (t, $J = 8.0$ Hz, 1H), 7.77 (d, $J = 8.5$ Hz, 2H), 6.14 (bs, 1H), 5.98 (d, $J = 5.5$ Hz, 1H), 5.63 (d, $J = 10.5$ Hz, 1H), 4.40 (bs, 1H), 3.50 (bs, 1H), 3.18 (m, 1H), 2.57-2.34 (m, 3H); $^{13}\text{C NMR}$ (125 MHz, CD_3OD) δ 159.1, 155.4, 141.0, 140.3, 136.3, 132.2, 131.4, 131.2, 129.8, 126.8, 126.0, 122.9, 122.8, 121.7, 69.8, 59.4, 41.4, 22.6; **IR** (solid, cm^{-1}) 3319, 3030, 2954, 1672, 1596, 1092; **HRMS** (ESI) for $(\text{M})^+$ $\text{C}_{21}\text{H}_{20}\text{ClN}_2\text{O}$: calcd. 351.1259; found 351.1257.



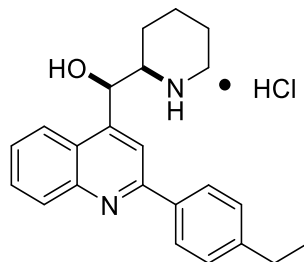
2-(4-bromophenyl)-2-5,6-dihydropyridinyl-4-quinolinemethanol, hydrochloride (28): Off-white solid (99% yield). $^1\text{H NMR}$ (500 MHz, CD_3OD) δ 8.58 (m, 2H), 8.45 (d, $J = 8.5$ Hz, 1H), 8.20 (t, $J = 8.0$ Hz, 1H), 8.11 (d, $J = 8.0$ Hz, 2H), 8.02 (t, $J = 8.0$ Hz, 1H), 7.93 (d, $J = 8.0$ Hz, 2H), 6.14 (bs, 1H), 5.98 (d, $J = 5.0$ Hz, 1H), 5.63 (d, $J = 10.5$ Hz, 1H), 4.40 (bs, 1H), 3.50 (bs, 1H), 3.18 (m, 1H), 2.57-2.34 (m, 3H); $^{13}\text{C NMR}$ (125 MHz, CD_3OD) δ 158.9, 155.6, 140.5, 136.2, 134.2, 132.3, 132.0, 131.4, 129.8, 129.3, 126.8, 126.0, 123.1, 122.9, 121.5, 69.8, 59.5, 41.5, 22.6; **IR** (solid, cm^{-1}) 3194, 3055, 2925, 1724, 1597, 1073; **HRMS** (ESI) for $(\text{M})^+$ $\text{C}_{21}\text{H}_{20}\text{BrN}_2\text{O}$: calcd. 395.0754; found 395.0733.



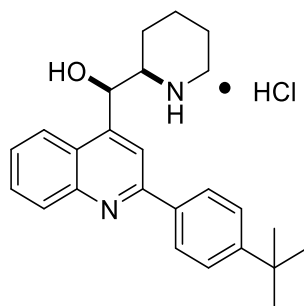
2-(4-iodophenyl)-2-5,6-dihydropyridinyl-4-quinolinemethanol, hydrochloride (29): Yellow solid (99% yield). $^1\text{H NMR}$ (500 MHz, CD_3OD) δ 8.49 (m, 2H), 8.39 (m, 1H), 8.12 (m, 3H), 7.94 (m, 3H), 6.12 (m, 1H), 5.98 (d, $J = 6.0$ Hz, 1H), 5.58 (d, $J = 10.0$ Hz, 1H), 4.38 (bs, 1H), 3.51 (m, 1H), 3.19 (m, 1H), 2.56-2.34 (m, 3H); $^{13}\text{C NMR}$ (125 MHz, CD_3OD) δ 156.2, 142.3, 140.2, 135.3, 131.6, 130.8, 129.7, 126.7, 125.6, 124.7, 122.8, 120.8, 116.1, 100.9, 69.9, 59.5, 41.3, 30.8, 22.6; **IR** (solid, cm^{-1}) 3314, 3066, 2922, 1596, 1005; **HRMS** (ESI) for $(\text{M})^+$ $\text{C}_{21}\text{H}_{20}\text{IN}_2\text{O}$: calcd. 443.0615; found 443.0614.



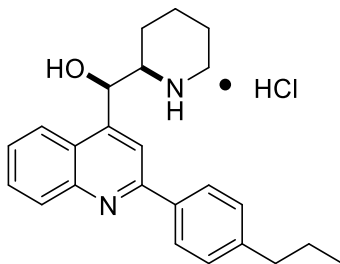
4-quinolinemethanol, 2-(4-methylphenyl)- α -2-piperidinyl-, hydrochloride (47): Light brown solid (80% yield). $^1\text{H NMR}$ (700 MHz, CD_3OD) δ 8.58 (d, $J = 8.4$ Hz, 1H), 8.53 (s, 1H), 8.45 (d, $J = 8.4$ Hz, 1H), 8.18 (t, $J = 7.0$ Hz, 1H), 8.12 (d, $J = 8.4$ Hz, 2H), 8.00 (t, $J = 7.0$ Hz, 1H), 7.60 (d, $J = 8.4$ Hz, 2H), 5.77 (d, $J = 6.3$ Hz, 1H) 3.66 (m, 1H), 3.41 (d, $J = 12.6$ Hz, 1H), 2.97 (td, $J = 13.3$ Hz 2.8 Hz, 1H), 2.53 (s, 3H) 1.94-1.50 (m, 6H); $^{13}\text{C NMR}$ (125 MHz, CD_3OD) δ 158.7, 156.6, 145.8, 140.7, 135.8, 131.7, 130.9, 130.4, 130.2, 126.6, 126.0, 123.2, 121.4, 71.0, 62.3, 46.3, 27.2, 23.3, 22.8, 21.7; **IR** (solid, cm^{-1}): 3500-2500, 3030, 2946, 1634, 1428, 1126; **HRMS** (ESI) for $(\text{M})^+$ $\text{C}_{22}\text{H}_{25}\text{N}_2\text{O}$: calcd. 333.1961; found 333.1961.



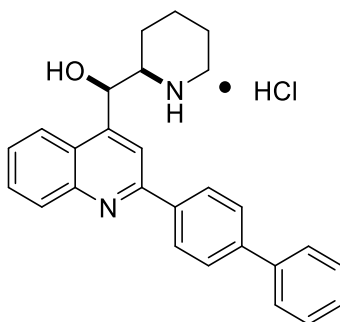
4-quinolinemethanol, 2-(4-ethylphenyl)- α -2-piperidinyl-, hydrochloride (48): White solid (99% yield). $^1\text{H NMR}$ (400 MHz, CD_3OD) δ 8.58 (d, $J = 8.8$ Hz, 1H), 8.54 (s, 1H), 8.45 (d, $J = 8.8$ Hz, 1H), 8.19 (t, $J = 7.6$ Hz, 1H), 8.13 (d, $J = 8.0$ Hz, 2H), 8.02 (t, $J = 7.6$ Hz, 1H), 7.63 (d, $J = 8.0$ Hz, 2H), 5.77 (d, $J = 6.3$ Hz, 1H) 3.66 (m, 1H), 3.42 (d, $J = 12.8$ Hz, 1H), 2.97 (t, $J = 12.8$ Hz, 1H), 2.83 (q, $J = 7.6$ Hz, 2H) 1.98-1.47 (m, 6H), 1.33 (t, $J = 7.6$ Hz, 3H); $^{13}\text{C NMR}$ (100 MHz, CD_3OD) δ 158.5, 155.9, 151.6, 139.6, 135.4, 130.5, 130.0, 129.5, 126.0, 125.5, 122.2, 120.9, 70.4, 61.7, 45.7, 29.3, 26.6, 22.7, 22.2, 15.1; **IR** (solid, cm^{-1}): 3300-2500, 3055, 2938, 1611, 1415, 1126; **HRMS** (ESI) for $(\text{M})^+$ $\text{C}_{23}\text{H}_{27}\text{N}_2\text{O}$: calcd. 347.2118; found 347.2118.



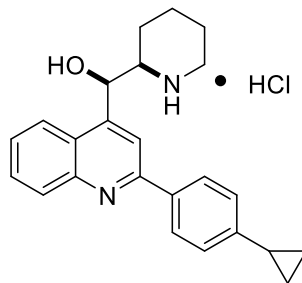
4-quinolinemethanol, 2-(4-*tert*-butylphenyl)- α -2-piperidinyl-, hydrochloride (49): White solid (99% yield). $^1\text{H NMR}$ (400 MHz, CD_3OD) δ 8.60 (d, $J = 8.4$ Hz, 1H), 8.54 (s, 1H), 8.46 (d, $J = 8.4$ Hz, 1H), 8.21 (t, $J = 7.2$ Hz, 1H), 8.16 (d, $J = 8.4$ Hz, 2H), 8.02 (t, $J = 7.2$ Hz, 1H), 7.83 (d, $J = 8.4$ Hz, 2H), 5.75 (d, $J = 6.4$ Hz, 1H) 3.65 (m, 1H), 3.42 (d, $J = 12.8$ Hz, 1H), 2.97 (td, $J = 13.2$ Hz, 3.2 Hz, 1H), 1.98-1.43 (m, 15H); $^{13}\text{C NMR}$ (100 MHz, CD_3OD) δ 158.2, 155.9, 135.4, 130.4, 129.7, 127.5, 126.0, 125.4, 122.3, 120.8, 70.4, 61.7, 45.7, 35.6, 30.8, 26.6, 22.7, 22.2, 10.10; **IR** (solid, cm^{-1}): 3200-2500, 3055, 2935, 1634, 1423, 1113; **HRMS** (ESI) for $(\text{M})^+$ $\text{C}_{25}\text{H}_{31}\text{N}_2\text{O}$: calcd. 375.2431; found 375.2431.



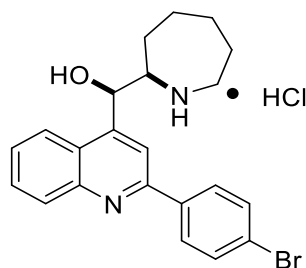
4-quinolinemethanol, 2-(4-propylphenyl)- α -2-piperidinyl-, hydrochloride (50): Beige solid (99% yield). $^1\text{H NMR}$ (400 MHz, CD_3OD) δ 8.60 (d, $J = 8.4$ Hz, 1H), 8.55 (s, 1H), 8.48 (d, $J = 8.4$ Hz, 1H), 8.21 (t, $J = 8.0$ Hz, 1H), 8.13 (d, $J = 8.0$ Hz, 2H), 8.02 (t, $J = 8.0$ Hz, 1H), 7.63 (d, $J = 8.0$ Hz, 2H), 5.77 (d, $J = 6.3$ Hz, 1H) 3.66 (m, 1H), 3.42 (d, $J = 12.8$ Hz, 1H), 2.97 (t, $J = 11.2$ Hz, 1H), 2.79 (t, $J = 7.6$ Hz, 2H) 1.91-1.47 (m, 8H), 0.998 (t, $J = 7.6$ Hz, 3H); $^{13}\text{C NMR}$ (100 MHz, CD_3OD) δ 150.2, 135.6, 130.7, 130.0, 122.0, 121.0, 70.4, 61.7, 45.7, 38.3, 26.6, 24.8, 22.7, 22.3, 13.4; **IR** (solid, cm^{-1}): 3200-2500, 3055, 2938, 1634, 1414, 1126; **HRMS** (ESI) for $(\text{M})^+$ $\text{C}_{24}\text{H}_{29}\text{N}_2\text{O}$: calcd. 361.2274; found 361.2274.



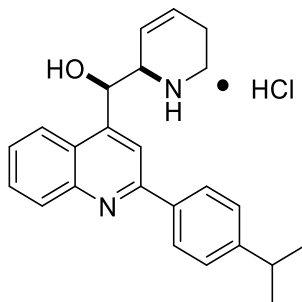
4-quinolinemethanol, 2-(4-biphenyl)- α -2-piperidinyl-, hydrochloride (51): Yellow solid (99% yield). $^1\text{H NMR}$ (400 MHz, CD_3OD) δ 8.60 (m, 2H), 8.48 (d, $J = 8.4$ Hz, 1H), 8.29 (d, $J = 8.4$ Hz, 2H), 8.22 (t, $J = 7.6$ Hz, 1H), 8.05 (m, 3H), 7.79 (m, 2H) 7.54 (m, 2H), 7.46 (m, 1H), 5.78 (d, $J = 6.0$ Hz, 1H) 3.68 (m, 1H), 3.41 (d, $J = 13.2$ Hz, 1H), 2.97 (t, $J = 12.8$ Hz, 1H), 1.96-1.51 (m, 6H); $^{13}\text{C NMR}$ (125 MHz, CD_3OD) δ 158.2, 154.6, 146.1, 138.9, 138.6, 134.8, 134.8, 129.9, 129.8, 128.9, 128.5, 128.0, 126.9, 125.4, 124.8, 121.2, 120.3, 69.6, 60.9, 44.9, 25.8, 21.8, 21.4; **IR** (solid, cm^{-1}): 3200-2600, 3059, 2954, 1634, 1417, 1350, 1006; **HRMS** (ESI) for $(\text{M})^+$ $\text{C}_{27}\text{H}_{27}\text{N}_2\text{O}$: calcd. 395.2118; found 395.2119.



4-quinolinemethanol, 2-(4-cyclopropylphenyl)- α -2-piperidinyl-, hydrochloride (52): Yellow solid (76% yield). $^1\text{H NMR}$ (600 MHz, CD_3OD) δ 8.56 (d, $J = 8.4$ Hz, 1H), 8.52 (s, 1H), 8.43 (d, $J = 8.4$ Hz, 1H), 8.19 (t, $J = 6.6$ Hz, 1H), 8.09 (d, $J = 8.4$ Hz, 2H), 8.00 (t, $J = 6.6$ Hz, 1H) 7.45 (d, $J = 8.4$ Hz, 2H), 5.75 (d, $J = 6.0$ Hz, 1H) 3.65 (m, 1H), 3.40 (d, $J = 12.6$ Hz, 1H), 2.95 (td, $J = 13.2$ Hz, 3.0 Hz, 1H), 2.10 (m, 1H), 1.93-1.48 (m, 6H), 1.17 (m, 2H), 0.883 (m, 2H); $^{13}\text{C NMR}$ (175 MHz, CD_3OD) δ 159.0, 156.4, 153.0, 140.2, 135.9, 131.0, 130.5, 129.3, 127.9, 126.5, 126.0, 122.7, 121.3, 71.0, 62.2, 46.3, 27.2, 23.2, 22.8, 16.6, 11.4; **IR** (solid, cm^{-1}): 3200-2500, 2937, 1603, 1513, 1423, 1111; **HRMS** (ESI) for $(\text{M})^+$ $\text{C}_{24}\text{H}_{27}\text{N}_2\text{O}$: calcd. 359.2118; found 359.2118.

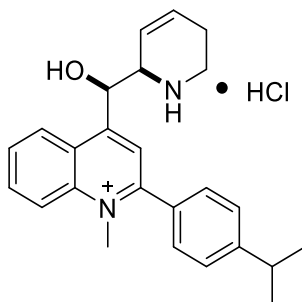


4-quinolinemethanol, 2-(4-bromophenyl)- α -2-azepanyl-, hydrochloride (53): Green solid (99% yield). $^1\text{H NMR}$ (600 MHz, CD_3OD) δ 8.55 (d, $J = 9.0$ Hz, 1H), 8.51 (s, 1H), 8.39 (d, $J = 9.0$ Hz, 1H), 8.14 (t, $J = 7.2$ Hz, 1H), 8.11 (d, $J = 8.4$ Hz, 2H), 7.97 (t, $J = 7.2$ Hz, 1H), 7.90 (d, $J = 8.4$ Hz, 2H), 5.77 (d, $J = 6.6$ Hz, 1H), 3.80 (ddd, $J = 9.0$ Hz, 6.6 Hz, 3.6 Hz, 1H), 3.40 (ddd, $J = 13.8$ Hz, 11.4, 2.4 Hz, 1H), 3.28-3.26 (m, 1H), 2.01-1.28 (m, 8H); $^{13}\text{C NMR}$ (125 MHz, CD_3OD) δ 155.9, 135.3, 134.0, 131.9, 130.9, 126.9, 125.7, 124.6, 121.1, 71.4, 64.7, 46.9, 29.5, 27.9, 26.2, 25.9; **IR** (solid, cm^{-1}): 3400-2800, 3066, 2932, 1633, 1415, 1341, 1008; **HRMS** (ESI) for $(\text{M})^+$ $\text{C}_{21}\text{H}_{24}\text{BrN}_2\text{O}$: calcd. 411.1067; found 411.1068.



2-(4-isopropylphenyl)-2-5,6-dihydropyridinyl-4-quinolinemethanol, hydrochloride (54):

White solid (99% yield). $^1\text{H NMR}$ (500 MHz, CD_3OD) δ 8.59 (s, 1H), 8.54 (d, $J = 8.4$ Hz, 1H), 8.44 (d, $J = 8.4$ Hz, 1H), 8.17 (m, 3H), 7.99 (app t, $J = 7.16$, 1H), 7.64 (d, $J = 8.4$ Hz, 2H), 6.19 (m, 1H), 5.94 (d, $J = 5.06$ Hz, 1H), 5.62 (dd, $J = 10.4$ Hz, 2.0 Hz, 1H), 4.42 (bs, 1H), 3.52 (m, 1H), 3.19 (m, 1H), 3.22-3.05 (m, 2H), 2.60-2.35 (m, 2H), 1.34 (d, $J = 6.8$ Hz); $^{13}\text{C NMR}$ (125 MHz, CD_3OD) δ 158.2, 156.6, 156.6, 140.5, 135.9, 131.0, 130.6, 130.4, 129.8, 129.2, 126.4, 125.9, 123.0, 122.7, 121.3, 69.8, 59.4, 41.3, 35.5, 24.0, 22.5; **IR** (solid, cm^{-1}) 3205, 3029, 2946, 1612, 1425, 1117; **HRMS** (ESI) for $(\text{M})^+$ $\text{C}_{21}\text{H}_{20}\text{IN}_2\text{O}$: calcd. 359.2118; found 359.2119.



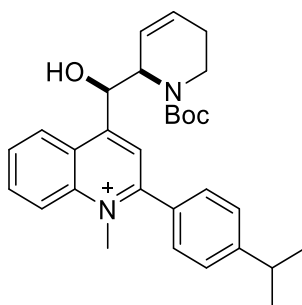
2-(4-isopropylphenyl)-2-5,6-dihydropyridinyl-4-methylquinoliniummethanol,

hydrochloride (75): Red solid (99% yield). $^1\text{H NMR}$ (500 MHz, CD_3OD) δ 8.63 (t, $J = 8.0$ Hz, 2H), 8.31 (t, $J = 8.0$ Hz, 1H), 8.28 (s, 1H), 8.08 (t, $J = 8.0$ Hz, 1H), 7.75 (d, $J = 8.5$ Hz, 2H), 7.59 (d, $J = 8.5$ Hz, 2H), 6.13 (m, 1H), 5.98 (d, $J = 5.5$ Hz, 1H), 5.66 (dd, $J = 10.5$ Hz, 2.5 Hz, 1H), 4.50 (s, 3H), 4.35 (bs, 1H), 3.46 (m, 1H), 3.16-3.05 (m, 2H), 2.51-2.32 (m, 2H), 1.34 (d, $J = 6.5$ Hz, 6H); $^{13}\text{C NMR}$ (175 MHz, CD_3OD) δ 161.5, 157.6, 155.0, 141.5, 136.9, 132.3, 131.2, 131.2, 131.0, 129.8, 128.8, 128.6, 127.6, 126.8, 125.1, 123.0, 121.5, 69.4, 59.5, 43.5, 41.5, 35.5, 24.1,

22.4; **IR** (solid, cm^{-1}): 3371, 3061, 2961, 1607, 1467, 1362, 1113; **HRMS** (ESI) for $(\text{M})^+$ $\text{C}_{25}\text{H}_{30}\text{N}_2\text{O}_3$: calcd. 374.2347; found 374.2346.

2.13.13 General Procedure for Simmons-Smith/N-Methylation

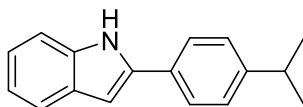
Diiodomethane (70.2 μL , 0.872 mmol, 4.00 equiv) was added to a solution of diethylzinc (1.0 M, 436 μL , 0.436 mmol, 2.00 equiv) in dichloromethane (1.00 mL) in a flame-dried 50 mL round bottom flask with stir bar under argon at $-78\text{ }^\circ\text{C}$. The mixture warmed to $0\text{ }^\circ\text{C}$, and was stirred 15 min. A solution of **39d** (100 mg, 0.218 mmol, 1.00 equiv) in dichloromethane (1.00 mL) was added dropwise via syringe. The reaction warmed to rt, and was stirred 1 h. Saturated ammonium chloride (5.00 mL) was added dropwise, and the layers were separated. The aqueous layer was extracted with dichloromethane ($3 \times 20.0\text{ mL}$), and the combined organic phases were washed with brine (60.0 mL), dried with sodium sulfate, and concentrated *in vacuo*. The residue was purified by HPLC using the conditions from 2.13.1.



1(2H)-pyridinecarboxylic acid, 2-[[2-(4-isopropylphenyl)-4-1-methylquinolinium] hydroxymethyl]-5,6-dihydro-, 1,1-dimethylethyl ester (74): Red solid (63% yield). $^1\text{H NMR}$ (600 MHz, CD_3OD) rotamers are present: δ 8.76-8.54 (m, 2H), 8.32 (m, 1H), 8.10 (m, 2H), 7.66 (m, 4H), 6.03-5.55 (m, 3H), 5.48 (s, 3H), 4.49 (m, 1H), 4.11 (m, 1H), 3.18-3.08 (m, 2H), 2.15-1.93 (m, 2H), 1.36 (d, $J = 6.6\text{ Hz}$, 6H), 1.23 (s, 9H); $^{13}\text{C NMR}$ (175 MHz, CD_3OD) rotamers are present: δ 167.9, 155.1, 137.0, 136.5, 132.1, 131.0, 130.9, 130.7, 130.0, 128.9, 128.8, 128.1, 127.1, 125.8, 124.7, 124.2, 121.2, 120.9, 81.2, 72.3, 58.4, 58.1, 54.8, 43.2, 40.6, 39.4, 35.5, 28.5, 28.2, 28.0, 25.5, 25.2, 24.1; **IR** (cast film, $\text{CH}_2\text{Cl}_2\text{ cm}^{-1}$): 3103, 2966, 1686, 1602, 1415, 1365, 1169; **HRMS** (ESI) for $(\text{M})^+$ $\text{C}_{30}\text{H}_{37}\text{N}_2\text{O}_3$: calcd. 473.2799; found 473.2804.

2.13.14 General Procedure for Fischer Indole Synthesis

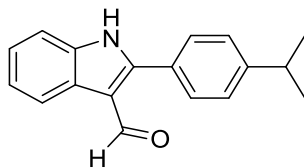
To a flame-dried 100 mL round bottom flask with a stir bar was added phenylhydrazine hydrochloride (1.60 g, 11.0 mmol, 1.10 equiv), 4-isopropylacetophenone (1.70 mL, 10.0 mmol, 1.00 equiv), and phosphoric acid (20.0 mL). A condenser was equipped, the mixture heated to 110 °C, and stirred 6 h under air. The solution was initially a yellow slurry that gradually turned dark red over time. The reaction was cooled to rt, and poured into ice water (150 mL), which precipitated the indole product. The solid was filtered, washed with water (100 mL), and dried under high vacuum giving the indole as a light brown solid, which was used without further purification.



1H-indole, 2-[4-(1-methylethyl)phenyl]- (67): Brown solid (84% yield). Spectral data matched that previously reported.⁶⁴

2.13.15 General Procedure for Vilsmeier-Haack Formylation

To a flame-dried 100 mL pear flask with a stir bar under argon at 0 °C was added dimethylformamide (1.50 mL), and phosphoryl chloride (0.600 mL, 5.65 mmol, 1.20 equiv), and the reagents stirred for 10 min. Indole intermediate **67** (1.10 g, 4.70 mmol, 1.00 equiv) in DMF (3.00 mL) was added dropwise to the solution via syringe, and the reaction stirred 2 h at 0 °C. The yellow-brown slurry was quenched with 1 M sodium hydroxide (35.0 mL) and a solid precipitated out of solution. The solid was collected by vacuum filtration, triturated with water (50.0 mL), ethyl acetate (50.0 mL), and dichloromethane (50.0 mL), and dried under high vacuum giving the indole aldehyde, which was used without further purification.



1H-indole-3-carboxaldehyde, 2-[4-(1-methylethyl)phenyl]- (68): Yellow solid (26% yield). ¹H NMR (400 MHz, DMSO-d₆) δ 9.98 (s, 1H), 8.20 (d, *J* = 7.6 Hz, 1H), 7.49 (m, 3H), 7.26 (m, 2H), 3.02 (sep, *J* = 6.8 Hz, 1H), 1.29 (d, *J* = 6.8 Hz, 6H); ¹³C NMR (175 MHz, DMSO-d₆) δ 201.1, 185.41, 150.32, 149.17, 135.84, 129.84, 127.49, 127.32, 126.92, 125.82, 123.56, 122.32, 120.97, 113.30, 111.89, 33.30, 23.74, 23.68; IR (direct deposit, cm⁻¹): 3024, 2970, 2759, 1647, 1448, 1305, 1103; HRMS (EI) for C₁₈H₁₇NO: calcd. 263.1310; found 263.1312.

2.14 References

- [1] American Association of Neurological Surgeons. Glioblastoma Multiforme. <https://www.aans.org/Patients/Neurosurgical-Conditions-and-Treatments/Glioblastoma-Multiforme> (accessed January 7, 2019).
- [2] Ohgaki, H.; Kleihues, P. *Am. J. Pathol.* **2007**, *170*, 1445-1453.
- [3] Urbańska, K.; Sokołowska, J.; Szmidt, M.; Sysa, P. *Contemp. Oncol. (Pozn)*. **2014**, *18*, 307-312.
- [4] John Hopkins Medicine. Neurology and Neurosurgery: Brain Tumour Centre. Brain Tumour Grades: Biopsy and Prognosis. https://www.hopkinsmedicine.org/neurology_neurosurgery/centers_clinics/brain_tumor/diagnosis/brain-tumor-grade.html (accessed January 9, 2018).
- [5] American Brain Tumour Association. Glioblastoma (GBM). https://www.abta.org/tumor_types/glioblastoma-gbm/ (accessed January 7, 2019).

- [6] Brain Tumour Foundation of Canada. Glioblastoma multiforme (GBM). <https://www.braintumour.ca/4869/glioblastoma-multiforme> (accessed January 7, 2019).
- [7] Shi, Y.; Lim, S. K.; Parada, L. F. *Cell Research*. **2014**, *24*, 910-911.
- [8] Appin, C. L.; et al. *Brain Pathol.* **2013**, *23*, 454-461.
- [9] Takeuchi, H.; Kitai, R.; Hosoda, T.; Yamada, S.; Hashimoto, N.; Kikuta, K.; Shimizu, Y.; Kimura, H. *J. Neurooncol.* **2016**, *127*, 337-344.
- [10] Barbashina, V.; Salazar, P.; Ladanyi, M.; Rosenblum, M. K.; Edgar, M. A. *Am. J. Surg. Pathol.* **2007**, *31*, 1196-1202.
- [11] Ohgaki, H.; Kleihues, P. *Clin. Cancer. Res.* **2012**, *19*, 764-772.
- [12] Rodriguez, F. J.; Orr, B. A.; Ligon, K. L.; Eberhart, C. G. *Oncotarget* **2012**, *3*, 98-106.
- [13] a) Messaoudi, K.; Clavreu, A.; Lagarce, F. *Drug Discov. Today* **2015**, *20*, 899-905. b) Lathia, J. D.; Mack, S. C.; Mulkearns-Hubert, E. E.; Valentim, C. L. L.; Rich, J. N. *Genes Dev.* **2015**, *29*, 1203–1217.
- [14] Bastiancich, C.; Bastiat, G.; Lagarce, F. *Drug Discov. Today* **2018**, *23*, 416-423.
- [15] Kitambi, S. S.; et al. *Cell* **2014**, *157*, 313–328.
- [16] Silverman, R. B.; and Holladay, M. W. *The Organic Chemistry of Drug Design and Drug Action*; Academic Press: San Diego, 2014.
- [17] Baell, J. B.; Nissink, J. W. M. *ACS. Chem. Biol.* **2018**, *13*, 36-44.
- [18] Roberts, S. A. *Xenobiotica* **2001**, *31*, 557-589.

[19] Gilbertson, R. J. *Cell* **2014**, *157*, 289-290.

[20] Lee, J. *Cancer Cell* **2006**, *9*, 391-403.

[21] a) Rapport, M. M.; Senear, A. E.; Mead, J. F.; Koepfli, J. B. *J. Am. Chem. Soc.* **1946**, *68*, 2695-2697. b) Rapport, M. M.; Senear, A. E.; Mead, J. F.; Koepfli, J. B. *J. Am. Chem. Soc.* **1946**, *68*, 2697-2703. c) Mead, J. F.; Rapport, M. M.; Koepfli, J. B. *J. Am. Chem. Soc.* **1946**, *68*, 2704-2705. d) Brown, R. F.; et al. *J. Am. Chem. Soc.* **1946**, *68*, 2705-2708. d) Mead, J. F.; Senear, A. E.; Koepfli, J. B. *J. Am. Chem. Soc.* **1946**, *68*, 2708-2710. e) Buchman, E. R.; Sargent, H.; Myers, T. C.; Howton, D. R. *J. Am. Chem. Soc.* **1946**, *68*, 2710-2714. f) Winstein, S.; Jacobs, T. L.; Levy, E. F.; Seymour, D.; Linden, G. B.; Henderson, R. B. *J. Am. Chem. Soc.* **1946**, *68*, 2714-2718. g) Buchman, E. R.; Howton, D. R. *J. Am. Chem. Soc.* **1946**, *68*, 2718-2720. h) Seibert, R. A.; Norton, T. R.; Benson, A. A.; Bergstrom, F. W. **1946**, *68*, 2721-2723.

[22] Pinder, R. M.; Burger, A. *J. Med. Chem.* **1968**, *11*, 267-269.

[23] Fernández-Álvaro, E.; Hong, W. D.; Nixon, G. L.; O'Neill, P. M.; Calderón, F. *J. Med. Chem.* **2016**, *59*, 5587-5603.

[24] Fuhler, G. M.; et al. *Mol. Med.* **2012**, *18*, 65-75.

[25] León, B.; Fong, J. C. N.; Peach, K. C.; Wong, W. R.; Yildiz, F. H.; Linington, R. G. *Org. Lett.* **2013**, *15*, 1234-1237.

[26] Hammarström, L. G. J. et al. *J. Med. Chem.* **2016**, *59*, 8577-8592.

[27] Färnegårdh, K.; Gravenfors, Y.; Ernfors, P.; Hammarström, L. G. J.; Kitambi, S. Compounds and Use for Treating Cancer. WO Patent 2015/033228 A2, March 12, 2015.

[28] a) Pfitzinger, W. *J. Prakt. Chem.* **1886**, 33, 100. b) Pfitzinger, W. *J. Prakt. Chem.* **1888**, 38, 582-584.

[29] Hofmann, A. W. *Berichte der Deutschen Chemischen Gesellschaft.* **1881**, 14, 2725-2736.

[30] Schönherr, H.; Cernak, T. *Angew. Chem. Int. Ed.* **2013**, 52, 12256-12267.

[31] a) Brooks, W. H.; Guida, W. C.; Daniel, K. G. *Curr. Top. Med. Chem.* **2011**, 11, 760-770. b) Lovering, F.; Bikker, J.; Humblet, C. *J. Med. Chem.* **2009**, 52, 6752-6756. c) McConathy, J.; Owens, M. J. *Primary Care Companion J. Clin. Psychiatry* **2003**, 5, 70-73.

[32] Bao, R. L-Y.; Zhao, R.; Shi, L. *Chem. Commun.* **2015**, 51, 6884-6900.

[33] Tan, S. K.; Jermakowicz, A.; Mookhtiar, A. K.; Nemeroff, C. B.; Schürer, S. C.; Ayad, N. G. *Front. Pharmacol.* **2018**, 9(218), 1-19.

[34] a) Doherty, G. J.; McMahon, H. T. *Annu. Rev. Biochem.* **2009**, 78, 857-902. b) Elkin, S. R.; Lakoduk, A. M.; Schmid, S. L. *Wien. Med. Wochenschr.* **2016**, 166, 196-204. c) Lim, J. P.; Gleeson, P. A. *Immunology and Cell Biology* **2011**, 89, 836-843. d) Naslavsky, N.; Caplan, S. J. *Cell. Sci.* **2018**, 131, 1-14.

[35] a) Overmeyer, J. H.; Young, A. M.; Bhanot, H.; Maltese, W. A. *Molecular Cancer* **2011**, 10(69), 1-17. b) Maltese, W. A.; Overmeyer, J. H. *Am. J. Pathol.* **2014**, 184, 1630-1642. c) Mbah, N. E.; Overmeyer, J. H.; Maltese, W. A. *Cell Biol. Toxicol.* **2017**, 33, 263-282. d) Li, Z.; Mbah, N. E.; Overmeyer, J. H.; Sarver, J. G.; George, S.; Trabbic, C. J.; Erhardt, P. W.; Maltese, W. A. *BMC Cancer* **2019**, 19(77), 1-20.

[36] Hutagalung, A. H.; Novick, P. J. *Physiol. Rev.* **2011**, 91, 119-149.

[37] Settembre, C.; Fraldi, A.; Medina, D. L.; Ballabio, A. *Nat. Rev. Mol. Cell Biol.* **2013**, 14, 283-296.

- [38] Elmore, S. *Toxicol. Pathol.* **2007**, *35*, 495-516.
- [39] Paddison, P. J.; Caudy, A. A.; Bernstein, E.; Hannon, G. J.; Conklin, D. S. *Genes Dev.* **2002**, *16*, 948-958.
- [40] a) Pavese, J. M.; Ogden, I. M.; Voll, E. A.; Huang, X.; Xu, L.; Jovanovic, B.; Bergan, R. C. *PLoS ONE* **2014**, *9*(7), 1-12. b) Pearson, G.; Robinson, F.; Gibson, T. B.; Xu, B-E.; Karandikar, M.; Berman, K.; Cobb, M. H. *Endocrine Reviews* **2001**, *22*, 153-183.
- [41] a) Cho, H.; Geno, E.; Patoor, M.; Reid, A.; McDonald, R.; Hild, M.; Jenkins, J. L. *ACS Omega* **2018**, *3*, 6097-6103. b) Falkenburger, B. H.; Jensen, J. B.; Dickson, J. E.; Suh, B-C.; Hille, B. J. *Physiol.* **2010**, *588*, 3179-3185.
- [42] a) Cingolani, F.; Simbari, F.; Abad, J. L.; Casasampere, M.; Fabrias, G.; Futerman, A. H.; Casas, J. J. *Lipid. Res.* **2017**, *58*, 1500-1513. b) Sun, L.; Li, B.; Su, X.; Chen, G.; Li, Y.; Li, L.; Wei, W. *J. Med. Chem.* **2017**, *60*, 6638-6648. c) Huang, W.; et al. *J. Med. Chem.* **2018**, *61*, 5424-5434.
- [43] Kwok, S. Application and Substrate Scope Expansion of a Unique Borylative Migration Transformation. M.Sc. Thesis, The University of Alberta, 2016.
- [44] Wilcken, R.; Zimmermann, M. O.; Bauer, M. R.; Rutherford, T. J.; Fersht, A. R.; Joerger, A. C.; Boeckler, F. M. *ACS Chem. Biol.* **2015**, *10*, 2725-2732.
- [45] Clement, H. A.; Hall, D. G. *Tetrahedron Lett.* **2018**, *59*, 4334-4339.
- [46] a) Russo, C. M.; Adhikari, A. A.; Wallach, D. R.; Fernandes, S.; Balch, A. N.; Kerr, W. G.; Chisholm, J. D. *Bioorg. Med. Chem. Lett.* **2015**, *25*, 5344-5348. b) Brown, W. G. *Org. React.* **1951**, *6*, 469-509.

- [47] Collin, G.; Höke, H. *Quinoline and Isoquinoline. Ullmann's Encyclopedia or Industrial Chemistry*; Wiley-VCH Verlag GmbH & Co. KGaA: Weinheim, 2012.
- [48] DasGupta, S.; Murumkar, P. R.; Giridhar, R.; Yadav, M. R. S. *Bioorg. Med. Chem.* **2009**, *17*, 3604–3617.
- [49] Kim, Y-R.; Hall, D. G. *Org. Biomol. Chem.* **2016**, *14*, 4739-4748.
- [50] Di, L.; Kerns, E. H. *Drug Discov. Today* **2006**, *11*, 446-451.
- [51] Dunleavy, J. K. *Platinum Metals Rev.* **2006**, *50*(2), 110.
- [52] Iwasaki, K.; Wan, K. K.; Oppedisano, A.; Crossley, S. W. M.; Shenvi, R. A. *J. Am. Chem. Soc.* **2014**, *136*, 1300–1303.
- [53] Jègou, G.; Jenekhe, S. A. *Macromolecules* **2001**, *34*, 7926-7928.
- [54] Zanon, J.; Kalpars, A.; Buchwald, S. L. *J. Am. Chem. Soc.* **2003**, *125*, 2890-2891.
- [55] *CellTiter 96® AQueous One Solution Cell Proliferation Assay*; Technical Bulletin #TB112; Promega Corporation: Madison, WI, 2012; 1-12.
- [56] Fang, G-H.; Yan, Z-J.; Deng, M-Z. *Org. Lett.* **2004**, *6*, 357-360.
- [57] Chen, W-L.; Wu, S-Y.; Mo, X-L.; Wei, L-X.; Lang, C.; Mo, D-L. *Org. Lett.* **2018**, *20*, 3527–3530.
- [58] Abdelwaly, A.; Salama, I.; Gomaa, M. S.; Helal, M. A. *Med. Chem. Res.* **2017**, *26*, 3173–3187.
- [59] Dhani, R.; et al. *J. Chem. Pharm. Res.* **2011**, *3*, 519-523.

[60] Kato, A.; et al. *Bioorg. Med. Chem.* **2011**, *19*, 3558–3568.

[61] Davies, S. G.; Ling, K. B.; Roberts, P. M.; Russell, A. J.; Thomson, J. E. *Chem. Commun.* **2007**, *0*, 4029–4031.

[62] Quartararo, C. E.; Reznik, E.; deCarvalho, A. C.; Mikkelsen, T.; Stockwell, B. R. *ACS Med. Chem. Lett.* **2015**, *6*, 948–952.

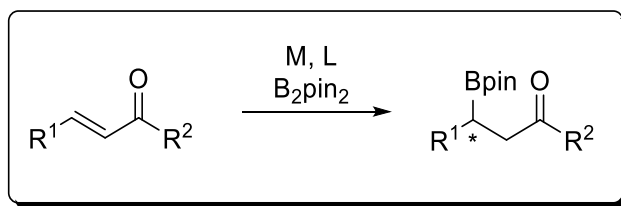
[63] Narlawar, R.; et al. *Chem. Asian J.* **2018**, *13*, 3321-3327.

[64] Jiang, C.; Zheng, Z-J.; Tian-Yang Yu, T-Y.; Wei, H. *Org. Biomol. Chem.*, **2018**, *16*, 7174-7177.

Chapter 3: Preparation of Enantioenriched Trisubstituted Cyclobutylboronates by Asymmetric Conjugate Borylation of Cyclobutenones

3.1 Conjugate Borylation

β -Borylation or conjugate borylation is the addition of a nucleophilic boryl species onto an electrophilic α,β -unsaturated acceptor.¹ This active reagent is generated by reaction of bis(pinacolato)diboron (B_2pin_2) with various transition metals, such as platinum (Pt), nickel (Ni), palladium (Pd), rhodium (Rh), or copper (Cu) (Scheme 3-1).¹ Asymmetric conjugate borylation is possible with an appropriate chiral metal or organocatalyst, which can give enantioenriched organoboron products.¹⁻²



Scheme 3-1: General conjugate borylation reaction.¹

To create C–C, C–O, C–X, and C–N bonds, chiral organoboron compounds can be employed through their diverse synthetic applications, such as transition metal catalyzed cross-coupling, homologation, halogenation, oxidation, amination, and olefination (Figure 3.1).³ Conjugate borylation is a common reaction that can readily prepare these valuable synthetic intermediates, and is an incredibly powerful tool to help create complex molecules or access privileged drug scaffolds in synthetic organic and medicinal chemistry endeavours.³

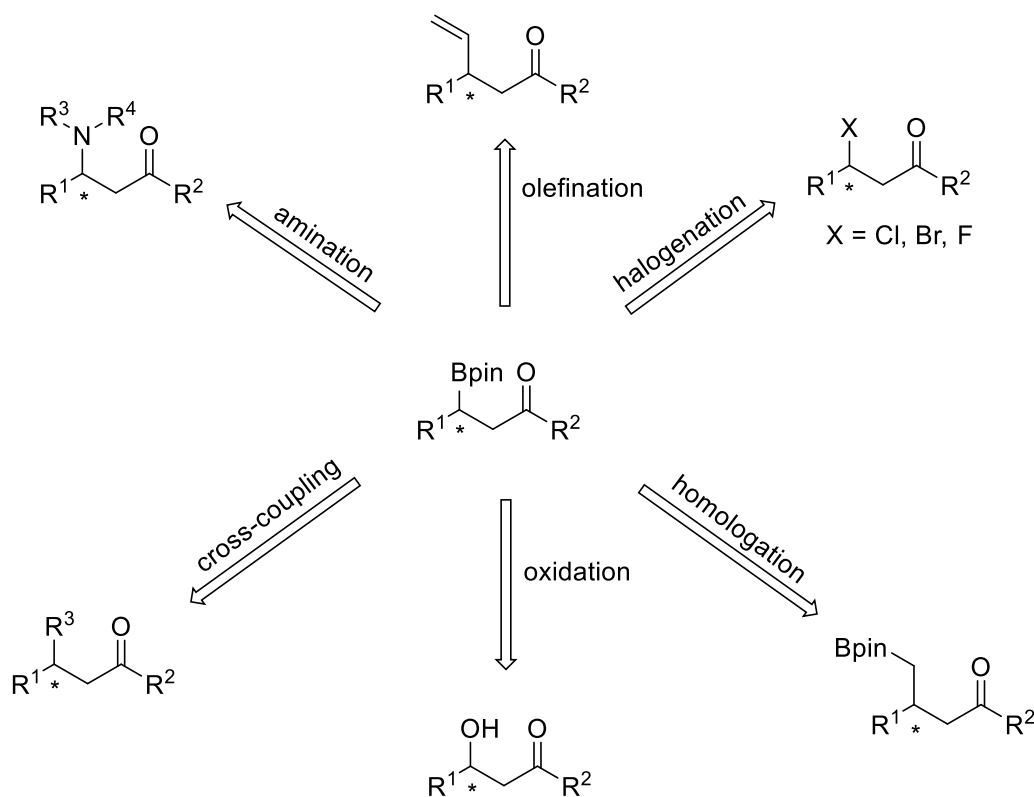
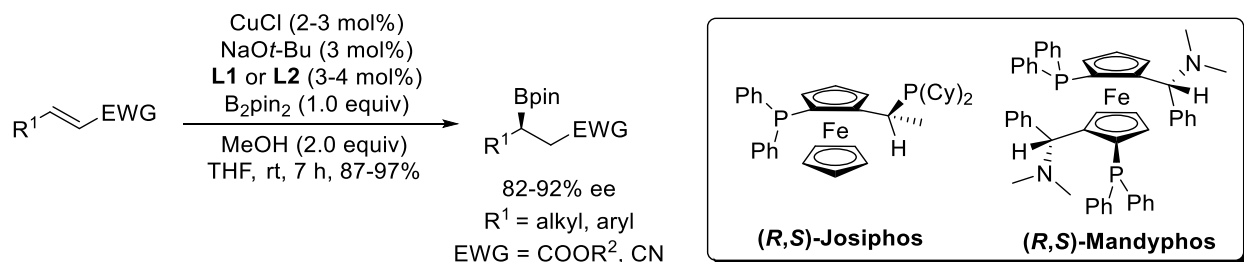


Figure 3-1: Stereospecific applications of organoboron compounds.³

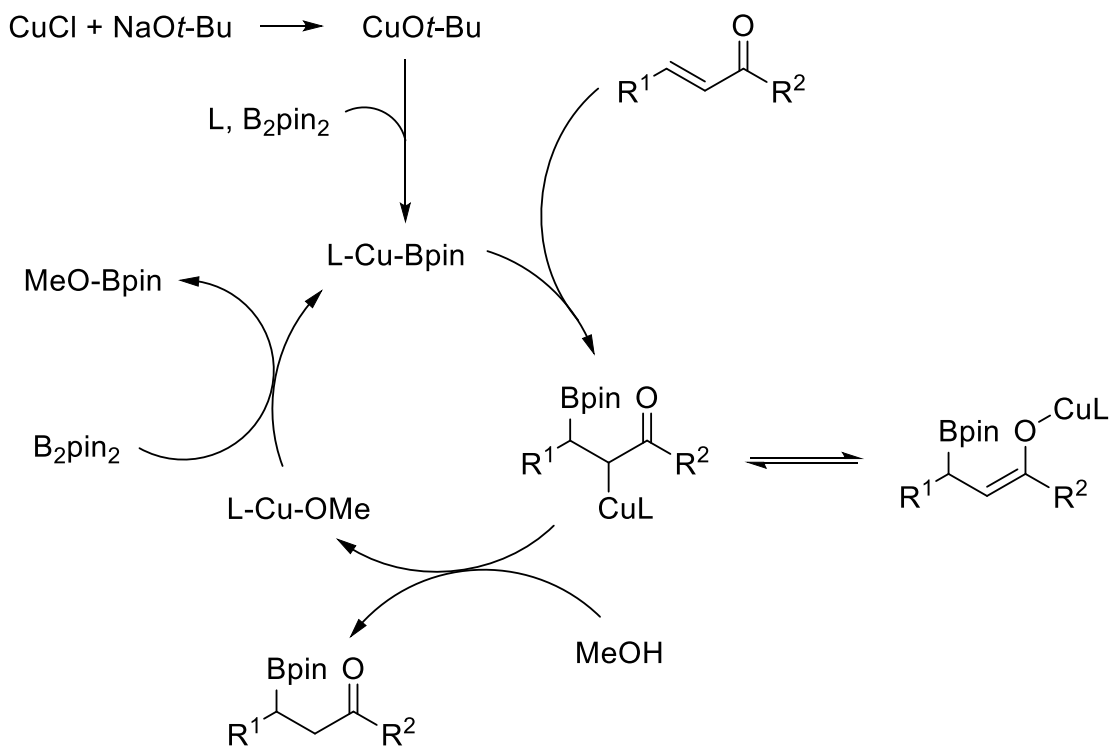
The preliminary development of the conjugate borylation reaction came from Marder and co-workers on their Pt catalyzed 1,4-diboration of α,β -unsaturated ketones with B_2pin_2 .⁴ This methodology formed the corresponding racemic α,β -hydroxy ketones after Bpin oxidation.⁴ Hosomi and Miyaura expanded upon this work by employing the first Cu(I) catalyzed borylation of enones using trialkyl phosphines or potassium acetate (KOAc) in the presence of CuCl and B_2pin_2 to form the borylated products in good yields.⁵ The Cu(I) conjugate borylation is a desirable way to generate organoboron compounds, due to commercial availability, ease of handling, and lower toxicity profile of Cu catalysts compared to other transition metals.¹ Despite the benefits of using Cu, there were significant limitations to Cu β -borylation at the time of its discovery.⁶ High catalyst loadings and temperature were necessary for good conversion to the borylated products, and only unhindered enones were viable substrates.⁶

To improve the generality of conjugate borylation, Yun and co-workers modified Hosomi and Miyaura's reaction conditions by using CuCl, the phosphine ligand DPEphos, sodium *tert*

butoxide (NaO*t*-Bu), and a methanol additive.⁶ The hindered based was found to work well with the ligand and improve product conversion, but it was the methanol additive that facilitated a much higher reaction rate, and improved the scope of this borylation chemistry to include α,β -unsaturated esters, phosphonates, nitriles, and β,β -disubstituted enones at milder temperatures and lower catalyst loadings.⁶ The authors were able to make the reaction enantioselective by employing the josiphos and mandyphos ligands on acyclic substrates (Scheme 3-2).⁷



Scheme 3-2: Yun's optimal conditions for a catalytic enantioselective Cu(I) conjugate borylation.

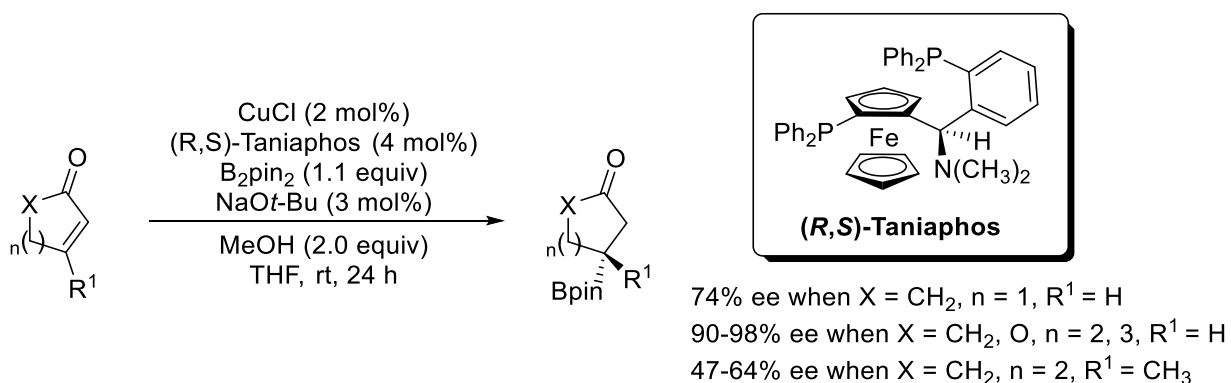


Scheme 3-3: Proposed catalytic cycle of Yun's Cu(I) conjugate borylation.⁶⁻⁹

Yun and co-workers hypothesized that the robustness of the reaction was due to protonation of the organocopper species with the MeOH after alkene addition from the boryl species.⁶⁻⁸ This protonation would generate a copper alkoxide that would be regenerated to the active catalyst by subsequent reaction with another equivalent of B₂pin₂.⁶⁻⁸ Marder and co-workers were able to corroborate this theory with high-level calculations, which resulted in the generally accepted catalytic cycle shown above (Scheme 3-3).⁶⁻⁹

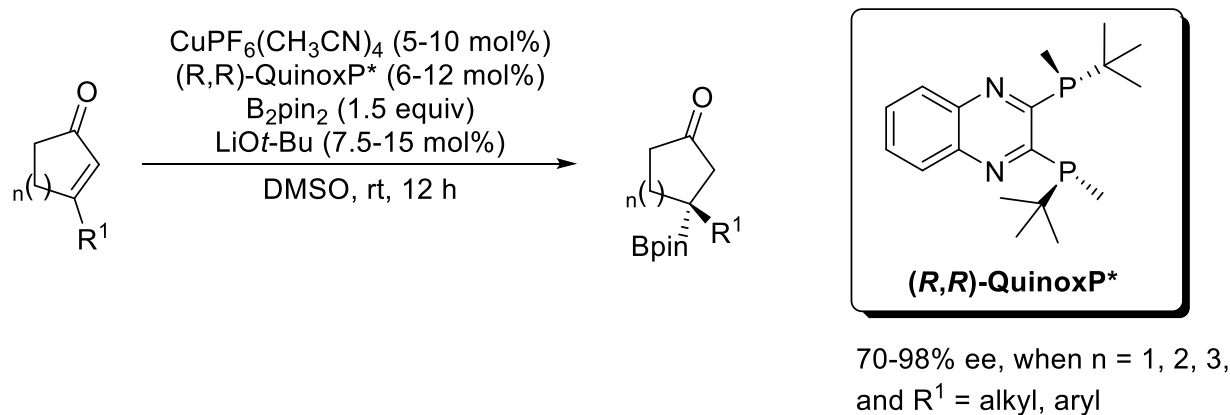
3.2 Conjugate Borylation of Cyclic Enones

Using the system of Cu, alkoxide base, and methanol, conjugate borylation became a very high-yielding and enantioselective process towards a variety of acyclic α,β -unsaturated acceptors. A limiting substrate using this methodology however, were the cyclic enones, as there were no enantioselective conditions available for these substrates.¹⁰ Furthermore, if these substrates were substituted in the β -position, their reactivity was also very sluggish due to the difficulty in forming a quaternary chiral centre.¹¹ Once again, Yun and co-workers were able to make another contribution towards the field with a successful enantioselective conjugate borylation of cyclic enones using a Cu-Taniaphos complex (Scheme 3-4). The reaction is synthetically useful for cyclohexenones, cycloheptenones, and pentenolides. A major drawback of Yun and co-worker's methodology was lower enantioselectivities observed for cyclopentenones and β -substituted cyclohexenones.



Scheme 3-4: Asymmetric Cu-catalyzed conjugate borylation of cyclic enones with (R,S)-Taniaphos.¹⁰

Complementarily to the findings of Yun, Shibasaki and co-workers managed to overcome the limitations of conjugate borylation on cyclopentenones and β -substituted cyclic enones by employing the (*R,R*)-QuinoxP* ligand, which gave the desired cyclopentyl- and cyclohexylboronates in high yield and enantioselectivity (Scheme 3-5).¹¹ An interesting variation in their reaction conditions was the omission of MeOH as an additive, and the use of hexafluorophosphate (PF₆) counteranion, which was thought to form catalytic LiPF₆ *in situ* and increase the catalytic turnover of the Cu catalyst—thus, eliminating the need for a protic additive. The authors also highlighted the utility of the copper enolate formed during the borylation by trapping this intermediate with benzaldehyde to get the corresponding aldol addition products in high enantioselectivity and modest diastereoselectivity. Ultimately, the ability to form optically active tertiary boronates was a significant advance in conjugate borylation chemistry. Two other major methodologies followed that of Shibasaki to access tertiary boronates. The first was Takacs and co-workers' oxime-directed asymmetric hydroboration, and the second was a conjugate borylation using chiral N-heterocyclic carbenes (NHCs) by Hoveyda and co-workers.¹²⁻¹³ A glaring and lingering limitation despite all of the advances in β -borylation by Yun, Shibasaki, Hoveyda and Takacs, is the inability to form borylated cyclobutanones (cyclobutylboronates) from conjugate borylation of the respective cyclobutenones.

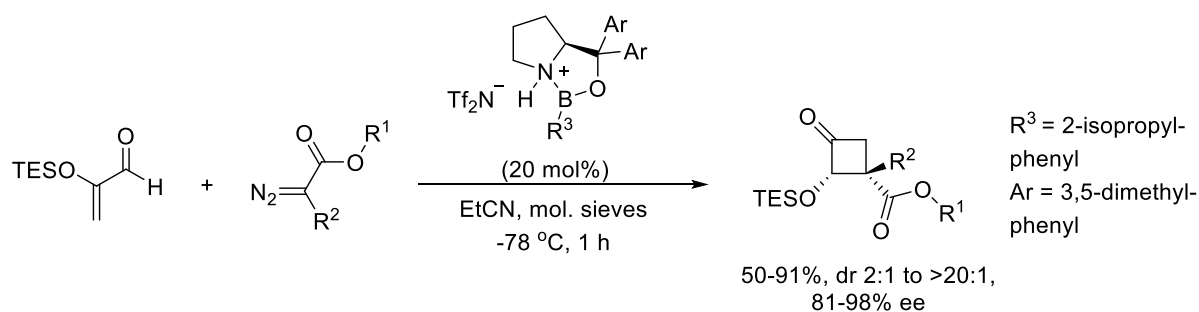


Scheme 3-5: Asymmetric Cu-catalyzed conjugate borylation of β -substituted cyclic enones with (*R,S*)-QuinoxP*.¹¹

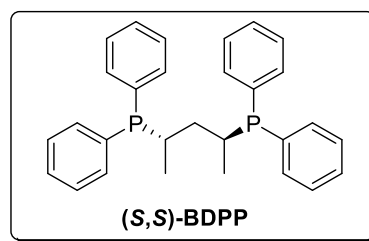
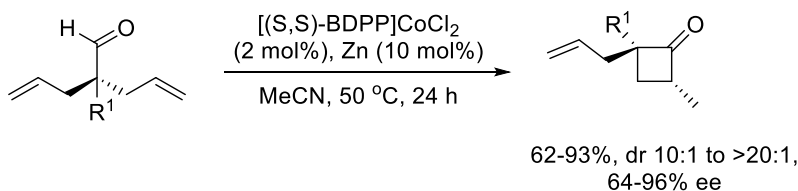
3.3 Cyclobutanones and Cyclobutylboronates

As described in Chapter 1, cyclobutanones are common scaffolds in medicinal chemistry that exhibit encouraging biological activity as penicillin mimics.¹⁴ Several routes of preparation and application of cyclobutanones exist that highlight their utility as a synthon, but there are limited reports to make chiral cyclobutanones enantioselectivity (Scheme 3-6).¹⁵

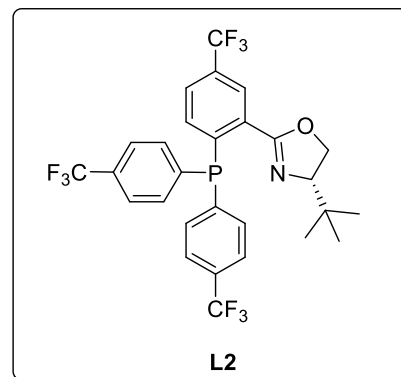
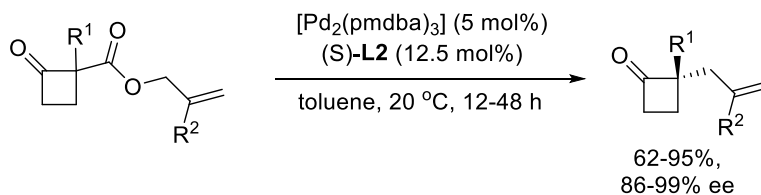
Tandem cyclopropanation/semipinacol rearrangement (Ryu)¹⁶



Intramolecular hydroacylation (Dong)¹⁷



Asymmetric allylic alkylation (Stoltz)¹⁸

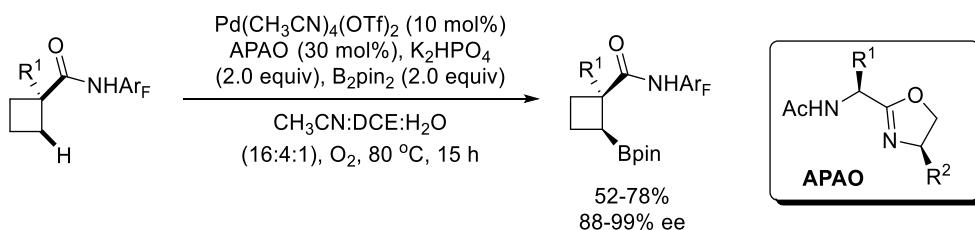


Scheme 3-6: Contemporary reactions to synthesize enantioenriched α/β substituted cyclobutanones.

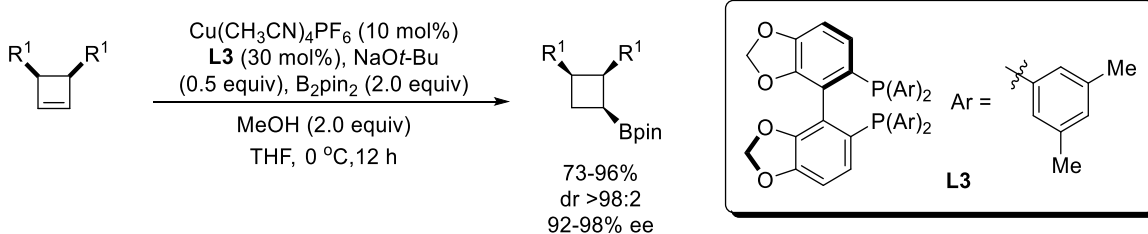
Ryu and co-workers reported a chiral Lewis acid catalyzed enantioselective formation of cyclobutanones through tandem cyclopropanation/semipinacol rearrangement starting from α -silyloxyacroleins and diazoesters.¹⁶ Dong and co-workers were able to synthesize enantioenriched cyclobutanones bearing chiral α -quaternary carbon centers by intramolecular hydroacylation of a prochiral dienyl aldehyde with a Co-catalyst.¹⁷ The catalytic asymmetric allylic alkylation developed by Stoltz and co-workers, was also successful in forming a cyclobutanone with an α -quaternary centre next to the carbonyl.¹⁸

While conjugate borylation methodologies are lacking to prepare cyclobutylboronates, they can be prepared indirectly through a few novel catalytic enantioselective transformations (Scheme 3-7).¹⁹⁻²¹

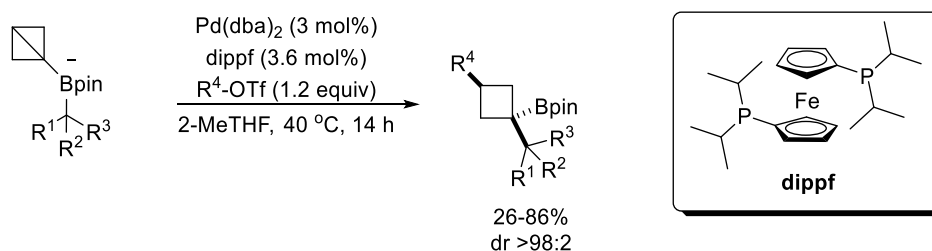
C-H activation (Yu)¹⁹



Desymmetrization (Tortosa)²⁰



Carbopalladation of strained boronates (Aggarwal)²¹



Scheme 3-7: Synthetic methods for the preparation of cyclobutylboronates.

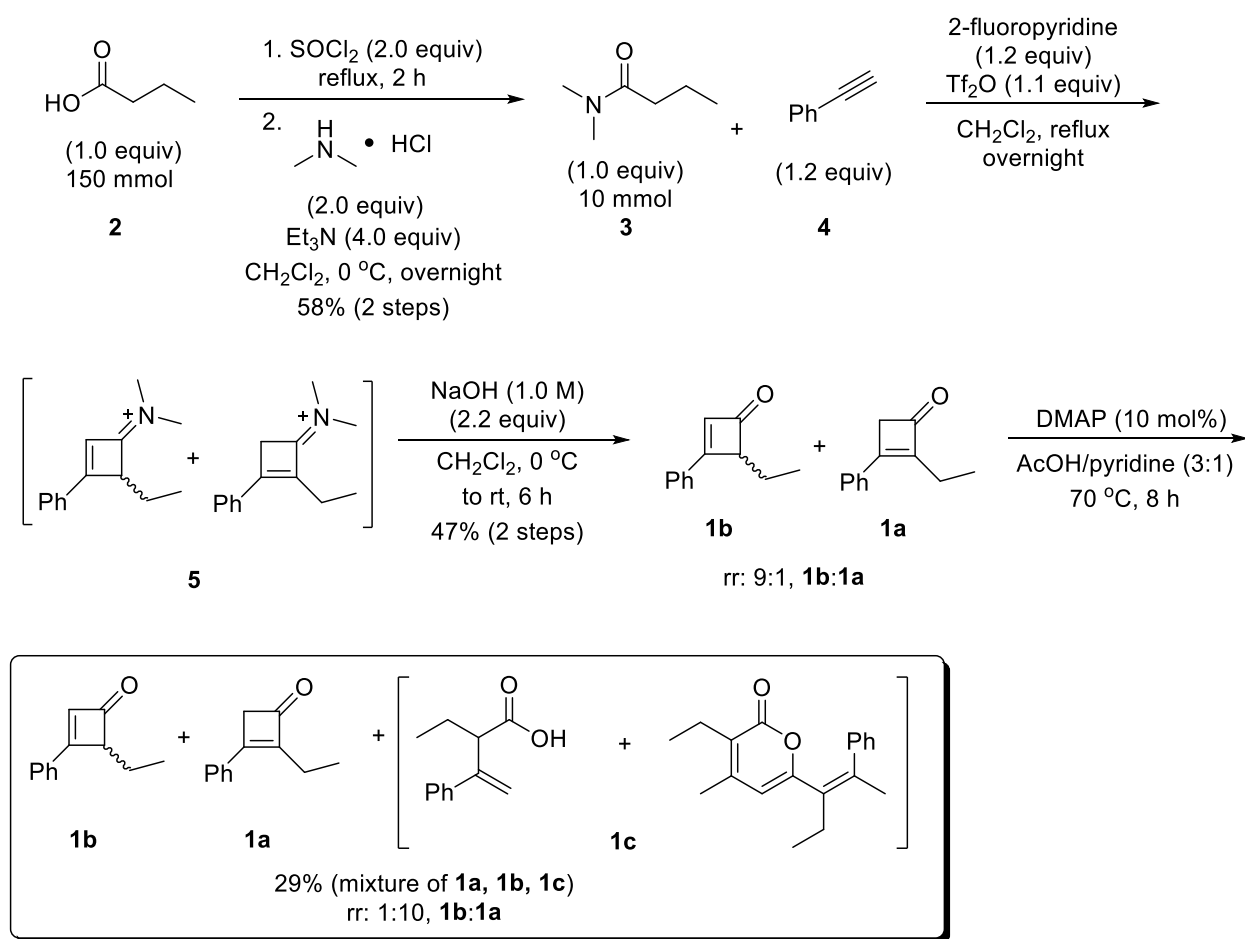
Desymmetrization of cyclobutenes to the corresponding cyclobutylboronate was accomplished by Tortosa and co-workers via a Cu-catalyzed hydroboration with B₂pin₂ in the presence of a chiral SEGPHOS ligand derivative.¹⁹ A Pd-catalyzed C-H activation with an APAO ligand facilitated a successful borylation of cyclobutyl carboxamides to generate the desired cyclobutylboronate.²⁰ Lastly, Aggarwal and co-workers were able to generate cyclobutylboronates diastereoselectively via an aryl palladium(II) complex interacting with a strained bicyclo[1.1.0]butyl boronate in the presence of various aryl triflates.²¹ While Tortosa and Yu were successful in preparing cyclobutylboronates enantioselectivity, there are some limitations to each reaction.¹⁹⁻²⁰ The desymmetrization limits the functionality and the variability that one can employ on the cyclobutene precursor. Yu is only able to vary one of the two stereogenic centres generated from the C-H activation, which limits diversification on the cyclobutylboronate scaffold. Aggarwal's Pd chemistry is a rare example of forming a cyclobutylboronate with a quaternary centre, which is extremely useful in drug discovery²¹; highly functionalized sp³ carbons tend to have better biological activity and binding affinities to biological targets.²² Aggarwal's methodology is complementary to Shibasaki's success in forming quaternary centres on four, five, six, and seven-membered cyclic enones, but the downside is the lack of chirality due to the symmetry of the tertiary cyclobutylboronate products. Taking all of the limitations of cyclobutylboronate preparation into consideration, the Hall Group and a small team at Pfizer wanted to contribute to this growing field by developing a catalytic enantioselective conjugate borylation reaction that could prepare tertiary cyclobutylboronates with diverse functional groups that would allow for greater synthetic elaboration of the cyclobutane drug scaffold—potentially leading to new biologically active molecules.²³

3.4 Alkene Migration Optimization for α,β -Substituted Cyclobutenones

As described in Chapter 1, The Hall Group and Pfizer succeeded in developing a Cu-catalyzed conjugate borylation of an α,β -substituted cyclobutenone to form the tertiary cyclobutylboronate product. The high-throughput screening (HTS) technology at Pfizer found that the (*S,S*)-BDPP ligand enabled the reaction to be performed in high enantioselectivity (>90%). Until a very recent paper published by Jiao and co-workers on cyclobutenone synthesis,²⁴ the cyclobutenone substrates used by the Hall Group and Pfizer for the conjugate borylation were

unknown. These novel substrates made the exploration of a substrate scope for the conjugate borylation difficult, as many of them could not tolerate the harsh conditions required for the alkene migration step to prepare the α,β -substituted cyclobutenones containing a tetrasubstituted alkene (Scheme 3-8). Milder conditions had to be developed to grow the library of cyclobutenone precursors.

The realization that milder conditions were required for the cyclobutenone preparation started with an attempted synthesis of an ethyl phenyl α,β -substituted cyclobutenone **1** using Boghi's route from Chapter 1 (Scheme 3-8).



Scheme 3-8: Attempted preparation of ethyl phenyl α,β -substituted cyclobutenone **1**.

This substrate was designed to probe substituent effects in the α -position for the conjugate borylation reaction. The synthesis begins by transforming butyric acid **2** into an acid chloride. The

acid intermediate reacts with dimethyl amine hydrochloride to form tertiary amide **3**. Then, a [2+2] cycloaddition between amide **3** and phenyl acetylene **4** in the presence of triflic anhydride and 2-fluoropyridine form the regioisomeric mixture of cyclobuteniminium salts **5**. Hydrolysis of the salts yield the title cyclobutenone as a 1:9 mixture of regioisomers **1a** and **1b**. When subjected to Boghi's alkene migration conditions, there was conversion to the desired regioisomer **1a**, but the undesired regioisomer **1b** still remained in significant quantities. More concerningly, there seemed to be competition between formation of **1a** and a combination of ring-opened and dimer byproducts **1c** from the thermal conditions of the reaction, based on relevant ethyl signals in the crude ^1H NMR spectrum (Figure 3-2).²⁵

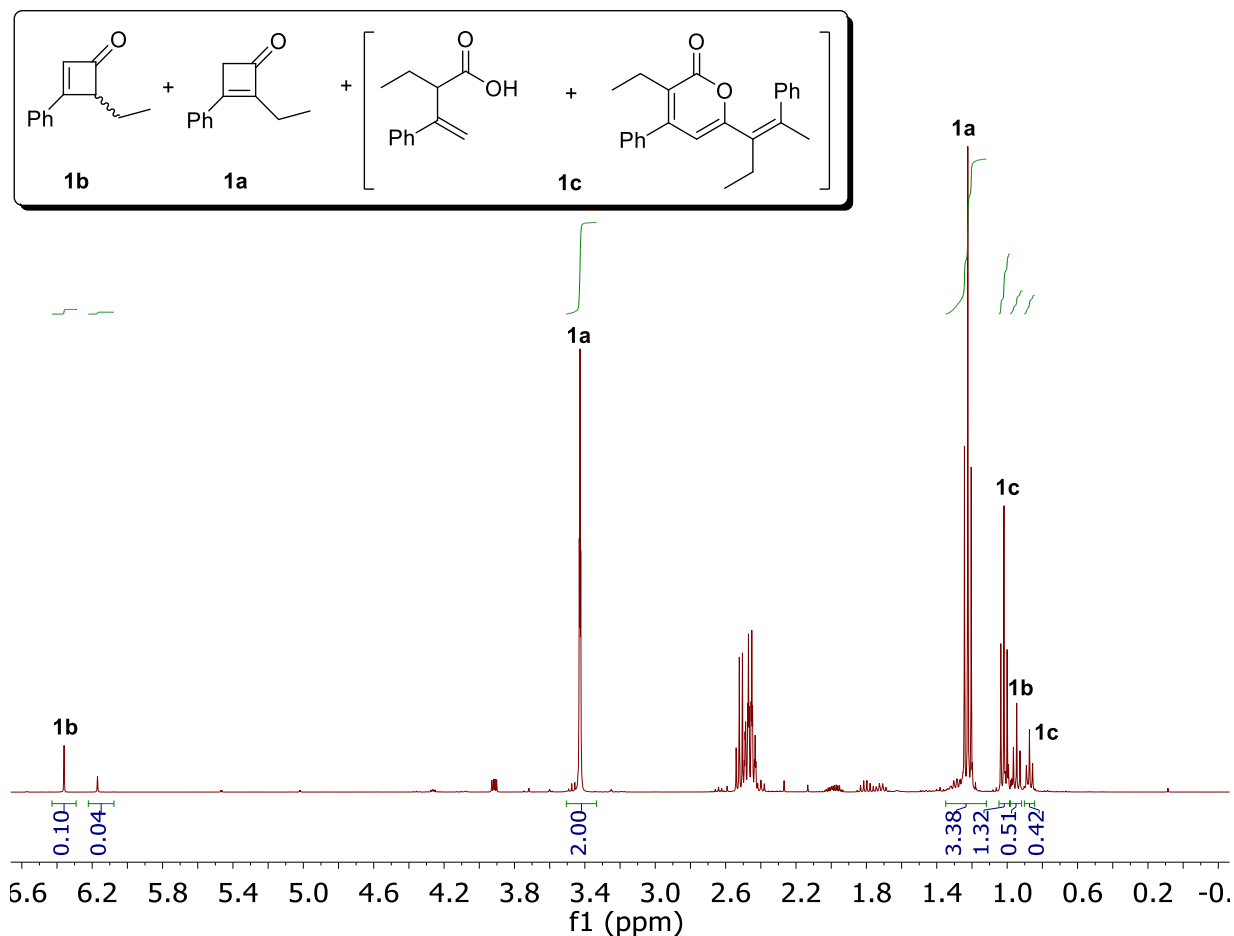
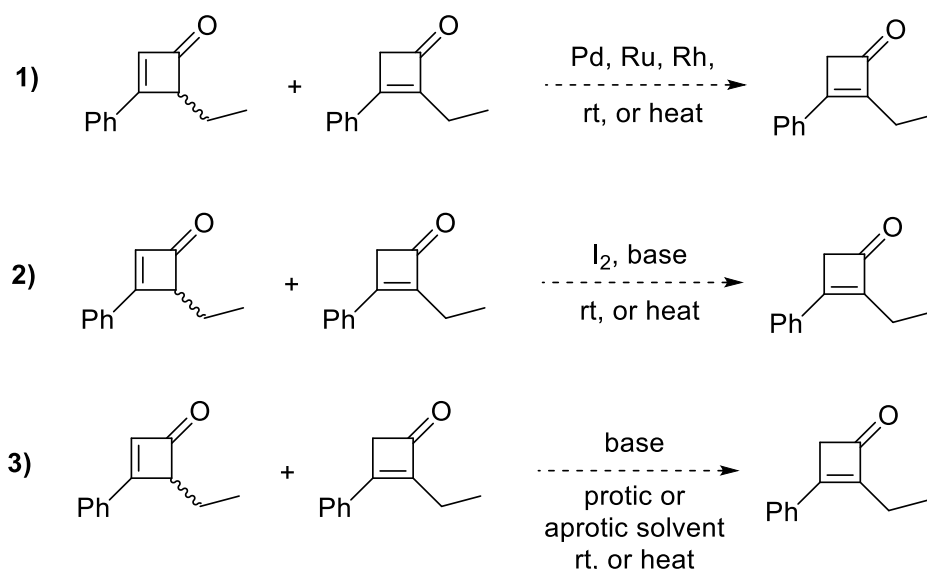


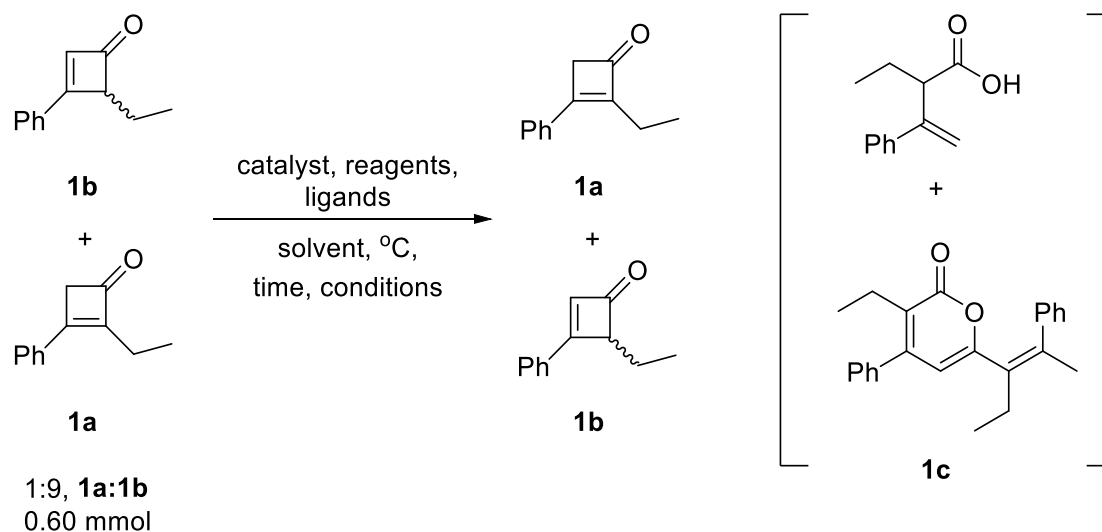
Figure 3-2: ^1H NMR of ethyl phenyl cyclobutenone regioisomers, as well as the proposed ring-opened and dimer byproducts.

The byproducts **1c** could likely be separated by flash column chromatography (FCC), however, previous attempt to separate the regioisomers by Boghi were unsuccessful. Thus, new alkene migration conditions needed to be implemented that could fully form the desired regioisomer **1a**, and eliminate the formation of the thermal byproducts **1c**.

Three alternative alkene migration reactions were tested: 1) transition metal catalyzed, 2) halogenation and elimination, and 3) base-catalyzed under protic and aprotic conditions (Scheme 3-9). Several metals such as Fe, Pd, Ru, and Rh, have been used to migrate alkenes in a variety of allylic substrates.²⁶ The more relevant examples towards cyclobutenone regioisomeric mixtures were $\text{RhCl}_3 \cdot 3\text{H}_2\text{O}$, $\text{RuH}_2(\text{CO})(\text{PPh}_3)_3$, and $\text{Rh}[(\text{CO})_2\text{Cl}]_2$ which are employed to migrate alkenes in cyclic enones, cyclic allylic acetals, and β,γ -unsaturated ketones respectively.²⁷ Iodination of olefins, followed by an E2 elimination is a well-established strategy towards a variety of synthetic applications and alkene migration scaffolds.²⁸ Double bond migrations of olefins and α,β -unsaturated ketones have also been thoroughly investigated using strong nucleophilic and non-nucleophilic bases.²⁹ The regioisomeric mixture of cyclobutenone **1a** and **1b** was used as the model substrate for alternative alkene migration conditions on a 0.6 mmol scale. Since the majority of these reactions were ran at higher temperature, thermal ring-opening products **1c** also had to be considered for optimization purposes—especially in the case of transition metal catalyzed alkene migrations.²⁵ The results of these optimizations are summarized in Table 3-1 below.



Scheme 3-9: Alternative approaches to alkene migration.²⁶⁻²⁹



Entry	Catalyst/ligands/reagents	Conditions	Solvent	°C	Time	1a:1b:1c ¹ (yield) ²
1	RuH ₂ (CO)(PPh ₃) ₃ (5 mol%)	Air	EtOH (95%)	80	24 h	1:0:4 (19%)
2	RhCl ₃ • 3H ₂ O (5 mol%)	Air	EtOH (95%)	50	24 h	1:9:0
3	[Rh(CO) ₂ Cl] ₂ (5 mol%) Ph ₃ PCH ₂ PPh ₃ (12 mol%)	Argon	DME*	65	20 h	0:5:95
4	[(<i>t</i> -Bu) ₃ PPdBr] ₂ (0.5 mol%)	N ₂	toluene	rt	18 h	1:9:0
5	Pd(OAc) ₂ (1 mol%)	N ₂	HFIP*	rt	24 h	1:9:0
6	(C ₆ H ₅ CN) ₂ PdCl ₂ (1 mol%)	N ₂	THF	rt	6 h	1:9:0
7	Pd(<i>dba</i>) ₃ • CHCl ₃ (10 mol%)	N ₂	DME	80	6 h	3:0:97
8	Grubb's II	Air	MeOH	60	3 h	1:9:0
9	I ₂ (30 mol%)	Air	pyridine	rt	48 hr	5:95:0
10	KO <i>t</i> -Bu (30 mol%)	N ₂	THF	rt	3 hr	2:0:98
11	KO <i>t</i> -Bu (30 mol%)	N ₂	EtOH (95%)	rt	3 hr	100:0:0 (97%)

¹ Ratios of products determined by integrations and peak heights of ethyl signals in ¹H NMR using 0.200 mmol of 1,3,5-trimethoxybenzene as an internal standard.

² Isolated yield after flash column chromatography (FCC).

* HFIP = hexafluoroisopropanol, DME = dimethoxyethane.

Table 3-1: Summary of alkene migration conditions for ethyl phenyl α,β -substituted cyclobutenone **1**.

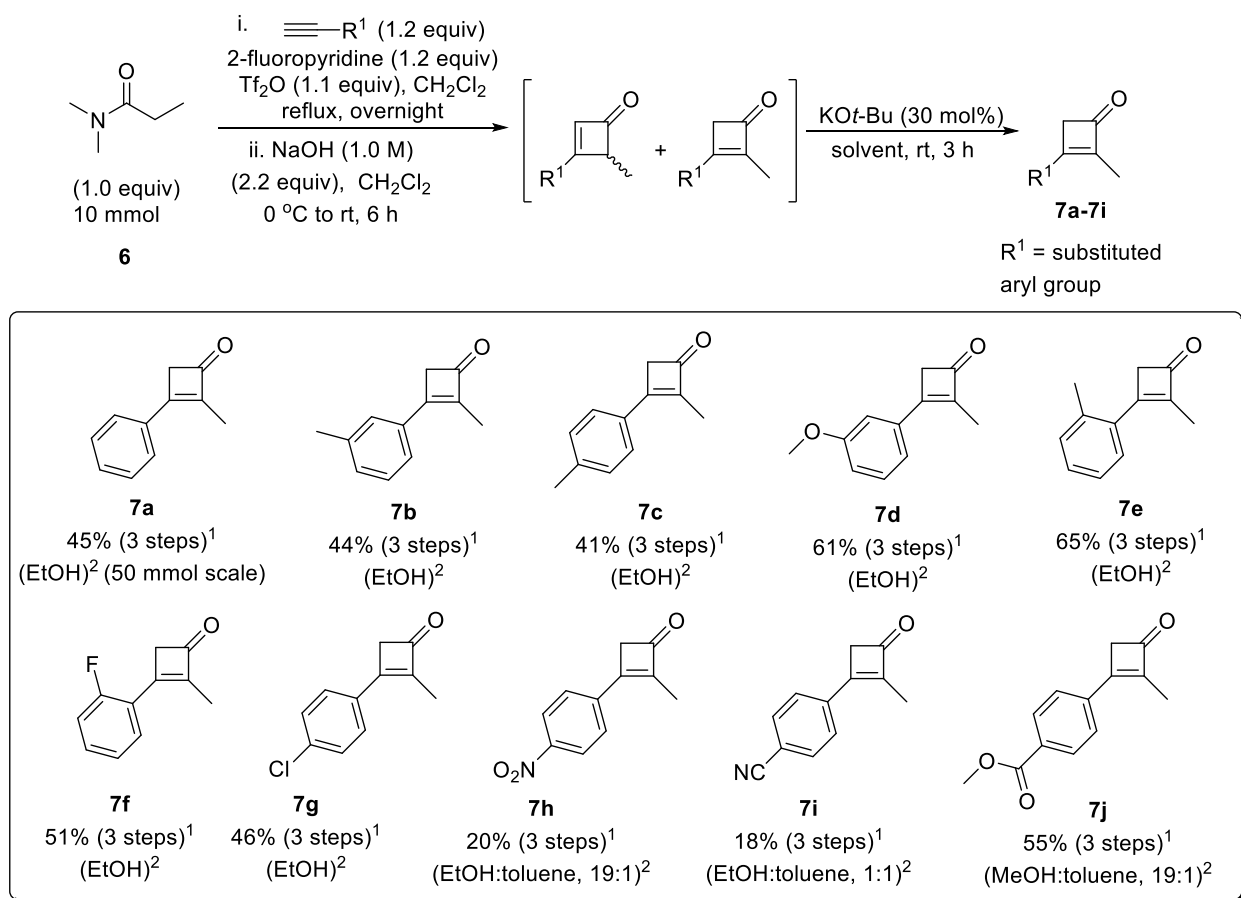
The RuH₂(CO)(PPh₃)₃ catalyst with high temperature, protic solvent, and open to air did facilitate full conversion to the desired regioisomer **1b** in low isolated yield (entry 1), however, the major products of the reaction were ring-opened or dimers **1c**.^{27b} Lowering temperature did not manage to improve this catalytic system, so other metals were attempted. Despite RhCl₃•3H₂O being well known to facilitate alkene migration of cyclic enones, when employed on the cyclobutenone mixture it only gave recovered starting material with mild heating and extended reaction time (entry 2).^{27a} Heating past 50 °C with this Rh catalyst began to promote the undesired formation of byproducts **1c**. Yu's conditions to isomerize β,γ-unsaturated ketones also failed on the cyclobutenone mixture, giving exclusive formation of **1c** products from the thermal conditions (entry 3).^{27c} Since Rh and Ru are known to insert into cyclobutenones and facilitate a variety of electrocyclic ring-opening reactions,²⁵ it was thought that Pd might be able to circumvent these detrimental side reactions.^{26d,30} Pd(II) species were unreactive, and only the regioisomeric mixture was recovered (entries 4-6). Pd(0) resulted in unwanted products **1c** (entry 7). Grub's II catalyst is known to migrate terminal allylic alkenes to give the more thermodynamically favoured *E*-alkene.³¹ Unfortunately, the regioisomeric cyclobutenone mixture remained inert towards the Ru catalyst (entry 8). Iodination and elimination favoured the undesired regioisomer **1b**, however, this did indicate that base catalysis had a profound effect on alkene migration without formation of the ring-opened or dimer products **1c** (entry 9). This observation led us to using catalytic amounts of potassium *tert*-butoxide (KO*t*-Bu) in an aprotic solvent that yielded the undesired decomposition products **1c** (entry 10). Remarkably, by changing from an aprotic to a protic solvent with the same catalytic amounts of KO*t*-Bu, the desired α,β-substituted cyclobutenone **1a** was exclusively formed (entry 11), and obtained in quantitative yield after FCC purification as a single regioisomer. Synthesis of a library of cyclobutenones could now commence by using these milder base-catalyzed alkene migration conditions.

3.5 Synthesis of a Small Library of α,β-Substituted Cyclobutenones

For the next series of cyclobutenone analogs, there was a desire to probe the steric and electronic effects of the β-substituted aryl group of the cyclobutenone in relation to the conjugate borylation. Different electron-donating (EDGs) and electron-withdrawing groups (EWGs) were added to the phenyl ring of terminal alkyne **4** used in the [2+2] cycloaddition. In addition, there

was an interest in switching to different aromatic heterocycles, alkyl groups, and silyl substituents in the β -position. Initial results of a conjugate borylation reaction conducted by group member Clement on a cyclobutenone with a benzyl group in the α -position showed a diminished enantioselectivity. The α -carbon of these new cyclobutenone analogs remained substituted with a methyl group as such.

The synthesis of the cyclobutenone analogs is shown in Scheme 3-10 with many similarities to Scheme 3-8, except for the tertiary amide in the Et substrate is replaced with the commercially available *N,N*-dimethylpropionamide **6**.



¹ Isolated yield of single regioisomer after FCC purification.

² Optimal solvent system for the alkene migration step.

Scheme 3-10: Scope of α,β -substituted cyclobutenones.

The rest of the synthesis follows the same conditions for the [2+2] cycloaddition and hydrolysis steps. Once the regioisomeric mixture of cyclobutenones are formed, they are subjected to the KOt-Bu-promoted isomerization conditions to acquire the desired α,β -substituted cyclobutenones in low to good isolated yields over the three steps (Scheme 3-10). The sequence to generate cyclobutenones is very tolerant towards weak EDGs and EWGs in the *ortho*, *para*, and *meta* positions (**7b-7c**, **7e** and **7f-7g**). The control substrate (methyl phenyl cyclobutenone) **7a** was particularly noteworthy, as it could be prepared on a multigram scale (50 mmol), highlighting the scalability of the milder alkene migration step in the synthetic route. Stronger EDGs were robust in the *meta* position (**7d**), and powerful EWGs were tolerated in the *para* position (**7h-7j**), but the yields of the nitro cyclobutenone **7h** and nitrile **7i**, were considerably lower. This diminished yield can be attributed to low solubility in protic solvents, and difficulty in purifying the product by FCC. Trituration or recrystallization may help improve the yields of **7h** and **7i** in the future.

There were several limitations to the cyclobutenone preparation (Figure 3-3). Strong EDGs in the *para* position of the aryl ring were unsuccessful at forming cyclobuteniminium salts, possibly as a result of unfavourable electronics stymieing the [2+2] cycloaddition.³² Attempting to replace the β -phenyl group with alkyl, and silyl groups was also not possible due to volatility, decomposition, or only partial conversion to the desired cyclobutenone regioisomer. Replacing the α methyl group with EDG and EWGs was also not tolerated during the [2+2] cycloaddition.

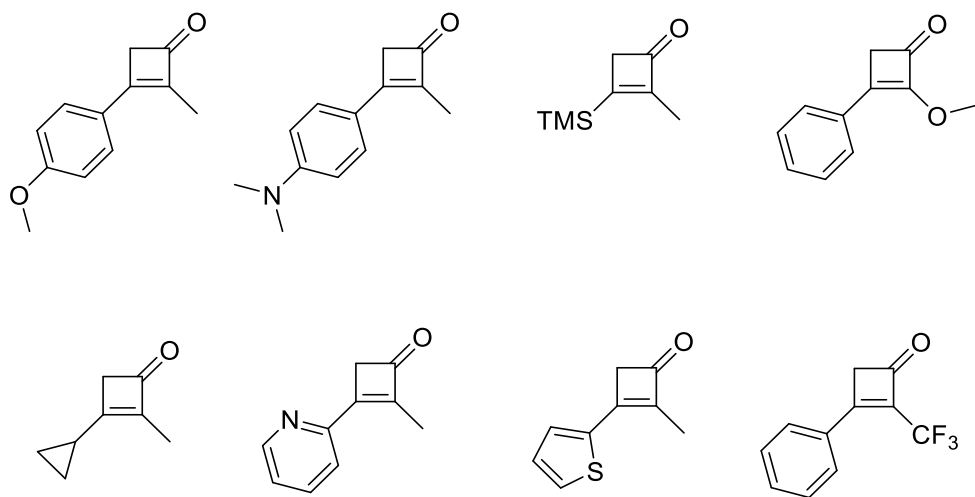


Figure 3-3: Unsuccessful substrates in the cyclobutenone synthetic route.

A pyridine heterocycle gave no reaction in the [2+2] cycloaddition, likely because its nucleophilicity interfered with the formation of the cyclobuteniminium salts. The thiophene heterocycle gave trace yield with several impurities that could not be eliminated by FCC.

3.6 Preliminary Substrate Scope of Conjugate Borylation

Following the optimized conditions and reaction setup from Clement, the cyclobutenone library was subjected to the enantioselective conjugate borylation reaction to obtain the desired tertiary cyclobutylboronates (Scheme 3-11). Special attention was given to the tolyl substrates **7b-7c**, **7e** and the simpler electronic cyclobutenones **7d**, **7f**, and **7g**. The enantioselectivity for the control substrate **7a** has already been determined, but it was run in tandem with the α -ethyl substituted cyclobutenone **1a** and other substrates to ensure accuracy in reaction reproducibility, and enantioselectivity. The stronger EWG cyclobutenones **7h-7j**, were not attempted until it was determined if EWGs on the phenyl ring detrimentally impacted the conjugate borylation. The *syn* stereochemistry of the cyclobutylboronates in Scheme 3-11 are representative of the major diastereomer, based on a crystal structure obtained by Clement (Figure 3-4).

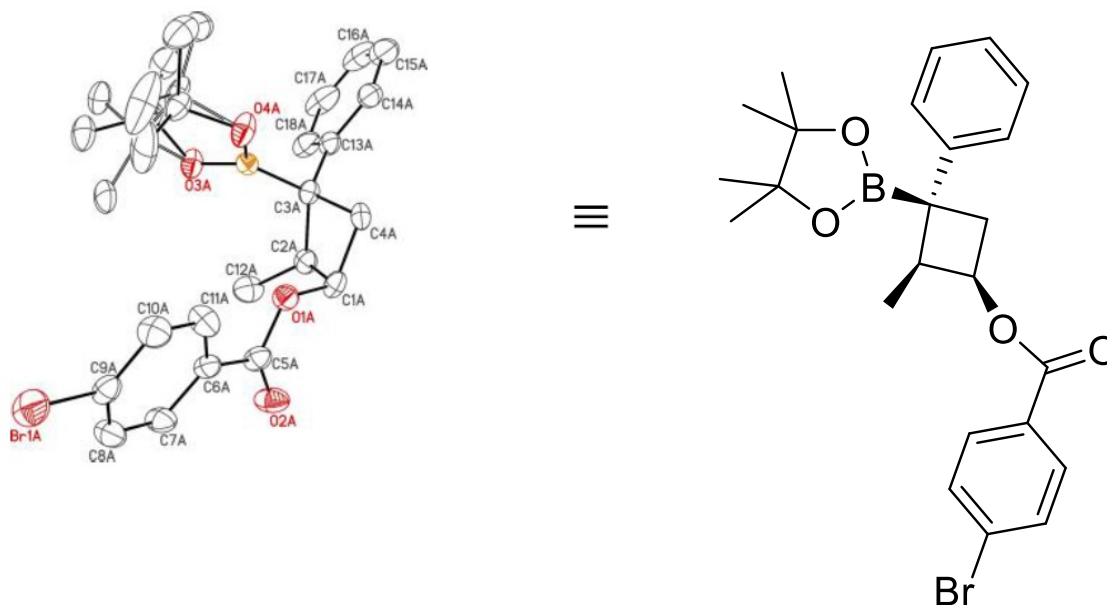


Figure 3-4: ORTEP representation of Clement's cyclobutylboronate crystal structure revealing the stereochemistry of the major diastereomer after conjugate borylation.

The absolute stereochemistry of the major cyclobutylboronate diastereomer can also be rationalized based on the diastereofacial selectivity of the conjugate borylation (Figure 3-5). After insertion of the C–C double bond of the cyclobutenone into the B–Cu bond, the copper enolate intermediate undergoes the methanol-catalyzed proto-decupration, which follows a kinetic control and occurs from the bottom face of the cyclobutanone.³³ One can rationalize that protonation from the bottom face avoids larger steric penalties with the Bpin group compared to the flatter phenyl ring and methyl group. Thus, the observed major product has the Bpin and α -substituent with a *syn* configuration. The minor thermodynamic product would put the α -substituent and Bpin unit *anti* to each other.

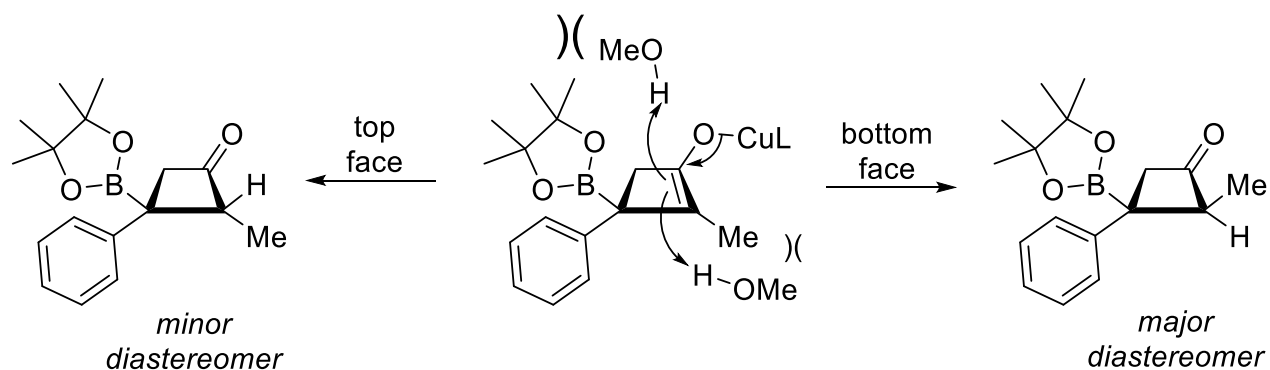
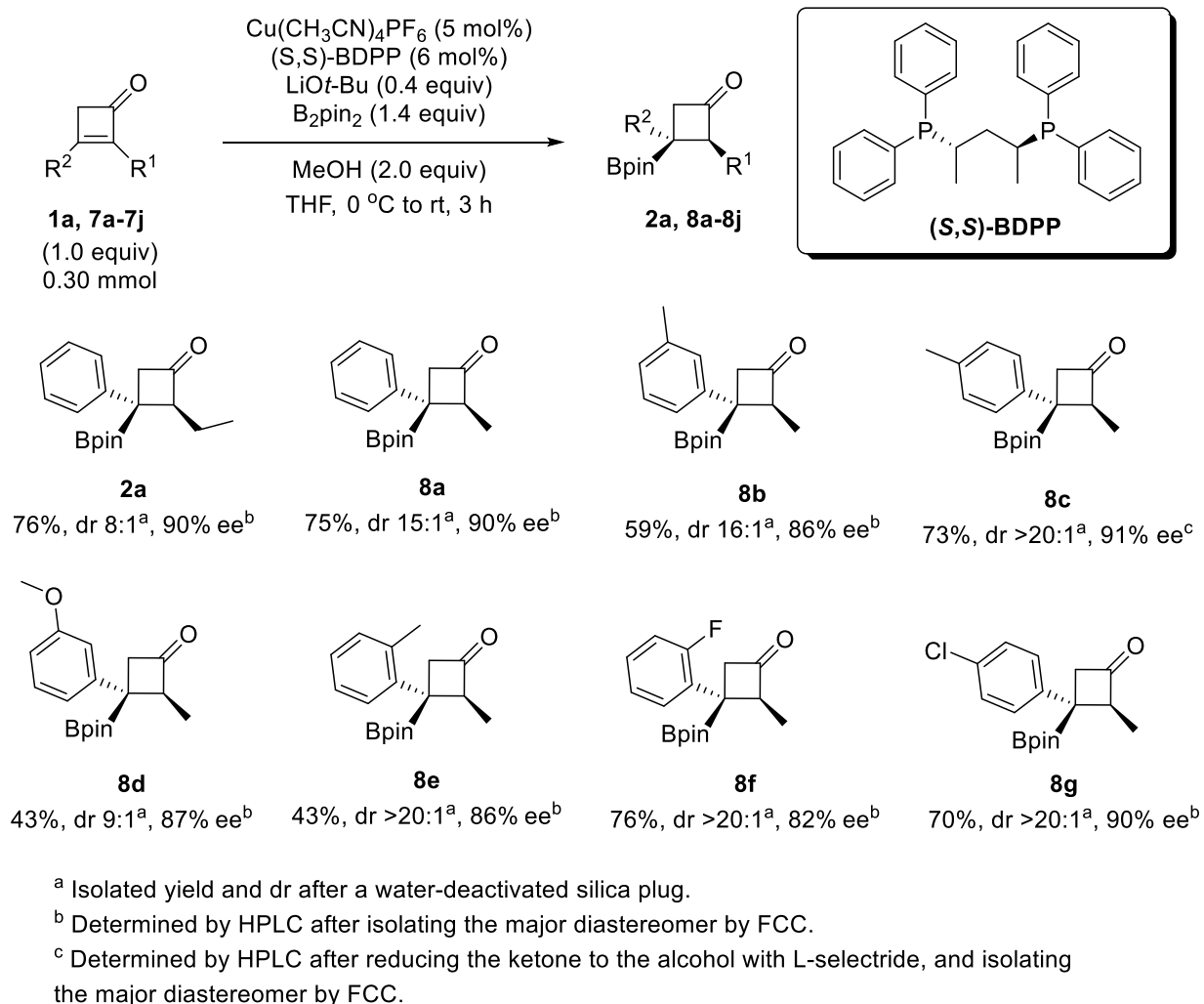


Figure 3-5: Proposed diastereofacial selectivity model for the conjugate borylation of cyclobutenones.

In general, the reaction converted the cyclobutenone to the desired cyclobutylboronate in all attempted substrates, however, there was some variation in diastereoselectivity and enantioselectivity. The tolyl substrates (**8b-8c**, **8e**) afforded modest to good isolated yields and dr, with only a minor loss of ee when the methyl substituent was placed in the *meta* or *ortho* position. The halogen cyclobutylboronates (**8f-8g**) gave encouraging yields and excellent dr. While there was a drop in enantioselectivity for an *ortho* fluoro group, the substrate with the *para* chloro group retained a high ee comparable to the *para* tolyl **8c**, and the methyl phenyl cyclobutylboronate **8a**.



Scheme 3-11: Preliminary substrate scope for the preparation of cyclobutylboronates by catalytic enantioselective conjugate borylation.

These results suggest that substituents in the *para* position of the phenyl ring are generally tolerated under the conjugate borylation conditions used, which suggests that the nitro **7h**, nitrile **7i**, and methyl ester **7j** could be efficient substrates as well. The *meta* methoxy substrate **8d** afforded high ee despite the discouraging yield and dr. The α -ethyl cyclobutylboronate **2a**, gave a good yield, low dr, and high ee, which highlights the potential generality of α -substituents on cyclobutylboronates.

3.7 Summary and Future Work

An optimized alkene migration reaction was developed to generate a library of α,β -substituted cyclobutenones in good yield, and high purity, on a multigram scale. This novel reaction methodology allowed the α -carbon to be derivatized with larger alkyl substituents, as well as a variety of electron donating- and electron-withdrawing groups in various positions on the β -phenyl moiety of the cyclobutenone. The synthetic route was less general for phenyl acetylene precursors with an EDG in the *para* position, as it led to an unfavourable [2+2] cycloaddition. Use of a cyclopropyl and trimethylsilyl group was unsuccessful due to the volatility of the cyclobutenone products. Nitrogen and sulfur heterocycles were unreactive or gave poor conversion. A small library of cyclobutenones was subjected to the optimal conditions to give the desired cyclobutylboronates in low to good yields and fair to excellent dr. Enantioselectivity was high with substrates substituted in the *para* position of the β -phenyl ring, with only a slight decline in ee observed with *ortho* and *meta* substituents. EWGs were generally tolerated better compared to a strong EDG, and the reaction efficacy and enantioselectivity was maintained when the cyclobutenone had an alkyl group larger than a methyl on the α -carbon.

The next substrates to evaluate will be the nitro **7h**, nitrile **7i**, and methyl ester **7j** cyclobutenones, which are auspicious based on the success of the *para* chlorophenyl cyclobutylboronate **8g** (Figure 3-6). A *para* trifluoromethyl cyclobutenone **9** should also be attempted to further push the limitations of electron withdrawing groups on the phenyl ring. A *para* and *meta* haloaryl cyclobutenone **10-11** should be attempted as well for its use as a potential intermediate in cross-coupling reactions. Since the *para* tolyl cyclobutylboronate **8c** gave a high ee, a variety of other *para* substituted alkyl and aryl substituents, like a naphthyl **12**, *tert*-butyl **13** and biphenyl **14** could also be tested in the conjugate borylation. Based on the success of the α -substituted ethyl group, a larger phenyl group **15** could be attempted to see if an aromatic maintains high enantioselectivity. This study on the scope of functionalized substrates has been completed by Helen Clement.

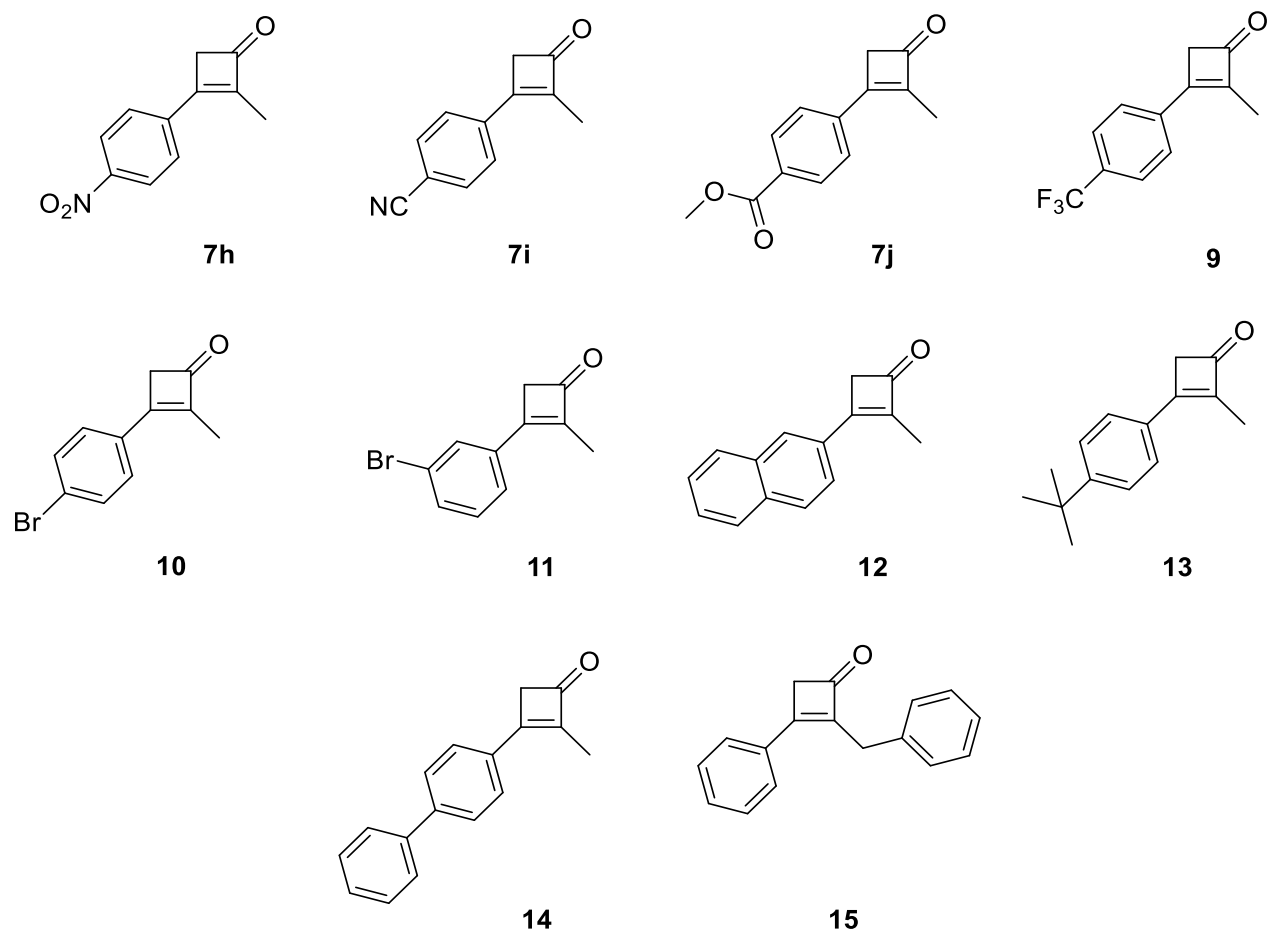


Figure 3-6: Additional cyclobutenones to test the scope of the conjugate borylation.

Since a major goal of the project was the development of a reaction to produce cyclobutylboronates with exploitable functionality, Clement successfully demonstrated the synthetic applications of the cyclobutylboronate products with various reactions on the Bpin or ketone groups (Figure 3-7).

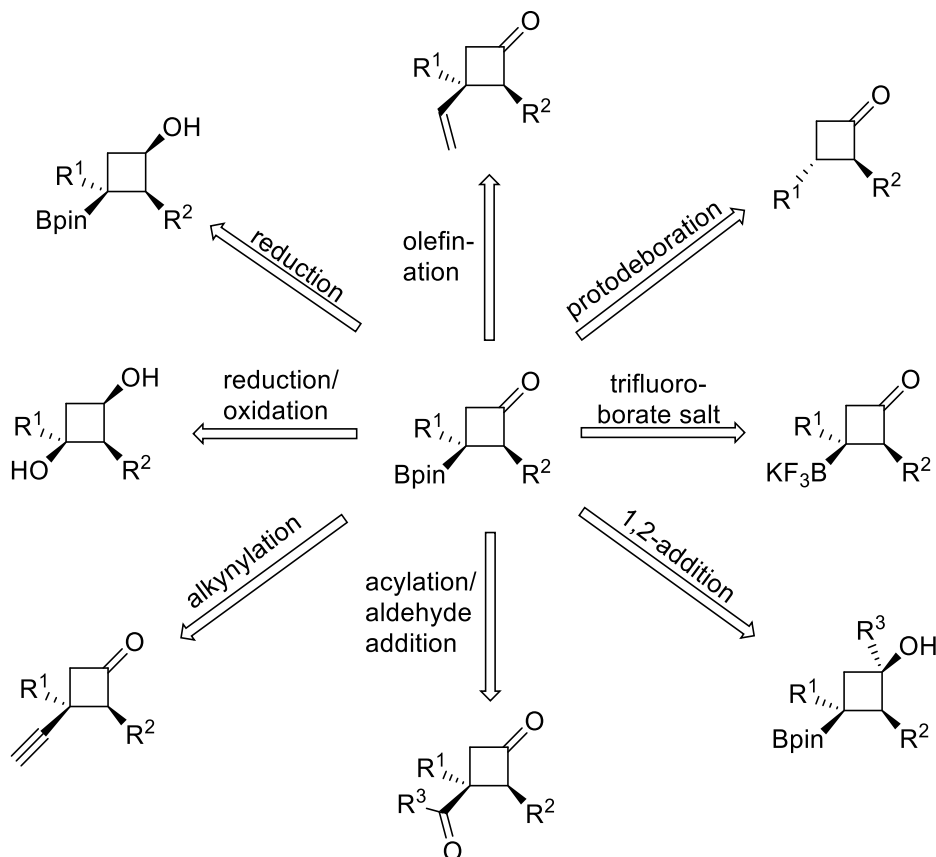


Figure 3-7: Examples of some synthetic applications of cyclobutylboronates utilizing the Bpin and ketone units.

3.8 Experimental Procedures

3.8.1 General Information

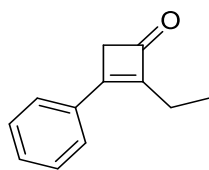
Unless otherwise indicated, all reactions were performed under a nitrogen or argon atmosphere using glassware that was washed thoroughly with water and acetone and flame-dried *in vacuo* prior to use. Dichloromethane and toluene were used directly from a MBraun Solvent Purification System. Tetrahydrofuran was obtained from the MBraun Solvent Purification System, and was freeze-pump-thawed for three cycles and stored under nitrogen before use. Methanol (reagent grade, 99%) was dried over 3Å molecular sieves for 3-24 h and stored under nitrogen before use. Ethanol (reagent grade, 95%) was obtained from chemical stores, and used without further purification. Bis(pinacolato)diboron (reagent grade 97%) was purchased from Combi-

Blocks Inc., and recrystallized from pentanes prior to use. Thionyl chloride was purchased from Sigma Aldrich, and distilled prior to use. Triflic anhydride was purchased from Oakwood Chemicals (reagent grade 99.5%) and was used without further purification if the solution was clear. If the triflic anhydride was dark brown it was distilled over phosphorous pentoxide and stored under argon before use. Lithium *tert*-butoxide solution (1.0 M in THF), potassium *tert*-butoxide solution (1.0 M in THF), (2*S*,4*S*)-2,4-bis(diphenylphosphino)pentane (reagent grade, 97%), tetrakis(acetonitrile)copper(I) hexafluorophosphate (reagent grade, 97%), dimethylamine hydrochloride (reagent grade, 99%), *N*-*N*-dimethylpropionamide (reagent grade, 98%), triethylamine (reagent grade, >99%), 4-(dimethylamino)pyridine (reagent grade, >99%), were purchased from Sigma Aldrich and were used without further purification. 2-fluoropyridine (reagent grade, 98%), and ethynyl building blocks for the [2+2] cycloaddition were purchased from Combi-Blocks Inc., and used without further purification. Thin layer chromatography (TLC) was performed on Merck Silica Gel 60 F254 plates, and visualized with UV light, KMnO₄, and PMA stain. Flash chromatography was performed on ultra-pure silica gel 230-400 mesh. Nuclear magnetic resonance (NMR) spectra were recorded on Agilent/Varian INOVA-400, INOVA-500, INOVA-600, or INOVA-700 MHz instruments. ¹H NMR data are presented as follows: chemical shift in ppm downfield from tetramethylsilane (multiplicity, coupling constant, integration). High resolution mass spectra were recorded by the University of Alberta Mass Spectrometry Services Laboratory using either electron impact (EI) ion source with double focusing sector analyzer (Kratos Analytical MS-50G), or electrospray (ESI) ion source with orthogonal acceleration TOF analyzer (Agilent Technologies 6220 oaTOF). Infrared spectra (performed on a Nicolet Magna-IR 750 instrument equipped with a Nic-Plan microscope) and optical rotations (performed using a Perkin-Elmer 241 polarimeter) were recorded by the University of Alberta Analytical and Instrumentation Laboratory. The enantiomeric excess for chiral compounds were determined using a HPLC Agilent instrument with a Chiralpak IC column. Specific conditions indicated in individual compound procedures.

3.8.2 General Procedure for the Synthesis of α,β -Disubstituted Cyclobutenones

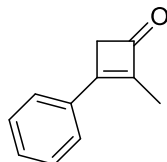
To a flame-dried 3-neck 250 mL round bottom flask equipped with a condenser and a stir bar was added *N*-*N*-dimethylpropionamide (5.50 mL, 50.0 mmol, 1.00 equiv), and the flask was

evacuated and backfilled with nitrogen for three cycles. Dichloromethane (100 mL) was added, and the reagents stirred vigorously forming a clear solution. Triflic anhydride (10.0 mL, 55.0 mmol, 1.10 equiv) was slowly added dropwise to the solution via syringe, forming a yellow-white slurry. The alkyne (6.5 mL, 60.0 mmol, 1.20 equiv) and 2-fluoropyridine (5.5 mL, 60.0 mmol, 1.20 equiv) as a mixed solution was added dropwise to the slurry via syringe, forming a bright yellow solution that slowly turned dark red. The reaction heated to 55 °C, and was stirred overnight. The reaction was cooled to rt, poured into a 500 mL Erlenmeyer flask, cooled to 0 °C in an ice bath, and 1 M sodium hydroxide (110 mL, 110 mmol, 2.20 equiv) was added with vigorous stirring. The reaction stirred for 6 h while warming to rt. The organic and aqueous layers were separated, and the aqueous layer was extracted with dichloromethane (3×50.0 mL). The combined organic layers were washed with 1 M hydrochloric acid (100 mL), water (100 mL), saturated sodium bicarbonate (100 mL), brine (100 mL), dried with sodium sulfate, filtered, and concentrated *in vacuo*. The crude oil was filtered through a short silica plug (3:17 ethyl acetate:hexanes), and the fractions were combined and concentrated *in vacuo* giving a mixture of cyclobutenone regioisomers as a yellow oil. Ethanol (100 mL) was added to the crude cyclobutenone regioisomer mixture followed by dropwise addition of potassium *tert*-butoxide (1.0 M, 15.0 mL, 0.30 equiv). The mixture stirred for 4 h at rt under nitrogen. The light orange solution was quenched with saturated ammonium chloride (100 mL), and the aqueous and organic layers were separated. The aqueous layer was extracted with ethyl acetate (3×50.0 mL), and the combined organic layers were washed with water (150 mL), brine (150 mL), dried with sodium sulfate, filtered, and concentrated *in vacuo* giving the crude cyclobutenone as an oil or solid, which was purified by flash column chromatography (1:19 ethyl acetate:hexanes).

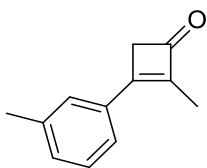


2-ethyl-3-phenylcyclobut-2-enone (1a): Clear yellow oil (46% yield over three steps). $^1\text{H NMR}$ (500 MHz, CDCl_3) δ 7.58-7.44 (m, 5H), 3.43 (app t, $J = 2.0$ Hz, 2H), 2.46 (qt, $J = 8.0$ Hz, 2.0 Hz, 2H), 1.22 (t, $J = 8.0$ Hz, 3H); $^{13}\text{C NMR}$ (125 MHz, CDCl_3) δ 190.0, 162.4, 146.7, 132.7, 130.9,

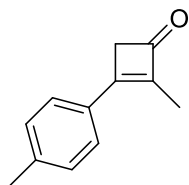
129.1, 129.0, 48.3, 18.2, 11.4; **IR** (cast film, CHCl₃ cm⁻¹): 3057, 2978, 1748, 1613, 1448, 1353, 1068; **HRMS** (EI) for C₁₂H₁₂O: calcd. 172.0888; found 172.0888.



2-methyl-3-phenylcyclobut-2-enone (7a): White-yellow solid (44% yield over three steps). **¹H NMR** (500 MHz, CDCl₃) δ 7.60-7.45 (m, 5H), 3.45 (app q, *J* = 2.5 Hz, 2H), 2.00 (app t, *J* = 2.5 Hz, 3H); **¹³C NMR** (125 MHz, CDCl₃) δ 190.0, 163.5, 141.0, 132.8, 131.0, 129.2, 129.0, 48.2, 9.4; **IR** (cast film, CHCl₃ cm⁻¹): 3070, 2918, 1750, 1616, 1447, 1348, 1068; **HRMS** (EI) for C₁₁H₁₀O: calcd. 158.0732; found 158.0732.

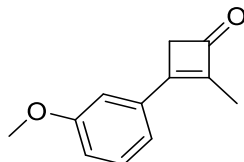


2-methyl-3-(*m*-tolyl)cyclobut-2-enone (7b): White solid (44% yield over three steps). **¹H NMR** (500 MHz, CDCl₃) δ 7.44-7.38 (m, 3H), 7.30 (m, 1H), 3.46 (app q, *J* = 2.5 Hz, 2H), 2.44 (s, 3H), 2.02 (app t, *J* = 2.5 Hz, 3H); **¹³C NMR** (125 MHz, CDCl₃) δ 190.2, 163.8, 140.8, 138.7, 132.8, 131.8, 129.8, 128.8, 126.4, 48.2, 21.4, 9.4; **IR** (cast film, CHCl₃ cm⁻¹): 3045, 2918, 1753, 1624, 1425, 1348, 1085; **HRMS** (EI) for C₁₂H₁₂O: calcd. 172.0888; found 172.0888.

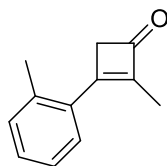


2-methyl-3-(*p*-tolyl)cyclobut-2-enone (7c): White solid (41% yield over three steps). **¹H NMR** (500 MHz, CDCl₃) δ 7.50 (d, *J* = 8.5 Hz, 2H), 7.32 (d, *J* = 8.5 Hz, 2H), 3.44 (app q, *J* = 2.5 Hz, 2H), 2.44 (s, 3H), 2.00 (app t, *J* = 2.5 Hz, 3H); **¹³C NMR** (125 MHz, CDCl₃) δ 190.1, 163.6, 141.7,

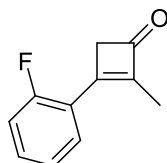
139.9, 130.2, 129.7, 129.2, 48.1, 21.7, 9.4; **IR** (cast film, CHCl₃ cm⁻¹): 3013, 2945, 1747, 1619, 1448, 1345, 1011; **HRMS** (EI) for C₁₂H₁₂O: calcd. 172.0888; found 172.0888.



3-(3-methoxyphenyl)-2-methylcyclobut-2-enone (7d): Yellow solid (61% yield over three steps). **¹H NMR** (500 MHz, CDCl₃) δ 7.44 (t, *J* = 8.0 Hz, 1H), 7.21 (d, *J* = 8.0 Hz, 1H), 7.10 (app t, *J* = 1.5 Hz, 1H), 7.04 (dd, *J* = 8.0 Hz, 3.0 Hz, 1H), 3.88 (s, 3H), 3.46 (app q, *J* = 2.5 Hz, 2H), 2.02 (app t, *J* = 2.5 Hz, 3H); **¹³C NMR** (125 MHz, CDCl₃) δ 190.0, 163.4, 159.8, 141.3, 134.0, 130.0, 121.7, 116.4, 114.4, 55.4, 48.3, 9.3; **IR** (cast film, CHCl₃ cm⁻¹): 3075, 2949, 1747, 1621, 1458, 1351, 1167, 1017; **HRMS** (EI) for C₁₂H₁₂O₂: calcd. 188.0837; found 188.0840.

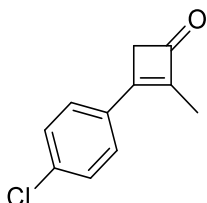


2-methyl-3-(o-tolyl)cyclobut-2-enone (7e): White solid (65% yield over three steps). **¹H NMR** (500 MHz, CDCl₃) δ 7.46 (dd, *J* = 7.5 Hz, 1.5 Hz, 1H), 7.37-7.27 (m, 3H), 3.60 (app q, *J* = 2.5 Hz, 2H), 2.46 (s, 3H), 1.90 (app t, *J* = 2.5 Hz, 3H); **¹³C NMR** (125 MHz, CDCl₃) δ 190.6, 165.8, 143.6, 137.0, 132.4, 131.4, 130.4, 129.1, 126.0, 51.7, 21.1, 9.5; **IR** (cast film, CHCl₃ cm⁻¹): 3057, 2967, 1741, 1592, 1447, 1337, 1017; **HRMS** (EI) for C₁₂H₁₂O: calcd. 172.0888; found 172.0888.

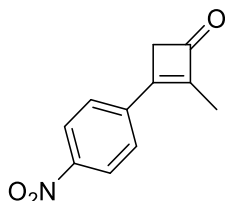


3-(2-fluorophenyl)-2-methylcyclobut-2-enone (7f): Brown solid (51% yield over three steps). **¹H NMR** (500 MHz, CDCl₃) δ 7.54-7.46 (m, 2H), 7.28 (td, *J* = 8.0 Hz, 1.0 Hz, 1H), 7.20 (ddd,

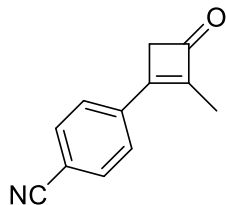
10.5 Hz, 8.0 Hz, 1.0 Hz), 3.57 (ddd, $J = 5.5$ Hz, 2.5 Hz, 1.0 Hz, 2H), 1.99 (app q, $J = 2.5$ Hz, 3H); ^{13}C NMR (125 MHz, CDCl_3) δ 190.7, 161.4, 159.4, 158.2, 143.7, 132.9, 130.7, 124.5, 121.0, 50.0, 9.6; IR (cast film, CHCl_3 cm^{-1}): 3057, 2967, 1756, 1619, 1458, 1333, 1015; HRMS (EI) for $\text{C}_{11}\text{H}_9\text{FO}$: calcd. 176.0637; found 176.0639.



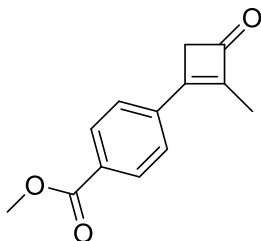
3-(4-chlorophenyl)-2-methylcyclobut-2-enone (7g): Yellow solid (46% yield over three steps). ^1H NMR (500 MHz, CDCl_3) δ 7.49 (app q, $J = 10.5$ Hz, 4H), 3.44 (app q, $J = 3.0$ Hz, 2H), 1.99 (app t, $J = 3.0$ Hz, 3H); ^{13}C NMR (125 MHz, CDCl_3) δ 189.5, 162.0, 141.5, 137.0, 131.2, 130.2, 129.3, 48.3, 9.4; IR (cast film, CHCl_3 cm^{-1}): 3056, 2945, 1748, 1623, 1444, 1338, 1090; HRMS (EI) for $\text{C}_{11}\text{H}_9\text{ClO}$: calcd. 192.0342; found 192.0339.



2-methyl-3-(4-nitrophenyl)cyclobut-2-enone (7h): Orange-red solid (20% yield over three steps). ^1H NMR (500 MHz, CDCl_3) δ 8.37 (dt, $J = 8.5$ Hz, 2.5 Hz, 2H), 7.76 (dt, $J = 8.5$ Hz, 2.5 Hz, 2H), 3.57 (app q, $J = 2.0$ Hz, 2H), 1.99 (app t, $J = 2.0$ Hz, 3H); ^{13}C NMR (125 MHz, CDCl_3) δ 189.1, 160.3, 148.5, 145.3, 138.3, 129.7, 124.2, 48.8, 9.7; IR (cast film, CHCl_3 cm^{-1}): 3104, 2963, 1755, 1620, 1517, 1349, 855; HRMS (EI) for $\text{C}_{11}\text{H}_9\text{NO}_3$: calcd. 203.0582; found 203.0584.



4-(2-methyl-3-oxocyclobut-1-en-1-yl)benzonitrile (7i): Yellow solid (18% yield over three steps). $^1\text{H NMR}$ (500 MHz, CDCl_3) δ 7.77 (d, $J = 8.5$ Hz, 2H), 7.65 (d, $J = 8.5$ Hz, 2H), 3.49 (app q, $J = 2.5$ Hz, 2H), 2.03 (app t, $J = 2.5$ Hz, 3H); $^{13}\text{C NMR}$ (175 MHz, CDCl_3) δ 189.1, 160.7, 144.7, 136.5, 132.6, 129.2, 118.1, 113.9, 48.5, 9.6; **IR** (cast film, CHCl_3 cm^{-1}): 3089, 2968, 2227, 1751, 1618, 1342, 848; **HRMS** (EI) for $\text{C}_{12}\text{H}_9\text{NO}$: calcd. 183.0684; found 183.0687.

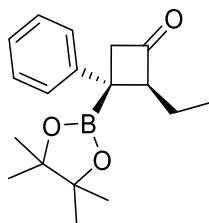


methyl 4-(2-methyl-3-oxocyclobut-1-en-1-yl)benzoate (7j): Yellow solid (55% yield over three steps). $^1\text{H NMR}$ (500 MHz, CDCl_3) δ 8.17 (d, $J = 8.5$ Hz, 2H), 7.66 (d, $J = 8.5$ Hz, 2H), 3.98 (s, 3H), 3.52 (app q, $J = 2.5$ Hz, 2H), 2.06 (app t, $J = 2.5$ Hz, 3H); $^{13}\text{C NMR}$ (175 MHz, CDCl_3) δ 189.7, 166.2, 161.9, 143.4, 136.5, 131.7, 130.0, 128.9, 52.4, 48.4, 9.5; **IR** (cast film, CHCl_3 cm^{-1}): 2953, 2919, 1746, 1716, 1618, 1276, 1107; **HRMS** (EI) for $\text{C}_{13}\text{H}_{12}\text{O}_3$: calcd. 216.0786; found 216.0787.

3.8.3 General Procedure for the Synthesis of Trisubstituted Cyclobutylboronates

To a flame-dried 10 mL microwave vial with a stir bar was added (2*S*,4*S*)-2,4-bis(diphenylphosphino)pentane (7.90 mg, 0.0180 mmol, 0.0600 equiv), tetrakis(acetonitrile)copper(I) hexafluorophosphate (5.60 mg, 0.0150 mmol, 0.0500 equiv), and bis(pinacolato)diboron (107 mg, 0.420 mmol, 1.40 equiv). The microwave vial was then capped and evacuated and backfilled with argon for five cycles. Tetrahydrofuran (0.500 mL) was added

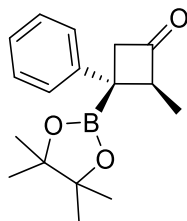
to the vial via syringe, the catalysts were stirred for 15 min forming a clear solution, while cooling to 0 °C in an ice-water bath. Lithium *tert*-butoxide (1.0 M, 0.130 mL, 0.120 mmol, 0.400 equiv) was added to the vial dropwise via a microsyringe, and the reaction stirred 5 min forming a yellow-brown solution. Cyclobutenone **7** (47.6 mg, 0.300 mmol, 1.00 equiv) in tetrahydrofuran (0.500 mL) was added to the vial, followed immediately by methanol (0.0250 mL, 0.600 mmol, 2.00 equiv), and the reaction was stirred for 3 h warming to rt. The solution quickly turned cloudy white or cloudy yellow over this time. The reaction was diluted with diethyl ether (8.00 mL), and poured into saturated ammonium chloride (15.0 mL) in a separatory funnel. The layers were separated, and the aqueous was extracted with diethyl ether (3×20.0 mL). The combined organic layers were washed with brine (60.0 mL), dried with sodium sulfate, filtered, and concentrated *in vacuo*. The crude ¹H NMR yield was determined with dibromomethane as an internal standard (26.0 mg, 0.150 mmol, 0.500 equiv). The crude mixture was then purified by a water-deactivated silica plug (7.00 g silica gel, 3.30 g water, 1:15 ethyl acetate to hexanes) to acquire the isolated yield and dr. The diastereoselectivity of the isolated products was determined by the relative peak height of the corresponding methyl protons for which had signals consistently around 1.40 and 0.75 ppm for the major and minor diastereomers, respectively. The cyclobutylboronate was then purified using regular flash chromatography (1:19 ethyl acetate:hexanes) to isolate the major diastereomer for full characterization.



(2*S*,3*R*)-2-ethyl-3-phenyl-3-(4,4,5,5-tetramethyl-1,3,2-dioxaborolan-2-yl)cyclobutanone

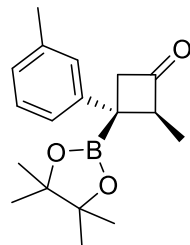
(2a): White solid after water-deactivated silica plug, (76% yield, dr 8:1). A second flash chromatography allowed isolation of the major diastereomer for characterization purposes: **mp** = 45.3–46.1 °C; ¹H NMR (500 MHz, CDCl₃) δ 7.36–7.29 (m, 2H), 7.25–7.16 (m, 3H), 3.53 (dd, *J* = 16.8, 2.4 Hz, 1H), 3.45 (dddd, *J* = 9.2, 7.0, 2.4, 2.4 Hz, 1H), 3.17 (dd, *J* = 16.8, 2.4 Hz, 1H), 2.01–1.85 (m, 1H), 1.80 (ddq, *J* = 14.5, 7.4, 7.4 Hz, 1H), 1.19 (s, 6H), 1.16 (s, 6H), 1.16 (t, *J* = 7.5 Hz, 3H); ¹³C NMR (125 MHz, CDCl₃) δ 209.4, 147.2, 128.3, 126.3, 125.5, 84.2, 71.0, 53.8, 24.7,

24.7, 22.4, 13.0 (the boron-bound carbon was not detected due to quadrupolar relaxation of boron); ^{11}B NMR (128 MHz, CDCl_3) δ 33.1; IR (cast film, CHCl_3 cm^{-1}): 3063, 2978, 1780, 1354, 1141; HRMS (EI) for $\text{C}_{18}\text{H}_{25}\text{BO}_3$: calcd. 300.1897; found 300.1894; $[\alpha]_{\text{D}}^{20}$: -82.78 ($c = 0.500$, CHCl_3); HPLC (Chiralpak IC): 5:95 iso-propanol:hexanes, 0.7 mL/min, 20 °C, $\lambda = 210$ nm, $T_{\text{minor}} = 4.9$ min, $T_{\text{major}} = 5.3$ min, er = 94.9:5.1.

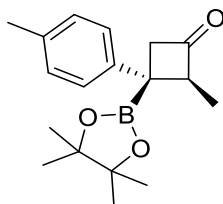


(2*S*,3*R*)-2-methyl-3-phenyl-3-(4,4,5,5-tetramethyl-1,3,2-dioxaborolan-2-yl)cyclobutanone

(8a): White solid after water-deactivated silica plug, (75% yield, dr 15:1). A second flash chromatography allowed isolation of the major diastereomer for characterization purposes: **mp** = 46.2–47.5 °C; ^1H NMR (400 MHz, CDCl_3) δ 7.36–7.29 (m, 2H), 7.24–7.17 (m, 3H), 3.58 (qdd, $J = 7.3, 2.2, 2.2$ Hz, 1H), 3.52 (dd, $J = 16.6, 2.3$ Hz, 1H), 3.22 (dd, $J = 16.6, 2.1$ Hz, 1H), 1.41 (d, $J = 7.4$ Hz, 3H), 1.19 (s, 6H), 1.16 (s, 6H); ^{13}C NMR (125 MHz, CDCl_3) δ 209.1, 128.4, 126.2, 125.6, 84.3, 77.3, 77.1, 76.8, 64.2, 53.5, 24.8, 24.7, 13.1 (the boron-bound carbon was not detected due to quadrupolar relaxation of boron); ^{11}B NMR (128 MHz, CDCl_3) δ 33.2; IR (cast film, CHCl_3 cm^{-1}): 3066, 2981, 1773, 1320, 1143; HRMS (EI) for $(\text{M}-\text{CO})^+$ $\text{C}_{16}\text{H}_{23}\text{BO}_2$: calcd. 258.1786; found 258.1794; $[\alpha]_{\text{D}}^{20}$: -86.51 ($c = 0.371$, CHCl_3); HPLC (Chiralpak IC): 1:99 iso-propanol:hexanes, 0.5 mL/min, 20 °C, $\lambda = 220$ nm, $T_{\text{minor}} = 14.2$ min, $T_{\text{major}} = 15.3$ min, er = 95.0:5.0.

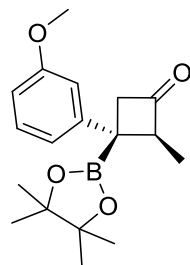


(2*S*,3*R*)-2-methyl-3-(4,4,5,5-tetramethyl-1,3,2-dioxaborolan-2-yl)-3-(*m*-tolyl)cyclobutanone (8b): White solid after water-deactivated silica plug, (59% yield, dr 16:1). A second flash chromatography allowed isolation of the major diastereomer for characterization purposes: $^1\text{H NMR}$ (500 MHz, CDCl_3) δ 7.24–7.18 (m, 1H), 7.04–6.97 (m, 3H), 3.57 (qdd, $J = 7.3, 2.8, 2.0$ Hz, 1H), 3.50 (dd, $J = 16.6, 2.3$ Hz, 1H), 3.20 (dd, $J = 16.6, 2.2$ Hz, 1H), 2.36 (s, 3H), 1.41 (d, $J = 7.4$ Hz, 3H), 1.19 (s, 6H), 1.16 (s, 6H); $^{13}\text{C NMR}$ (125 MHz, CDCl_3) δ 209.2, 147.1, 137.8, 128.2, 126.8, 126.3, 123.3, 84.2, 64.0, 53.6, 24.8, 24.7, 21.6, 13.1 (the boron-bound carbon was not detected due to quadrupolar relaxation of boron); $^{11}\text{B NMR}$ (128 MHz, CDCl_3) δ 33.0; **IR** (cast film, CHCl_3 cm^{-1}): 2980, 2929, 1775, 1323, 1167; **HRMS** (EI) for $\text{C}_{18}\text{H}_{25}\text{BO}_3$: calcd. 300.1897; found 300.1888; $[\alpha]_{\text{D}}^{20}$: -68.33 ($c = 0.446$, CHCl_3); **HPLC** (Chiralpak IC): 5:95 isopropanol:hexanes, 0.7 mL/min, 20 °C, $\lambda = 220$ nm, $T_{\text{minor}} = 6.4$ min, $T_{\text{major}} = 6.7$ min, er = 93.0:7.0.

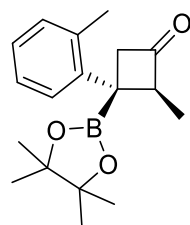


(2*S*,3*R*)-2-methyl-3-(4,4,5,5-tetramethyl-1,3,2-dioxaborolan-2-yl)-3-(*p*-tolyl)cyclobutanone (8c): White solid after water-deactivated silica plug, (86% yield, dr >20:1). A second flash chromatography allowed isolation of the major diastereomer for characterization purposes: **mp** = 50.7–52.3 °C; $^1\text{H NMR}$ (500 MHz, CDCl_3) δ 7.12 (dd, $J = 8.2, 8.2$ Hz, 4H), 3.59–3.44 (m, 2H), 3.19 (d, $J = 16.4$ Hz, 1H), 2.33 (s, 3H), 1.40 (d, $J = 7.4$ Hz, 3H), 1.19 (s, 6H), 1.16 (s, 6H); $^{13}\text{C NMR}$ (125 MHz, CDCl_3) δ 209.2, 144.2, 135.0, 129.1, 126.0, 84.2, 64.2, 53.6, 24.8, 24.7, 21.1, 13.1 (the boron-bound carbon was not detected due to quadrupolar relaxation of boron); $^{11}\text{B NMR}$ (128 MHz, CDCl_3) δ 33.1; **IR** (cast film, CHCl_3 cm^{-1}): 3046, 2982, 2930, 1782, 1380,

1372, 1324, 1138, 857, 815; **HRMS** (EI) for C₁₈H₂₅BO₃: calcd. 300.1897; found 300.1899; **[α]_D²⁰**: −96.11 (c = 0.160, CHCl₃). For enantioselectivity determination, see section 3.8.4.

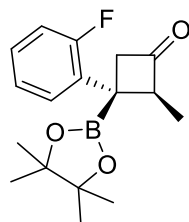


(2*S*,3*R*)-3-(3-methoxyphenyl)-2-methyl-3-(4,4,5,5-tetramethyl-1,3,2-dioxaborolan-2-yl)cyclobutanone (8d): White solid after water-deactivated silica plug, (43% yield, dr 10:1). A second flash chromatography allowed isolation of the major diastereomer for characterization purposes: **mp** = 72.6–74.2 °C; **¹H NMR** (500 MHz, CDCl₃) δ 7.28–7.21 (m, 1H), 6.81 (d, *J* = 7.9 Hz, 1H), 6.78–6.71 (m, 2H), 3.82 (s, 3H), 3.58 (qdd, *J* = 7.1, 2.1, 2.1 Hz, 1H), 3.49 (dd, *J* = 16.7, 2.3 Hz, 1H), 3.22 (dd, *J* = 16.6, 2.2 Hz, 1H), 1.40 (d, *J* = 7.4 Hz, 3H), 1.19 (s, 6H), 1.17 (s, 6H); **¹³C NMR** (125 MHz, CDCl₃) δ 209.0, 159.5, 148.9, 129.3, 118.7, 112.6, 110.4, 84.3, 64.1, 55.2, 53.5, 24.8, 24.7, 13.0 (the boron-bound carbon was not detected due to quadrupolar relaxation of boron); **¹¹B NMR** (128 MHz, CDCl₃) δ 32.0; **IR** (cast film, CHCl₃ cm^{−1}): 2979, 2931, 1779, 1355, 1141; **HRMS** (EI) for C₁₈H₂₅BO₄: calcd. 316.1846; found 316.1847; **[α]_D²⁰**: −63.12 (c = 0.204, CHCl₃); **HPLC** (Chiralpak IC): 5:95 iso-propanol:hexanes, 0.7 mL/min, 20 °C, λ = 220 nm, T_{minor} = 9.0 min, T_{major} = 9.9 min, er = 93.5:6.5.

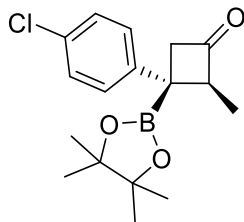


(2*S*,3*R*)-2-methyl-3-(4,4,5,5-tetramethyl-1,3,2-dioxaborolan-2-yl)-3-(*o*-tolyl)cyclobutanone (8e): White solid after water-deactivated silica plug, (43% yield, dr >20:1). A second flash chromatography allowed isolation of the major diastereomer for characterization purposes: **¹H NMR** (600 MHz, CDCl₃) δ 7.22–7.12 (m, 4H), 3.72 (qdd, *J* = 7.4, 2.0, 2.0 Hz, 1H), 3.54 (dd, *J* =

16.1, 2.0 Hz, 1H), 3.01 (dd, $J = 16.1, 1.8$ Hz, 1H), 2.22 (s, 3H), 1.42 (d, $J = 7.3$ Hz, 3H), 1.22 (s, 6H), 1.19 (s, 6H); ^{13}C NMR (125 MHz, CDCl_3) δ 209.0, 145.1, 135.6, 130.7, 126.0, 125.9, 125.6, 84.3, 61.8, 54.5, 25.0, 24.9, 20.6, 12.4 (the boron-bound carbon was not detected due to quadrupolar relaxation of boron); ^{11}B NMR (128 MHz, CDCl_3) δ 33.6; IR (cast film, CHCl_3 cm^{-1}): 2979, 2932, 1779, 1381, 1142; HRMS (EI) for $\text{C}_{18}\text{H}_{25}\text{BO}_3$: calcd. 300.1897; found 300.1888; $[\alpha]_{\text{D}}^{20}$: -117.85 ($c = 0.442$, CHCl_3); HPLC (Chiralpak IC): 5:95 iso-propanol:hexanes, 0.7 mL/min, 20 °C, $\lambda = 220$ nm, $T_{\text{minor}} = 7.5$ min, $T_{\text{major}} = 8.8$ min, er = 92.7:7.3.



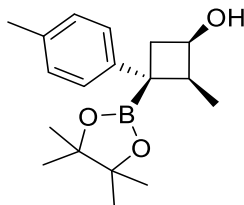
(2*S*,3*R*)-3-(2-fluorophenyl)-2-methyl-3-(4,4,5,5-tetramethyl-1,3,2-dioxaborolan-2-yl)cyclobutanone (8f) Yellow solid after water-deactivated silica plug, (76% yield, dr >20:1). A second flash chromatography allowed isolation of the major diastereomer for characterization purposes: mp = 56.3–57.8 °C; ^1H NMR (500 MHz, CDCl_3) δ 7.24–7.17 (m, 2H), 7.15–7.10 (m, 1H), 7.07–7.00 (m, 1H), 3.64 (qdd, $J = 7.5$ Hz, 2.0 Hz, 1.9 Hz, 1H), 3.53 (dt, $J = 16.7$ Hz, 2.0 Hz, 1H), 3.12 (dd, $J = 17.0$ Hz, 1.0 Hz, 1H), 1.37 (d, $J = 7.3$ Hz, 3H), 1.20 (s, 6H), 1.18 (s, 6H); ^{13}C NMR (100 MHz, CDCl_3 , ^{19}F decoupled) δ 208.8, 161.0, 133.9, 127.5, 127.0, 124.0, 115.4, 84.4, 77.4, 77.1, 76.7, 62.0, 54.0, 24.8, 24.7, 12.2 (the boron-bound carbon was not detected due to quadrupolar relaxation of boron); ^{11}B NMR (128 MHz, CDCl_3) δ 33.2; ^{19}F NMR (376 MHz, CDCl_3) δ -113.8 ; IR (cast film, CHCl_3 cm^{-1}): 2980, 2932, 1782, 1358, 1142; HRMS (EI) for $\text{C}_{17}\text{H}_{22}\text{BFO}_3$: calcd. 304.1646; found 304.1651; $[\alpha]_{\text{D}}^{20}$: -88.49 ($c = 0.602$, CHCl_3); HPLC (Chiralpak IC): 1:99 iso-propanol:hexanes, 0.5 mL/min, 20 °C, $\lambda = 220$ nm, $T_{\text{minor}} = 13.5$ min, $T_{\text{major}} = 15.2$ min, er = 90.8:9.2.



(2*S*,3*R*)-3-(4-chlorophenyl)-2-methyl-3-(4,4,5,5-tetramethyl-1,3,2-dioxaborolan-2-yl)cyclobutanone (8g) Yellow solid after water-deactivated silica plug, (70% yield, dr >20:1). A second flash chromatography allowed isolation of the major diastereomer for characterization purposes: **mp** = 50.6–53.1 °C; **¹H NMR** (500 MHz, CDCl₃) δ 7.28 (dt, *J* = 8.4, 2.8 Hz, 2H), 7.02 (dt, *J* = 8.4, 2.8 Hz, 2H), 3.53 (m, 2H), 3.18 (dd, *J* = 16.4 Hz, 2.0 Hz, 1H), 1.40 (d, *J* = 7.2 Hz, 3H), 1.17 (s, 6H), 1.15 (s, 6H); **¹³C NMR** (125 MHz, CDCl₃) δ 208.3, 131.3, 128.4, 127.5, 84.4, 64.4, 53.4, 24.8, 24.7, 24.6, 13.0 (the boron-bound carbon was not detected due to quadrupolar relaxation of boron); **¹¹B NMR** (128 MHz, CDCl₃) δ 33.2; **IR** (cast film, CHCl₃ cm⁻¹): 2979, 2930, 1782, 1492, 1141; **HRMS** (EI) for C₁₇H₂₂BClO₃: calcd. 320.1351; found 320.1351; **[α]_D²⁰**: –70.88 (c = 0.391, CHCl₃); **HPLC** (Chiralpak IC): 5:95 iso-propanol:hexanes, 0.7 mL/min, 20 °C, λ = 220 nm, T_{minor} = 6.7, T_{major} = 7.8 min, er = 95.2:4.8.

3.8.4 General Procedure for the Reduction of (2*S*,3*R*)-2-methyl-3-(4,4,5,5-tetramethyl-1,3,2-dioxaborolan-2-yl)-3-(*p*-tolyl)cyclobutanone (8c)

To a flame-dried 5 mL pear flask with a stir bar under nitrogen was added *para* tolyl cyclobutylboronate **8c** (66.7 mg, 0.220 mmol, 1.00 equiv) in THF (2 x 0.500 mL aliquots). The solution was stirred, and cooled to –78 °C. L-selectride (235 μL, 0.233 mmol, 1.05 equiv), was added dropwise to the mixture via syringe, and the mixture stirred for 4 h at –78 °C. The reaction was warmed to 0 °C, and quenched with saturated ammonium chloride (3.00 mL). The layers were separated, and the aqueous layer was extracted with diethyl ether (3×20.0 mL). The combined organic layers were washed with brine (60.0 mL), dried with sodium sulfate, filtered, and concentrated *in vacuo*. The crude oil was purified by flash chromatography (2:5 ethyl acetate:hexanes).



(1R,2S,3R)-2-methyl-3-(4,4,5,5-tetramethyl-1,3,2-dioxaborolan-2-yl)-3-(p-tolyl)cyclobutanol (8ca): White solid, (86% yield, >20:1 dr). $^1\text{H NMR}$ (500 MHz, CDCl_3) δ 7.09–7.05 (m, 2H), 7.03–6.97 (m, 2H), 4.27–4.18 (m, 1H), 3.11 (d, $J = 9.7$ Hz, 1H), 2.80 (dq, $J = 7.2, 7.2$ Hz, 1H), 2.31 (s, 3H), 1.28 (d, $J = 7.3$ Hz, 3H), 1.23 (s, 6H), 1.21 (s, 6H); $^{13}\text{C NMR}$ (125 MHz, CDCl_3) δ 145.6, 134.0, 128.7, 125.6, 84.1, 68.7, 46.1, 39.3, 24.8, 24.7, 21.1, 12.9. (the boron-bound carbon was not detected due to quadrupolar relaxation of boron); $^{11}\text{B NMR}$ (128 MHz, CDCl_3) δ 33.9; **IR** (cast film, CHCl_3 cm^{-1}): 3429, 3017, 2977, 2927, 1511, 1358, 1305, 1145, 1124, 860; **HRMS** (EI) for $(\text{M}-\text{H}_2\text{O})^+$ $\text{C}_{18}\text{H}_{25}\text{BO}_2$: calcd. 284.1948; found 284.1944; $[\alpha]_{\text{D}}^{20}$: -68.3 ($c = 0.210$, CHCl_3); **HPLC** (Chiralpak IC): 5:95 iso-propanol:hexanes, 0.7 mL/min, 20 °C, $\lambda = 220$ nm, $T_{\text{minor}} = 7.1$ min, $T_{\text{major}} = 8.0$ min, er = 95.5:4.5.

3.9 References:

[1] Fernández, E.; Whiting, A. *Synthesis and Application of Organoboron Compounds*; Springer International Publishing: Switzerland, 2015.

[2] Zheng, K.; Liu, X.; Feng, X. *Chem. Rev.* **2018**, *118*, 7586–7656.

[3] a) Hall, D. G. *Boronic Acids: Preparation and Applications in Organic Synthesis, Medicine, and Materials*, 1&2, 2nd Ed; Wiley-VCH Verlag & Co. KGaA: Weinheim, 2011. b) Sonawane, R. P.; Jheengut, V.; Rabalakos, C.; Larouche-Gauthier, R.; Scott, H. K.; Aggarwal, V. K. *Angew. Chem. Int. Ed.* **2011**, *50*, 3760-3763. c) Armstrong, R. J.; Aggarwal, V. K. *Synthesis* **2017**, *49*, 3323–3336.

- [4] Lawson, Y. G.; M. J. Lesley, M. J. G.; Marder, T. B.; Norman, N. C.; Rice, C. R. *Chem. Commun.* **1997**, 2051-2052.
- [5] a) Ito, J.; Yamanaka, H.; Tateiwab, J.; Hosomi, A.; *Tetrahedron Lett.* **2000**, *41*, 6821-6825. b) Takahashi, K.; Ishiyama, T.; Miyaura, N. *Chem. Lett.* **2000**, 982-983.
- [6] Mun, S.; Lee, J-E.; Yun, J. *Org. Lett.* **2006**, *8*, 4887-4889.
- [7] Lee, J-E.; Yun, J. *Angew. Chem. Int. Ed.* **2008**, *47*, 145-147.
- [8] Schiffner, J. A.; Müther, K.; Oestreich, M. *Angew. Chem. Int. Ed.* **2010**, *49*, 1194-1196.
- [9] Dang, L.; Lin, Z.; Marder, T. B. *Organometallics* **2008**, *27*, 4443-4454.
- [10] Feng, X.; Yun, J. *Chem. Commun.* **2009**, 6577-6579.
- [11] Chen, I-H.; Yin, L.; Itano, W.; Kanai, M.; Shibasaki, M. *J. Am. Chem. Soc.* **2009**, *131*, 11664-11665.
- [12] Shoba, V. M.; Thacker, N. C.; Bochat, A. J.; James M. Takacs, J. M. *Angew. Chem. Int. Ed.* **2016**, *55*, 1465-1469
- [13] Radomkit, S.; Hoveyda, A. H. *Angew. Chem. Int. Ed.* **2014**, *53*, 3387-3391.
- [14] Devi, P.; Rutledge, P. J. *ChemBioChem* **2017**, *18*, 338-351.
- [15] Bellus, D.; Ernst, B. *Angew. Chem. Int. Ed.* **1988**, *27*, 797-827.
- [16] Shim, S. Y.; Yuna Choi, Y.; Ryu, D. H. *J. Am. Chem. Soc.* **2018**, *140*, 11184-11188.
- [17] Kim, D. K.; Riedel, J.; Kim, R. S.; Dong, V. M. *J. Am. Chem. Soc.* **2017**, *139*, 10208-10211.

- [18] Reeves, C. M.; Eidamshaus, C.; Kim, J.; Stoltz, B. M. *Angew. Chem. Int. Ed.* **2013**, *52*, 6718-6721.
- [19] Guisán-Ceinos, M.; Parra, A.; Martin-Heras, V.; Tortosa, M. *Angew. Chem. Int. Ed.* **2016**, *55*, 6969–6972.
- [20] He, J.; Shao, Q.; Wu, Q.; Yu, J-Q. *J. Am. Chem. Soc.* **2017**, *139*, 3344–3347.
- [21] Fawcett, A.; Biberger, T.; Aggarwal, V. K. *Nat. Chem.* **2019**, *11*, 117-122.
- [22] Maciá, B. *Top. Organomet. Chem.* **2016**, *58*, 41-98.
- [23] Marson, C. M. *Chem. Soc. Rev.*, **2011**, *40*, 5514-5533.
- [24] Qixue, Q.; et al. *Angew. Chem. Int. Ed.* **2019**, *58*, 4376-4380.
- [25] Chen, P.; Dong, G. *Chem. Eur. J.* **2016**, *22*, 18290-18315.
- [26] a) Urbalaa, M.; Krompiecb, S.; Penkalab, M.; Danikiewicz, W.; Grelac, M. *Applied Catalysis A: General* **2013**, *451*, 101– 111. b) Hilt, G. *ChemCatChem* **2014**, *6*, 2484-2485. c) Lv, Z.; Chen, Z.; Hu, Y.; Zheng, W.; Wang, H.; Wanling Mo, W.; Yin, G. *ChemCatChem* **2017**, *9*, 3849-3859. d) Mamone, P.; Grünberg, M. F.; Fromm, A.; Khan, B. A.; Gooßen, L. J. *Org. Lett.* **2012**, *14*, 3716-3719.
- [27] a) Grieco, P. A.; Nishizawa, M.; Marinovic, N.; Ehmann, W. J. *J. Am. Chem. Soc.* **1976**, *98*, 7102-7104. b) Seo, K.; Kim, Y.; Rhee, Y. H. *Org. Lett.* **2018**, *20*, 979-982. c) Zhuo, L-G.; Yao, Z-K.; and Yu, Z-X. *Org. Lett.* **2013**, *15*, 4634-4637.
- [28] French, A. N. Bissmireb, S.; Wirth, T. *Chem. Soc. Rev.* **2004**, *3*, 354-362.

[29] a) D'incan, E.; Viout, P. *Tetrahedron* **1984**, *40*, 3421-3424. b) Schriesheim, A.; Hofmann, J. E.; Rowe, C. A. *J. Am. Chem. Soc.* **1961**, *83*, 3731-3732.

[30] a) Nishiwaki, N.; et al. *Tetrahedron Lett.* **2010**, *51*, 3590-3592. b) Sparke, M. B.; Turner, L.; Wenham, A. J. M. *J. Catal.* **1965**, *4*, 332-340.

[31] Hanessian, S.; Giroux, S.; Larsson, A. *Org. Lett.* **2006**, *8*, 5481-5484.

[32] a) Lumbroso, A.; Catak, S.; Sulzer-Mossé, S.; Mesmaeker, A. D. *Tetrahedron Lett.* **2015**, *56* 2397-2401. b) Madelaine, C.; Valerio, V.; Maulide, N. *Chem. Asian J.* **2011**, *6*, 2224-2239.

[33] H.-S. Sim, X. Feng, J. Yun *Chem. Eur. J.* **2009**, *15*, 1939–1943.

Chapter 4: Conclusions and Outlook

4.1 Overview

Cyclic chiral boronates are an emerging class of compounds that can be employed in several valuable transformations in synthetic organic chemistry. Despite the growing popularity of boron as a bioisostere and molecular editor of common drug scaffolds, there are relatively few examples of these organoboron compounds employed in drug discovery and medicinal chemistry programs. This thesis attempted to highlight how a cyclic chiral boronate is a valuable tool for a medicinal chemist to employ for preclinical drug discovery. The synthesis of two generations of vacquinol-1 (vac-1) analogs with allylic piperidinyl boronates illustrates the application of chiral boronates and how powerful they can be at accessing privileged scaffolds using novel chemistry. The unique functionality a chiral boronate can provide to a synthetic intermediate can also be readily diversified to help improve the biological activity of a preclinical candidate. Subjecting cyclobutenones to a catalytic enantioselective conjugate borylation reaction to form the corresponding cyclobutylboronate is another example of how the preparation of a cyclic chiral boronate could potentially serve as a precursor towards polysubstituted scaffolds with novel bioactivity. The Bpin and ketone unit of the cyclobutylboronates can likely provide many synthetic applications to add new diversity to the cyclobutane scaffold. This functionalization can pave the way towards new biological activity, leading to the discovery of new drug candidates, and new accessibility towards natural products of interest. The ability to have highly functionalized sp^3 stereogenic centres on these unique cyclobutylboronates is also highly desirable, as it will likely give any drug candidate that utilizes this scaffold a greater potency, higher binding affinity, and stronger pharmacokinetic profile.

4.2 Application of Allylic Piperidinyl Boronates for the Synthesis of Vac-1 analogs

Vac-1 was discovered by Ernfors and co-workers through a phenotypic high-throughput screening (HTS) campaign. This substance contains a quinoline β -amino alcohol with a 2-(4-chlorophenyl) moiety and displays promising activity against glioblastoma multiforme (GBM), a

highly malignant stage IV brain cancer with a miserable prognosis. Initially, the authors had no way to prepare the four possible stereoisomers of vac-1, so Kwok and Hall used a new stereocontrolled methodology via an allylboration of quinoline aldehydes and allylic piperidinyl boronates to access all individual stereoisomers. Ernfors and co-workers did eventually develop a stereoselective synthesis of vac-1, and both groups found that the *erythro* (anti) stereoisomers tended to have greater potency compared to the *threo* (syn) stereoisomers. Ultimately, Ernfors and co-workers abandoned their involvement with the drug candidate, as they were unable to reproduce one of their original observations that vac-1 attenuated GBM progression *in vivo* using mice implanted with brain tumours. It is possible that vac-1 is still active against GBM, but is not potent enough to significantly affect GBM *in vivo*. To this end, Kwok synthesized a small series of analogs replacing the *para* chlorine atom on the 2-(4-chlorophenyl moiety). These analogs were tested against U251 GBM cell lines *in vitro* through MTS assays conducted by Dr. Saket Jain in the laboratory of Dr. Roseline Godbout, and it was discovered that substitution of a larger bromine atom increased the biological activity of vac-1.

Based on the success of Kwok's analog, the main work of this thesis encompassed a structure-activity relationship (SAR) study on the 2-(4-bromophenyl) scaffold to create new generations of vac-1 analogs to increase further increase the potency. A library of racemic *threo* vac-1 analogs with *classical* and *nonclassical* bioisosteric bromine substitutions were prepared according to previous methods from Kwok with some slight modifications or alternative reactions in the synthetic routes. The results of these endeavours was the discovery of an analog where the replacement of a bromine with an isopropyl (*i*-Pr) group improved the potency four-fold in comparison to the vac-1 positive control. This promising analog prompted another small library of vac-1 analogs, looking at variable sized alkyl and aryl substituents in the 2-phenyl moiety, as well as attempted functionalization of the endocyclic alkene on the piperidine moiety and changing the quinoline scaffold to an indole. The alkene and scaffold hopping analogs were ultimately not synthesized due to difficulties, or decomposition in the synthetic route. The variable size alkyl and aryl analogs were successfully prepared, in addition to an *N*-methyl quinolinium dehydro vac-1 analog, accidentally synthesized while attempting to cyclopropanate the endocyclic alkene. After testing these analogs, Dr. Jain revealed that a *tert*-butyl (*t*-Bu) substituent in the *para* position of the 2-phenyl moiety had the greater biological activity compared to an *i*-Pr group in serum and patient-derived GBM cell lines, and it would become the new lead vac-1 analog as such. The *t*-Bu

compound indicates that large globular sterically bulky groups are necessary to maximize potency in the *para* position of the 2-phenyl moiety. Surprisingly, alkylating the nitrogen atom on the quinoline ring managed to produce biological activity at 10 and 5 μM respectively, despite the presence of an endocyclic alkene on the piperidine, which previously was detrimental towards potency. This dehydro vac-1 analog highlights the importance of the quinoline nitrogen atom as a pharmacophore and should be investigated in any future studies to further optimize vac-1.

Allylic piperidinyl boronates have been successful in advancing vac-1 as a preclinical candidate with the development of more potent analogs, but more diversification will be needed for the lead vac-1 analogs to progress to *in vivo* studies. Synthesizing enantioenriched stereoisomers of the lead analog, substituting the *t*-Bu with larger alkyl groups, scaffold hopping, substitutions on the quinoline ring, and substitutions in the *meta* and *ortho* positions on the 2-phenyl scaffold are just some of the many ways one could further optimize the vac-1 lead analog. Although initially unsuccessful with dihydroxylation and cyclopropanation reactions, functionalization of the endocyclic alkene may be possible with Heck chemistry, or perhaps [2+2] or [4+2] cycloaddition chemistry under catalyzed thermal or photochemical conditions. The many diversifications points coupled with the convergent assembly of vac-1 analogs make cyclic chiral boronates a key methodology to implement to advance vac-1 as a clinical candidate for GBM.

4.3 Preparation of Cyclobutylboronates through Asymmetric Conjugate Borylation of Cyclobutenones

New methodologies to prepare tertiary cyclobutylboronates with diverse functional groups and new biological activity are lacking in the field of conjugate borylation chemistry. A collaboration between the Hall Group and a small team at Pfizer resulted in the development of a catalytic enantioselective conjugate borylation reaction of cyclobutenones by taking advantage of modern HTS technology. Reaction optimization by Clement managed to produce the first cyclobutylboronate in good isolated yields (75-80%) and high ee (90-91%). Despite the initial success, a setback in exploring the generality of this novel conjugate borylation reaction came as a result of the unreliable synthetic route to prepare the cyclobutenone substrates. Many new analogs were not stable towards Boghi's conditions to migrate the endocyclic alkene and create the desired α,β -disubstituted cyclobutenone regioisomer with a tetrasubstituted alkene.

Consequently, new strategies were attempted to migrate the alkene under milder conditions. Transition metal catalysis, iodination and elimination, and base catalysis under protic and aprotic conditions were the three prongs of attack at solving this problem. Transition metals and iodination either led to the formation of the undesired regioisomer, or ring-opened/dimer products. The breakthrough came with base catalysis, where potassium *tert*-butoxide (KO*t*-Bu) in a protic media gave full conversion to the desired regioisomer. From this mild methodology, a library of cyclobutenone substrates were prepared in low to good yields.

Subjecting the library of cyclobutenones to the conjugate borylation conditions was successful, and gave the corresponding cyclobutylboronates in all attempted substrates. *Para*-substituted weakly electron-donating (EDG) and electron-withdrawing groups (EWGs) gave satisfactory isolated yields, good to excellent diastereoselectivity, and maintained the high enantioselectivity observed for Clement's cyclobutylboronate substrate. *Meta* and *ortho* substituents were also tolerated, albeit in slightly lowered yields and enantioselectivity. An ethyl group in place of a methyl group in the α -position next to the carbonyl had reduced diastereoselectivity, but maintained a good isolated yield and enantioselectivity.

The catalytic enantioselective preparation of cyclobutylboronates provides a significant advance in the field of β -borylation chemistry, as this methodology allows the first access to borylated cyclobutanones with a tertiary boronate. Since these substrates are relatively unknown, there are many possible future applications with these new scaffolds. One can imagine transforming the Bpin and ketone units to build C–C bonds or acquire different functional groups to rapidly generate libraries of enantioenriched polysubstituted cyclobutanes, which could be screened for biological activity against a variety of diseases for new drug discovery and medicinal chemistry projects at Pfizer or in the Hall Group. Another avenue would be to develop or optimize stereospecific Suzuki-Miyaura sp^3 - sp^2 cross-coupling methodologies on this unique scaffold. If successful, this reaction could rapidly assemble functionalized cyclobutyl units. These various applications will further highlight cyclic chiral boronates as a useful tool to exploit in drug discovery programs in academia and industry.

4.4 Bibliography

Blass, B. E. *Basic Principles of Drug Discovery and Development*; Academic Press: San Diego, 2015.

Drews, J. *Science* **2000**, *287*, 1960-1964.

Patrick, G. L. *An Introduction to Medicinal Chemistry 5th Ed*; Oxford University Press: Oxford, 2013.

Bosch, F.; Rosich, L. *Pharmacology* **2008**, *82*, 171-179.

a) Calcaterra, N. E.; Barrow, J. C. *ACS Chem. Neurosci.* **2014**, *5*, 253-260. b) Collins, R.; et al. *Lancet*, **2016**, *388*, 2532-2561. c) Pazuki, G.; Vossoughi, M.; Taghikhani, V. *J. Chem. Eng. Data.* **2010**, *55*, 243-248. d) Browning, R. J.; Reardon, P. J. T.; Parhizkar, M.; Pedley, R. B.; Edirisinghe, M.; Knowles, J. C.; Stride, E. *ACS Nano* **2017**, *11*, 8560-8578. e) Wang, Y-F.; Shi, Q-W.; Dong, M.; Kiyota, H.; Gu, Y-C.; Cong, B. *Chem. Rev.* **2011**, *111*, 7652-7709. f) Heffron, T. P. *J. Med. Chem.* **2016**, *59*, 10030-10066.

Dugger, S. A.; Platt, A.; Goldstein, D. B. *Nat. Rev. Drug. Discov.* **2018**, *17*, 183-196.

Tufféry, P. *Expert Opin. Drug Discov.* **2015**, *10*, 579-589.

Morrow, J. K.; Tian, L.; Zhang, S. *Critical Reviews™ in Biomedical Engineering* **2010**, *38*, 143-156.

a) Scannell, J. W.; Blanckley, A.; Boldon, H.; Warrinton, B. *Nat. Rev. Drug. Discov.* **2012**, *11*, 191-200. b) Moore, G. E. *Electronics.* **1965**, *38(8)*, 1-4.

Abou-Gharbia, M.; Childers, W. E. *J. Med. Chem.* **2014**, *57*, 5525-5553.

U.S. Food & Drug Administration. Generic Drug Facts. <https://www.fda.gov/drugs/resourcesforyou/consumers/buyingusingmedicinesafely/genericdrugs/ucm167991.htm> (accessed March 14, 2019)

Takebe, T.; Imai, R.; Ono, S. *Clin. Transl. Sci.* **2018**, *11*, 597-606.

Bolognesi, M. L. *ACS Med. Chem. Lett.* **2019**, *10*, 273-275.

Proschak, E.; Stark, H.; Merk, D. *J. Med. Chem.* **2019**, *62*, 420-444.

Aubé, J. *ACS Med. Chem. Lett.* **2012**, *3*, 442-444.

Polamreddy, P.; Gattu, N. *Drug Discov. Today* **2018**, *24*, 789-795.

Pushpakom, S.; et al. *Nat. Rev. Drug. Discov.* **2019**, *18*, 41-58.

a) Brown, D. G.; Boström, J. *J. Med. Chem.* **2018**, *61*, 9442-9468. b) Valeur, E.; Jimonet, P. *J. Med. Chem.* **2018**, *61*, 9004-9029.

a) Hall, D. G. *Boronic Acids: Preparation and Applications in Organic Synthesis, Medicine, and Materials, 1&2, 2nd Ed*; Wiley-VCH Verlag & Co. KGaA: Weinheim, 2011. b) Ban, H. S.; Nakamura, H. *Chem. Rec.* **2015**, *15*, 616-635. c) Yang, W.; Gao, X.; Wang, B. *Med. Res. Rev.* **2003**, *23*, 346-368.

Leśnikowski, Z. *J. Expert Opin. Drug Discov.* **2016**, *11*, 569-578.

Brooks, W. L. A.; Sumerlin, B. S. *Chem. Rev.* **2016**, *116*, 1375-1397.

Whyte, G. F.; Vilar, R.; Woscholski, R. *J. Chem. Biol.* **2013**, *6*, 161-174.

a) Meanwell, N. A. *J. Med. Chem.* **2011**, *54*, 2529-2591. b) Seddon, M. P.; Cosgrove, D. A.; Gillet, V. J. *ChemMedChem* **2018**, *13*, 607-613.

Ballatore, C.; Huryn, D. M.; III, Smith, A. B. *ChemMedChem* **2013**, *8*, 385-395.

Maynard, A.; and et al. *J. Med. Chem.* **2014**, *57*, 1902-1913.

Yang, F.; Zhu, M.; Zhang, J.; Zhou, H. *Med. Chem. Commun.* **2018**, *9*, 201-211.

Vshyvenko, S.; Clapson, M. L.; Suzuki, I.; Hall, D. G. *ACS Med. Chem. Lett.* **2016**, *7*, 1097-1101.

a) Adamczyk-Woźniak, A.; Borys, K. M.; Sporzyński, A. *Chem. Rev.* **2015**, *115*, 5224-5247. b) Liu, C. T.; Tomsho, J. W.; Benkovic, S. J. *Bioorg. Med. Chem.* **2014**, *22*, 4462-4473. c) Baker, S. J.; Tomsho, J. W.; Benkovic, S. J. *Chem. Soc. Rev.* **2011**, *40*, 4279-4285. d) Dowlut, M.; Hall, D. G. *J. Am. Chem. Soc.* **2006**, *128*, 4226-4227.

Meredydy, G. R.; Chakradhar, A.; Rutkoski, R. M.; Jonnalagadda, S. C. *J. Organomet. Chem.* **2018**, *865*, 12-22.

a) Sehl, T.; Maugeri, Z.; Rother, D. *J. Mol. Catal. B. Enzym.* **2015**, *114*, 65-71. b) Karjalainen, O. K.; Koskinen, A. M. P. *Org. Biomol. Chem.* **2012**, *10*, 4311-4326. c) Burchak, O. N.; Py, S. *Tetrahedron.* **2009**, *65*, 7333-7356. d) Lee, H-S.; Kang, S. H. *Synlett.* **2004**, *10*, 1673-1685. e) Bergmeier, S. C. *Tetrahedron* **2000**, *56*, 2561-2576.

Calleja, P.; Ernst, M.; Hashmi, A. S. K.; Schaub, T. *Chem. Eur. J.* **2019**, *10.1002/chem.201900531*.

Li, X.; Hall, D. G. *Angew. Chem. Int. Ed.* **2018**, *57*, 10304-10308.

a) Lachance, H.; Hall, D. G. *Org. React.* **2009**, *73*, 1-341. b) Hall, D. G.; Lee, J. C. H.; Ding, J. *Pure Appl. Chem.*, **2012**, *84*, 2263-2277.

a) Panda, S.; Coffin, A.; Nguyen, Q. N.; Tantillo, D. J.; Ready, J. M. *Angew. Chem. Int. Ed.* **2016**, *55*, 2205–2209. b) Hoffmann, R. W.; Brückner, D. *New. J. Chem.* **2001**, *25*, 369-373.

Murata, M.; Oyama, T.; Watanabe, S.; Masuda, Y. *Synthesis* **2000**, *6*, 778-780.

a) Kim, Y-R.; Hall, D. G. *Org. Biomol. Chem.* **2016**, *14*, 4739-4748. b) Lessard, S.; Peng, F.; Hall, D. G. *J. Am. Chem. Soc.* **2009**, *131*, 9612-9613.

Vitaku, E.; Smith, D. T.; Njardarson, J. T. *J. Med. Chem.* **2014**, *57*, 10257-10274.

Ding, J.; Rybak, T.; Hall, D. G. *Nat. Commun.* **2014**, *5*, 5474-5472.

Bräse, S. *Privileged Scaffolds in Medicinal Chemistry: Design, Synthesis, Evaluation*; The Royal Society of Chemistry: Cambridge, 2016.

Ramawat, K. G.; Mérillon, J. M. *Natural Products: Phytochemistry, Botany, and Metabolism of Alkaloids, Phenolics and Terpenes*; Springer-Verlag Berlin: Heidelberg, 2013.

Ding, J.; Hall, D. G. *Angew. Chem. Int. Ed.* **2013**, *52*, 8069-8073.

Kitambi, S. S.; et al. *Cell* **2014**, *157*, 313–328.

Kwok, S. Application and Substrate Scope Expansion of a Unique Borylative Migration Transformation. M.Sc. Thesis, The University of Alberta, 2016.

Hammarström, L. G. J.; et al. *J. Med. Chem.* **2016**, *59*, 8577-8592.

Dembitsky, V. M. *Phytomedicine* **2014**, *21*, 1559–1581.

a) Meanwell, N. A. *Chem. Res. Toxicol.* **2016**, *29*, 564–616. b) Hazelard, D.; Compain, P. *Org. Biomol. Chem.* **2017**, *15*, 3806–3827. c) Johnson, J. W.; et al. *J. Org. Chem.* **2008**, *73*, 6970–6982.

d) Kuchar, M.; Mamat, C. *Molecules* **2015**, *20*, 16186-16220. e) Wroblewski, M. L.; et al. *Bioorg. Med. Chem. Lett.* **2006**, *16*, 3859–3863. f) Lovering, F.; Bikker, J.; Humblet, C. *J. Med. Chem.* **2009**, *52*, 6752–6756.

a) Oun, R.; Moussa, Y. E.; Wheate, N. J. *Dalton Trans.* **2018**, *47*, 6645-6653. b) Pager, V. V.; RajanBabu, T. V. *Science* **2018**, *361*, 68-72. c) Berger, W. T.; et al. *PLOS ONE*. **2012**, *7*, e50968. d) Slade, J.; et al. *Org. Process Res. Dev.* **2007**, *11*, 825-835.

a) Lee-Ruff, E. *Synthesis of Cyclobutanes. PATAI'S Chemistry of Functional Groups*, Rappoport, Z. (Ed.); John Wiley & Sons, Ltd: 2009, doi:10.1002/9780470682531.pat0322.

b) Lee-Ruff, E.; Mladenova, G. *Chem. Rev.* **2003**, *103*, 1449-1484.

Chen, P-h.; Dong, G. *Chem. Eur. J.* **2016**, *22*, 18290-18315.

a) Lumbroso, A.; Catak, S.; Sulzer-Mossé, S.; Mesmaeker, A. D. *Tetrahedron Lett.* **2015**, *56*, 2397–2401. b) Falmagne, J-B.; Escudero, J.; Taleb-Sahraoui, S.; Ghosez, L. *Angew. Chem. Int. Ed.* **1981**, *20*, 879–880.

Danheiser, R. L.; Savariar, S. *Tetrahedron. Lett.* **1987**, *28*, 3299-3302.

Fernández, E.; Whiting, A. *Synthesis and Application of Organoboron Compounds*; Springer International Publishing: Switzerland, 2015.

American Association of Neurological Surgeons. Glioblastoma Multiforme. <https://www.aans.org/Patients/Neurosurgical-Conditions-and-Treatments/Glioblastoma-Multiforme> (accessed January 7, 2019).

Ohgaki, H.; Kleihues, P. *Am. J. Pathol.* **2007**, *170*, 1445-1453.

Urbańska, K.; Sokołowska, J.; Szmidt, M.; Sysa, P. *Contemp. Oncol. (Pozn)*. **2014**, *18*, 307-312.

John Hopkins Medicine. Neurology and Neurosurgery: Brain Tumour Centre. Brain Tumour Grades: Biopsy and Prognosis. https://www.hopkinsmedicine.org/neurology_neurosurgery/centers_clinics/brain_tumor/diagnos/s/brain-tumor-grade.html (accessed January 9, 2018).

American Brain Tumour Association. Glioblastoma (GBM). https://www.abta.org/tumor_types/glioblastoma-gbm/ (accessed January 7, 2019).

Brain Tumour Foundation of Canada. Glioblastoma multiforme (GBM). <https://www.braintumour.ca/4869/glioblastoma-multiforme> (accessed January 7, 2019).

Shi, Y.; Lim, S. K.; Parada, L. F. *Cell Research*. **2014**, *24*, 910-911.

Appin, C. L.; et al. *Brain Pathol*. **2013**, *23*, 454-461.

Takeuchi, H.; Kitai, R.; Hosoda, T.; Yamada, S.; Hashimoto, N.; Kikuta, K.; Shimizu, Y.; Kimura, H. *J. Neurooncol*. **2016**, *127*, 337-344.

Barbashina, V.; Salazar, P.; Ladanyi, M.; Rosenblum, M. K.; Edgar, M. A. *Am. J. Surg. Pathol*. **2007**, *31*, 1196-1202.

Ohgaki, H.; Kleihues, P. *Clin. Cancer. Res*. **2012**, *19*, 764-772.

Rodriguez, F. J.; Orr, B. A.; Ligon, K. L.; Eberhart, C. G. *Oncotarget* **2012**, *3*, 98-106.

a) Messaoudi, K.; Clavreu, A.; Lagarce, F. *Drug Discov. Today* **2015**, *20*, 899-905. b) Lathia, J. D.; Mack, S. C.; Mulkearns-Hubert, E. E.; Valentim, C. L. L.; Rich, J. N. *Genes Dev*. **2015**, *29*, 1203–1217.

Bastiancich, C.; Bastiat, G.; Lagarce, F. *Drug Discov. Today* **2018**, *23*, 416-423.

Silverman, R. B.; and Holladay, M. W. *The Organic Chemistry of Drug Design and Drug Action*; Academic Press: San Diego, 2014.

Baell, J. B.; Nissink, J. W. M. *ACS. Chem. Biol.* **2018**, *13*, 36-44.

Roberts, S. A. *Xenobiotica* **2001**, *31*, 557-589.

Gilbertson, R. J. *Cell* **2014**, *157*, 289-290.

Lee, J. *Cancer Cell* **2006**, *9*, 391-403.

a) Rapport, M. M.; Senear, A. E.; Mead, J. F.; Koepfli, J. B. *J. Am. Chem. Soc.* **1946**, *68*, 2695-2697. b) Rapport, M. M.; Senear, A. E.; Mead, J. F.; Koepfli, J. B. *J. Am. Chem. Soc.* **1946**, *68*, 2697-2703. c) Mead, J. F.; Rapport, M. M.; Koepfli, J. B. *J. Am. Chem. Soc.* **1946**, *68*, 2704-2705. d) Brown, R. F.; et al. *J. Am. Chem. Soc.* **1946**, *68*, 2705-2708. d) Mead, J. F.; Senear, A. E.; Koepfli, J. B. *J. Am. Chem. Soc.* **1946**, *68*, 2708-2710. e) Buchman, E. R.; Sargent, H.; Myers, T. C.; Howton, D. R. *J. Am. Chem. Soc.* **1946**, *68*, 2710-2714. f) Winstein, S.; Jacobs, T. L.; Levy, E. F.; Seymour, D.; Linden, G. B.; Henderson, R. B. *J. Am. Chem. Soc.* **1946**, *68*, 2714-2718. g) Buchman, E. R.; Howton, D. R. *J. Am. Chem. Soc.* **1946**, *68*, 2718-2720. h) Seibert, R. A.; Norton, T. R.; Benson, A. A.; Bergstrom, F. W. **1946**, *68*, 2721-2723.

Pinder, R. M.; Burger, A. *J. Med. Chem.* **1968**, *11*, 267-269.

Fernández-Álvaro, E.; Hong, W. D.; Nixon, G. L.; O'Neill, P. M.; Calderón, F. *J. Med. Chem.* **2016**, *59*, 5587-5603.

Fuhler, G. M.; et al. *Mol. Med.* **2012**, *18*, 65-75.

Léon, B.; Fong, J. C. N.; Peach, K. C.; Wong, W. R.; Yildiz, F. H.; Linington, R. G. *Org. Lett.* **2013**, *15*, 1234-1237.

Färnegårdh, K.; Gravenfors, Y.; Ernfors, P.; Hammarström, L. G. J.; Kitambi, S. Compounds and Use for Treating Cancer. WO Patent 2015/033228 A2, March 12, 2015.

a) Pfitzinger, W. *J. Prakt. Chem.* **1886**, 33, 100. b) Pfitzinger, W. *J. Prakt. Chem.* **1888**, 38, 582-584.

Hofmann, A. W. *Berichte der Deutschen Chemischen Gesellschaft.* **1881**, 14, 2725-2736.

Schönherr, H.; Cernak, T. *Angew. Chem. Int. Ed.* **2013**, 52, 12256-12267.

a) Brooks, W. H.; Guida, W. C.; Daniel, K. G. *Curr. Top. Med. Chem.* **2011**, 11, 760-770. b) Lovering, F.; Bikker, J.; Humblet, C. *J. Med. Chem.* **2009**, 52, 6752-6756. c) McConathy, J.; Owens, M. J. *Primary Care Companion J. Clin. Psychiatry* **2003**, 5, 70-73.

Bao, R. L-Y.; Zhao, R.; Shi, L. *Chem. Commun.* **2015**, 51, 6884-6900.

Tan, S. K.; Jermakowicz, A.; Mookhtiar, A. K.; Nemeroff, C. B.; Schürer, S. C.; Ayad, N. G. *Front. Pharmacol.* **2018**, 9(218), 1-19.

a) Doherty, G. J.; McMahon, H. T. *Annu. Rev. Biochem.* **2009**, 78, 857-902. b) Elkin, S. R.; Lakoduk, A. M.; Schmid, S. L. *Wien. Med. Wochenschr.* **2016**, 166, 196-204. c) Lim, J. P.; Gleeson, P. A. *Immunology and Cell Biology* **2011**, 89, 836-843. d) Naslavsky, N.; Caplan, S. *J. Cell. Sci.* **2018**, 131, 1-14.

a) Overmeyer, J. H.; Young, A. M.; Bhanot, H.; Maltese, W. A. *Molecular Cancer* **2011**, 10(69), 1-17. b) Maltese, W. A.; Overmeyer, J. H. *Am. J. Pathol.* **2014**, 184, 1630-1642. c) Mbah, N. E.; Overmeyer, J. H.; Maltese, W. A. *Cell Biol. Toxicol.* **2017**, 33, 263-282. d) Li, Z.; Mbah, N. E.; Overmeyer, J. H.; Sarver, J. G.; George, S.; Trabbic, C. J.; Erhardt, P. W.; Maltese, W. A. *BMC Cancer* **2019**, 19(77), 1-20.

Hutagalung, A. H.; Novick, P. J. *Physiol. Rev.* **2011**, 91, 119-149.

Settembre, C.; Fraldi, A.; Medina, D. L.; Ballabio, A. *Nat. Rev. Mol. Cell Biol.* **2013**, *14*, 283-296.

Elmore, S. *Toxicol. Pathol.* **2007**, *35*, 495-516.

Paddison, P. J.; Caudy, A. A.; Bernstein, E.; Hannon, G. J.; Conklin, D. S. *Genes Dev.* **2002**, *16*, 948-958.

a) Pavese, J. M.; Ogden, I. M.; Voll, E. A.; Huang, X.; Xu, L.; Jovanovic, B.; Bergan, R. C. *PLoS ONE* **2014**, *9*(7), 1-12. b) Pearson, G.; Robinson, F.; Gibson, T. B.; Xu, B-E.; Karandikar, M.; Berman, K.; Cobb, M. H. *Endocrine Reviews* **2001**, *22*, 153-183.

a) Cho, H.; Geno, E.; Patoor, M.; Reid, A.; McDonald, R.; Hild, M.; Jenkins, J. L. *ACS Omega* **2018**, *3*, 6097-6103. b) Falkenburger, B. H.; Jensen, J. B.; Dickson, J. E.; Suh, B-C.; Hille, B. *J. Physiol.* **2010**, *588*, 3179-3185.

a) Cingolani, F.; Simbari, F.; Abad, J. L.; Casasampere, M.; Fabrias, G.; Futerman, A. H.; Casas, J. *J. Lipid. Res.* **2017**, *58*, 1500-1513. b) Sun, L.; Li, B.; Su, X.; Chen, G.; Li, Y.; Li, L.; Wei, W. *J. Med. Chem.* **2017**, *60*, 6638-6648. c) Huang, W.; et al. *J. Med. Chem.* **2018**, *61*, 5424-5434.

Wilcken, R.; Zimmermann, M. O.; Bauer, M. R.; Rutherford, T. J.; Fersht, A. R.; Joerger, A. C.; Boeckler, F. M. *ACS Chem. Biol.* **2015**, *10*, 2725-2732.

Clement, H. A.; Hall, D. G. *Tetrahedron Lett.* **2018**, *59*, 4334-4339.

a) Russo, C. M.; Adhikari, A. A.; Wallach, D. R.; Fernandes, S.; Balch, A. N.; Kerr, W. G.; Chisholm, J. D. *Bioorg. Med. Chem. Lett.* **2015**, *25*, 5344-5348. b) Brown, W. G. *Org. React.* **1951**, *6*, 469-509.

Collin, G.; Höke, H. *Quinoline and Isoquinoline. Ullmann's Encyclopedia of Industrial Chemistry*; Wiley-VCH Verlag GmbH & Co. KGaA: Weinheim, 2012.

DasGupta, S.; Murumkar, P. R.; Giridhar, R.; Yadav, M. R. S. *Bioorg. Med. Chem.* **2009**, *17*, 3604–3617.

Di, L.; Kerns, E. H. *Drug Discov. Today* **2006**, *11*, 446-451.

a) Dunleavy, J. K. *Platinum Metals Rev.* **2006**, *50*(2), 110. b) Iwasaki, K.; Wan, K. K.; Oppedisano, A.; Crossley, S. W. M.; Shenvi, R. A. *J. Am. Chem. Soc.* **2014**, *136*, 1300–1303.

Jègou, G.; Jenekhe, S. A. *Macromolecules* **2001**, *34*, 7926-7928.

Zanon, J.; Kalpars, A.; Buchwald, S. L. *J. Am. Chem. Soc.* **2003**, *125*, 2890-2891.

CellTiter 96® AQueous One Solution Cell Proliferation Assay; Technical Bulletin #TB112; Promega Corporation: Madison, WI, 2012; 1-12.

Fang, G-H.; Yan, Z-J.; Deng, M-Z. *Org. Lett.* **2004**, *6*, 357-360.

Chen, W-L.; Wu, S-Y.; Mo, X-L.; Wei, L-X.; Lang, C.; Mo, D-L. *Org. Lett.* **2018**, *20*, 3527–3530.

Abdelwaly, A.; Salama, I.; Gomaa, M. S.; Helal, M. A. *Med. Chem. Res.* **2017**, *26*, 3173–3187.

Dhani, R.; et al. *J. Chem. Pharm. Res.* **2011**, *3*, 519-523.

Kato, A.; et al. *Bioorg. Med. Chem.* **2011**, *19*, 3558–3568.

Davies, S. G.; Ling, K. B.; Roberts, P. M.; Russell, A. J.; Thomson, J. E. *Chem. Commun.* **2007**, *0*, 4029–4031.

Quartararo, C. E.; Reznik, E.; deCarvalho, A. C.; Mikkelsen, T.; Stockwell, B. R. *ACS Med. Chem. Lett.* **2015**, *6*, 948–952.

Narlawar, R.; et al. *Chem. Asian J.* **2018**, *13*, 3321-3327.

Zheng, K.; Liu, X.; Feng, X. *Chem. Rev.* **2018**, *118*, 7586–7656.

a) Sonawane, R. P.; Jheengut, V.; Rabalakos, C.; Larouche-Gauthier, R.; Scott, H. K.; Aggarwal, V. K. *Angew. Chem. Int. Ed.* **2011**, *50*, 3760-3763. b) Armstrong, R. J.; Aggarwal, V. K. *Synthesis* **2017**, *49*, 3323–3336.

Lawson, Y. G.; M. J. Lesley, M. J. G.; Marder, T. B.; Norman, N. C.; Rice, C. R. *Chem. Commun.* **1997**, 2051-2052.

a) Ito, J.; Yamanaka, H.; Tateiwab, J.; Hosomi, A.; *Tetrahedron Lett.* **2000**, *41*, 6821-6825. b) Takahashi, K.; Ishiyama, T.; Miyaura, N. *Chem. Lett.* **2000**, 982-983.

Mun, S.; Lee, J-E.; Yun, J. *Org. Lett.* **2006**, *8*, 4887-4889.

Lee, J-E.; Yun, J. *Angew. Chem. Int. Ed.* **2008**, *47*, 145–147.

Schiffner, J. A.; Müther, K.; Oestreich, M. *Angew. Chem. Int. Ed.* **2010**, *49*, 1194-1196.

Dang, L.; Lin, Z.; Marder, T. B. *Organometallics* **2008**, *27*, 4443-4454.

Feng, X.; Yun, J. *Chem. Commun.* **2009**, 6577–6579.

Chen, I-H.; Yin, L.; Itano, W.; Kanai, M.; Shibasaki, M. *J. Am. Chem. Soc.* **2009**, *131*, 11664-11665.

Shoba, V. M.; Thacker, N. C.; Bochat, A. J.; James M. Takacs, J. M. *Angew. Chem. Int. Ed.* **2016**, *55*, 1465-1469

Radomkit, S.; Hoveyda, A. H. *Angew. Chem. Int. Ed.* **2014**, *53*, 3387-3391.

Devi, P.; Rutledge, P. J. *ChemBioChem* **2017**, *18*, 338-351.

Bellus, D.; Ernst, B. *Angew. Chem. Int. Ed.* **1988**, *27*, 797-827.

Shim, S. Y.; Yuna Choi, Y.; Ryu, D. H. *J. Am. Chem. Soc.* **2018**, *140*, 11184-11188.

Kim, D. K.; Riedel, J.; Kim, R. S.; Dong, V. M. *J. Am. Chem. Soc.* **2017**, *139*, 10208–10211.

Reeves, C. M.; Eidamshaus, C.; Kim, J.; Stoltz, B. M. *Angew. Chem. Int. Ed.* **2013**, *52*, 6718-6721.

Guisán-Ceinos, M.; Parra, A.; Martín-Heras, V.; Tortosa, M. *Angew. Chem. Int. Ed.* **2016**, *55*, 6969–6972

He, J.; Shao, Q.; Wu, Q.; Yu, J-Q. *J. Am. Chem. Soc.* **2017**, *139*, 3344–3347.

Fawcett, A.; Biberger, T.; Aggarwal, V. K. *Nat. Chem.* **2019**, *11*, 117-122.

Maciá, B. *Top. Organomet. Chem.* **2016**, *58*, 41-98.

Marson, C. M. *Chem. Soc. Rev.*, **2011**, *40*, 5514-5533.

Qixue, Q.; et al. *Angew. Chem. Int. Ed.* **2019**, *58*, 4376-4380.

Chen, P.; Dong, G. *Chem. Eur. J.* **2016**, *22*, 18290-18315.

a) Urbalaa, M.; Krompiecb, S.; Penkalab, M.; Danikiewicz, W.; Grelac, M. *Applied Catalysis A: General* **2013**, *451*, 101– 111. b) Hilt, G. *ChemCatChem* **2014**, *6*, 2484-2485. c) Lv, Z.; Chen, Z.; Hu, Y.; Zheng, W.; Wang, H.; Wanling Mo, W.; Yin, G. *ChemCatChem* **2017**, *9*, 3849-3859. d)

Mamone, P.; Grünberg, M. F.; Fromm, A.; Khan, B. A.; Gooßen, L. J. *Org. Lett.* **2012**, *14*, 3716-3719.

a) Grieco, P. A.; Nishizawa, M.; Marinovic, N.; Ehmman, W. J. *J. Am. Chem. Soc.* **1976**, *98*, 7102-7104. b) Seo, K.; Kim, Y.; Rhee, Y. H. *Org. Lett.* **2018**, *20*, 979-982. c) Zhuo, L-G.; Yao, Z-K.; and Yu, Z-X. *Org. Lett.* **2013**, *15*, 4634-4637.

French, A. N. Bissmireb, S.; Wirth, T. *Chem. Soc. Rev.* **2004**, *3*, 354-362.

a) D'incan, E.; Viout, P. *Tetrahedron* **1984**, *40*, 3421-3424. b) Schriesheim, A.; Hofmann, J. E.; Rowe, C. A. *J. Am. Chem. Soc.* **1961**, *83*, 3731-3732.

a) Nishiwaki, N.; et al. *Tetrahedron Lett.* **2010**, *51*, 3590-3592. b) Sparke, M. B.; Turner, L.; Wenham, A. J. M. *J. Catal.* **1965**, *4*, 332-340.

Hanessian, S.; Giroux, S.; Larsson, A. *Org. Lett.* **2006**, *8*, 5481-5484.

a) Lumbroso, A.; Catak, S.; Sulzer-Mossé, S.; Mesmaeker, A. D. *Tetrahedron Lett.* **2015**, *56* 2397-2401. b) Madelaine, C.; Valerio, V.; Maulide, N. *Chem. Asian J.* **2011**, *6*, 2224-2239.

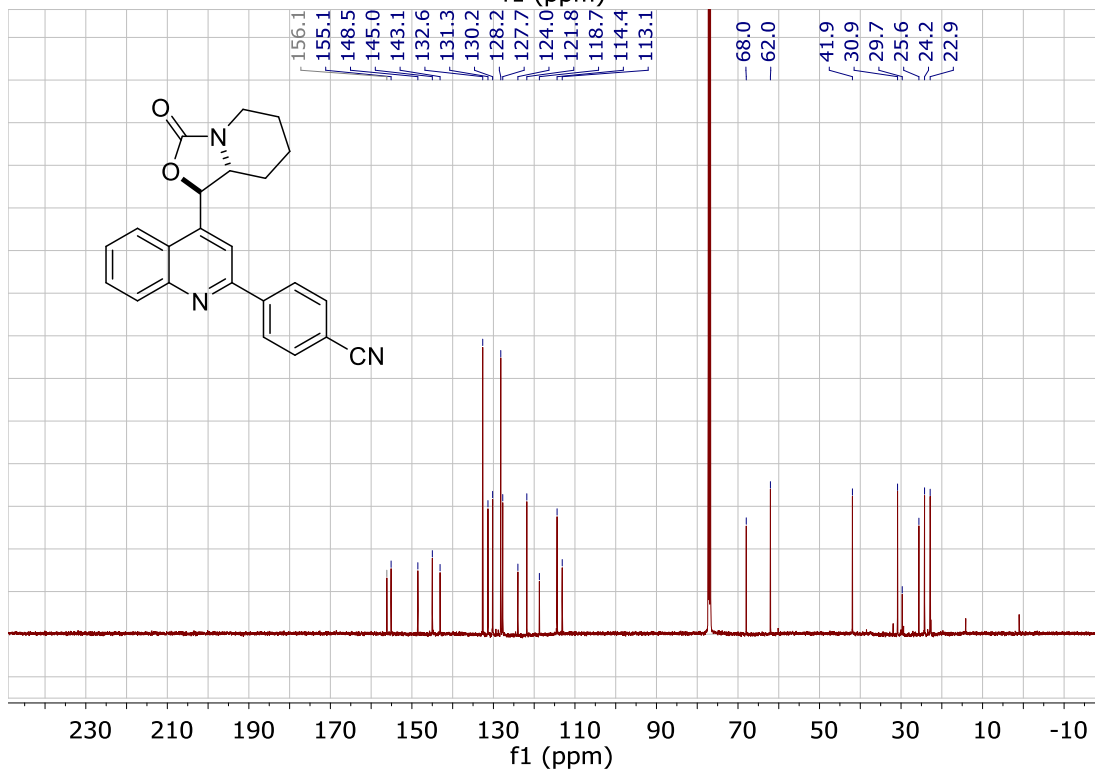
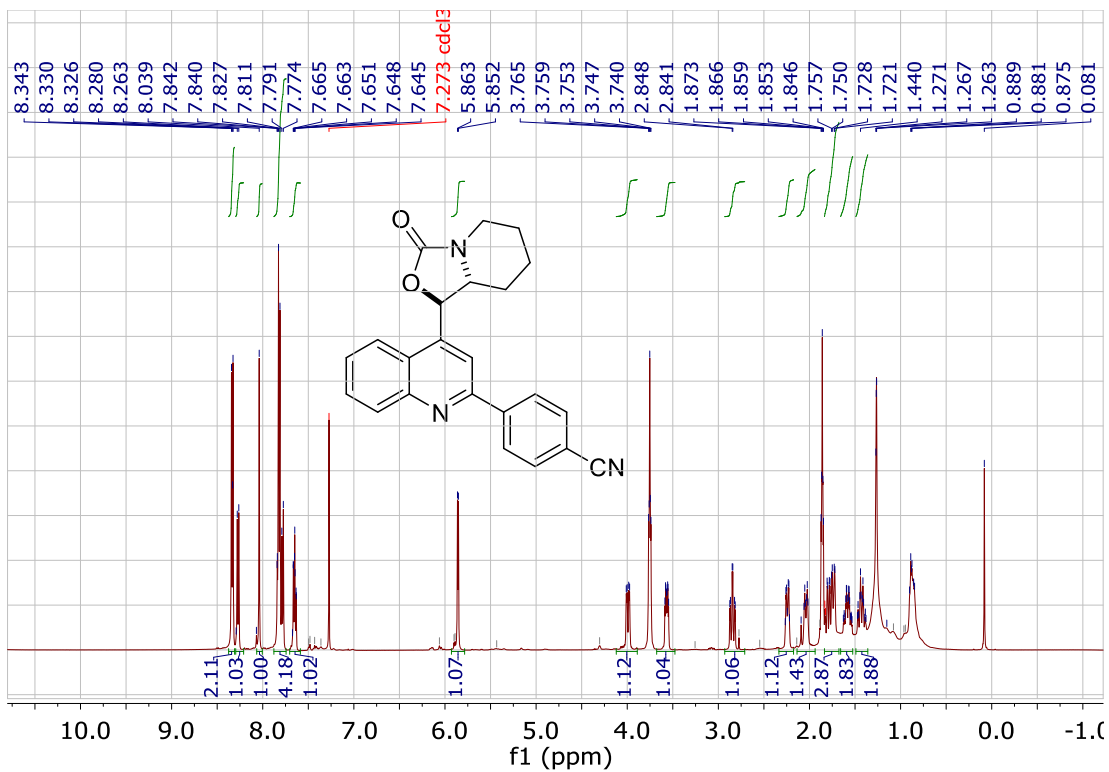
Jiang, C.; Zheng, Z-J.; Tian-Yang Yu, T-Y.; Wei, H. *Org. Biomol. Chem.*, **2018**, *16*, 7174-7177.

H.-S. Sim, X. Feng, J. Yun *Chem. Eur. J.* **2009**, *15*, 1939-1943.

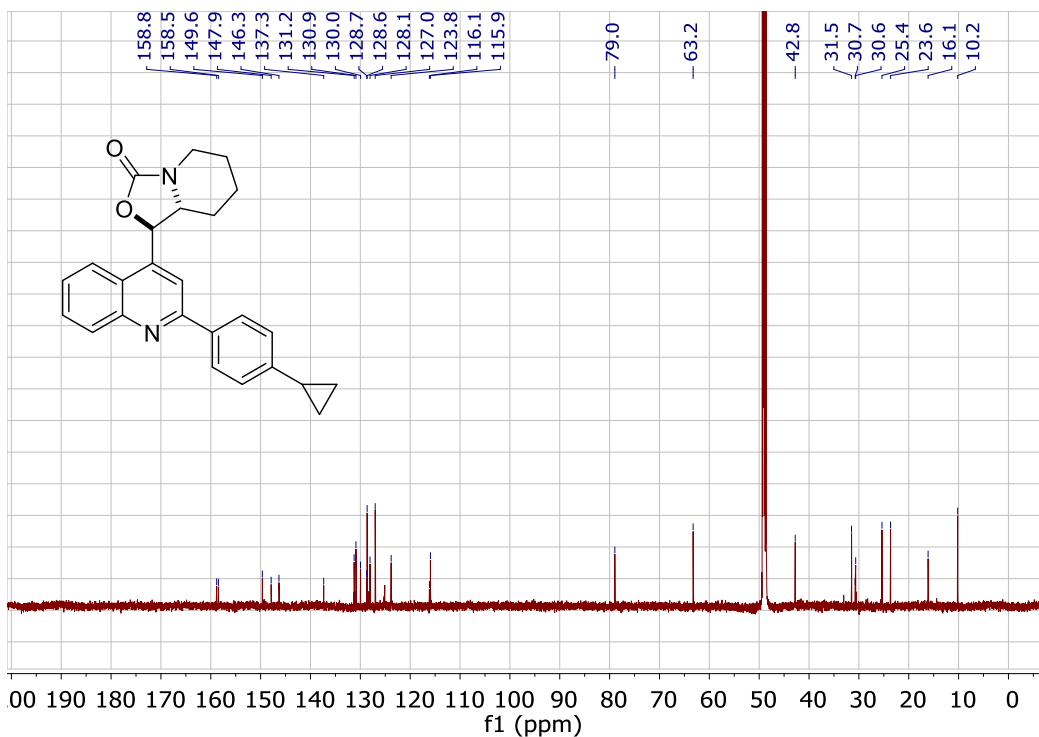
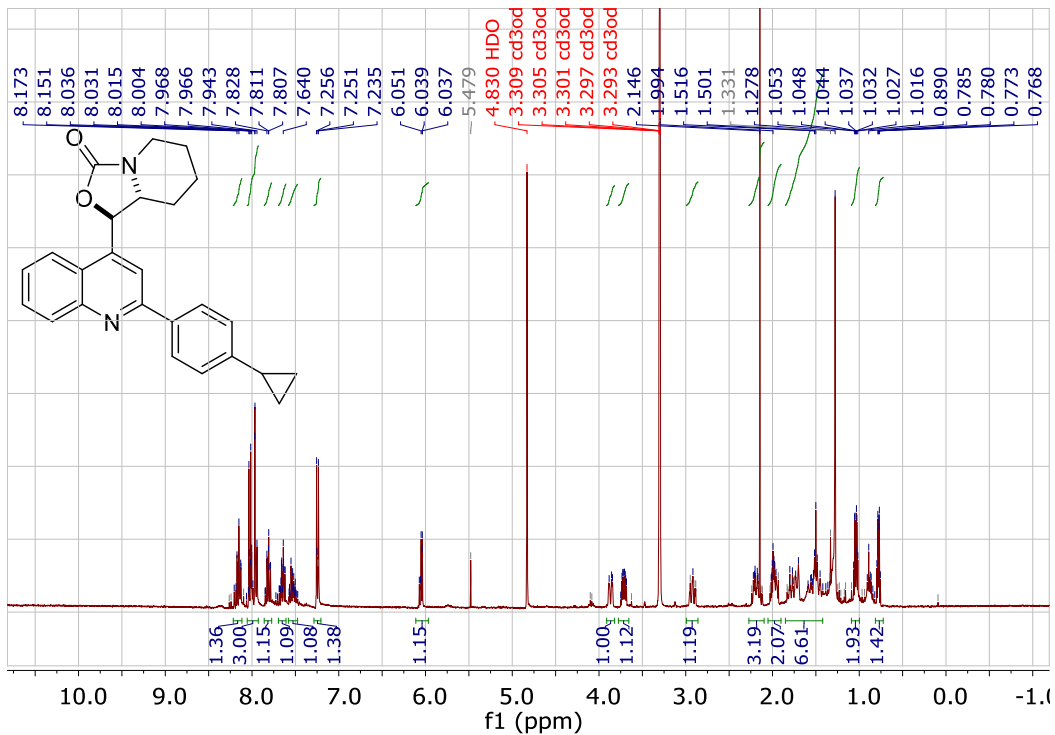
Appendix: Reproductions of Important NMR Spectra and Selected Chromatograms for Enantiomeric Excess Measurements

See experimental sections for conditions.

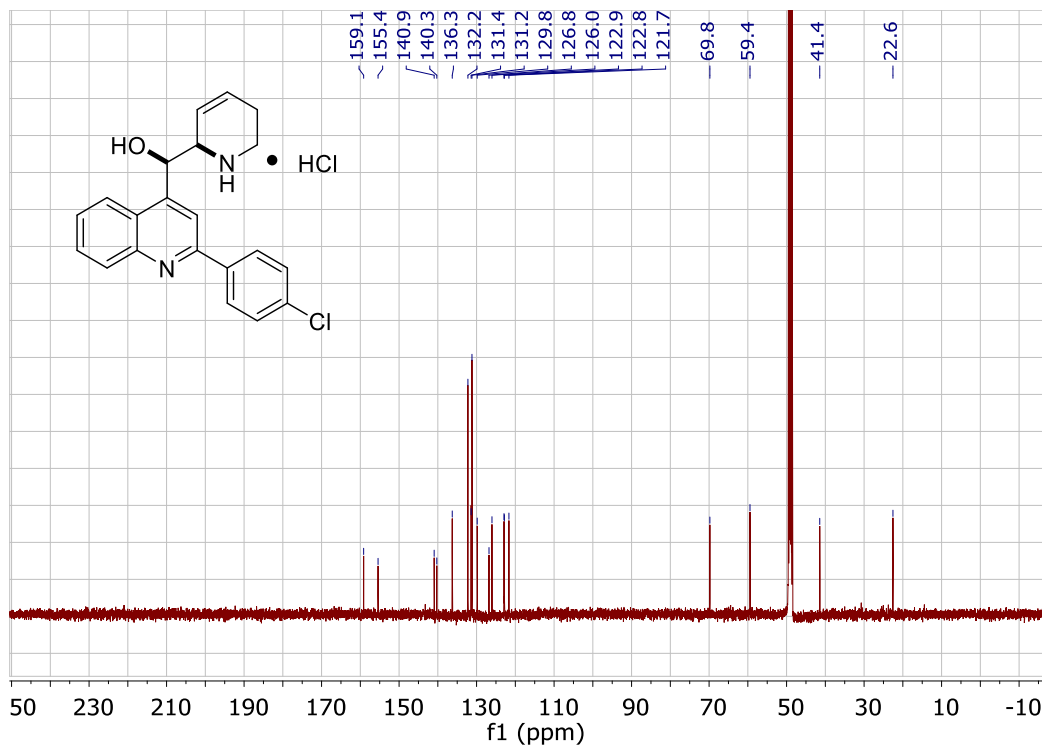
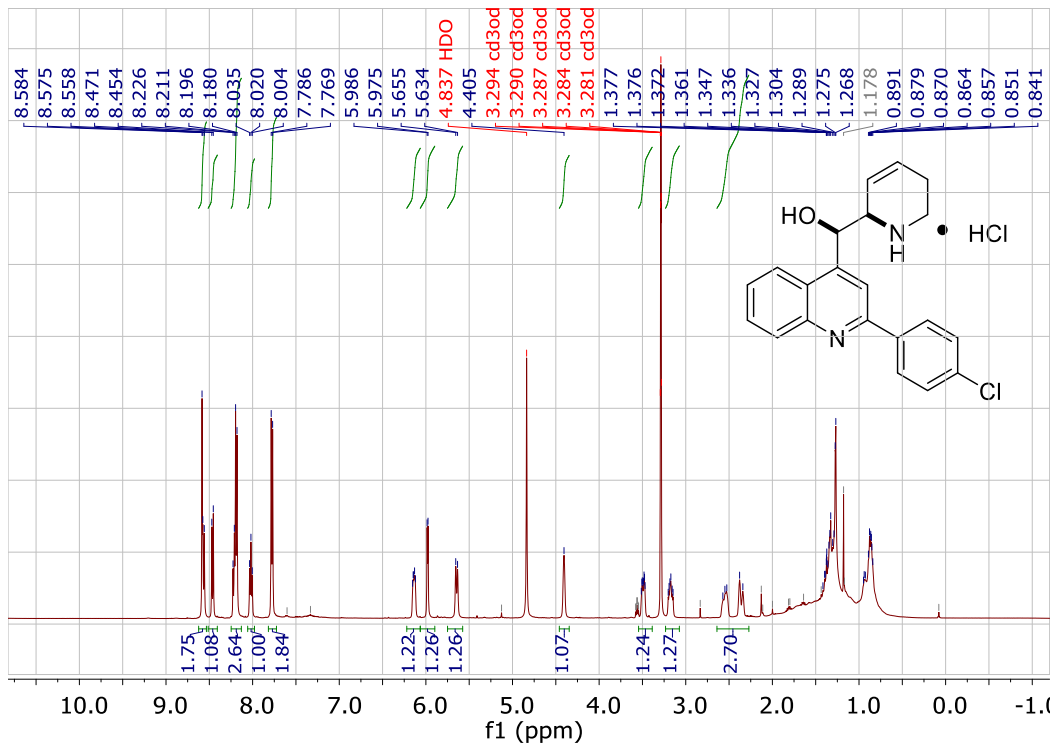
3H-oxazolo[3,4-a]pyridin-3-one, 1-[2-(4-nitrilephenyl)-4-quinoliny]-1,5,6,8a-tetrahydro-



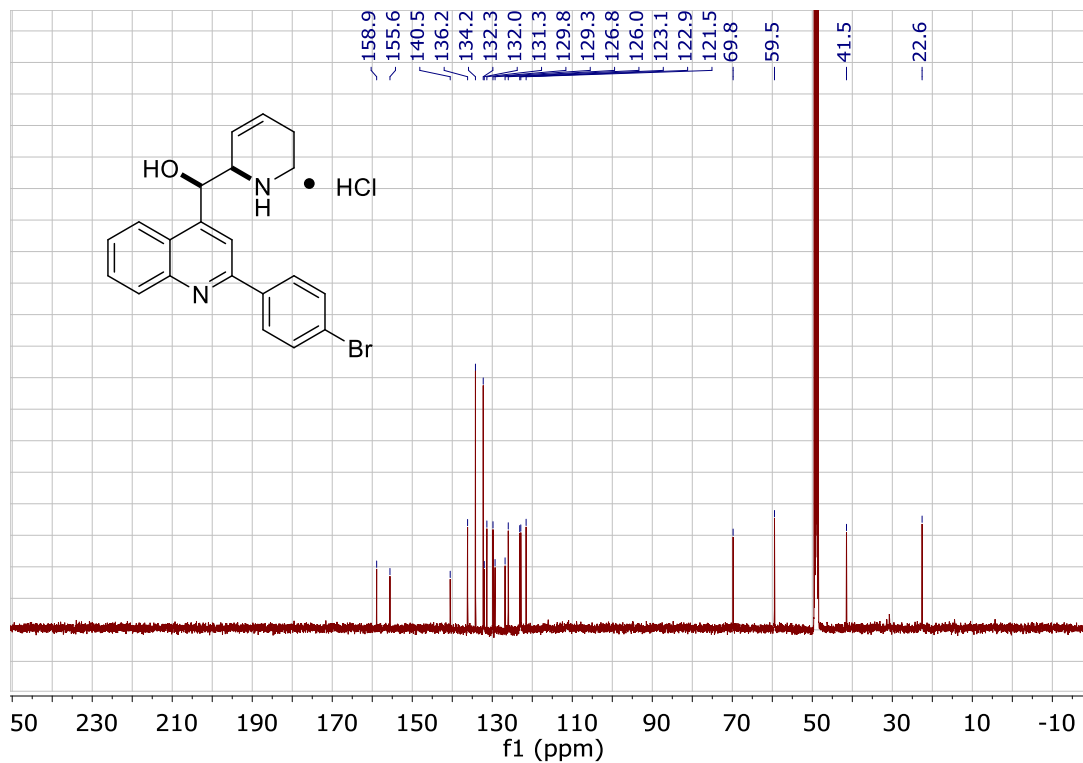
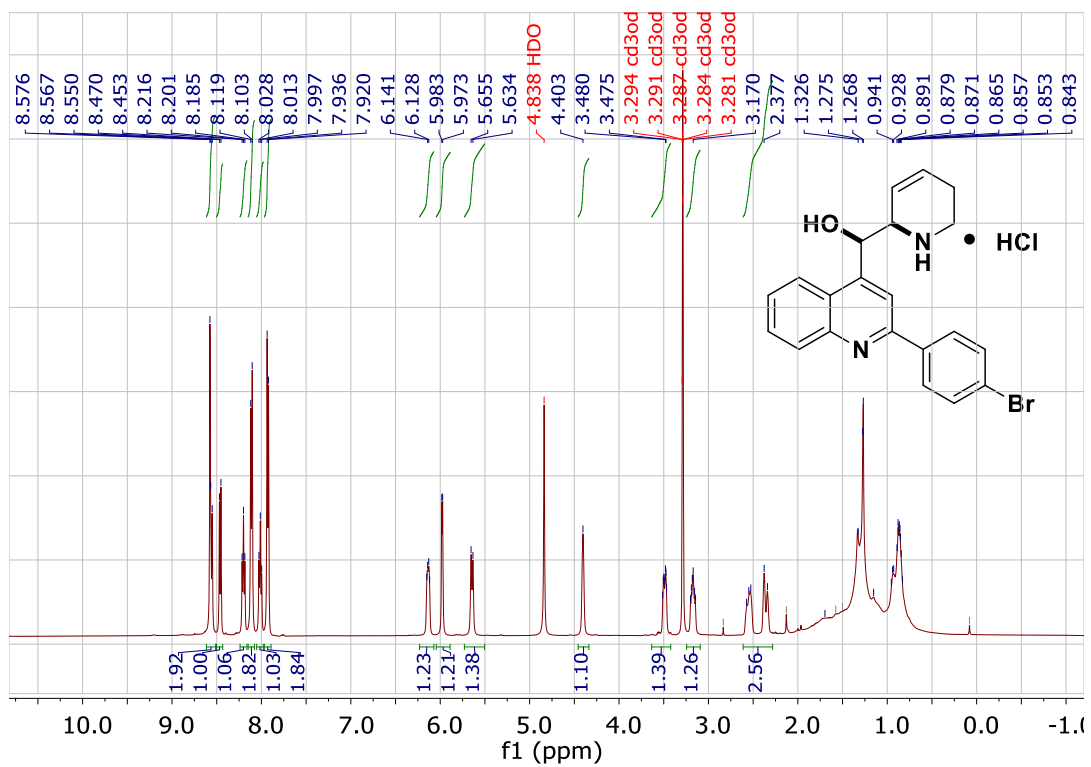
3H-oxazolo[3,4-a]pyridin-3-one, 1-[2-(4-cyclopropylphenyl)-4-quinolinyl]-1,5,6,8a-tetrahydro-



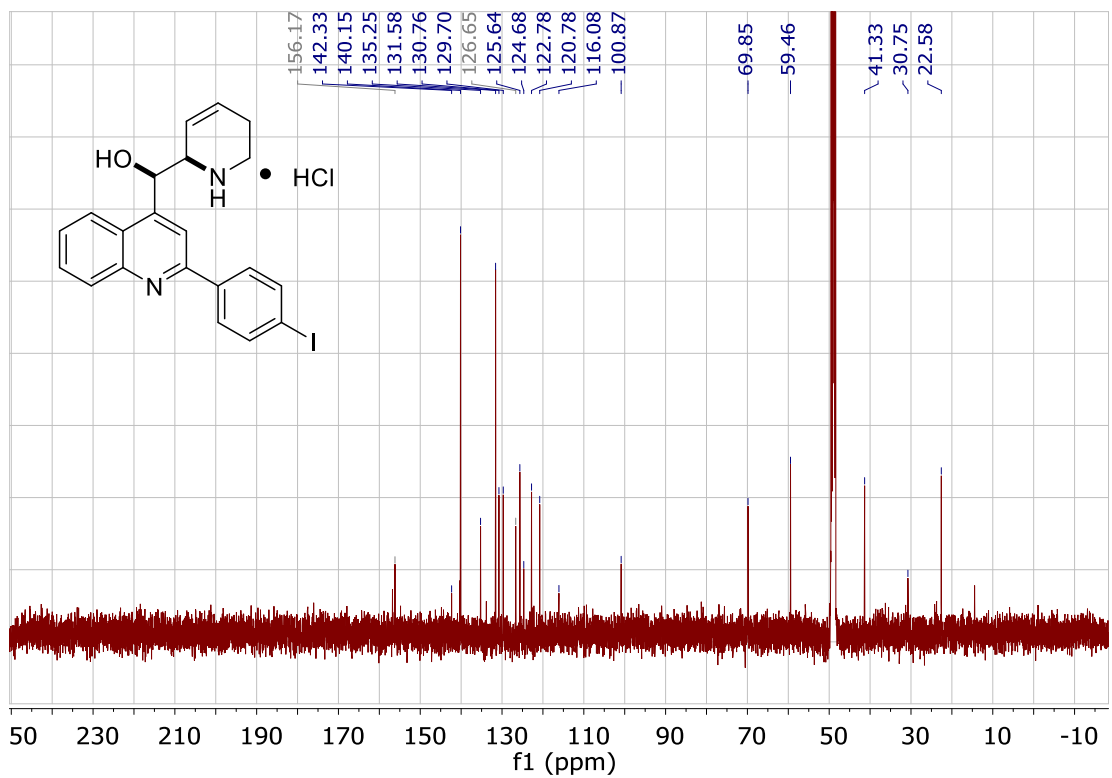
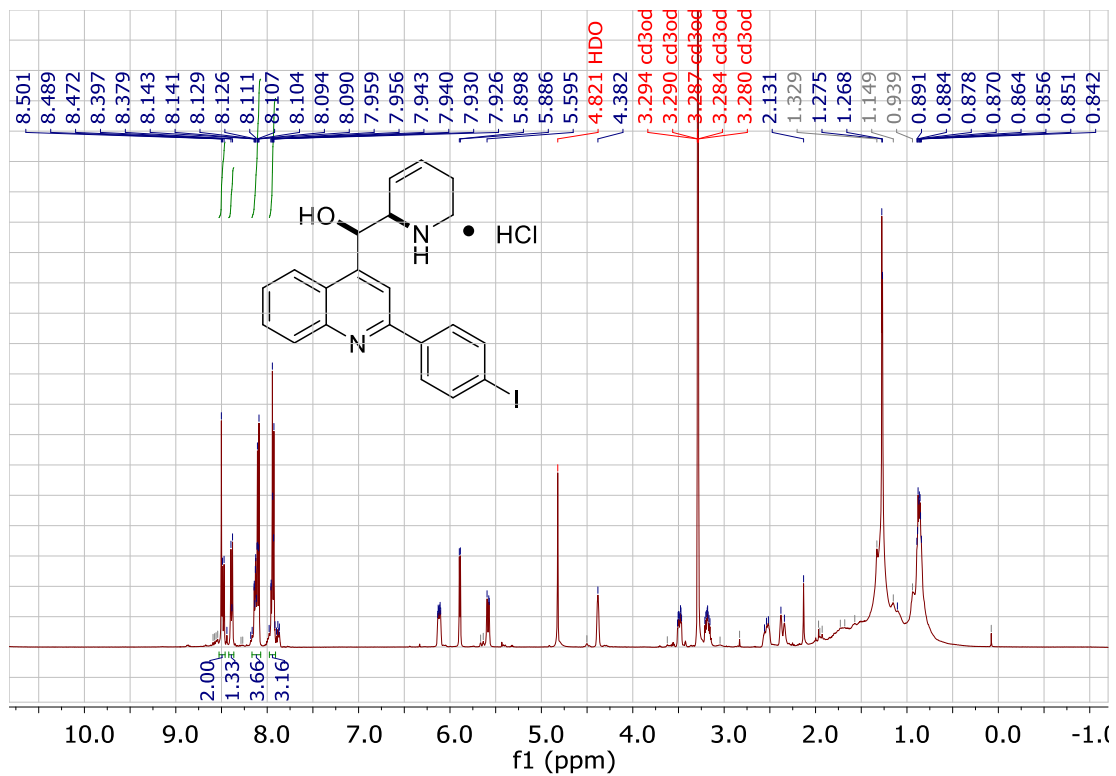
2-(4-chlorophenyl)-2-5,6-dihydropyridinyl-4-quinolinemethanol, hydrochloride



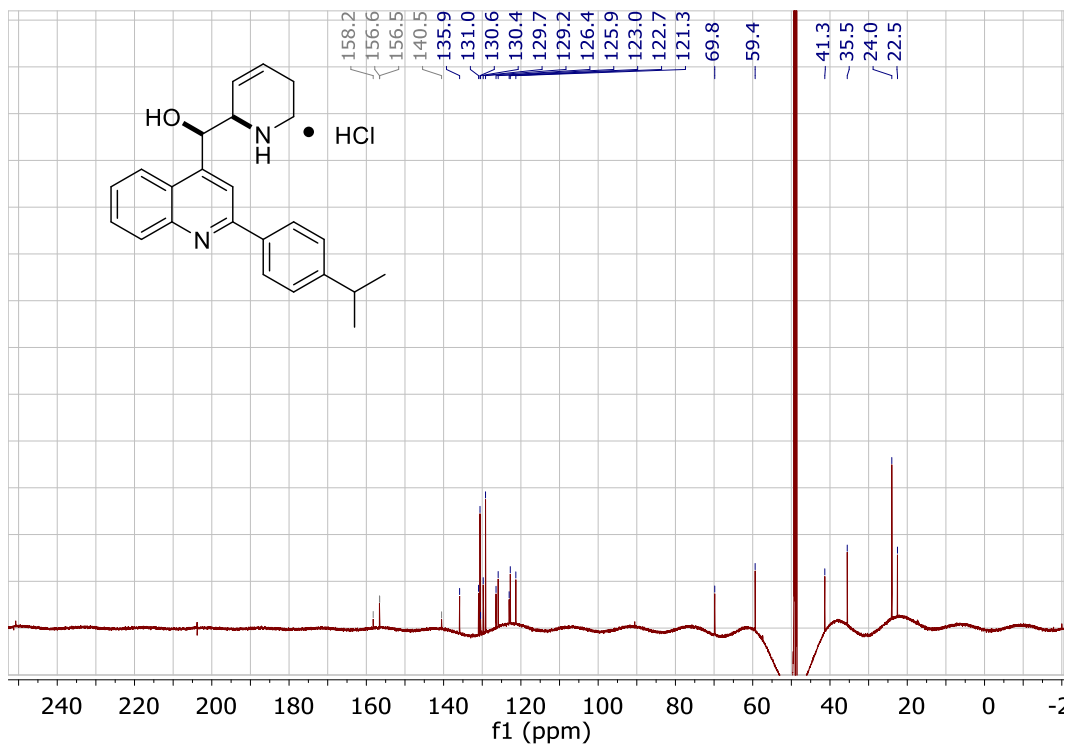
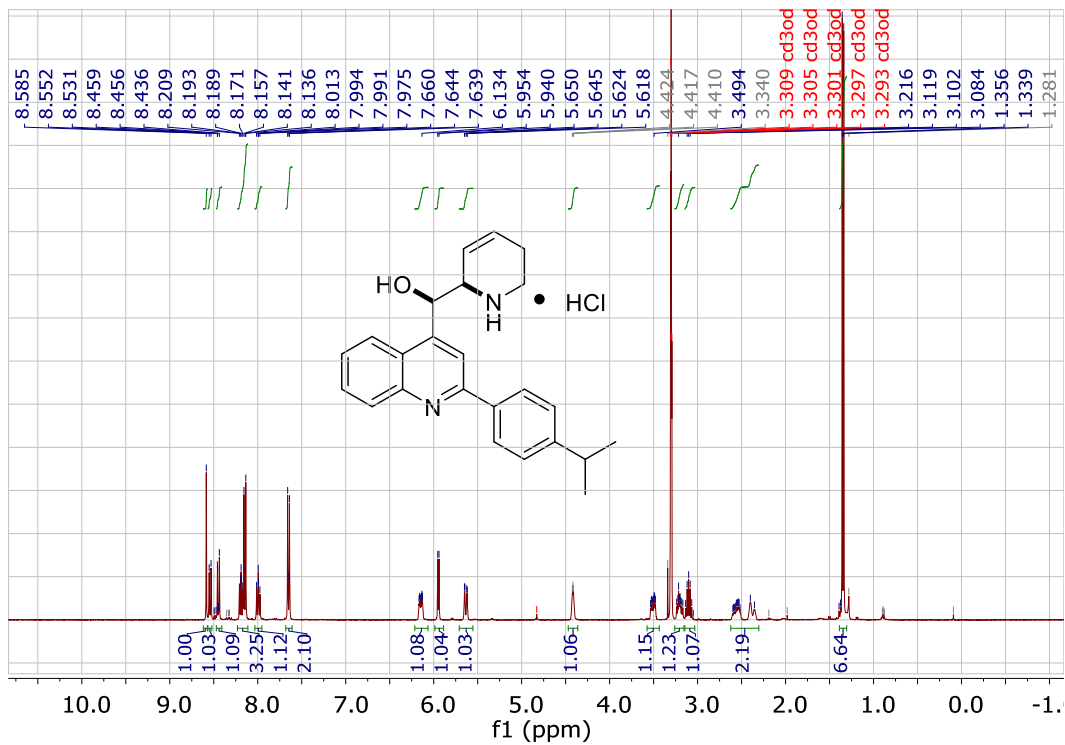
2-(4-bromophenyl)-2-5,6-dihydropyridinyl-4-quinolinemethanol, hydrochloride



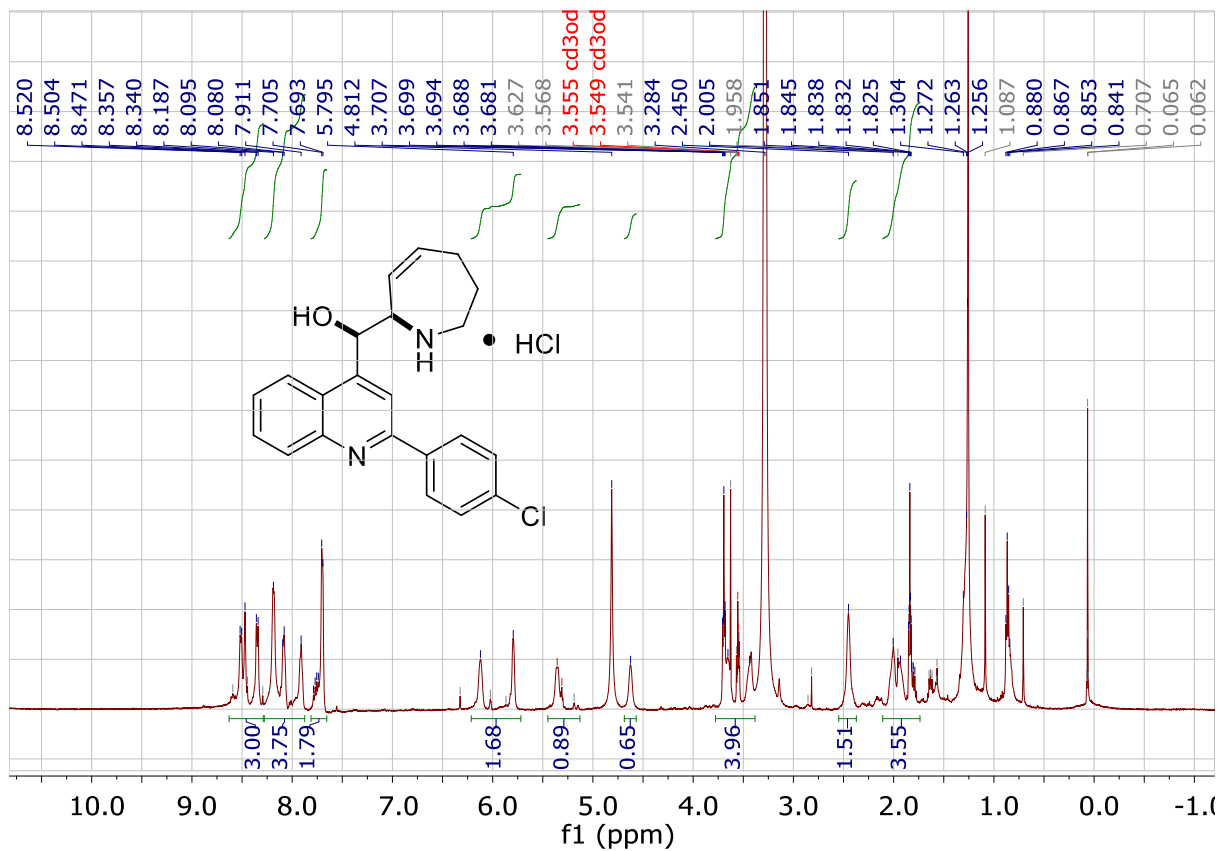
2-(4-iodophenyl)-2-5,6-dihydropyridinyl-4-quinolinemethanol, hydrochloride



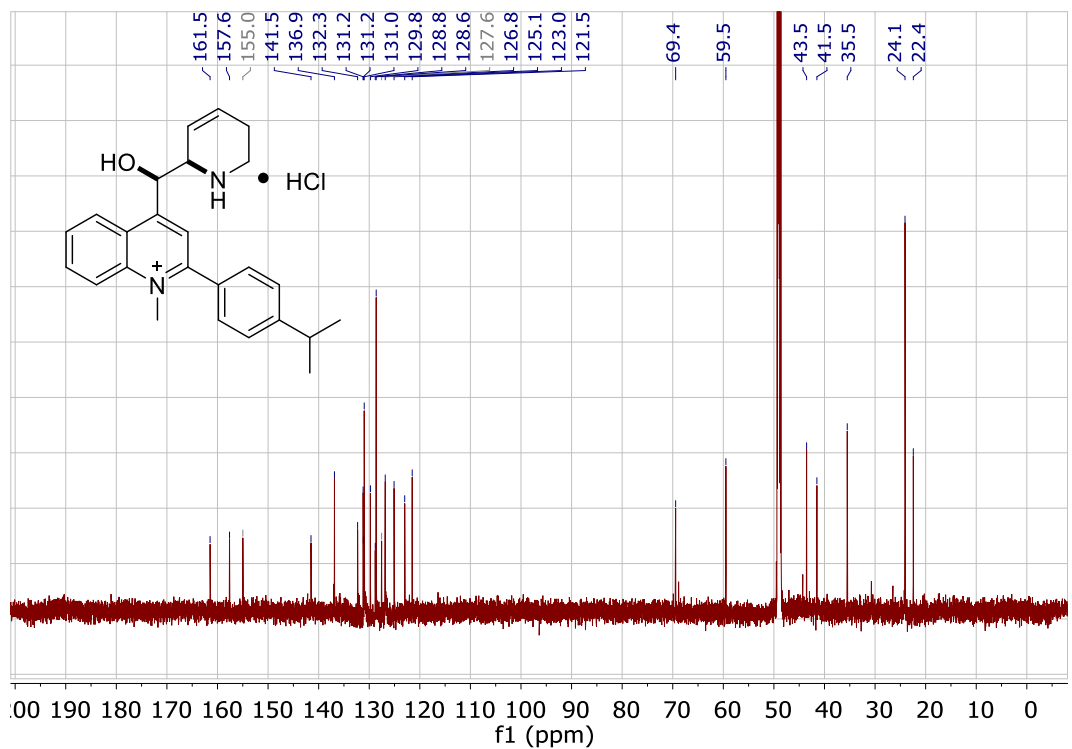
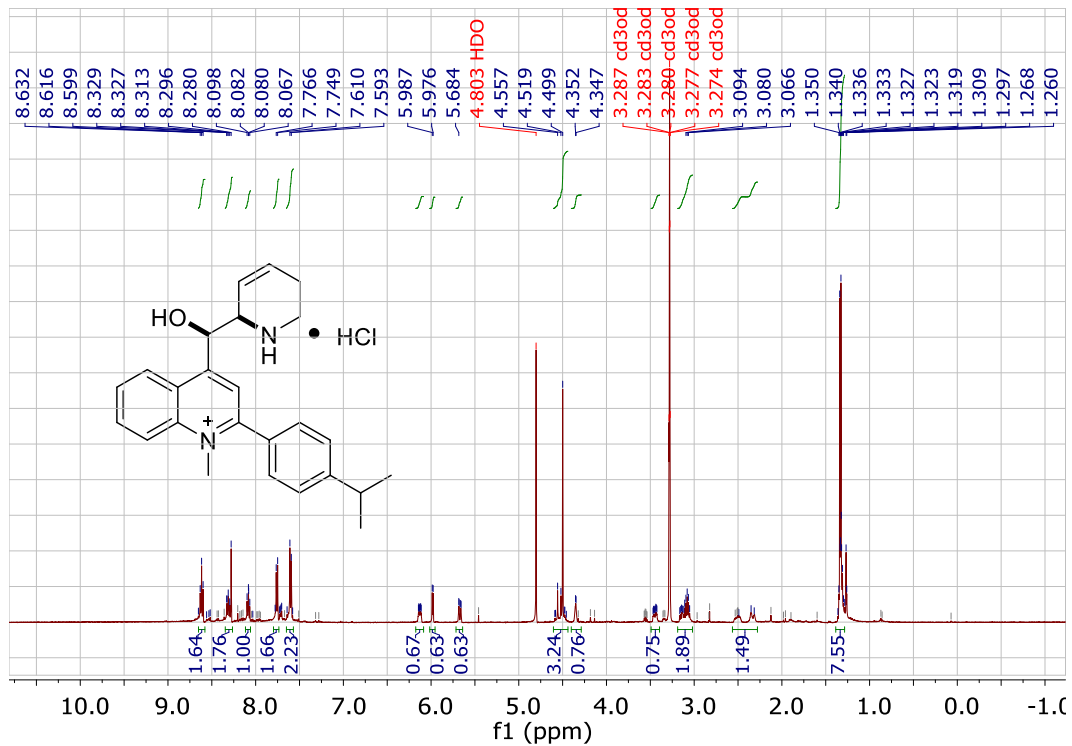
**2-(4-isopropylphenyl)-2-5,6-dihydropyridinyl-4-quinolinemethanol,
hydrochloride**



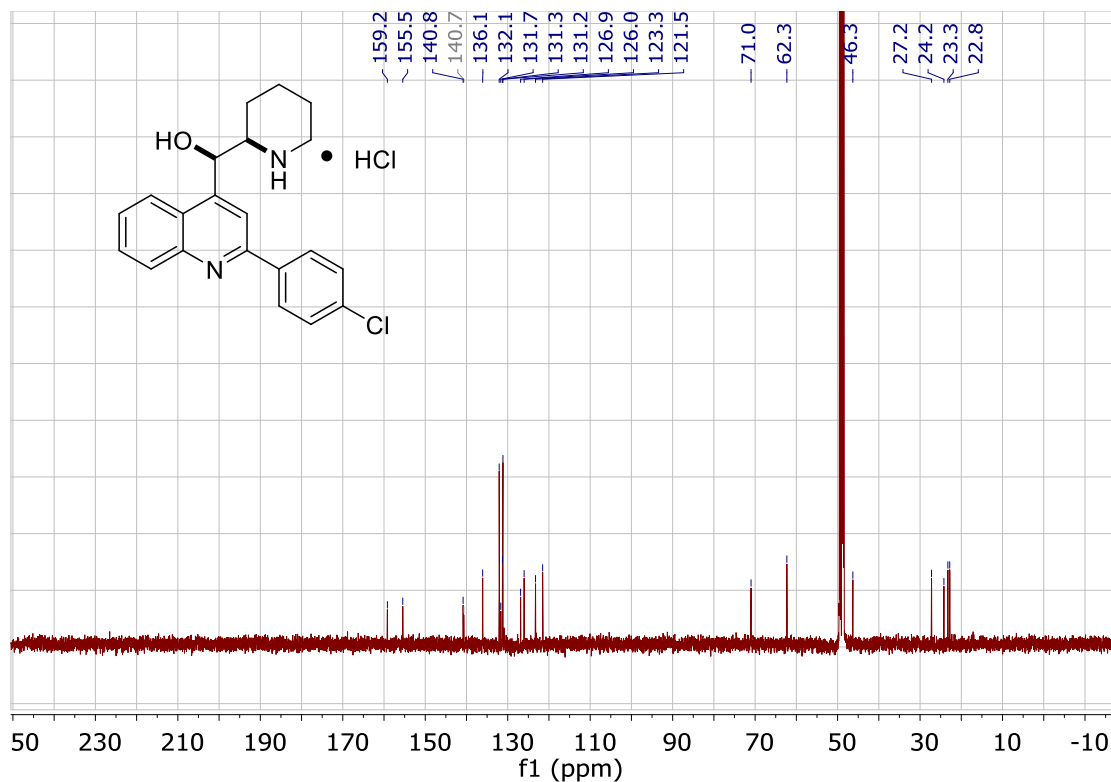
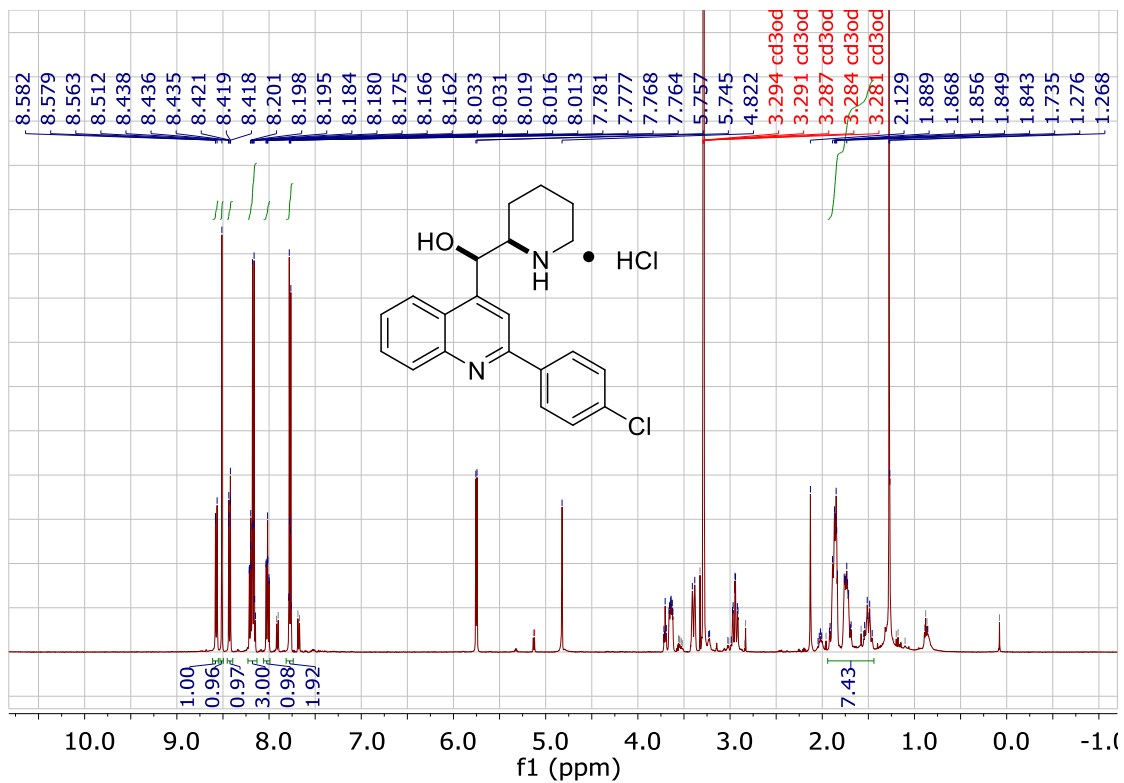
**2-(4-chlorophenyl)-2,3,4,7-tetrahydro-1H-azepine-4-quinolinemethanol,
hydrochloride**



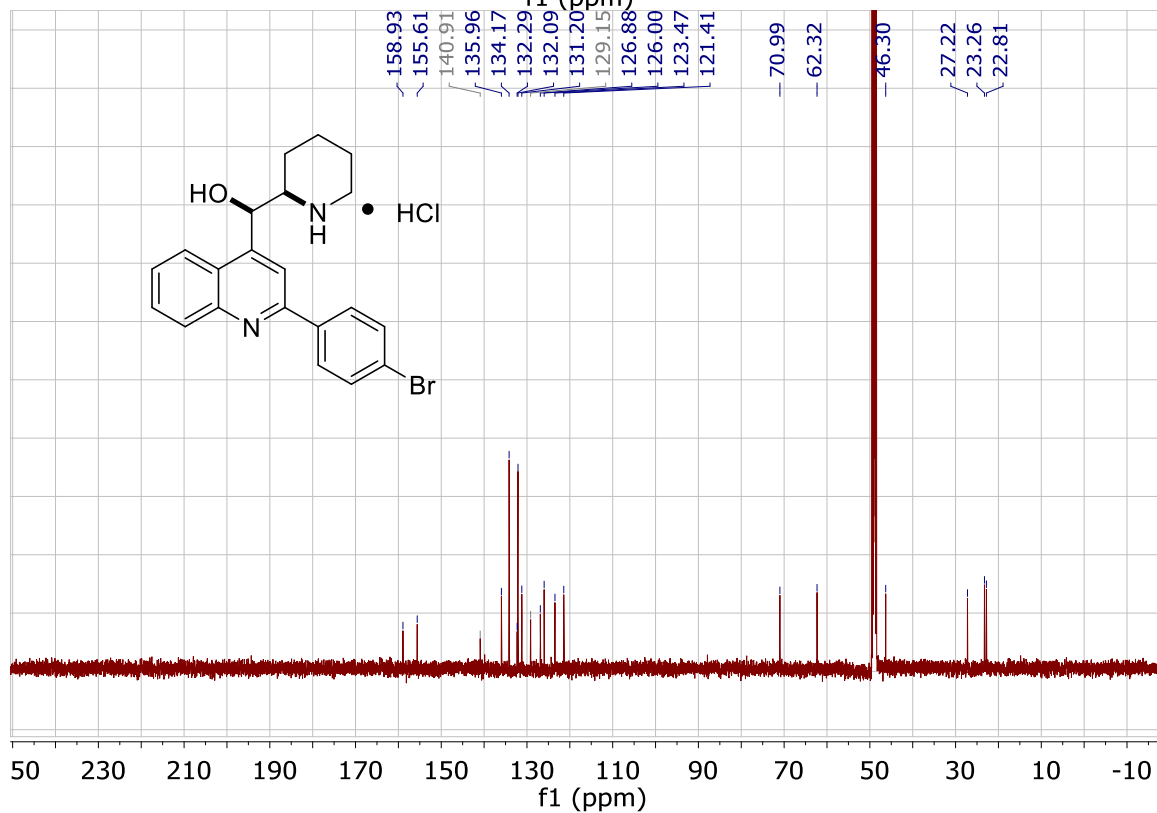
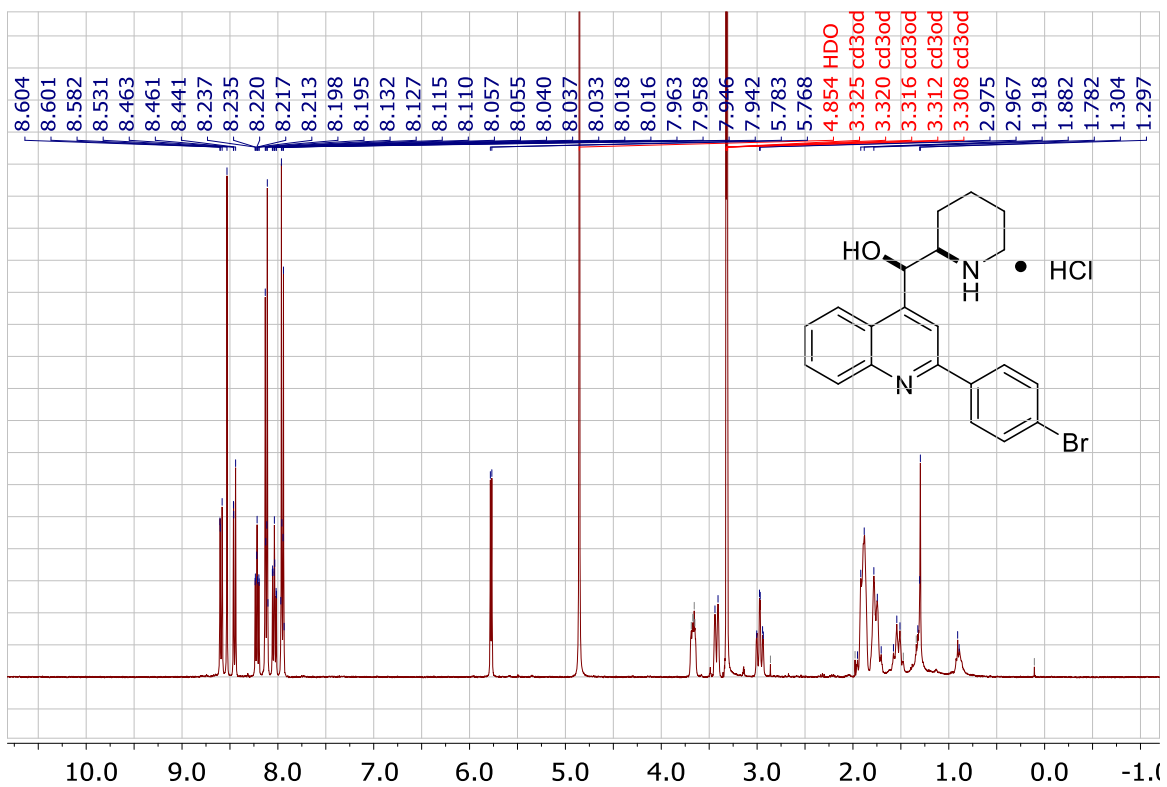
2-(4-isopropylphenyl)-2-5,6-dihydropyridinyl-4-methylquinoliniummethanol, hydrochloride



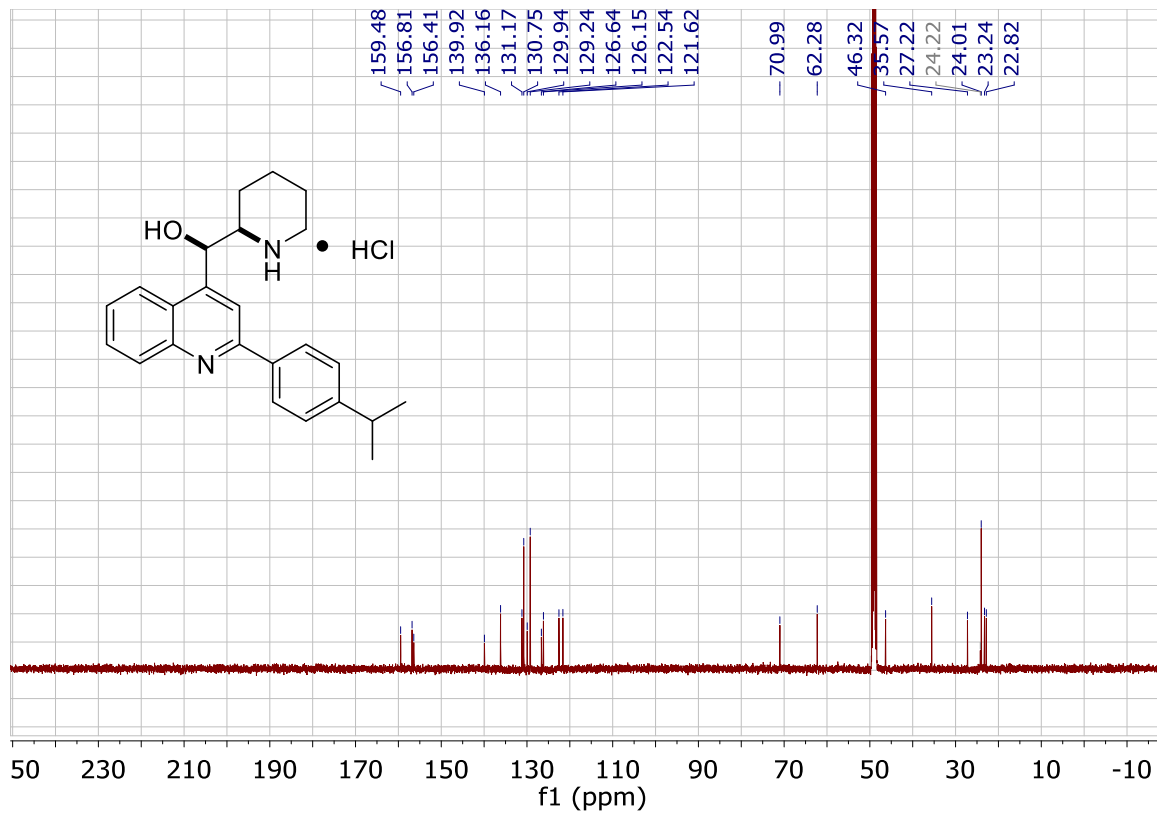
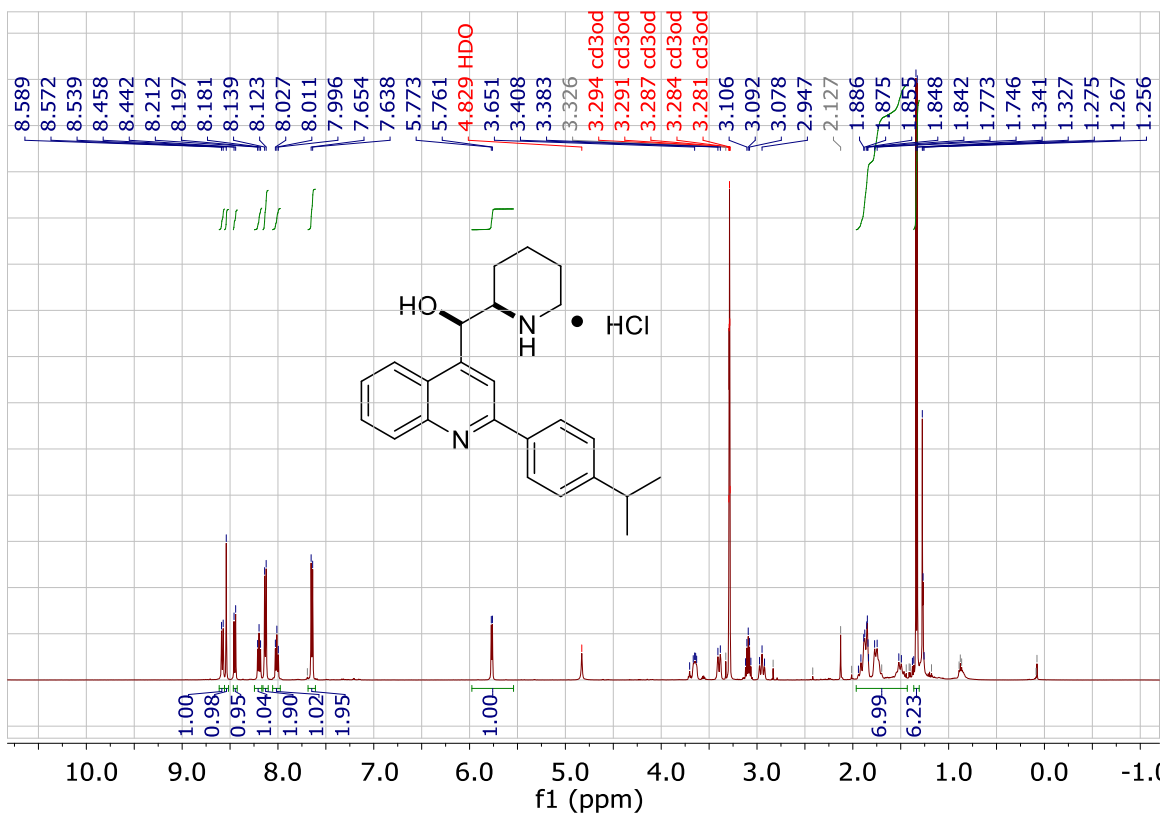
4-quinolinemethanol, 2-(4-chlorophenyl)- α -2-piperidiny-, hydrochloride



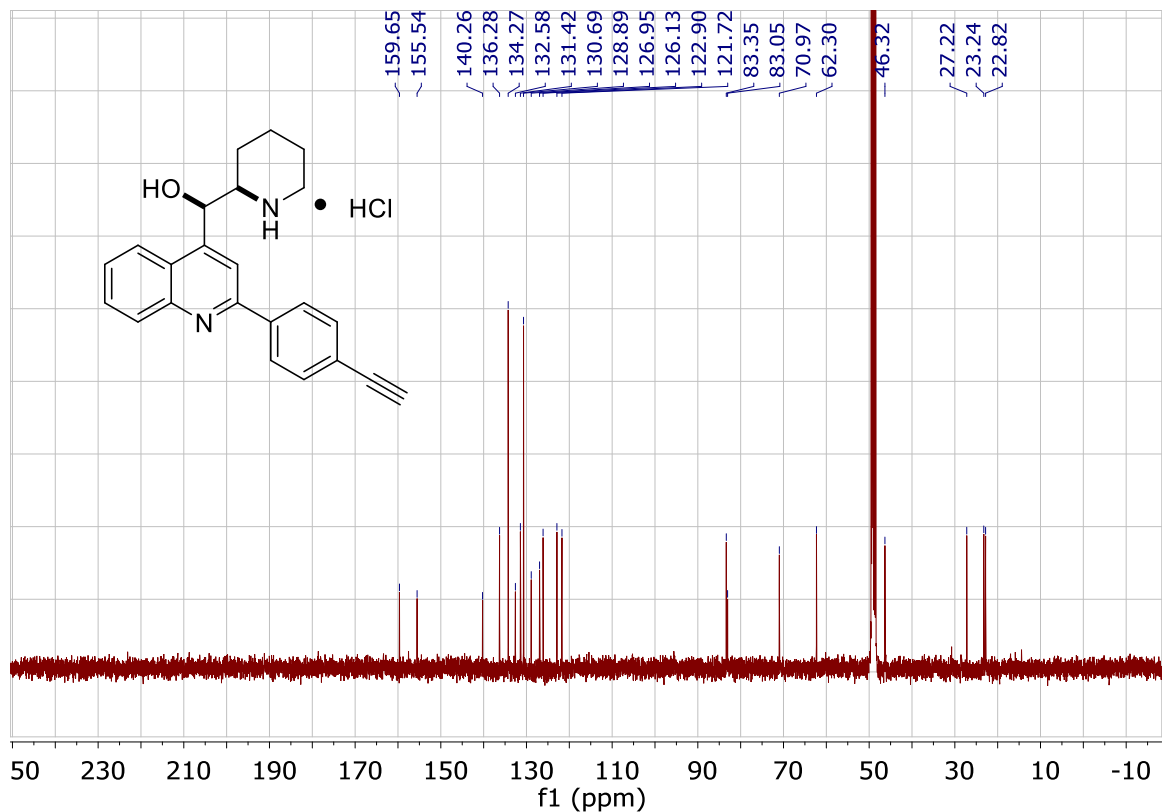
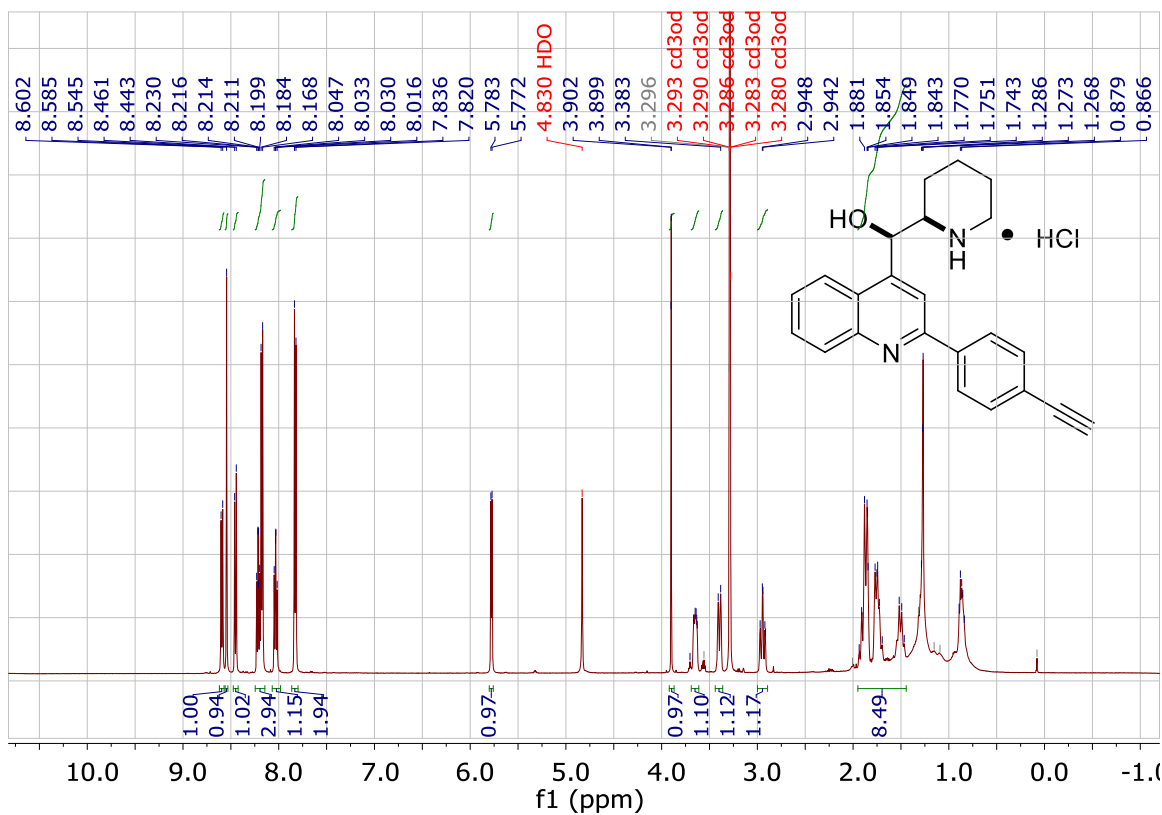
4-quinolinemethanol, 2-(4-bromophenyl)- α -2-piperidinyl-, hydrochloride



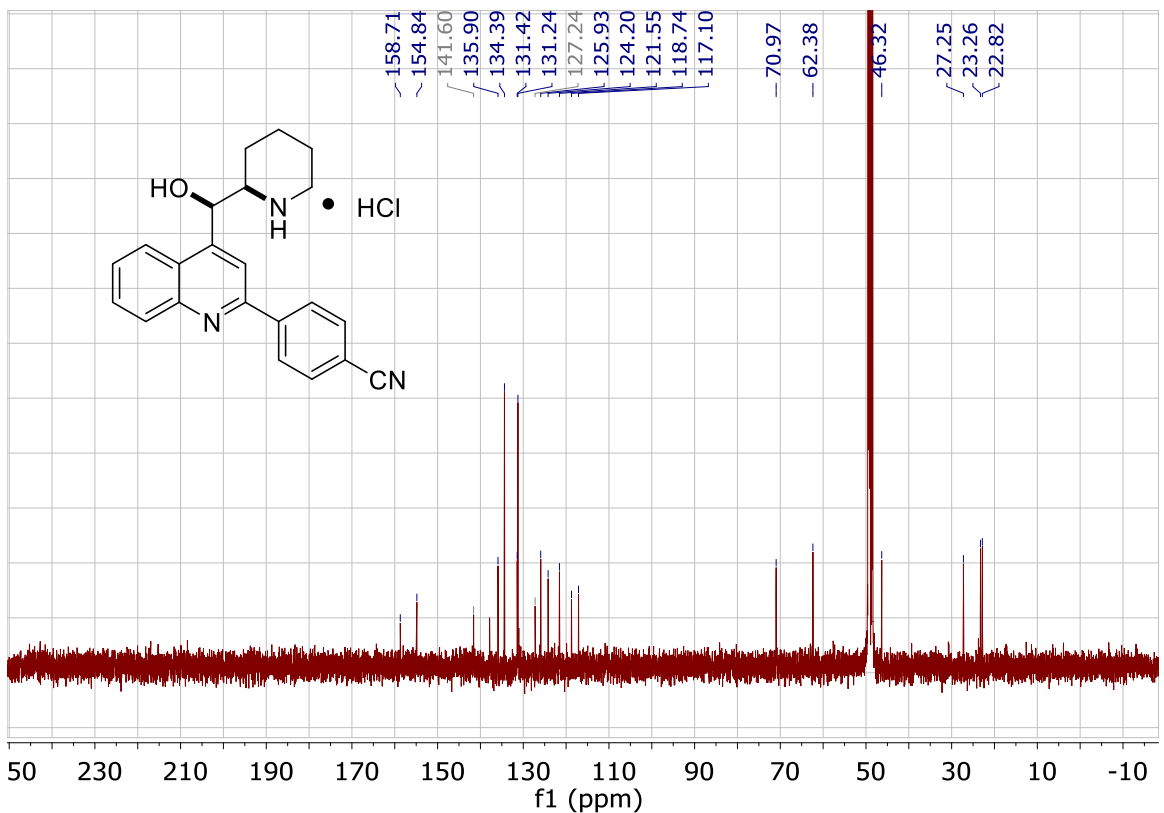
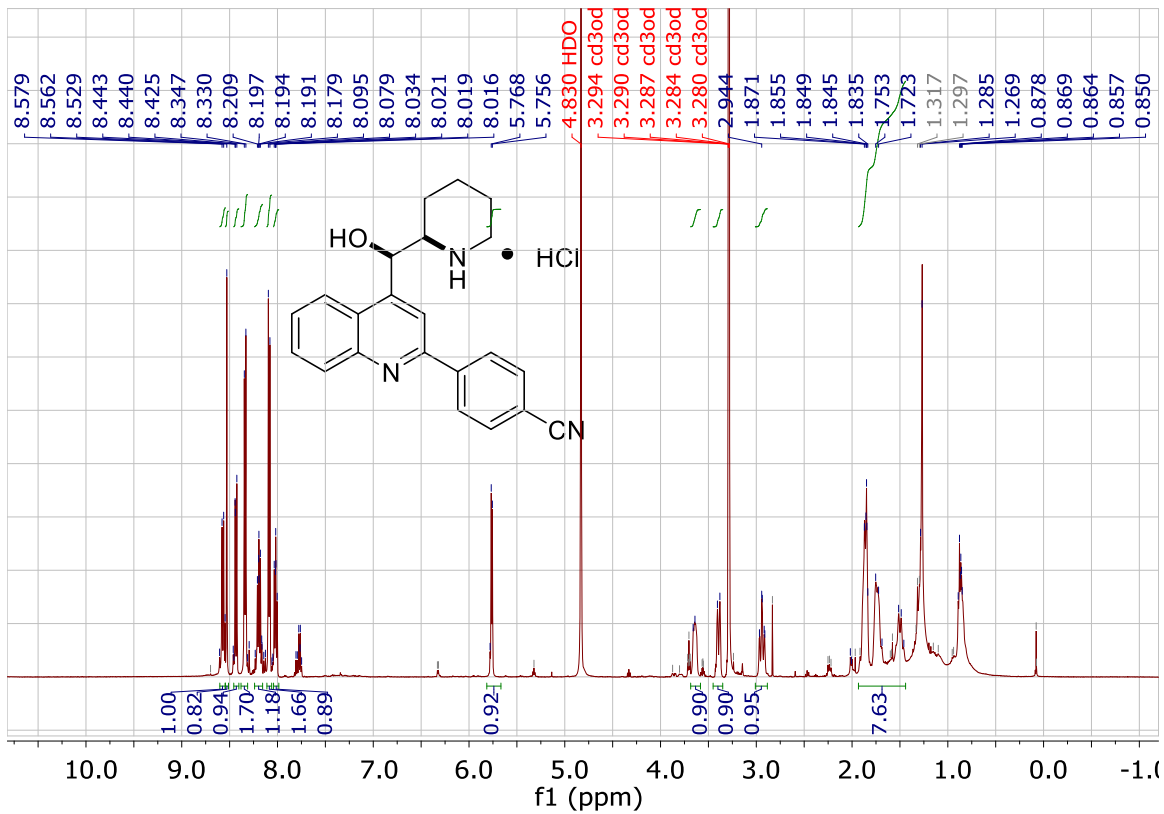
4-quinolinemethanol, 2-(4-isopropylphenyl)- α -2-piperidinyl-, hydrochloride



4-quinolinemethanol, 2-(4-ethynylphenyl)- α -2-piperidiny-, hydrochloride

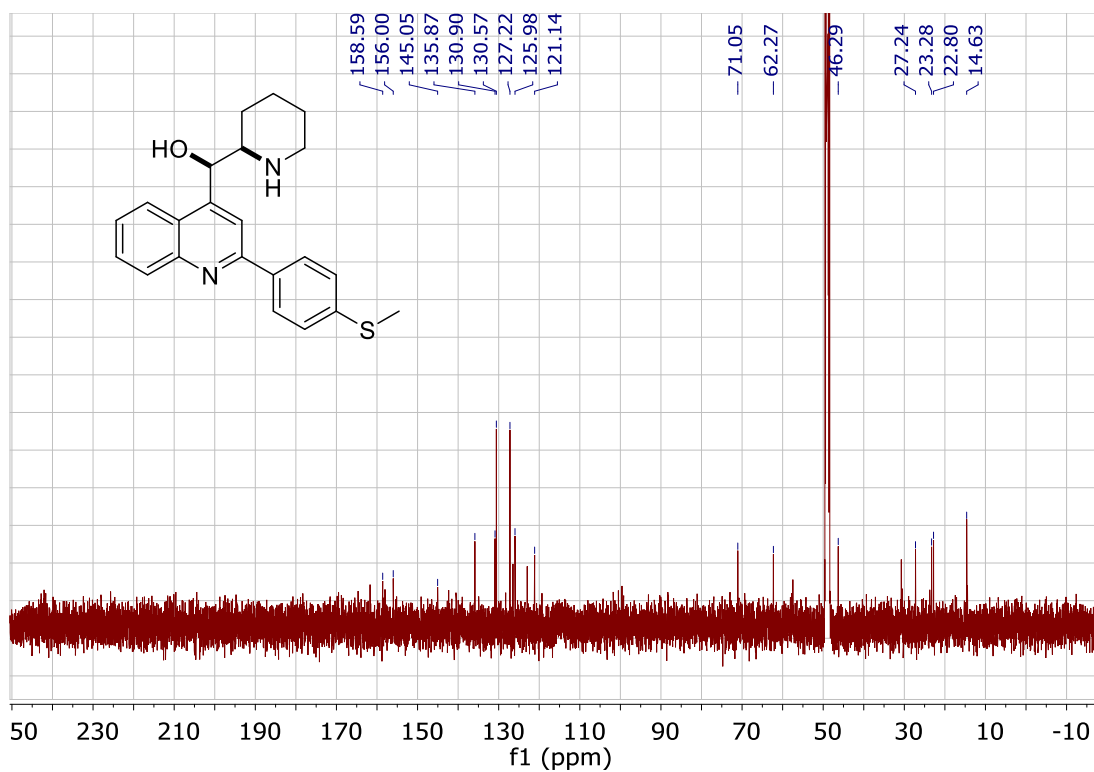
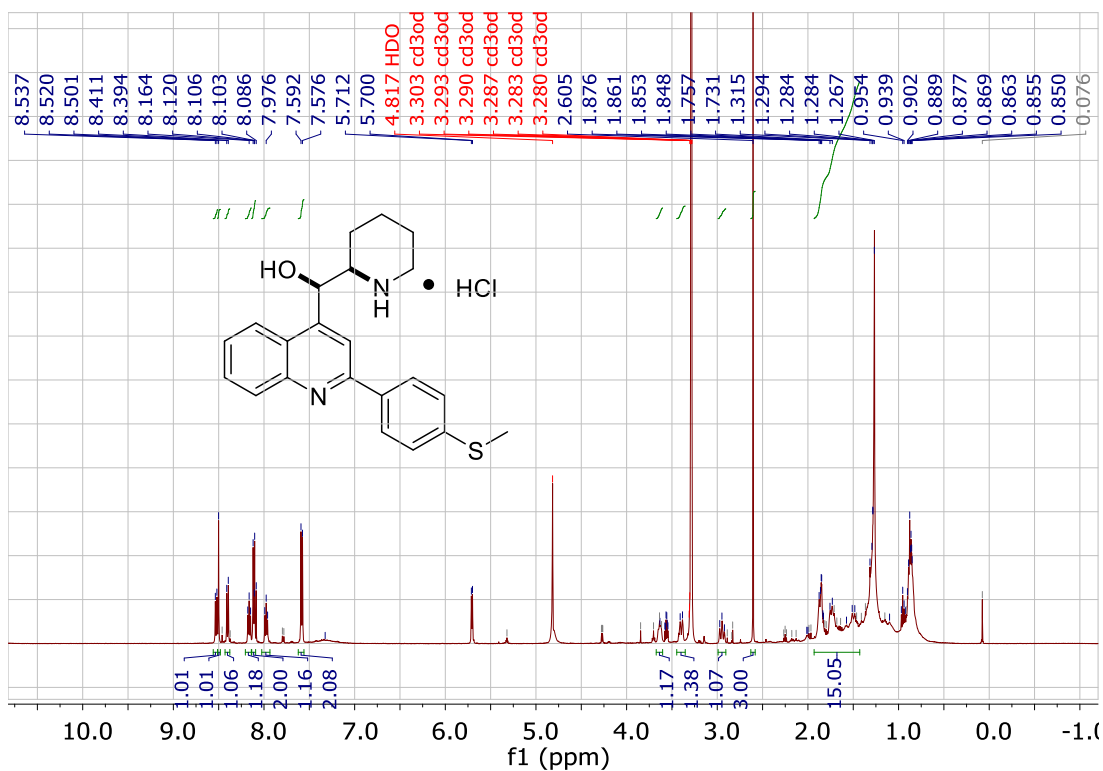


4-quinolinemethanol, 2-(4-nitrilephenyl)- α -2-piperidinyl-, hydrochloride



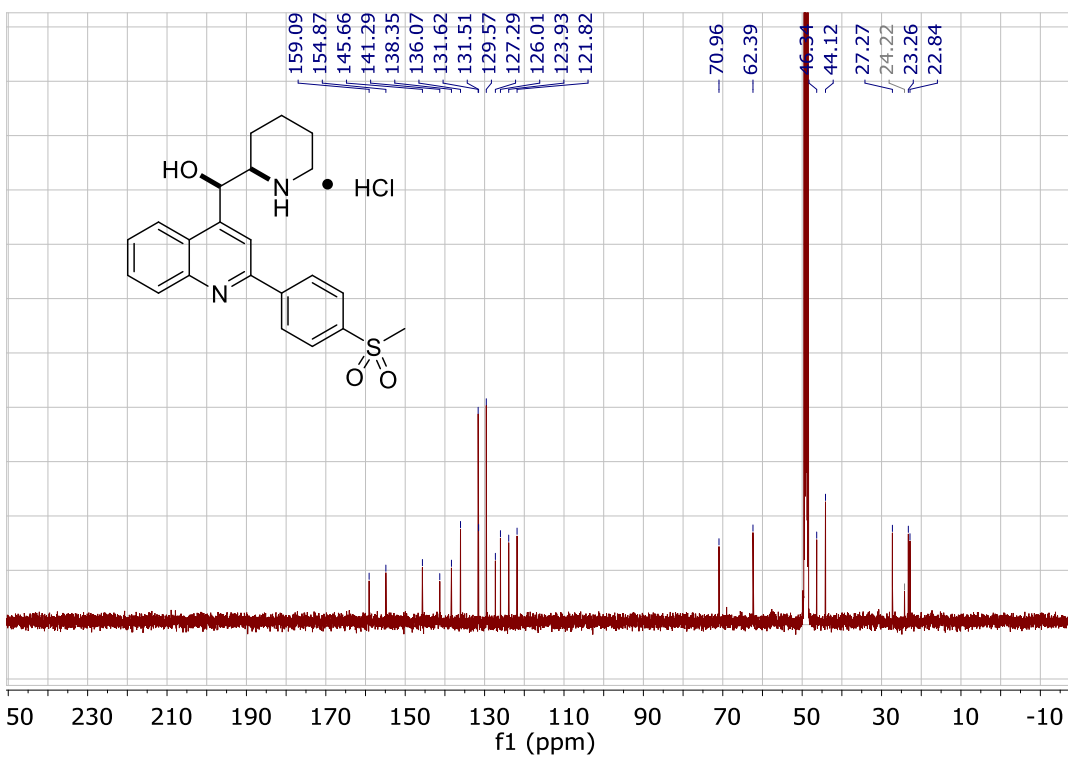
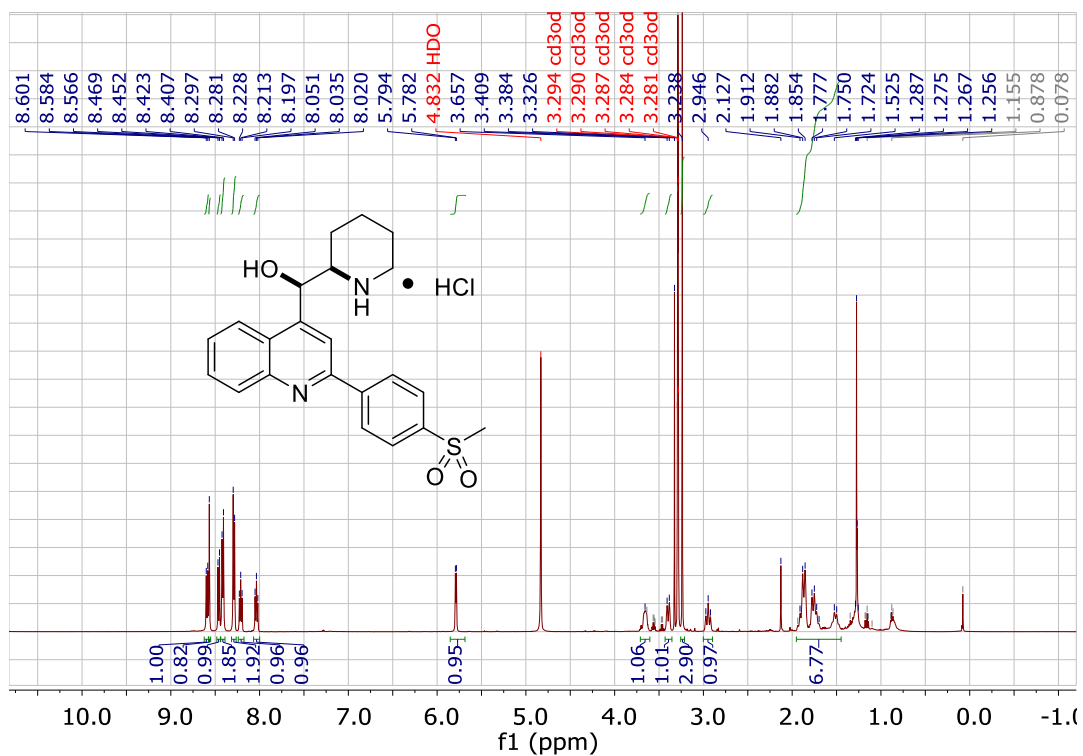
4-quinolinemethanol,
hydrochloride

2-(4-methylsulfanyphenyl)- α -2-piperidinyl-,

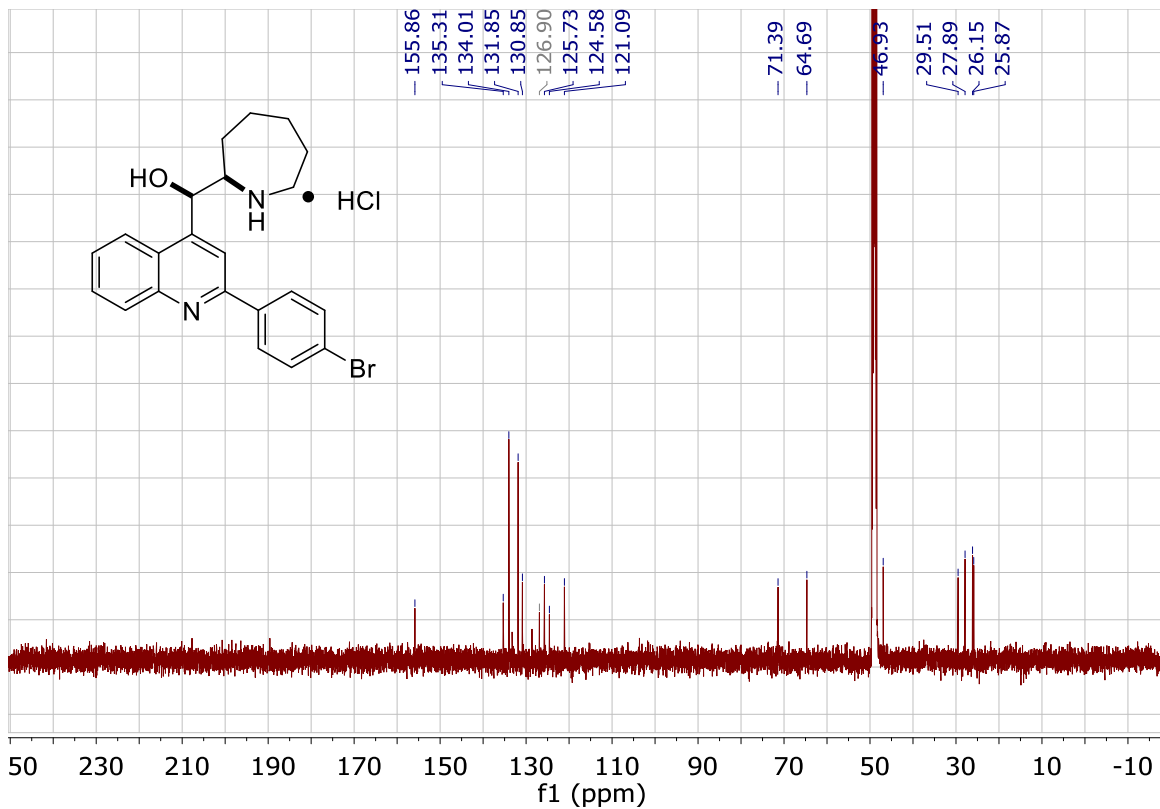
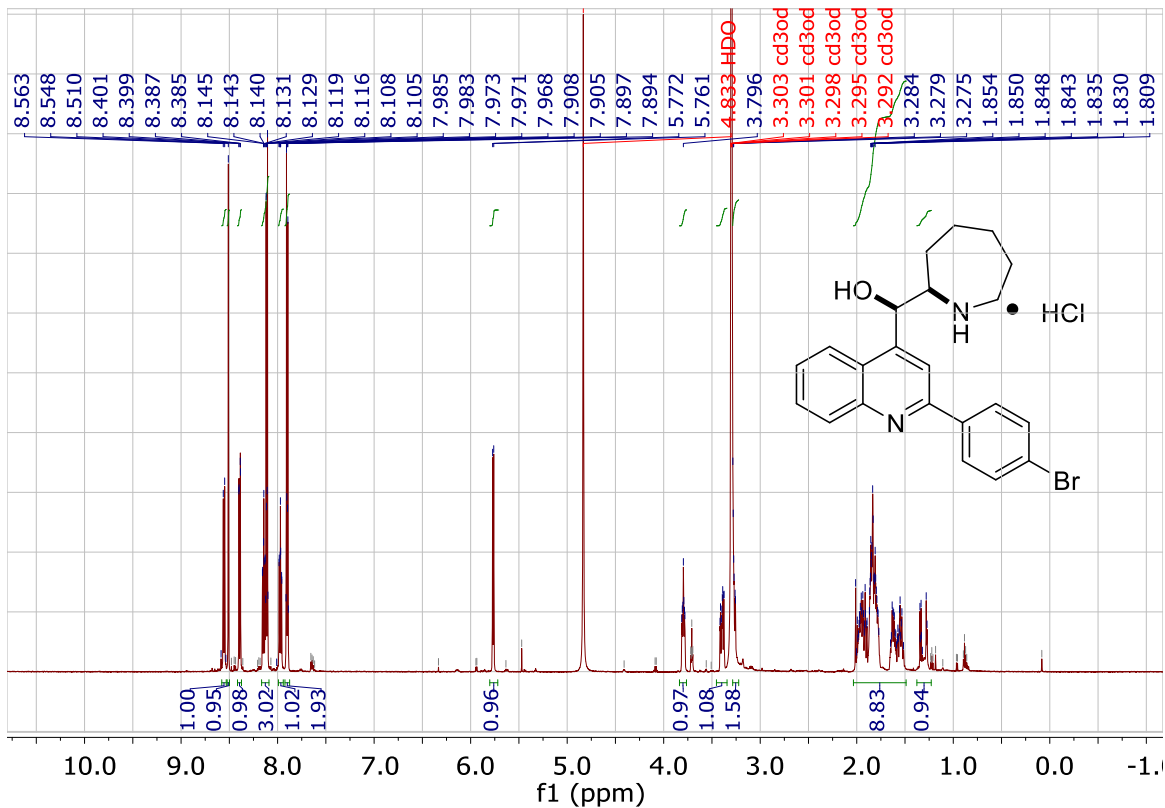


4-quinolinemethanol,
hydrochloride

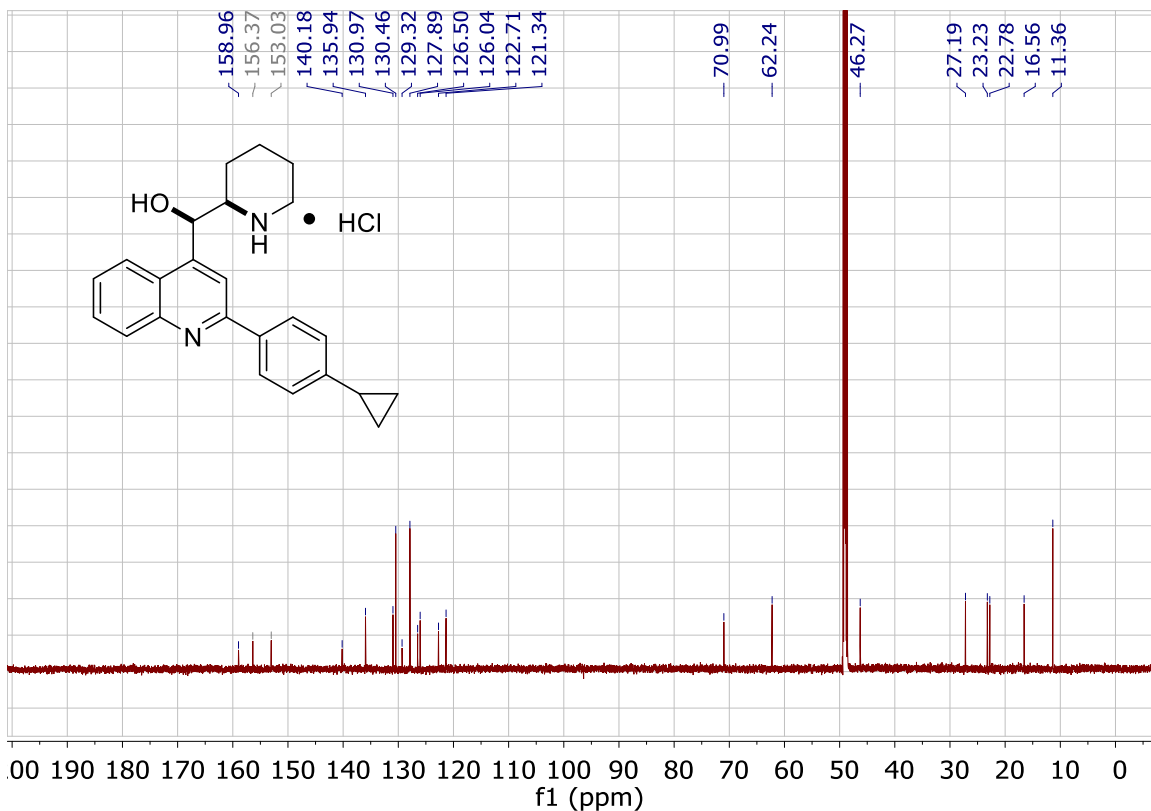
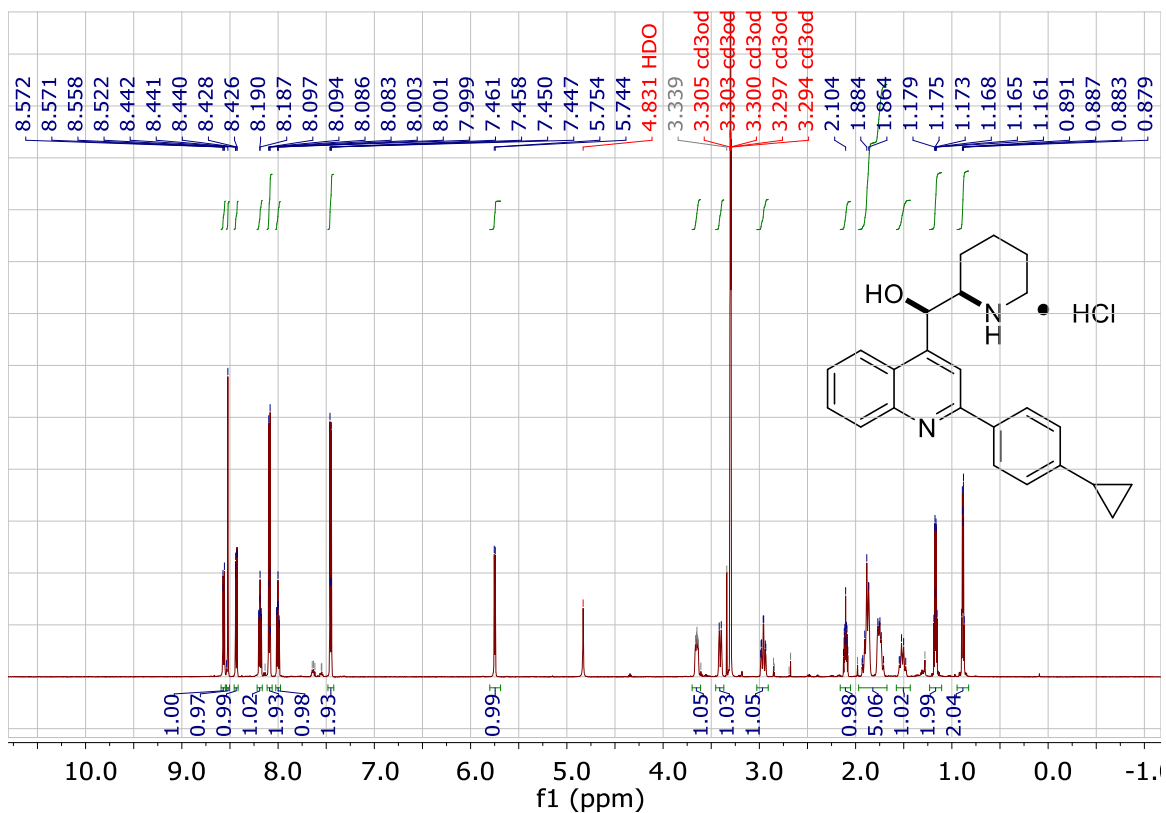
2-(4-methylsulfonylphenyl)- α -2-piperidinyl-,
hydrochloride



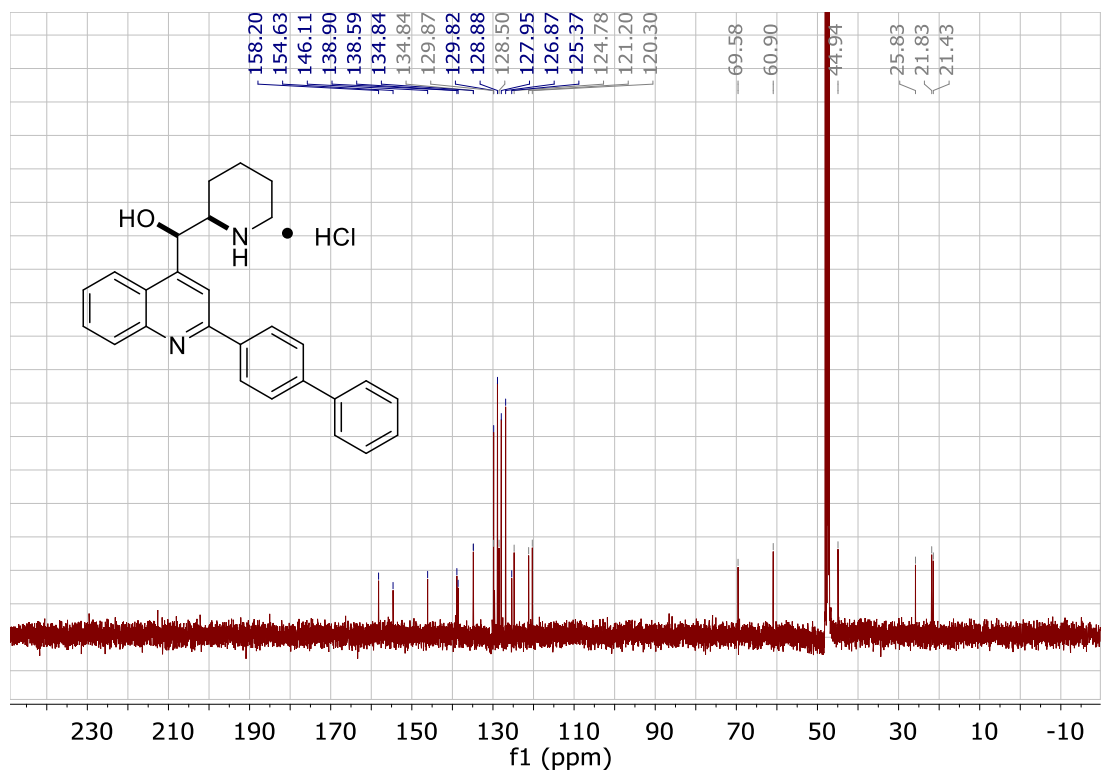
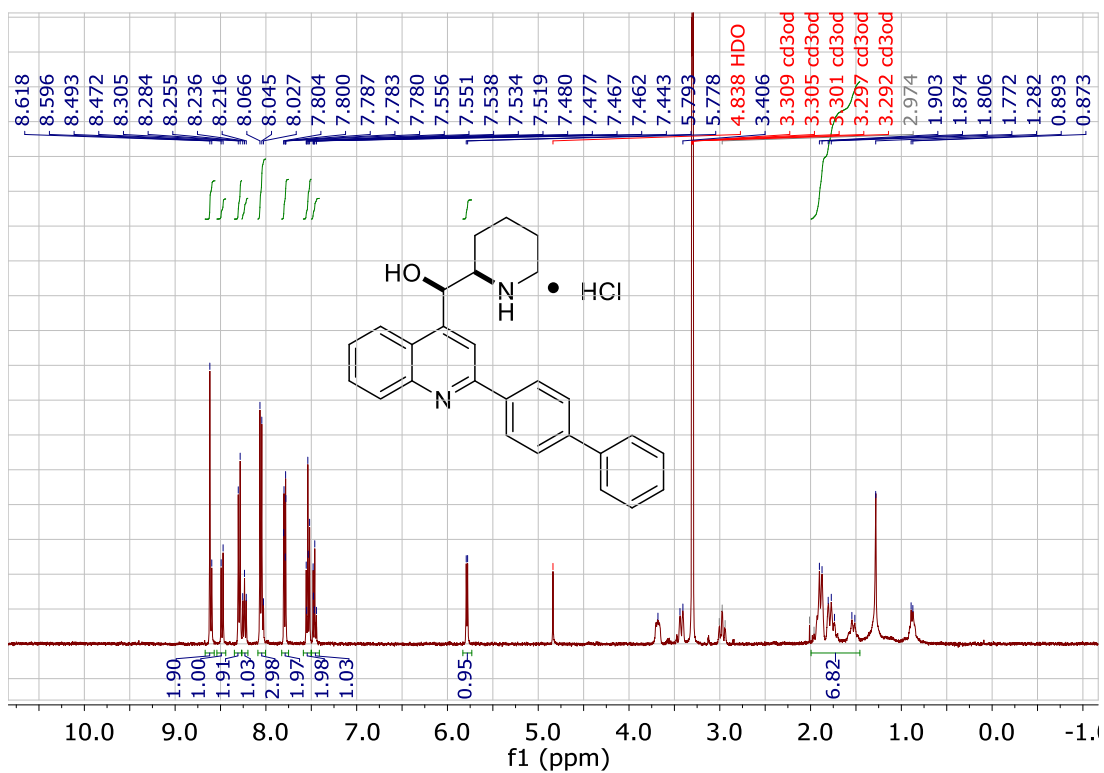
4-quinolinemethanol, 2-(4-bromophenyl)- α -2-azepanyl-, hydrochloride



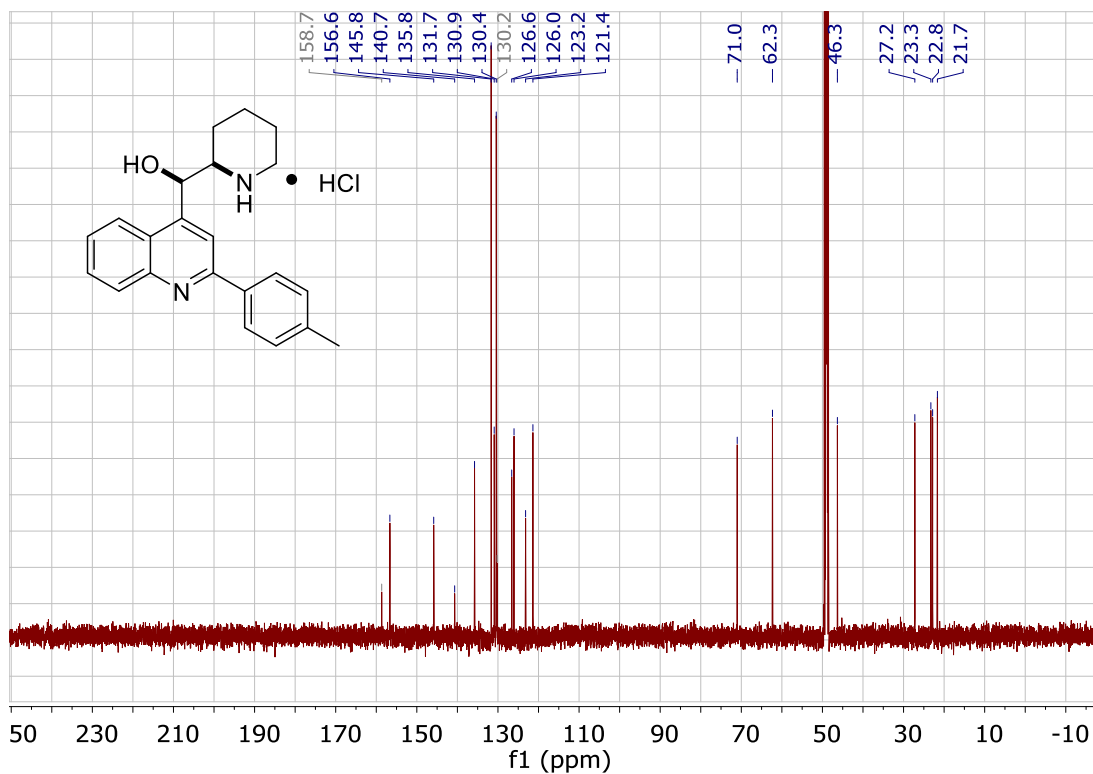
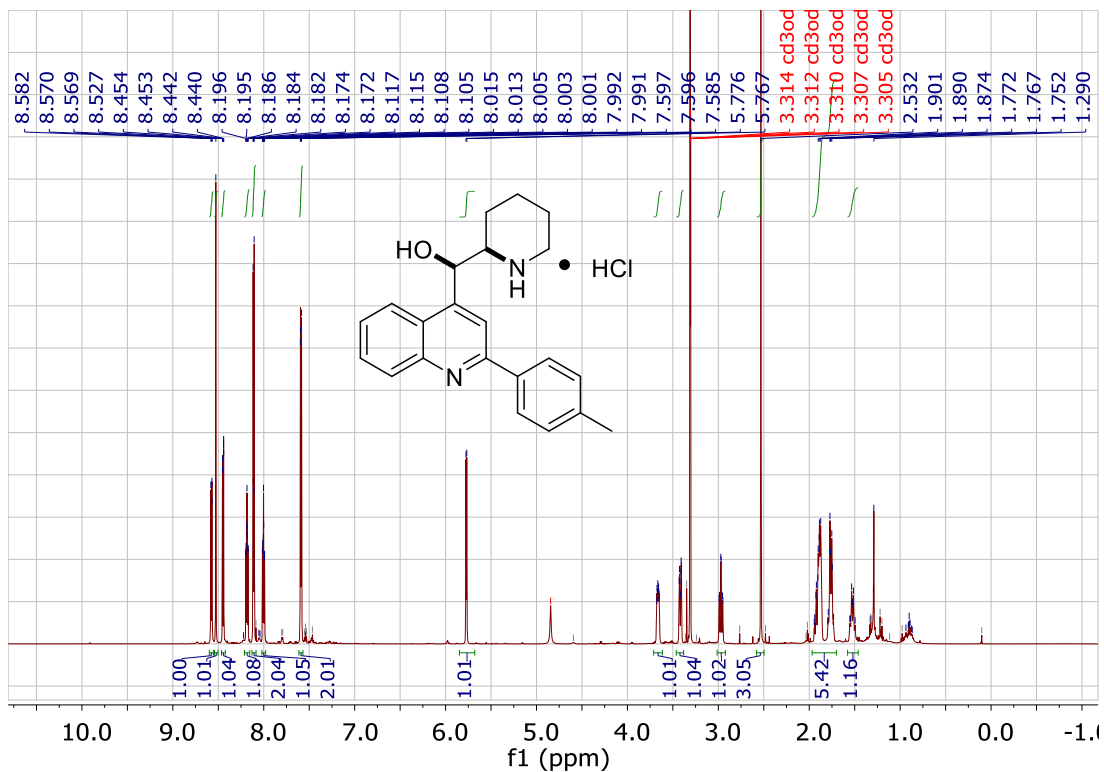
4-quinolinemethanol, 2-(4-cyclopropylphenyl)- α -2-piperidinyl-, hydrochloride



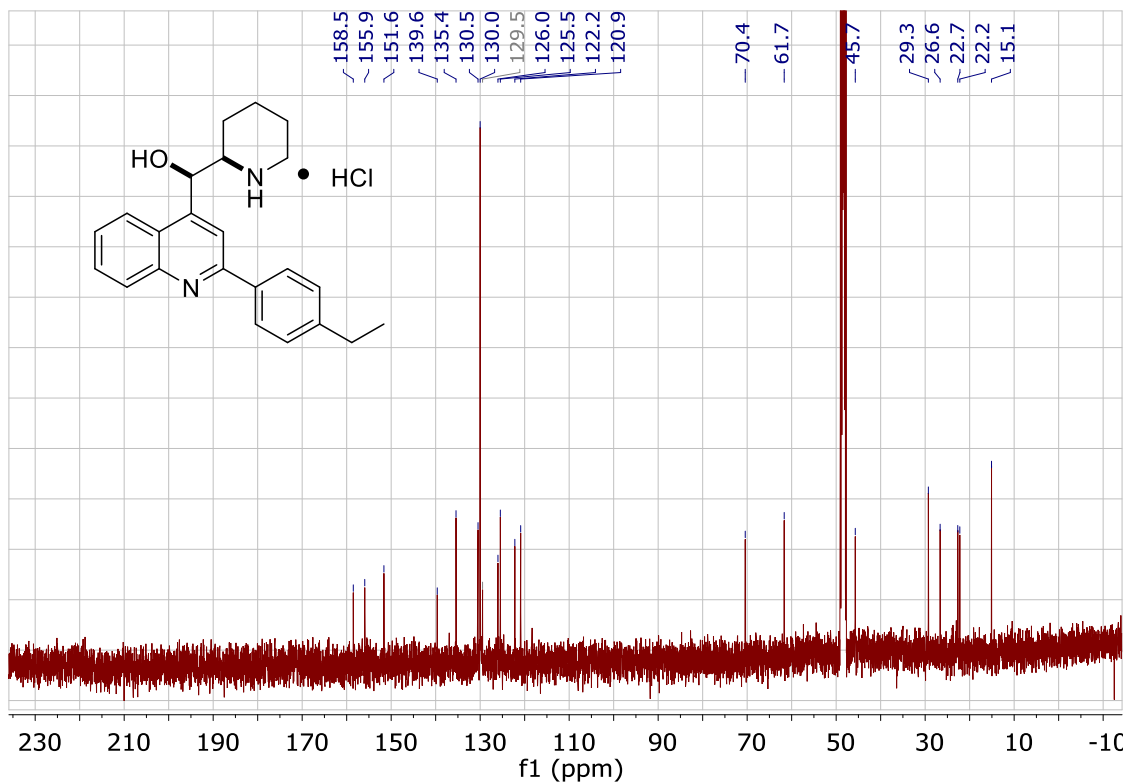
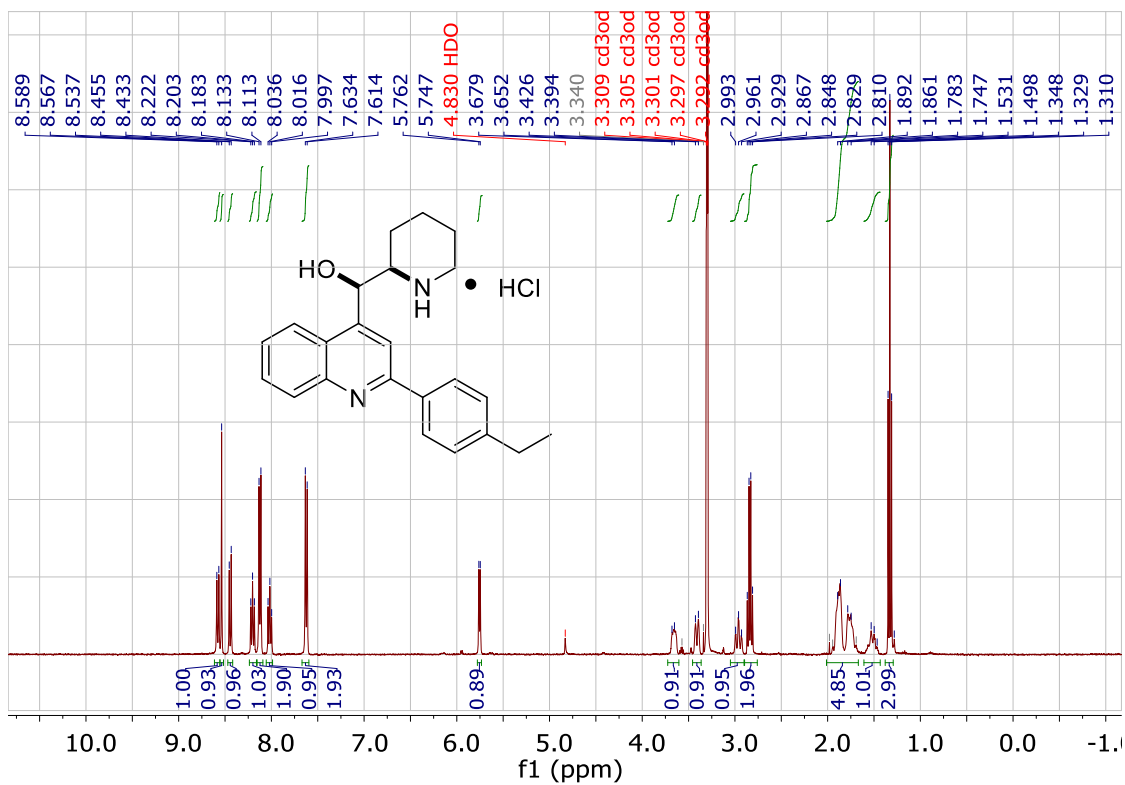
4-quinolinemethanol, 2-(4-biphenyl)- α -2-piperidinyl-, hydrochloride



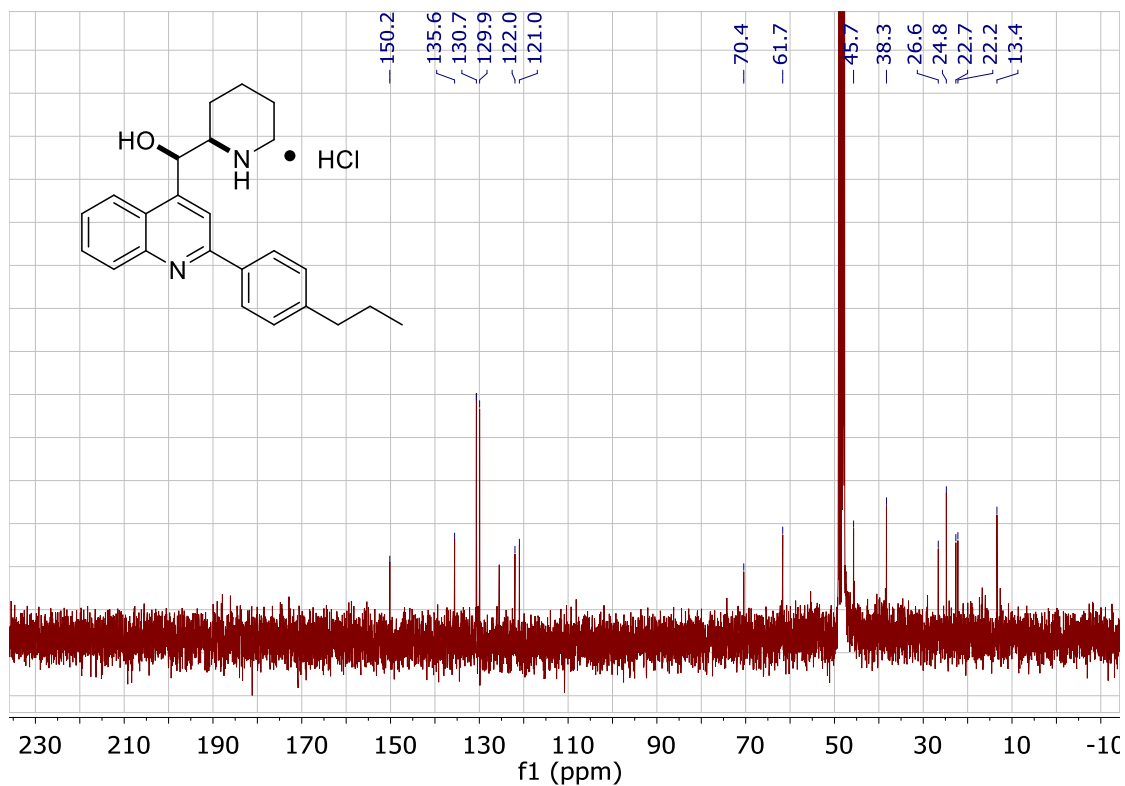
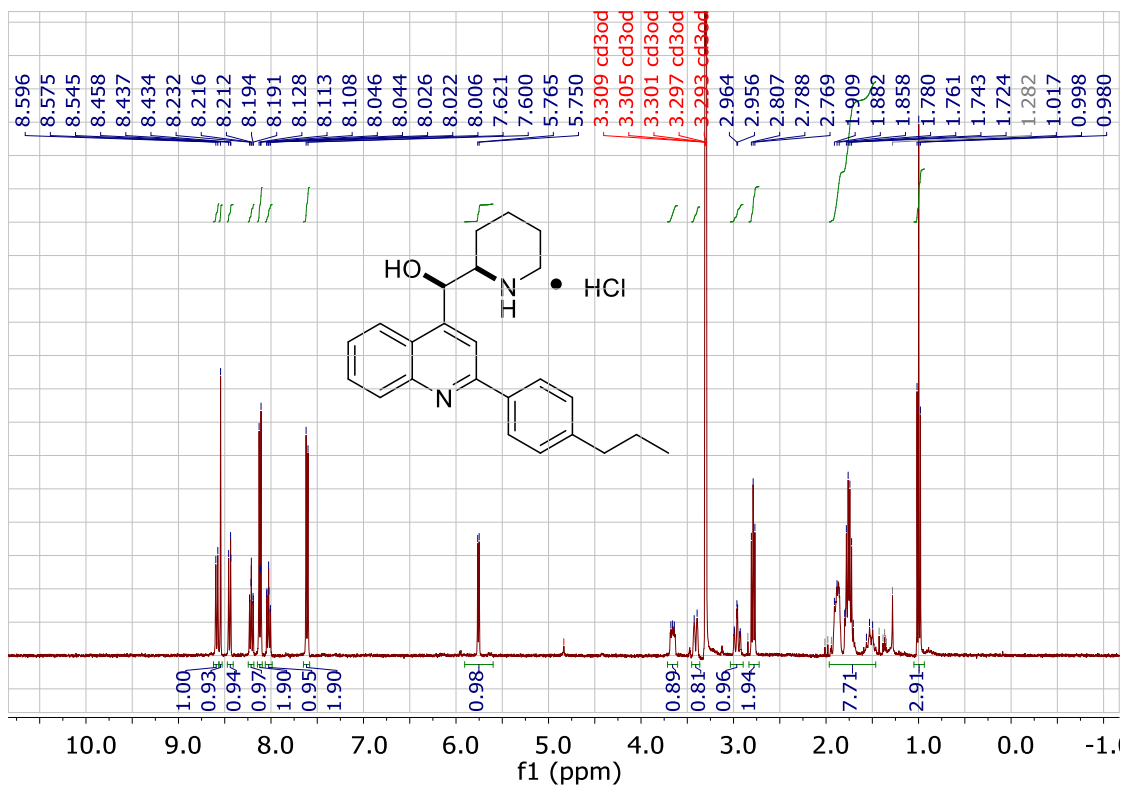
4-quinolinemethanol, 2-(4-methylphenyl)- α -2-piperidinyl-, hydrochloride



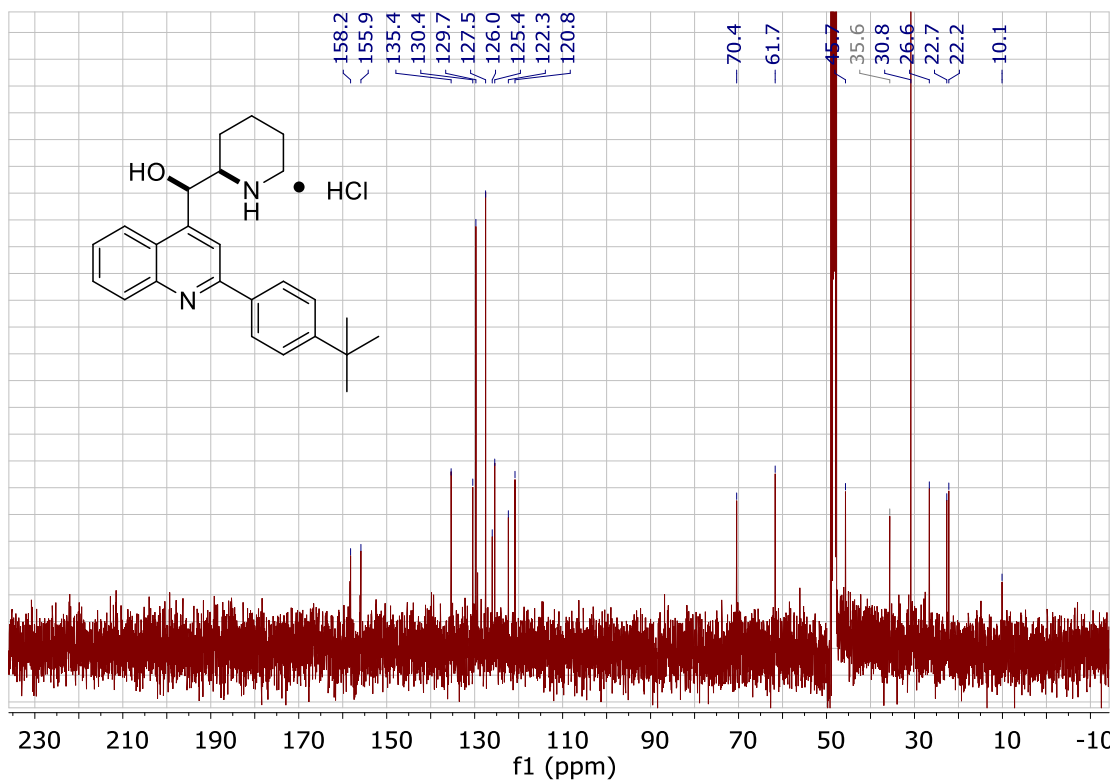
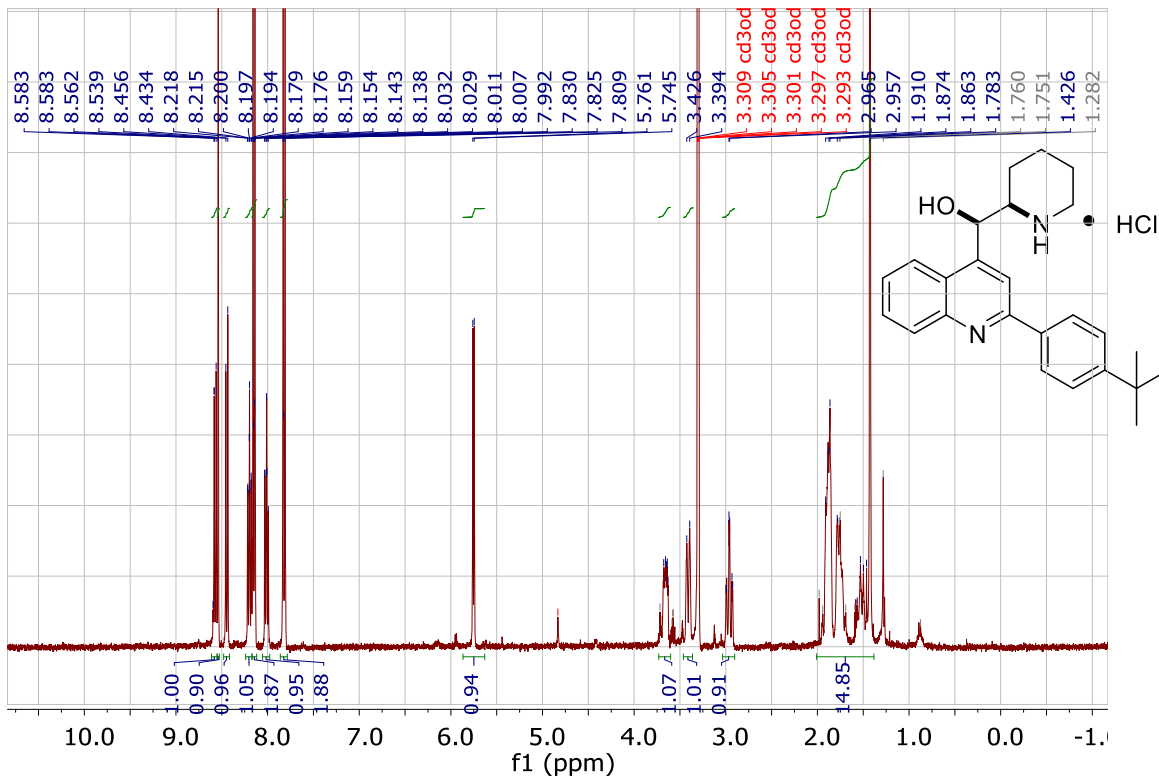
4-quinolinemethanol, 2-(4-ethylphenyl)- α -2-piperidinyl-, hydrochloride



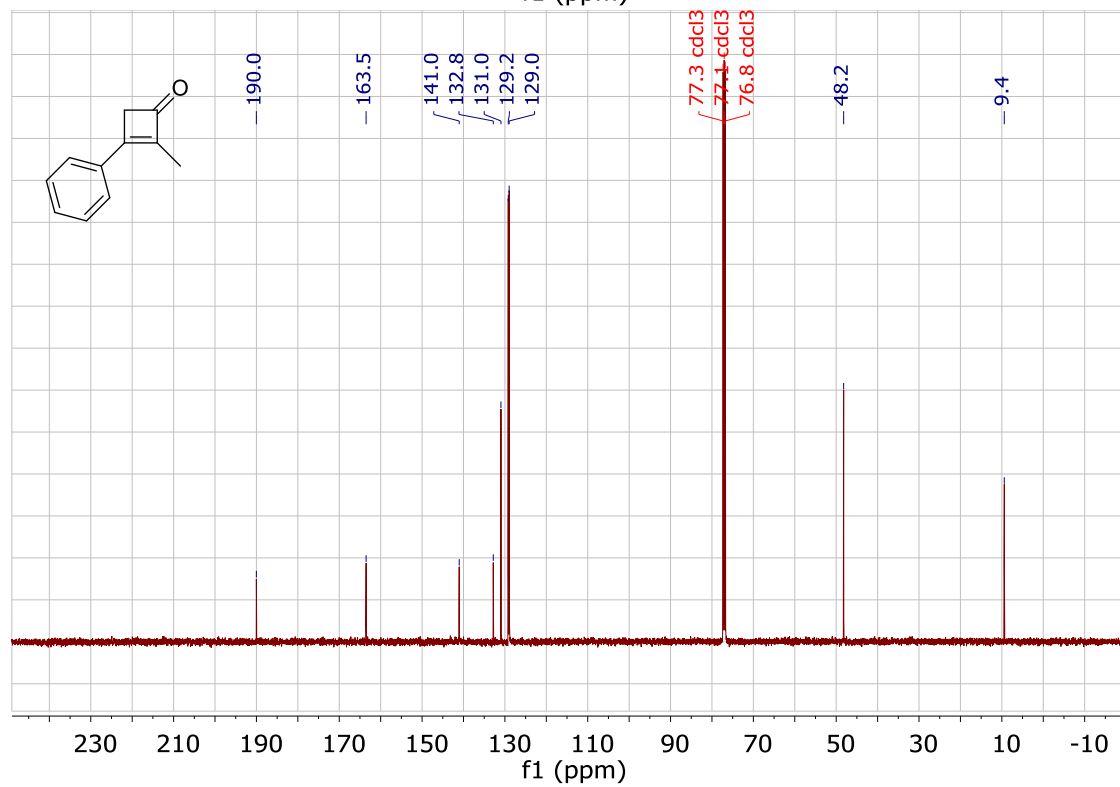
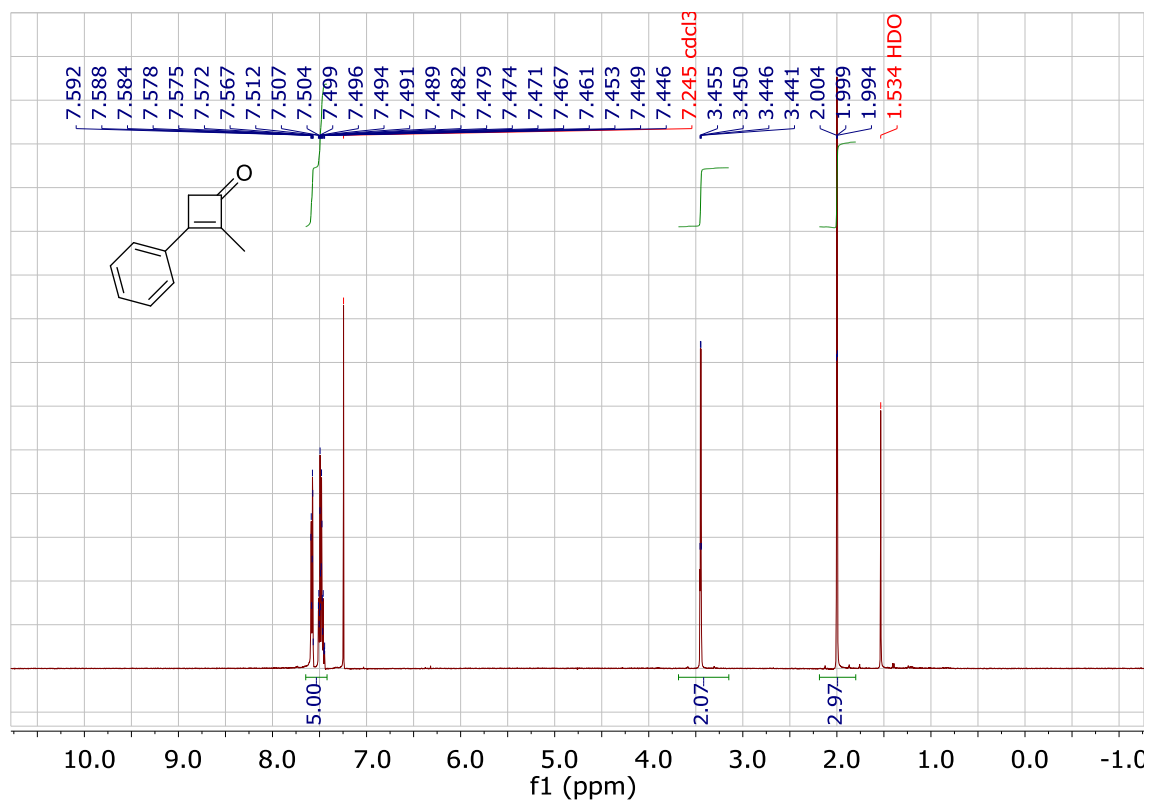
4-quinolinemethanol, 2-(4-propylphenyl)- α -2-piperidinyl-, hydrochloride



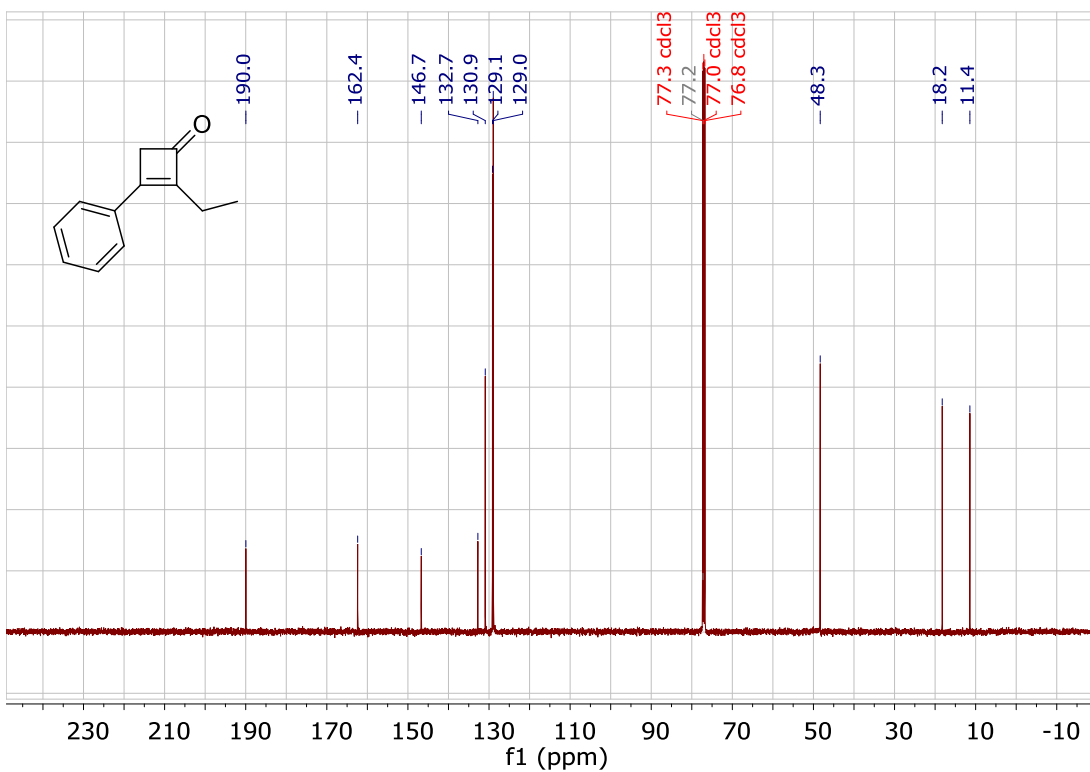
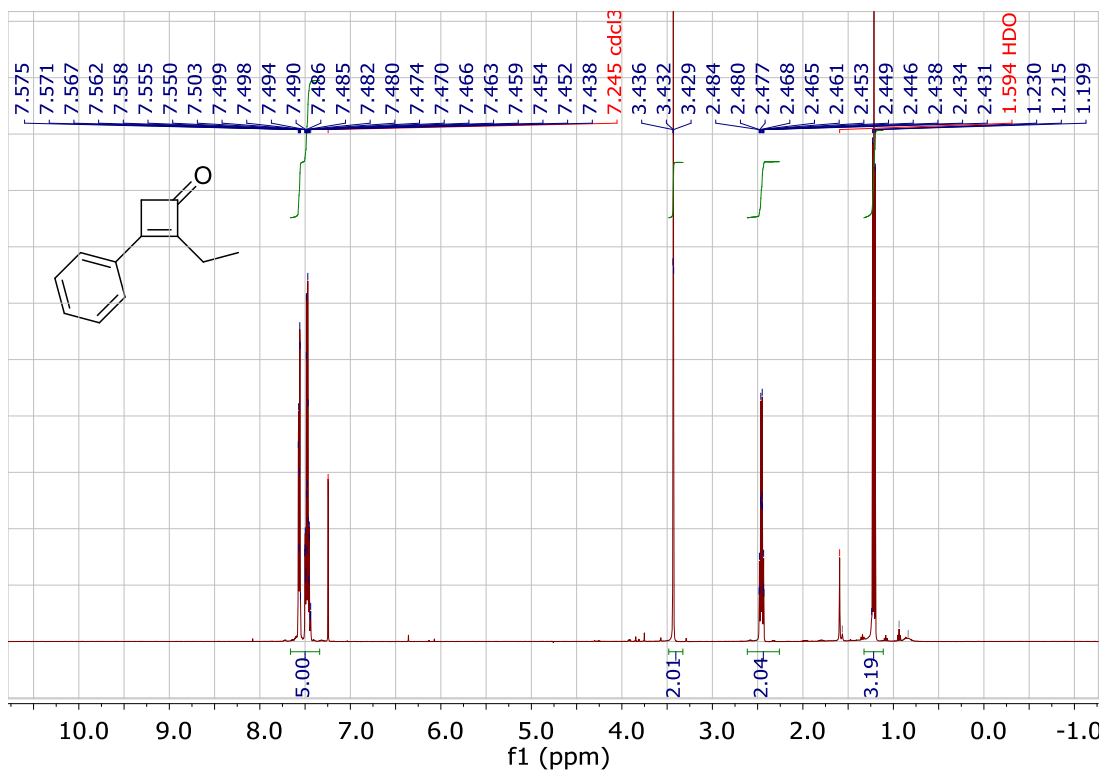
4-quinolinemethanol, 2-(4-*tert*-butylphenyl)- α -2-piperidinyl-, hydrochloride



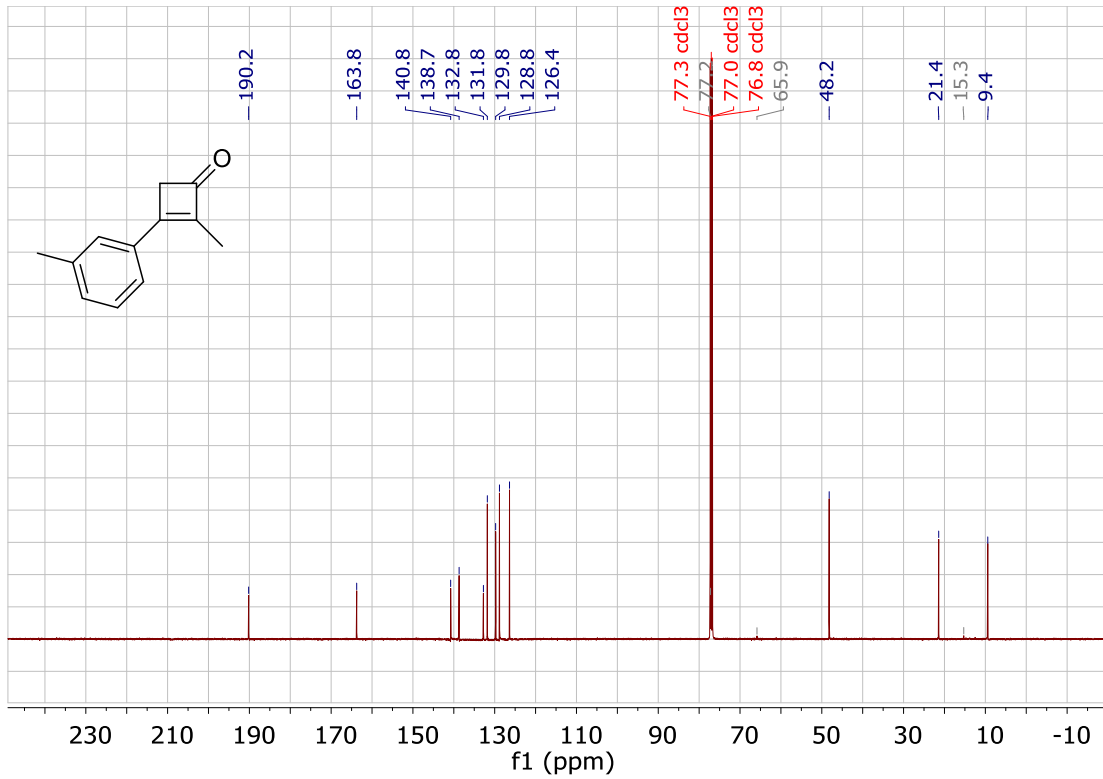
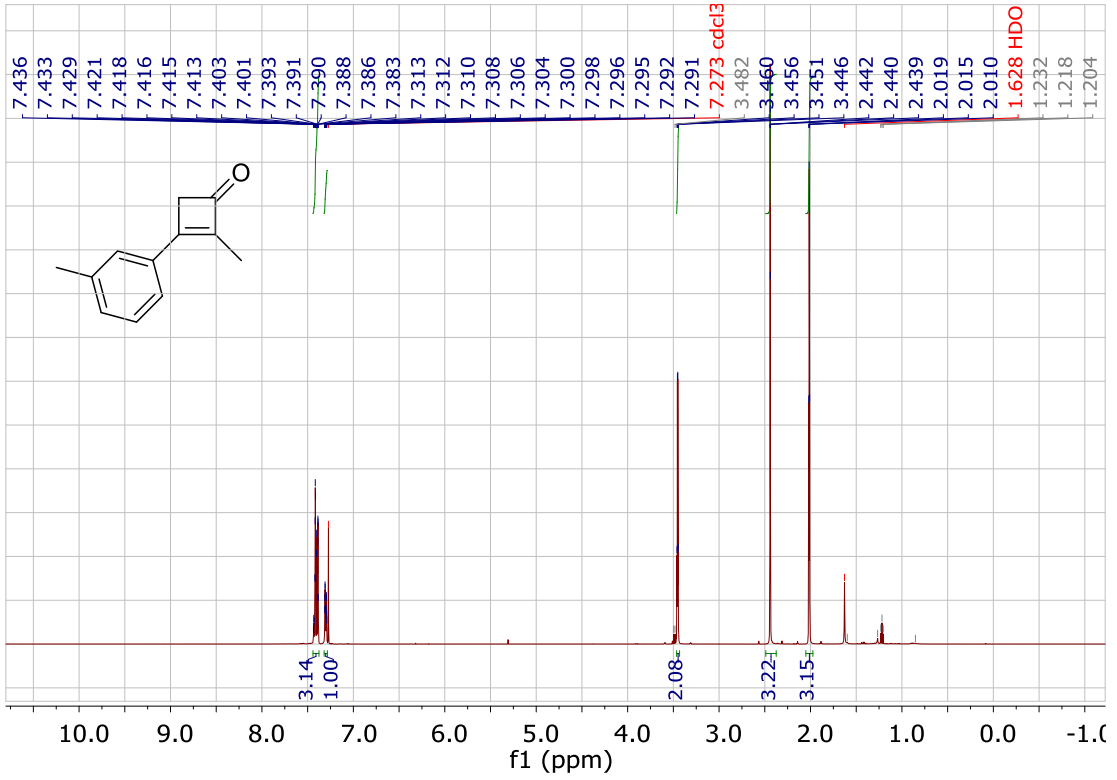
2-methyl-3-phenylcyclobut-2-enone



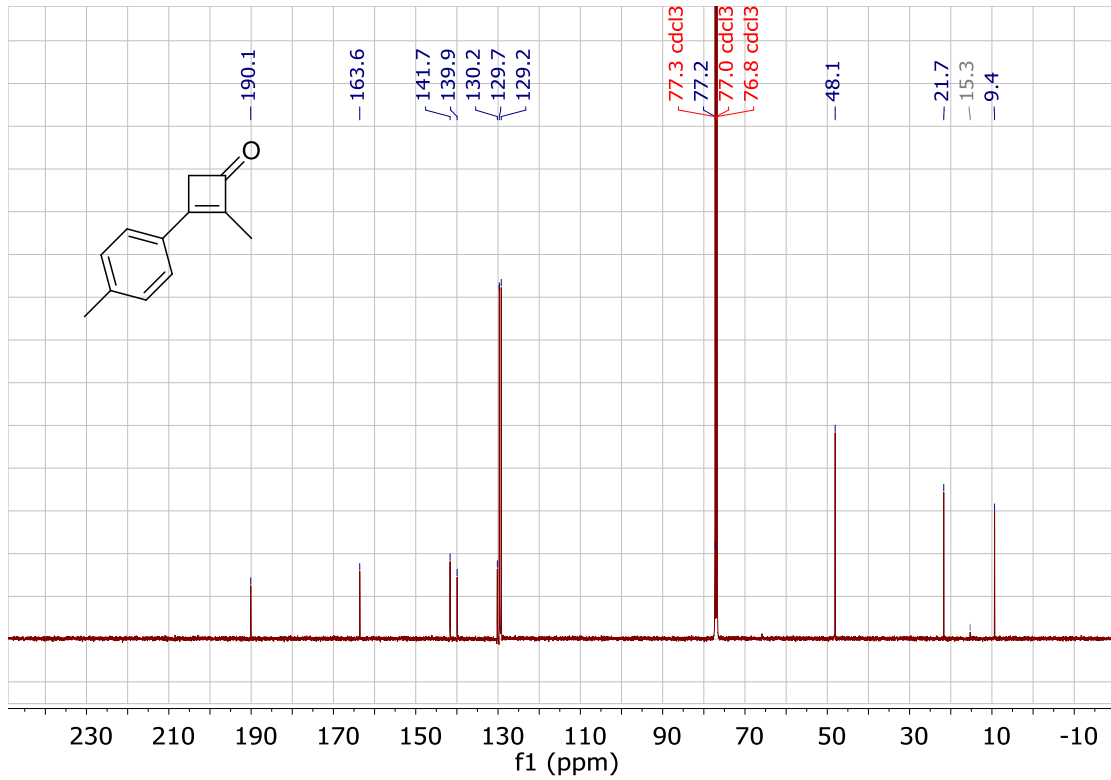
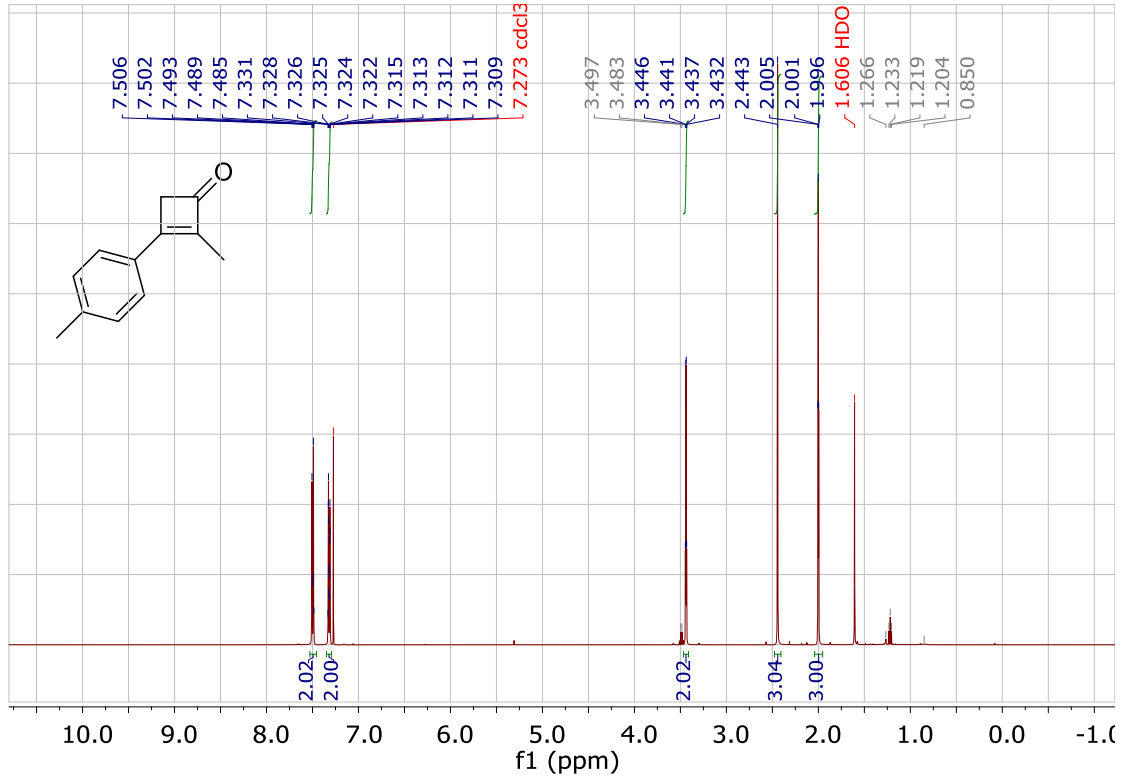
2-ethyl-3-phenylcyclobut-2-enone



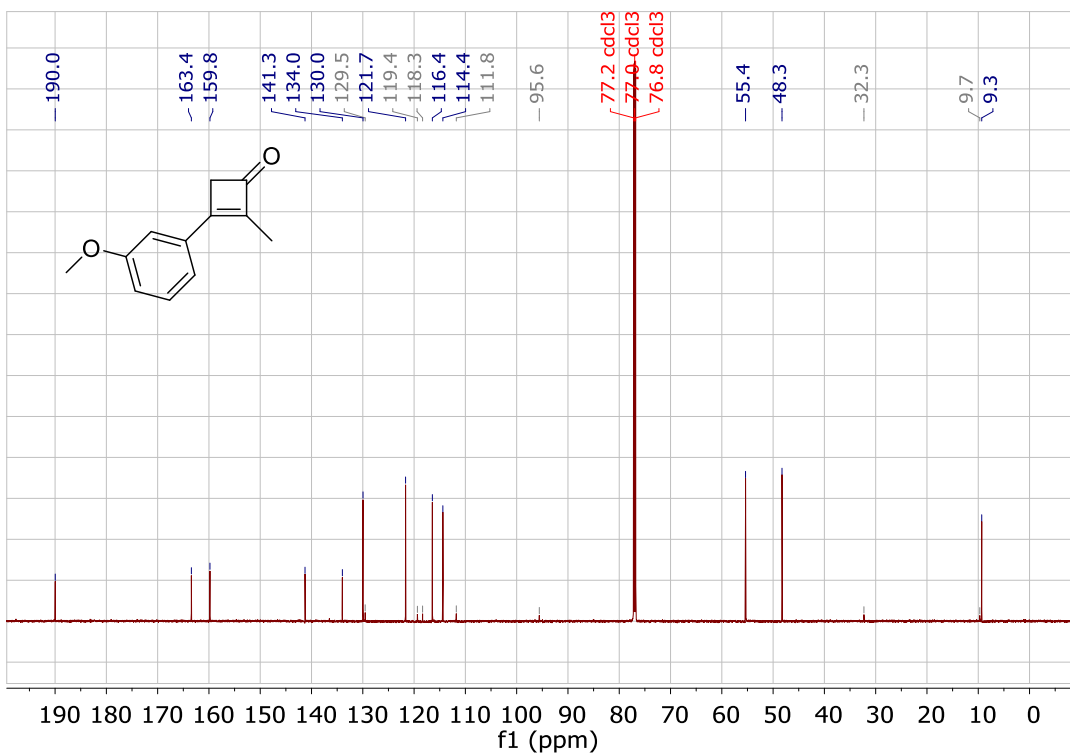
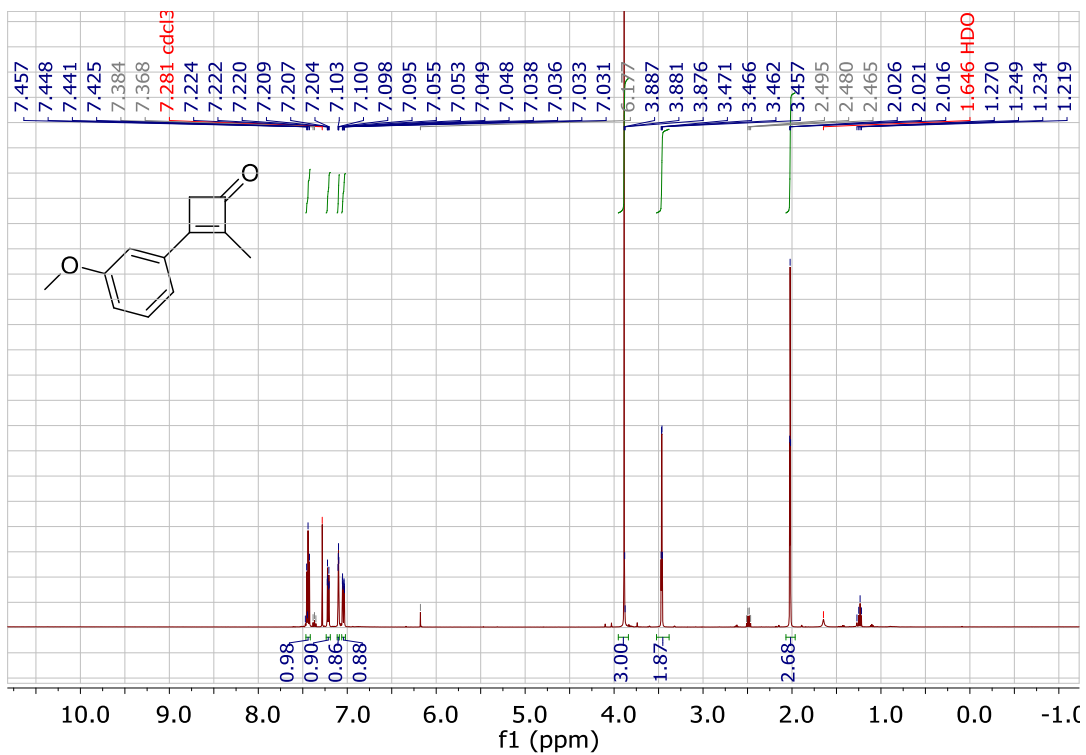
2-methyl-3-(*m*-tolyl)cyclobut-2-enone



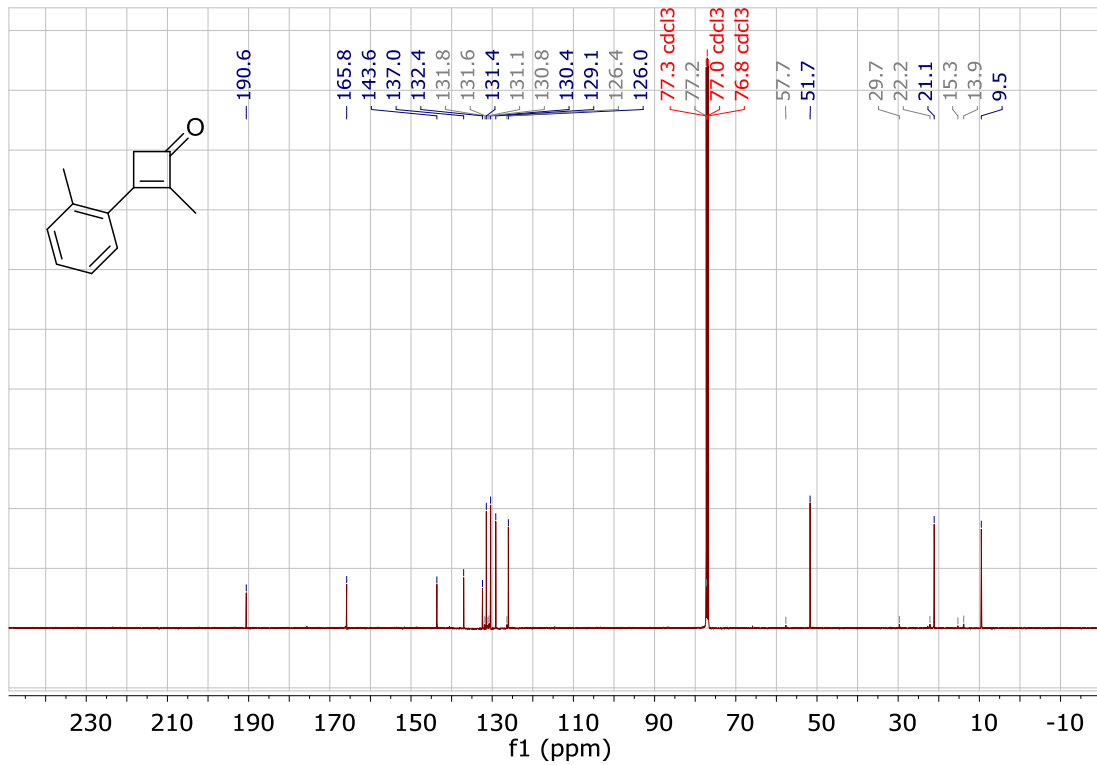
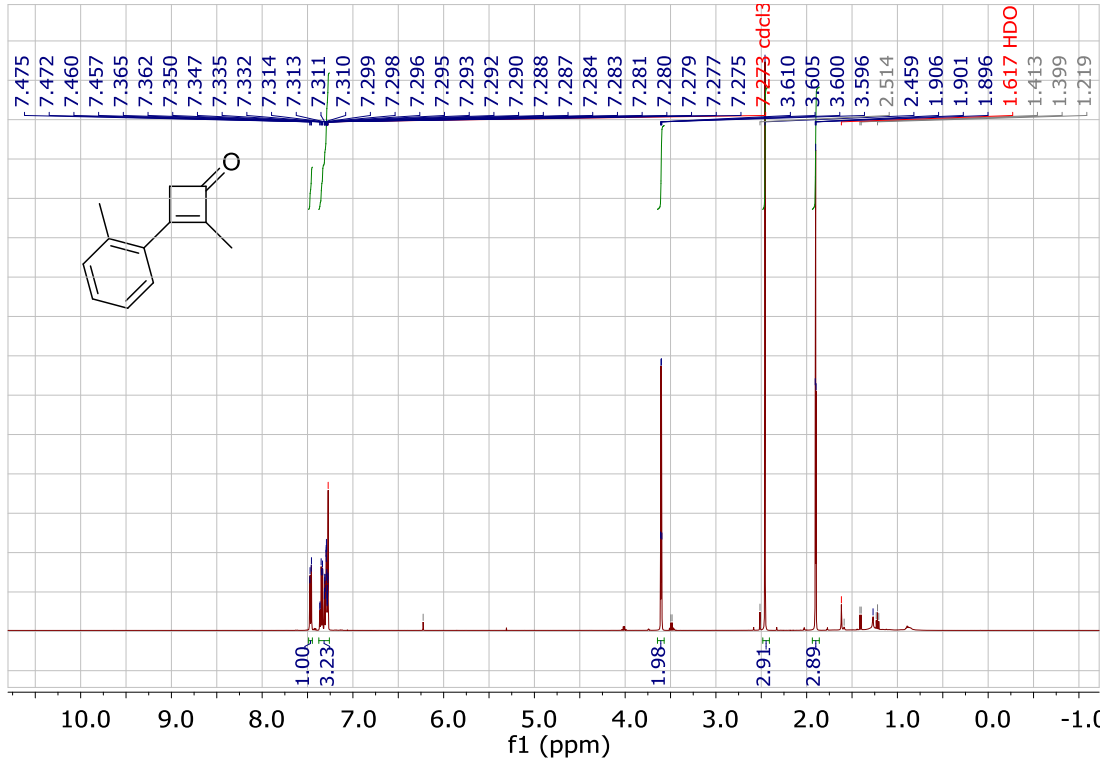
2-methyl-3-(*p*-tolyl)cyclobut-2-enone



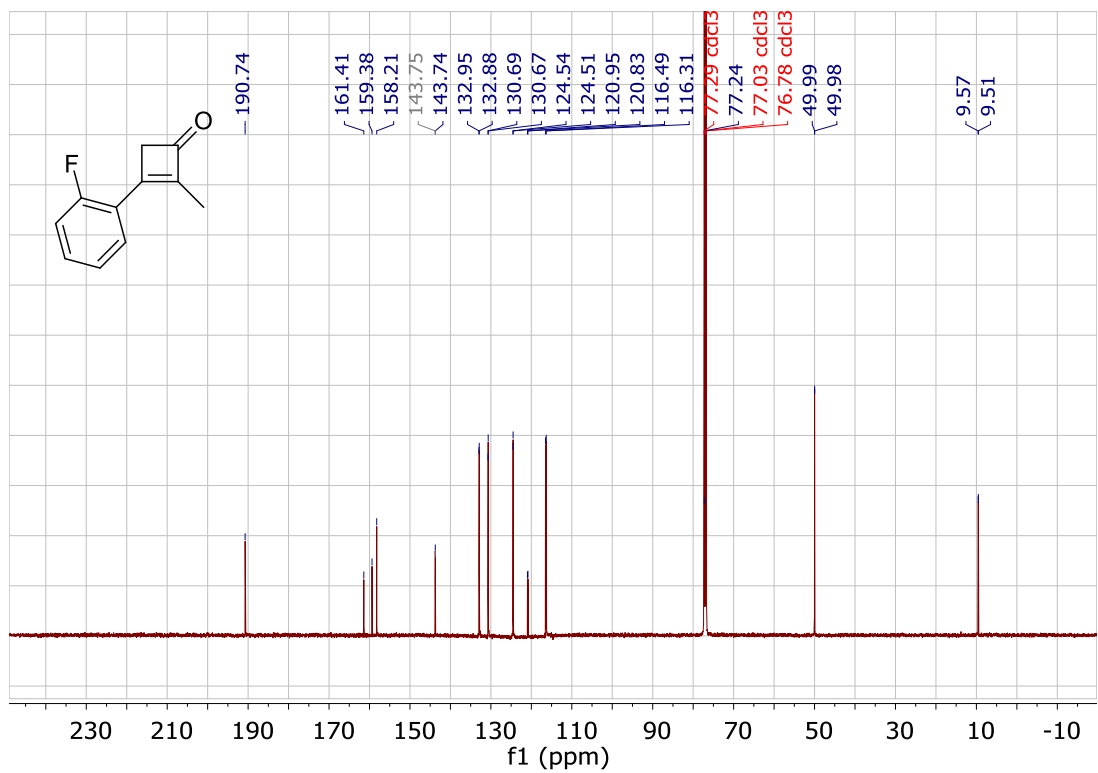
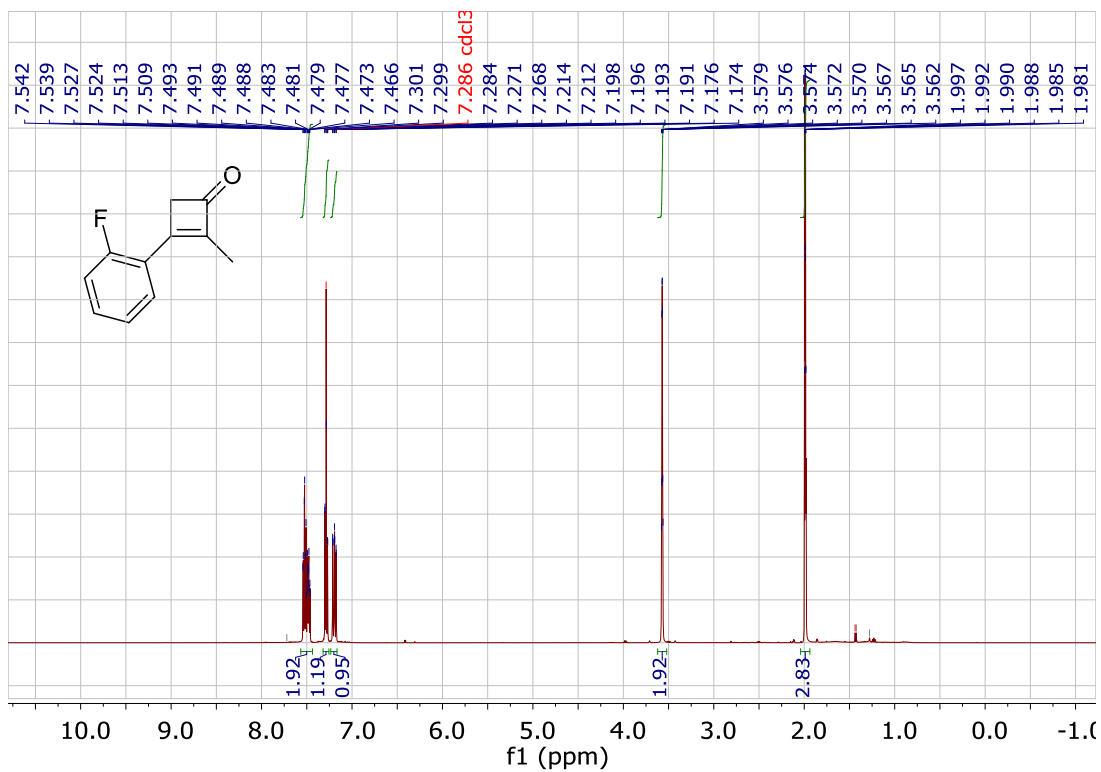
3-(3-methoxyphenyl)-2-methylcyclobut-2-enone



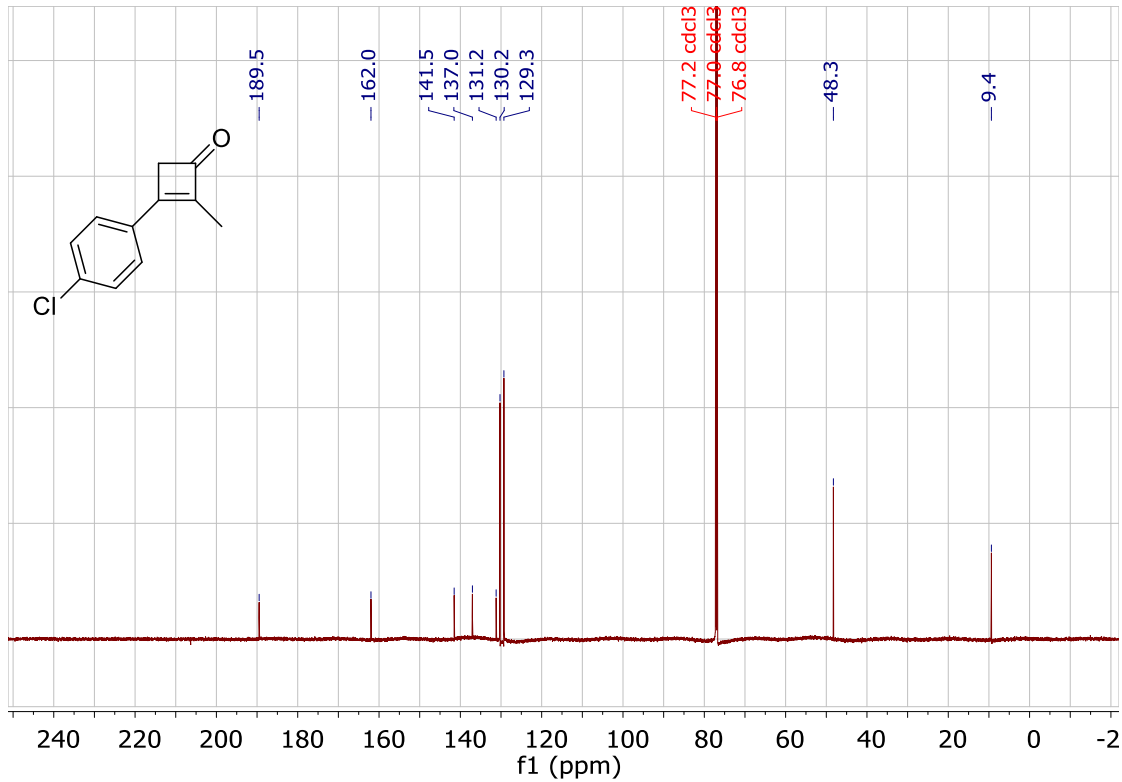
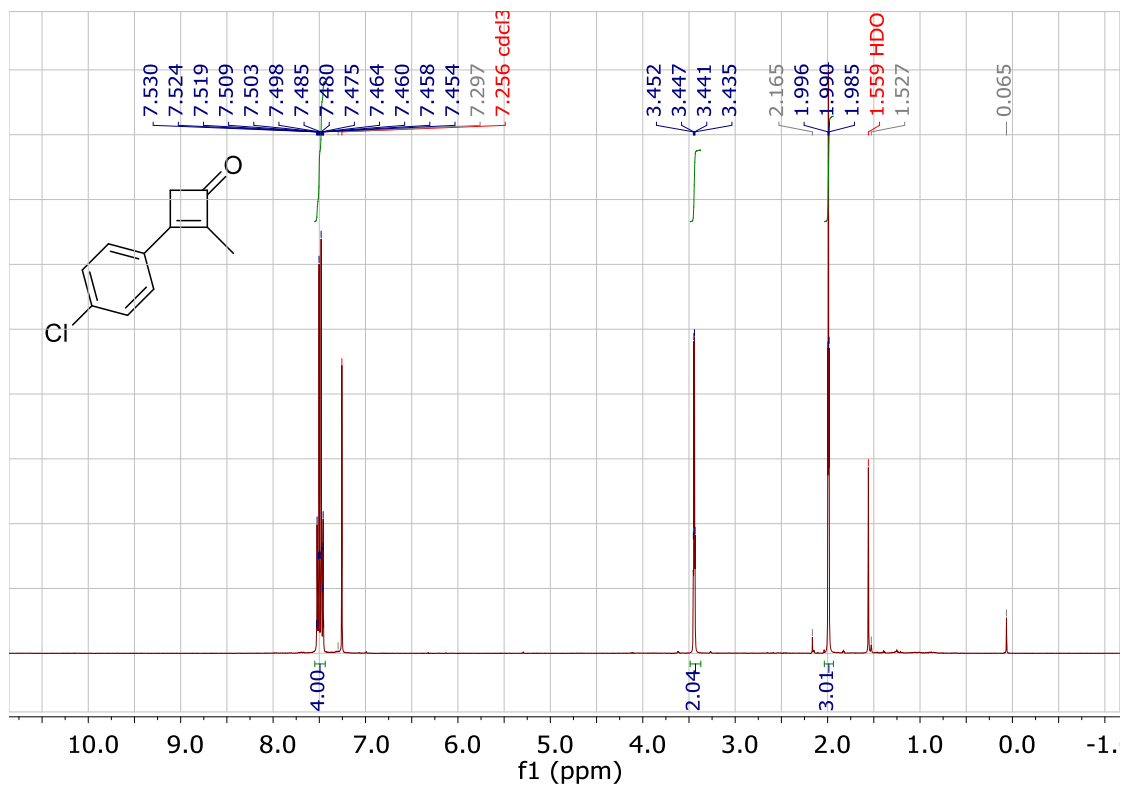
2-methyl-3-(*o*-tolyl)cyclobut-2-enone



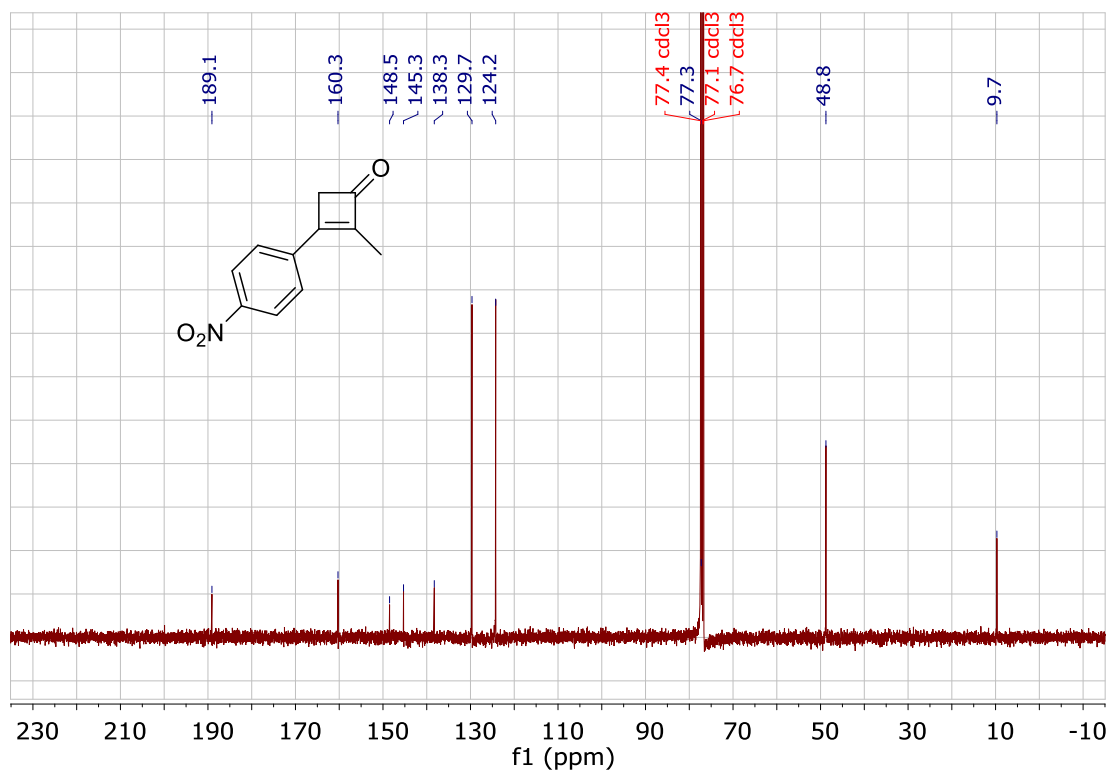
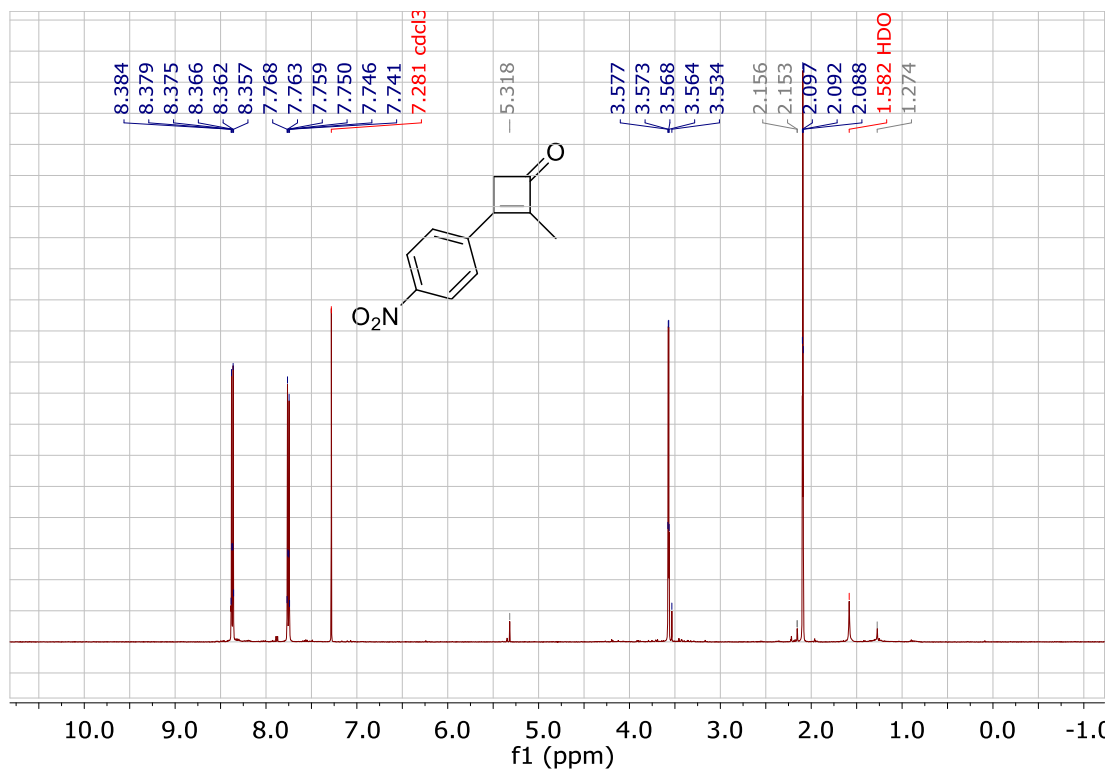
3-(2-fluorophenyl)-2-methylcyclobut-2-enone



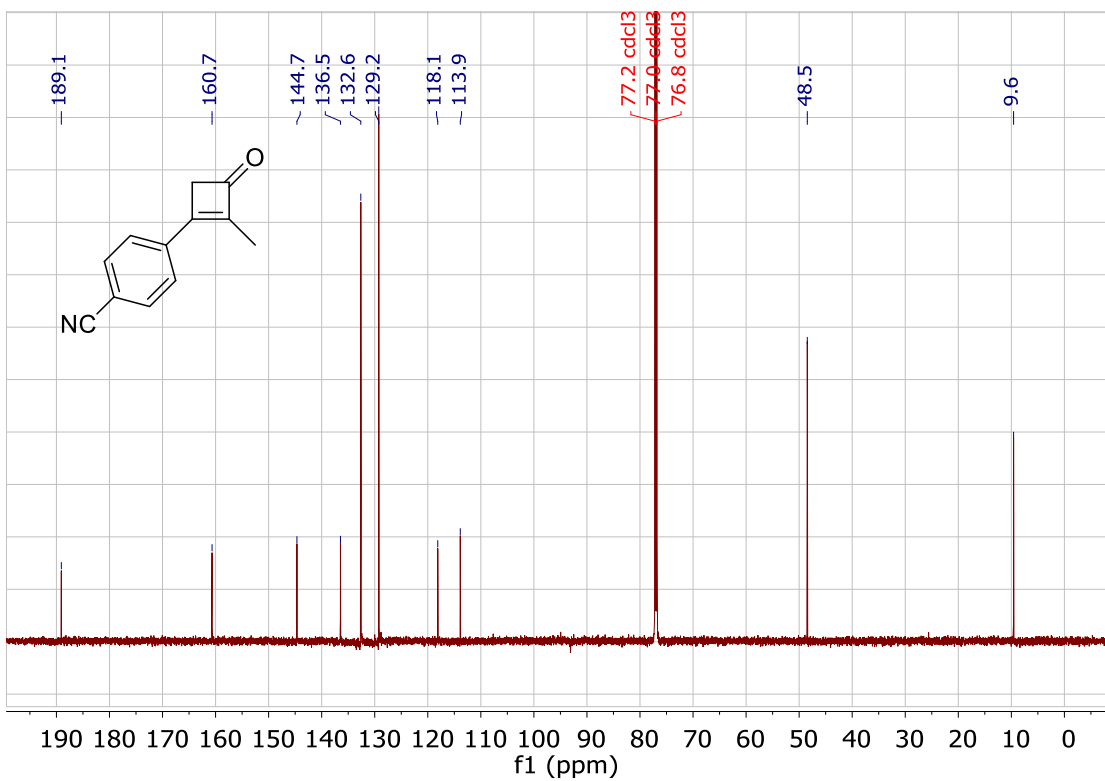
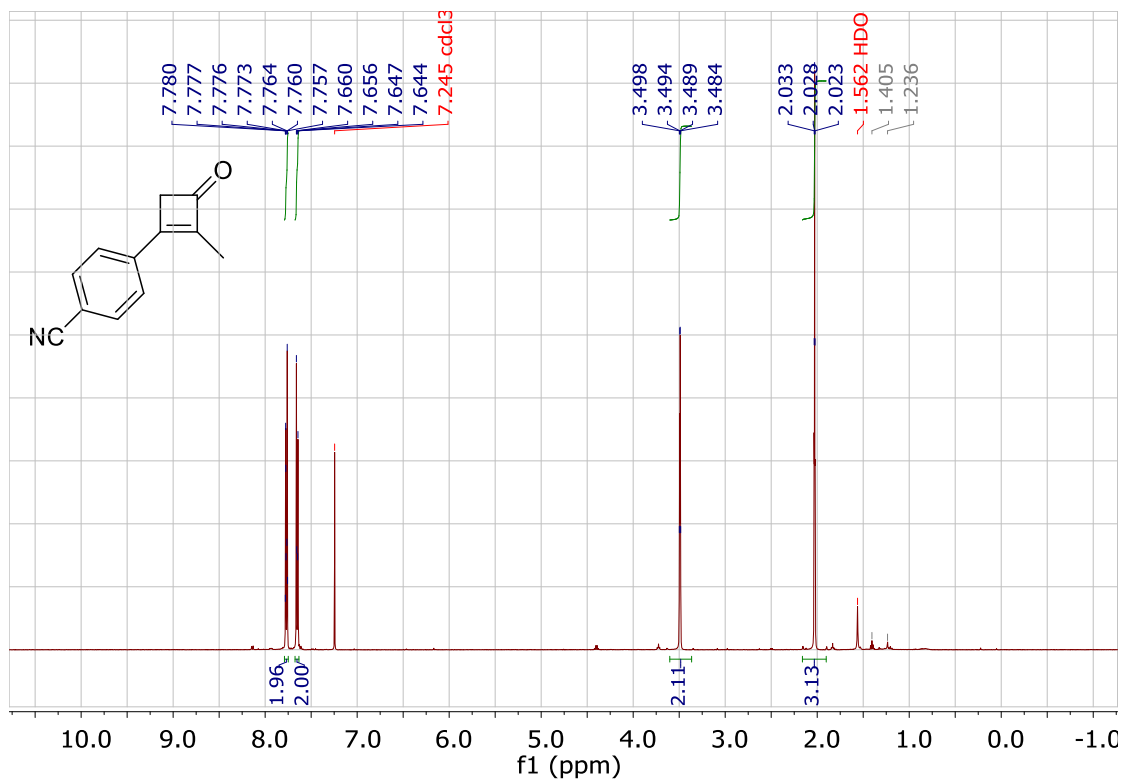
3-(4-chlorophenyl)-2-methylcyclobut-2-enone



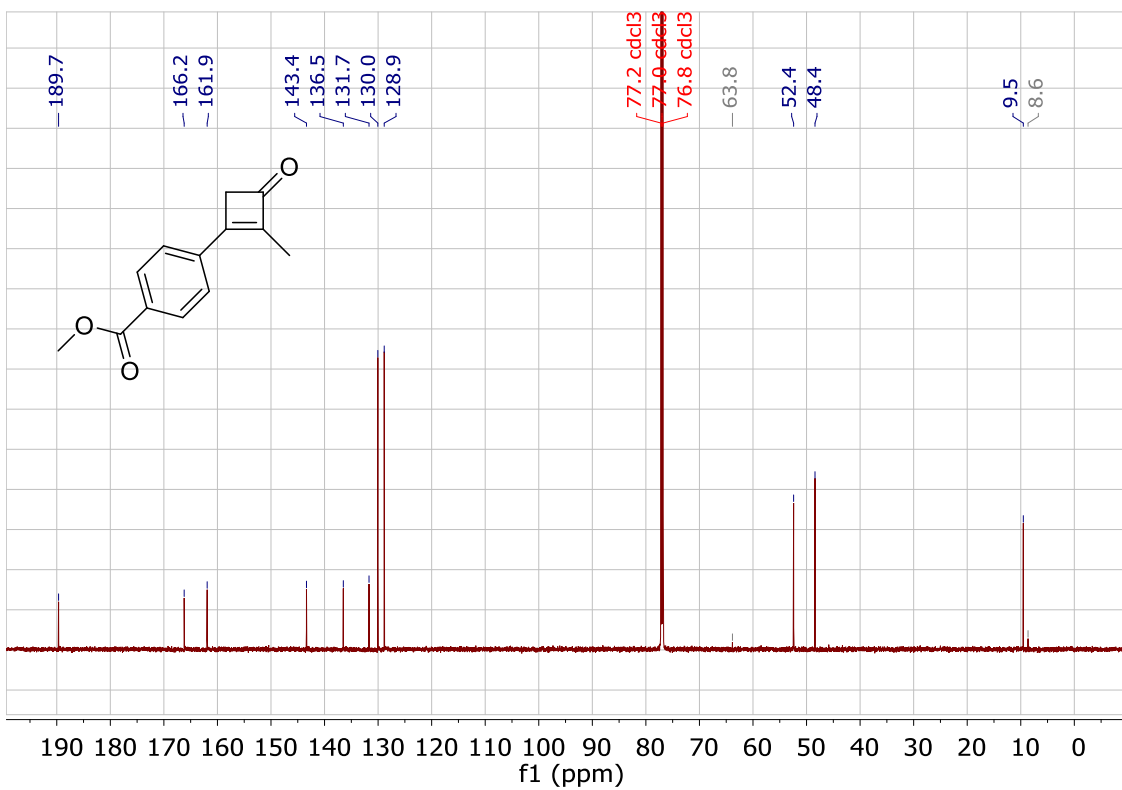
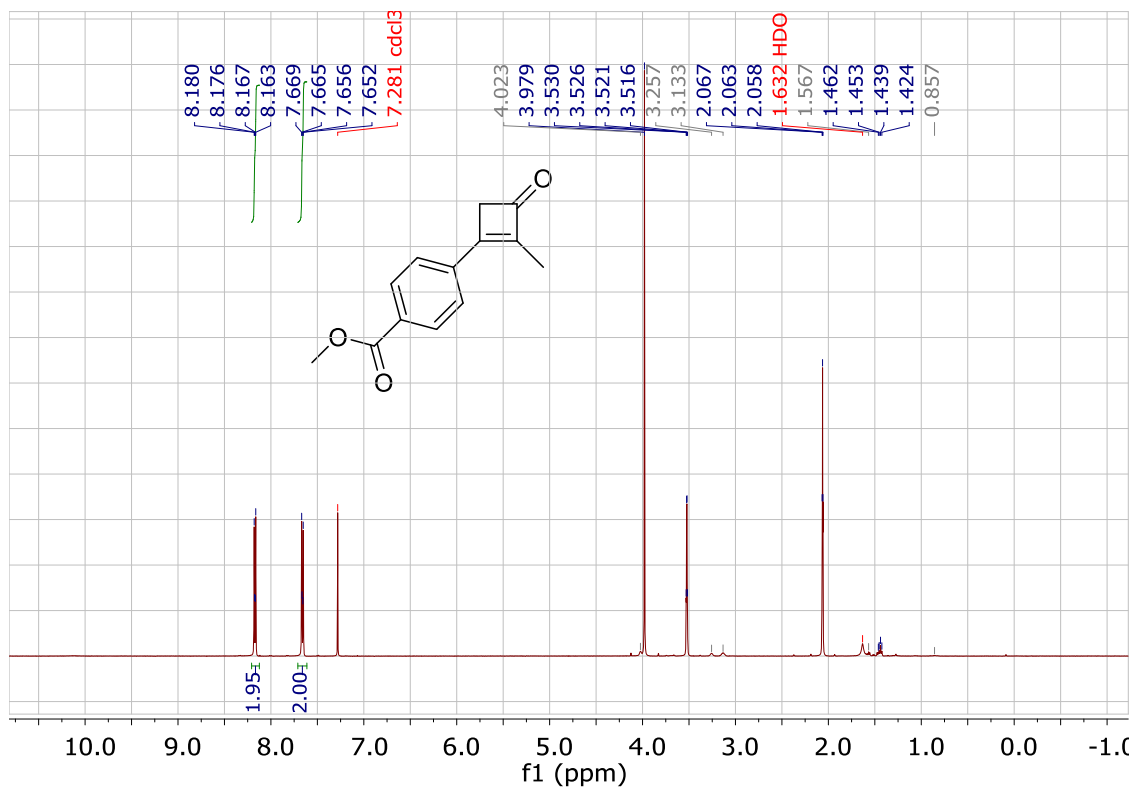
2-methyl-3-(4-nitrophenyl)cyclobut-2-ene



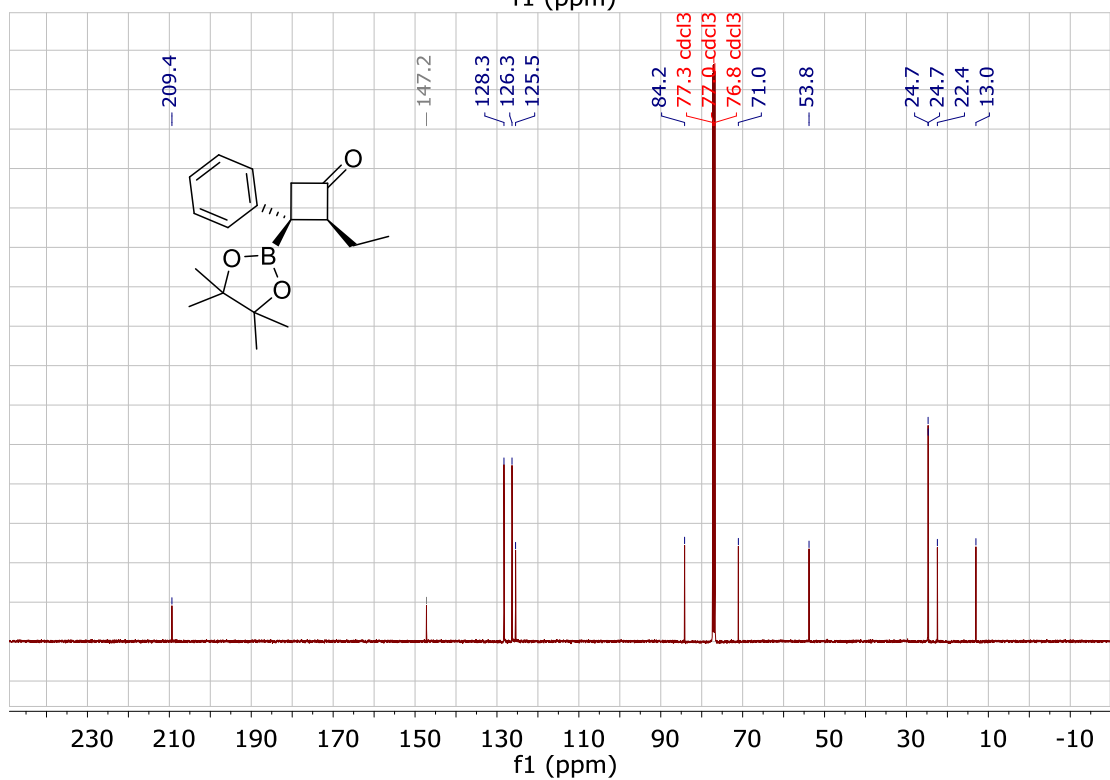
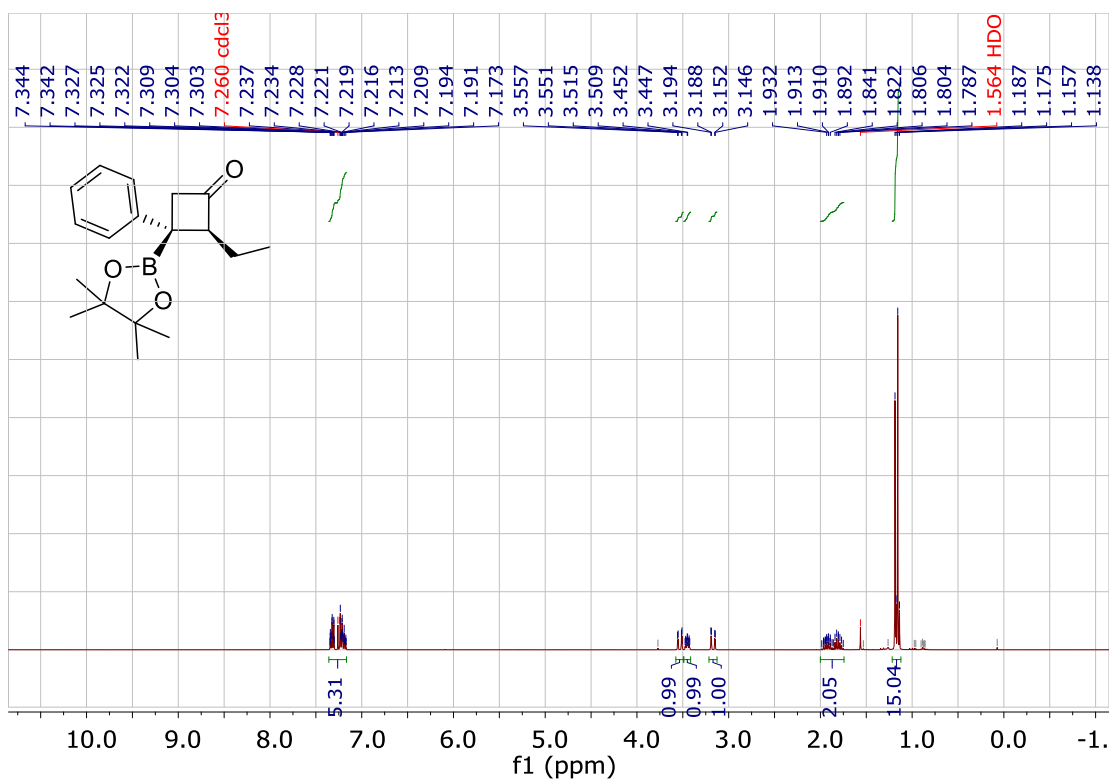
4-(2-methyl-3-oxocyclobut-1-en-1-yl)benzonitrile

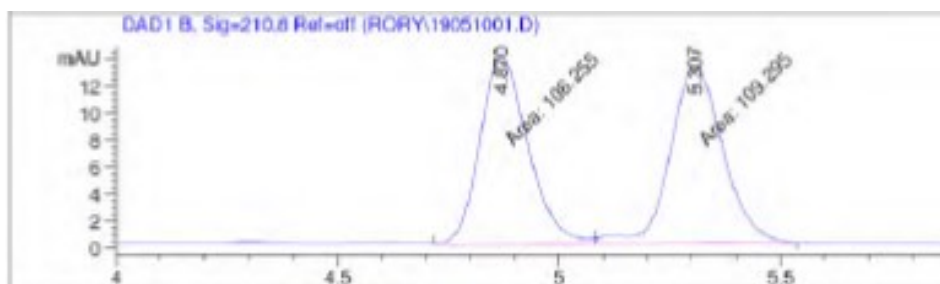


methyl 4-(2-methyl-3-oxocyclobut-1-en-1-yl)benzoate



(2*S*,3*R*)-2-ethyl-3-phenyl-3-(4,4,5,5-tetramethyl-1,3,2-dioxaborolan-2-yl)cyclobutanone





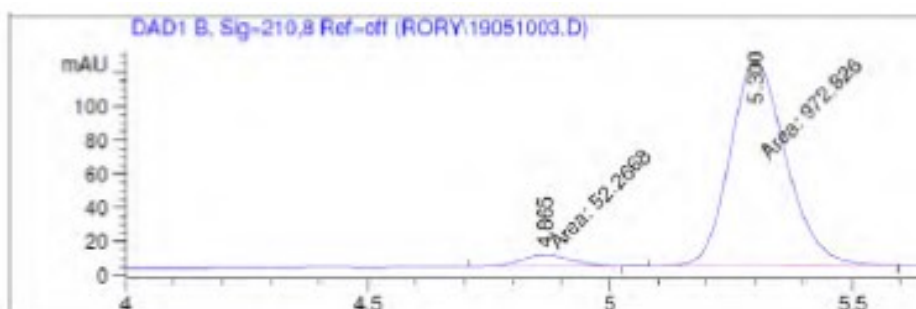
Area Percent Report

Sorted By : Signal
 Multiplier : 1.0000
 Dilution : 1.0000
 Use Multiplier & Dilution Factor with ISTDs

Signal 2: DAD1 B, Sig=210,8 Ref=off

Peak #	RetTime [min]	Type	Width [min]	Area [mAU*s]	Height [mAU]	Area %
1	4.870	MF	0.1265	106.25518	13.99622	49.2949
2	5.307	FM	0.1380	109.29498	13.20042	50.7051

Totals : 215.55016 27.19664



Area Percent Report

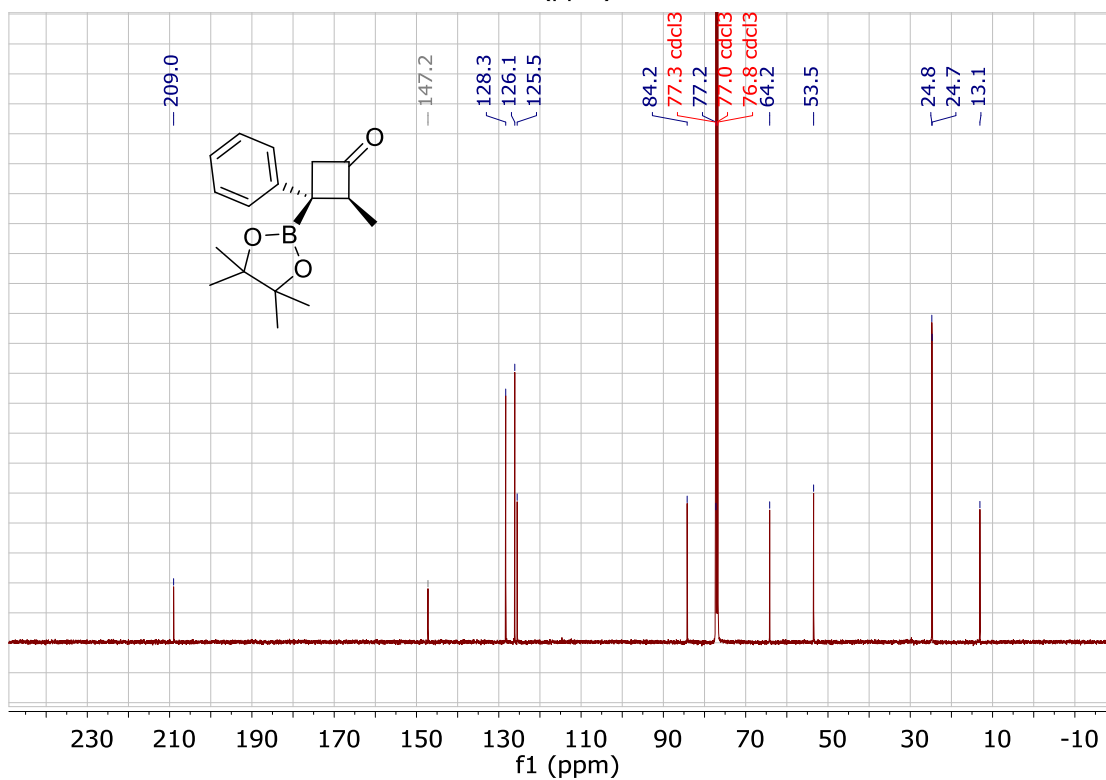
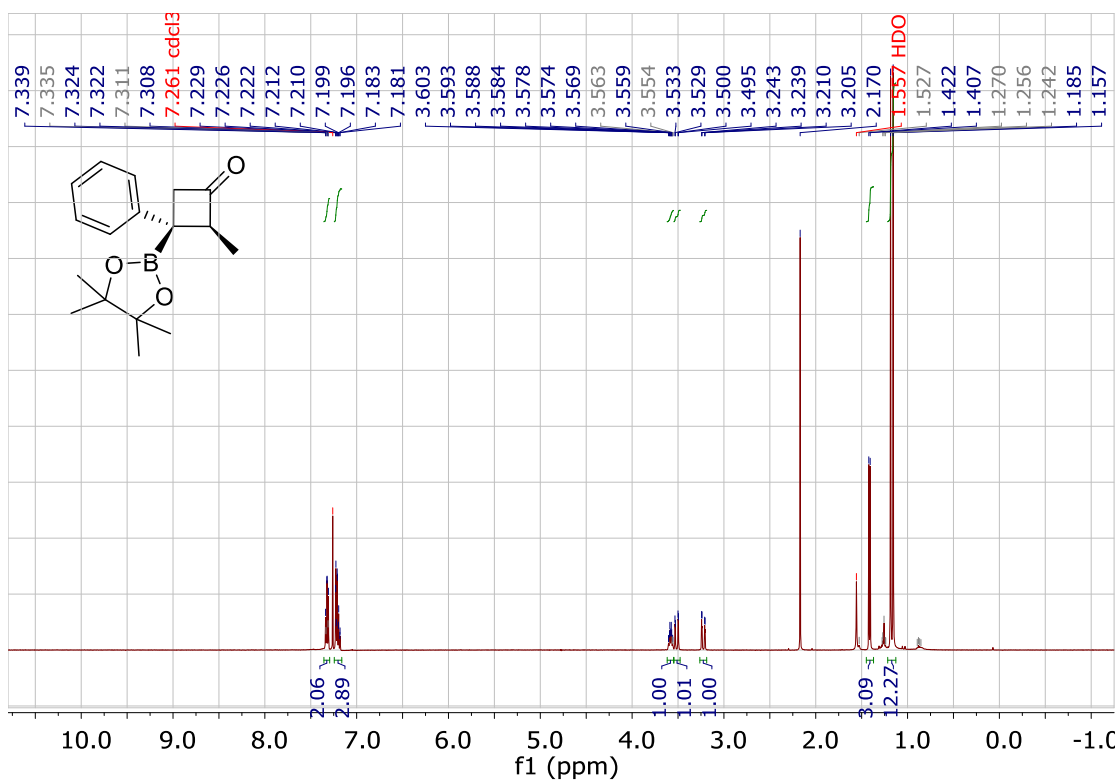
Sorted By : Signal
 Multiplier : 1.0000
 Dilution : 1.0000
 Use Multiplier & Dilution Factor with ISTDs

Signal 2: DAD1 B, Sig=210,8 Ref=off

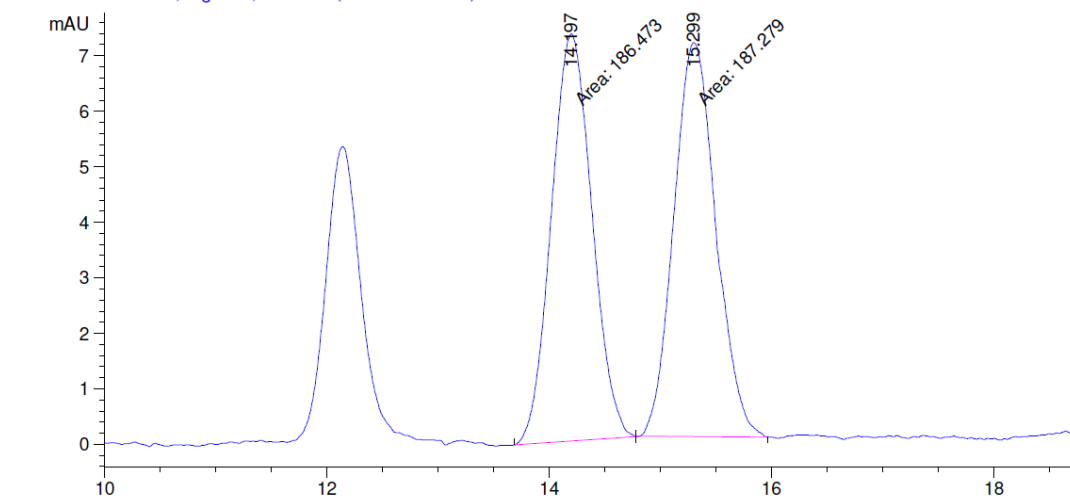
Peak #	RetTime [min]	Type	Width [min]	Area [mAU*s]	Height [mAU]	Area %
1	4.865	MM	0.1203	52.26679	7.24315	5.0987
2	5.300	MM	0.1342	972.82593	120.82475	94.9013

Totals : 1025.09272 128.06790

(2*S*,3*R*)-2-methyl-3-phenyl-3-(4,4,5,5-tetramethyl-1,3,2-dioxaborolan-2-yl)cyclobutanone



DAD1 A, Sig=220,4 Ref=off (ED\19021302.D)

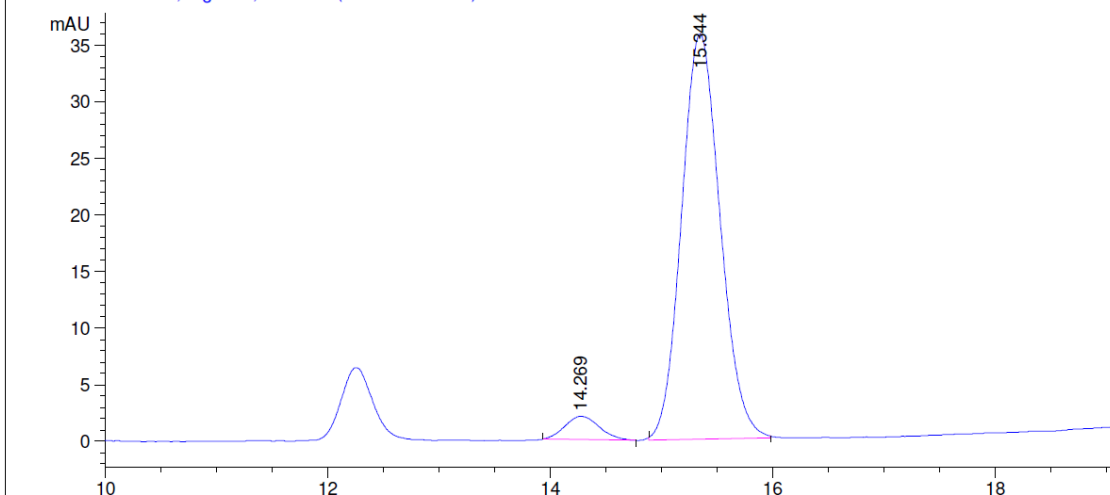


Peak #	RetTime [min]	Type	Width [min]	Area [mAU*s]	Height [mAU]	Area %
1	14.197	MM	0.4234	186.47258	7.34037	49.8922
2	15.299	MM	0.4393	187.27870	7.10538	50.1078

Totals : 373.75128 14.44575

*** End of Report ***

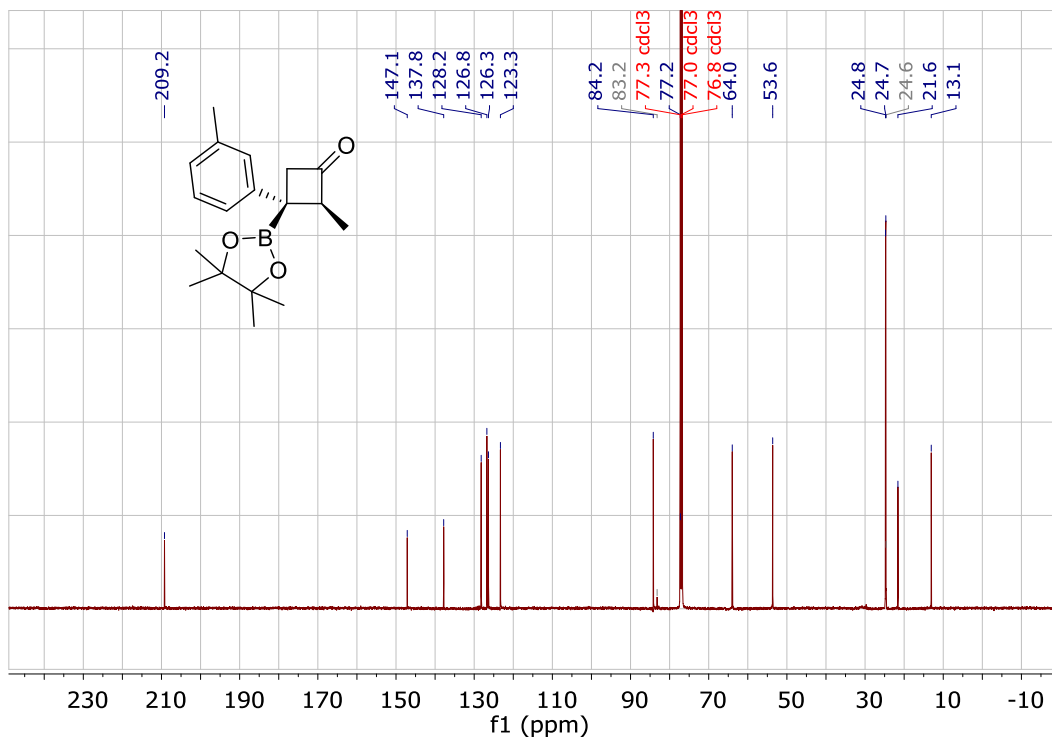
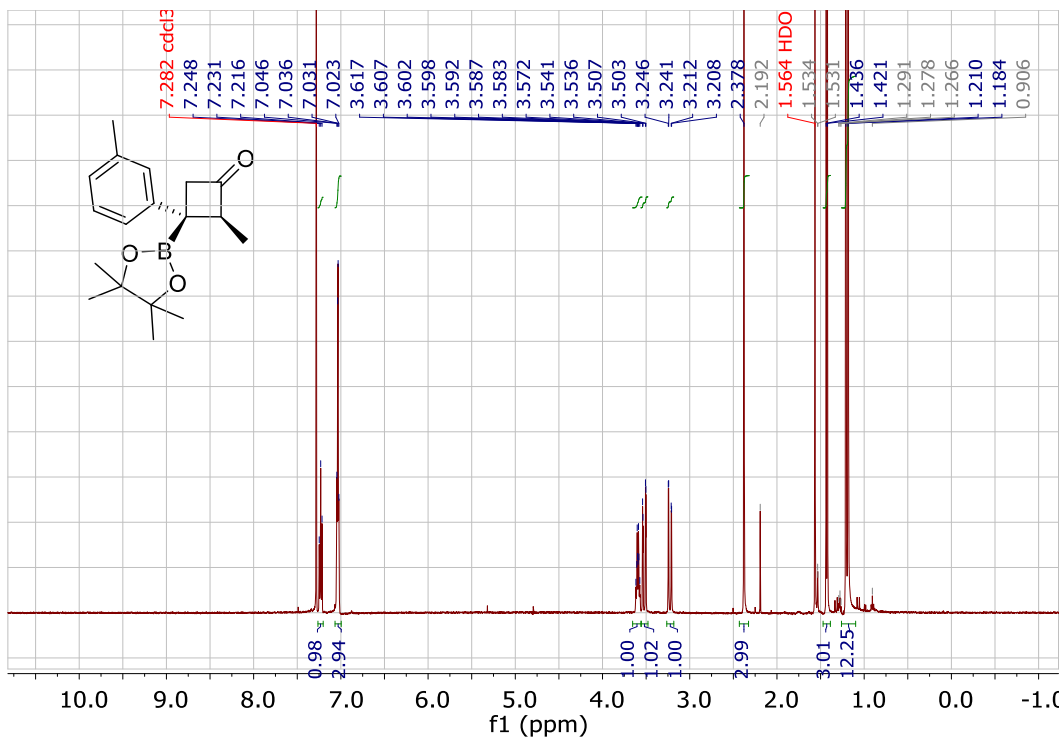
DAD1 A, Sig=220,4 Ref=off (ED\19021306.D)

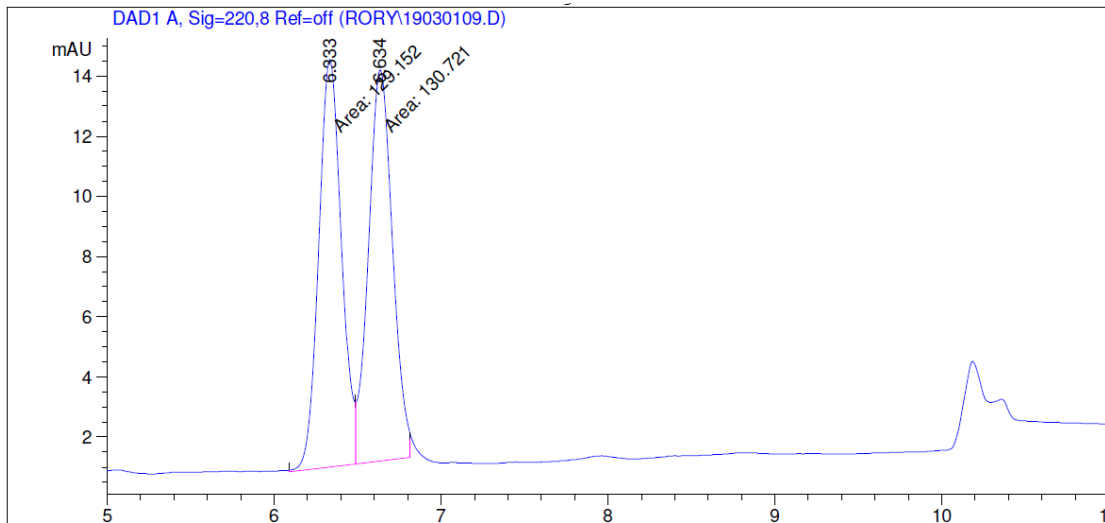


Peak #	RetTime [min]	Type	Width [min]	Area [mAU*s]	Height [mAU]	Area %
1	14.269	BP	0.3079	44.85875	2.07745	4.9351
2	15.344	BB	0.3715	864.11157	35.80891	95.0649

Totals : 908.97032 37.88637

(2*S*,3*R*)-2-methyl-3-(4,4,5,5-tetramethyl-1,3,2-dioxaborolan-2-yl)-3-(*m*-tolyl)cyclobutanone



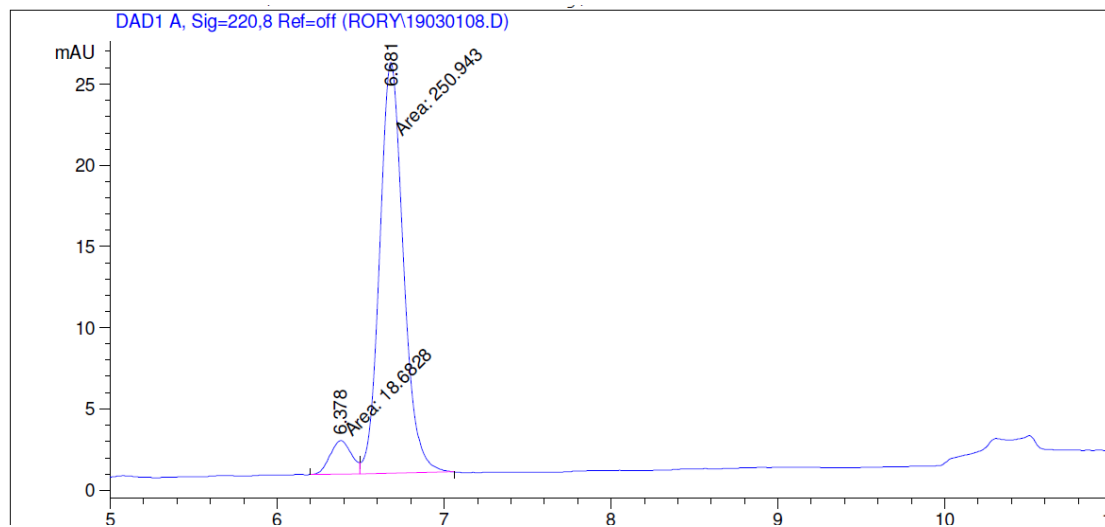


Signal 1: DAD1 A, Sig=220,8 Ref=off

Peak #	RetTime [min]	Type	Width [min]	Area [mAU*s]	Height [mAU]	Area %
1	6.333	MF	0.1587	129.15193	13.56356	49.6982
2	6.634	MF	0.1672	130.72070	13.03325	50.3018

Totals : 259.87263 26.59681

*** End of Report ***



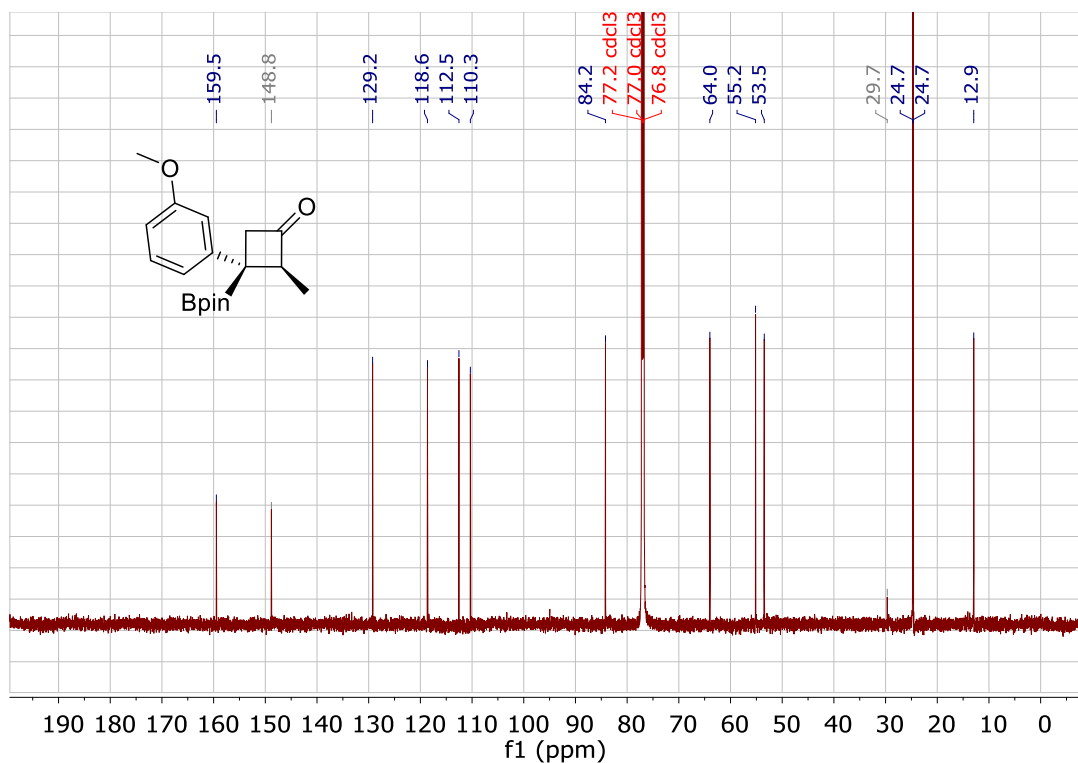
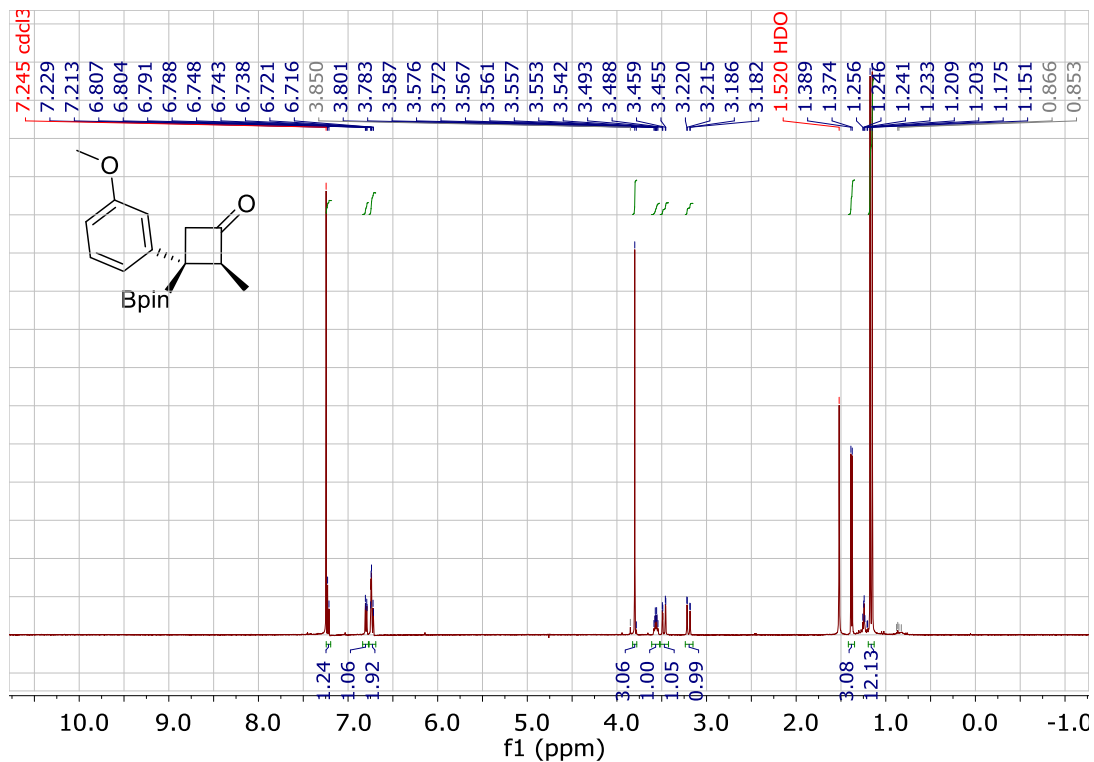
Signal 1: DAD1 A, Sig=220,8 Ref=off

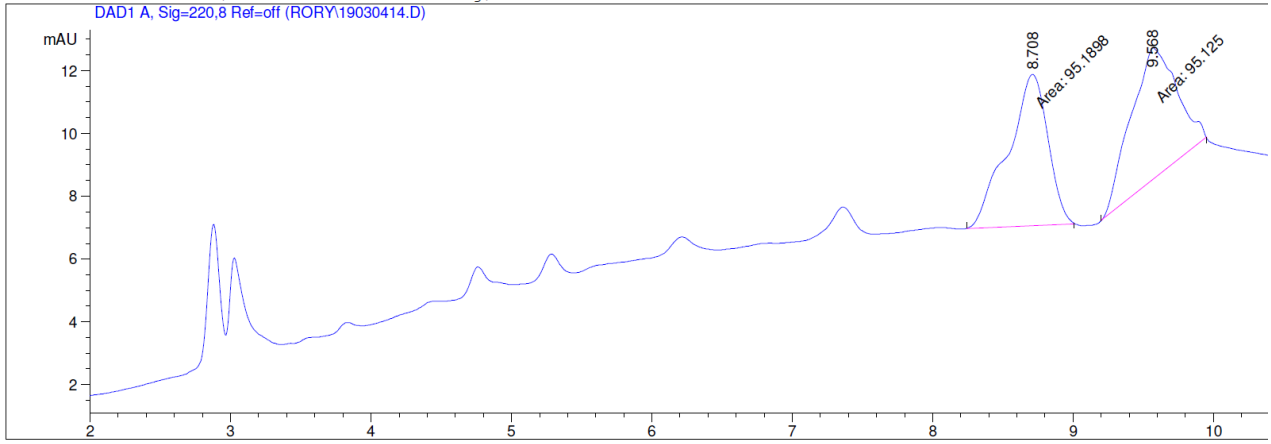
Peak #	RetTime [min]	Type	Width [min]	Area [mAU*s]	Height [mAU]	Area %
1	6.378	MF	0.1497	18.68276	2.08041	6.9292
2	6.681	FM	0.1652	250.94272	25.31918	93.0708

Totals : 269.62548 27.39959

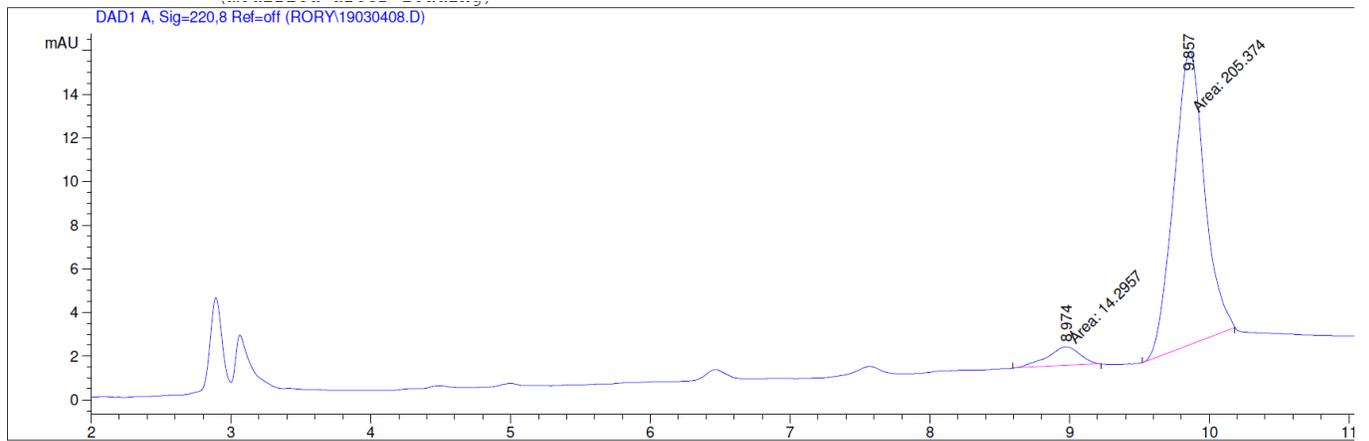
*** End of Report ***

(2*S*,3*R*)-3-(3-methoxyphenyl)-2-methyl-3-(4,4,5,5-tetramethyl-1,3,2-dioxaborolan-2-yl)cyclobutanone



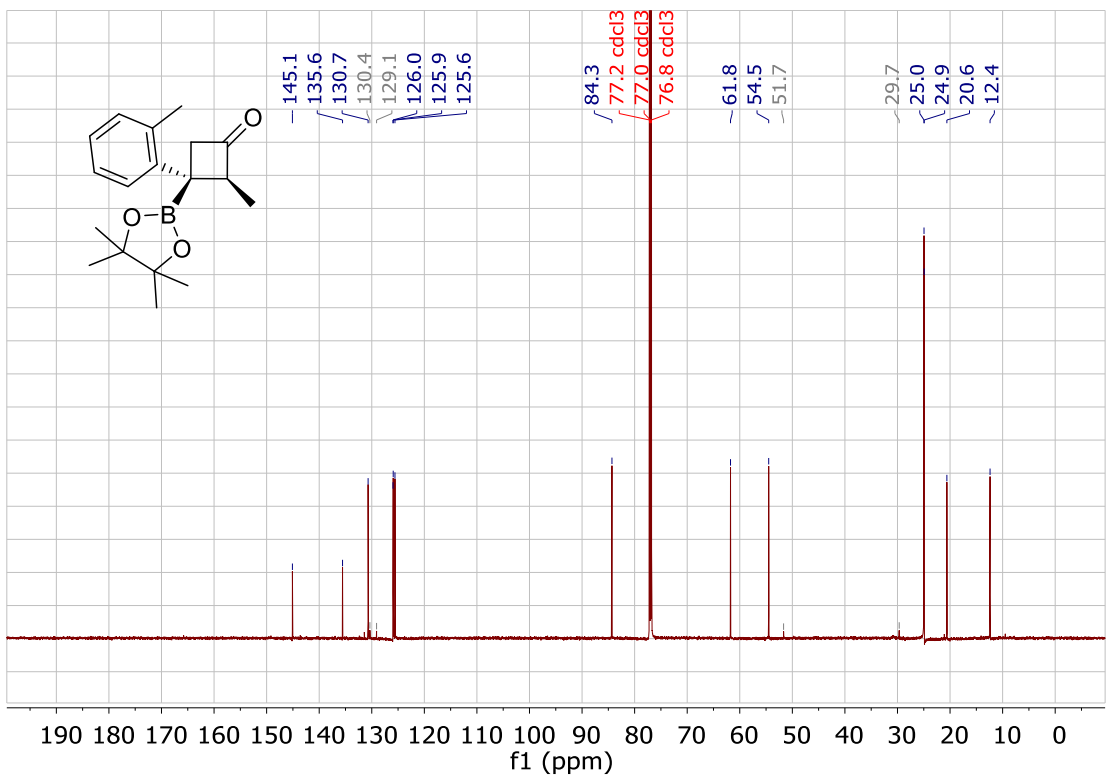
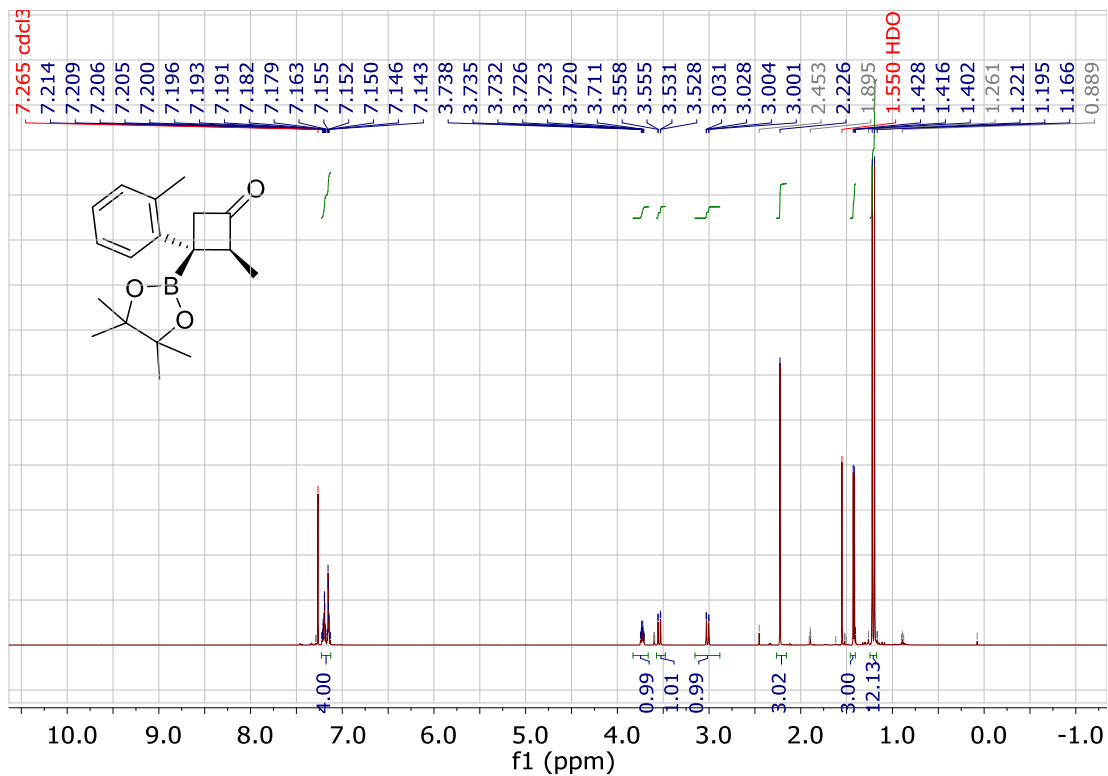


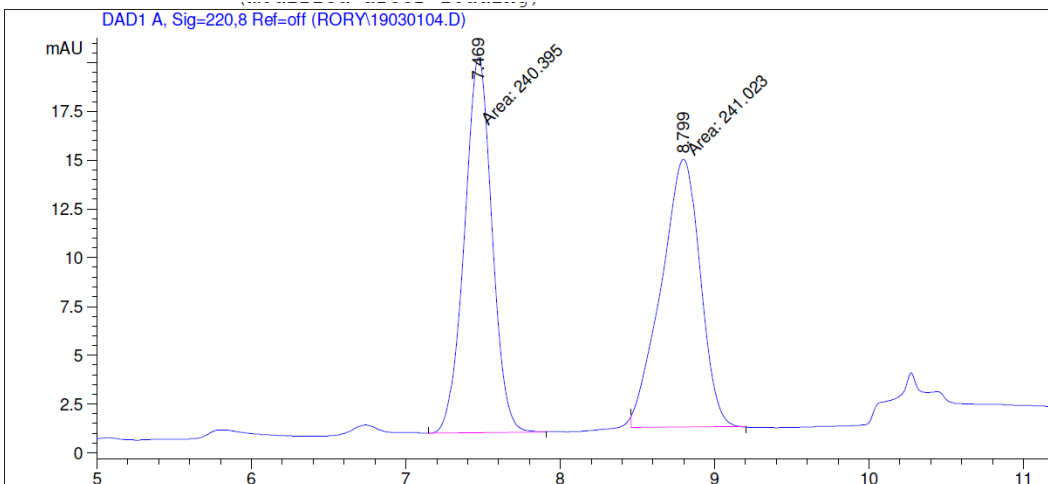
Peak #	RetTime [min]	Type	Width [min]	Area [mAU*s]	Height [mAU]	Area %
1	8.708	MM	0.3290	95.18982	4.82166	50.0170
2	9.568	MM	0.3754	95.12498	4.22306	49.9830
Totals :				190.31480	9.04472	



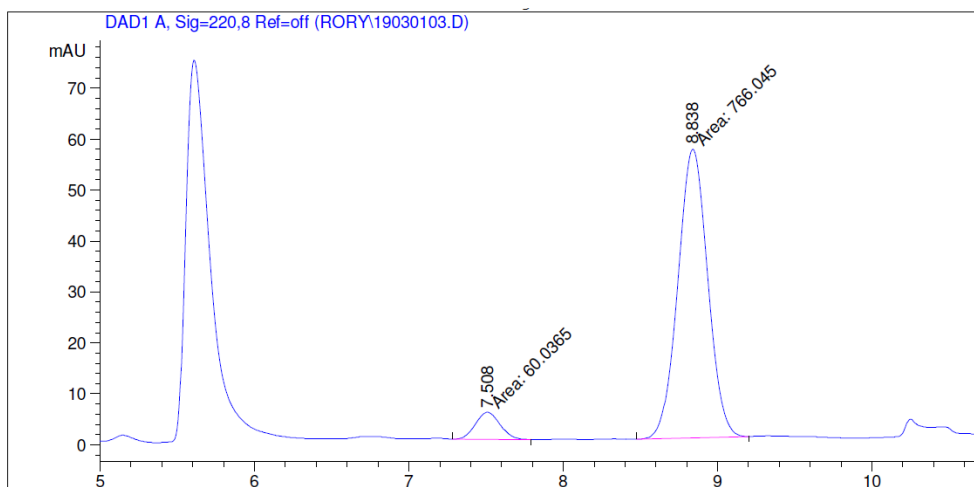
Peak #	RetTime [min]	Type	Width [min]	Area [mAU*s]	Height [mAU]	Area %
1	8.974	MM	0.2747	14.29565	8.67359e-1	6.5078
2	9.857	MM	0.2541	205.37358	13.46921	93.4922
Totals :				219.66923	14.33657	

(2*S*,3*R*)-2-methyl-3-(4,4,5,5-tetramethyl-1,3,2-dioxaborolan-2-yl)-3-(*o*-tolyl)cyclobutanone



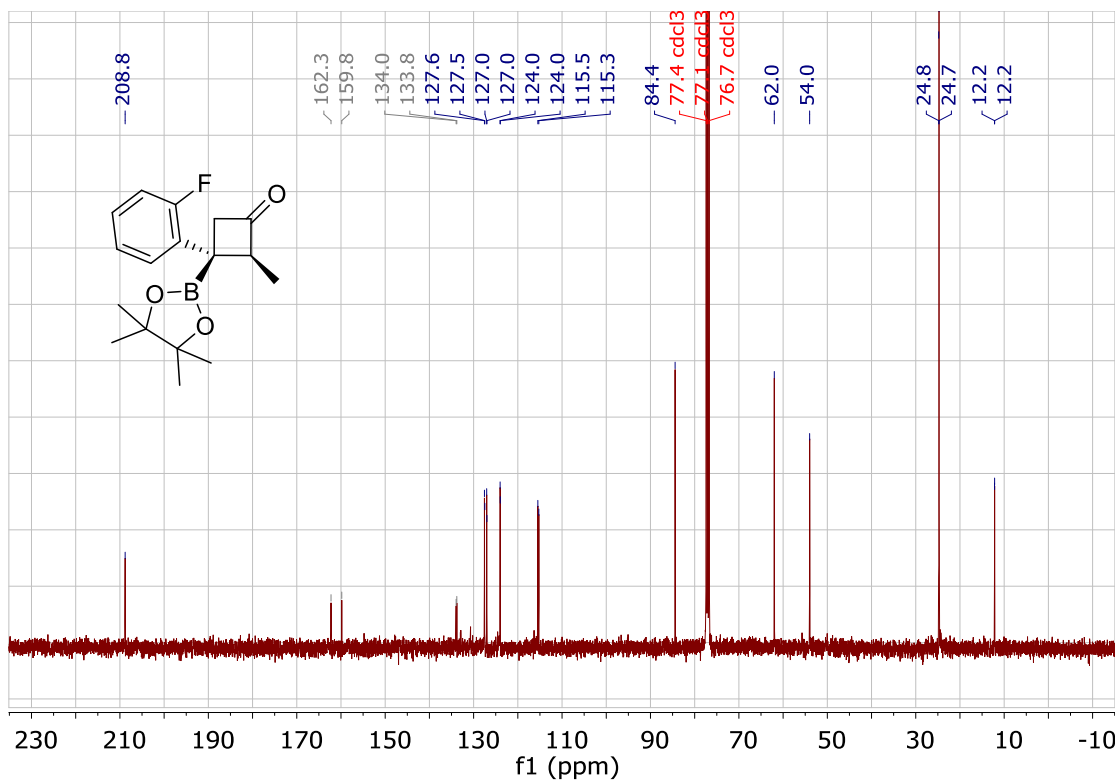
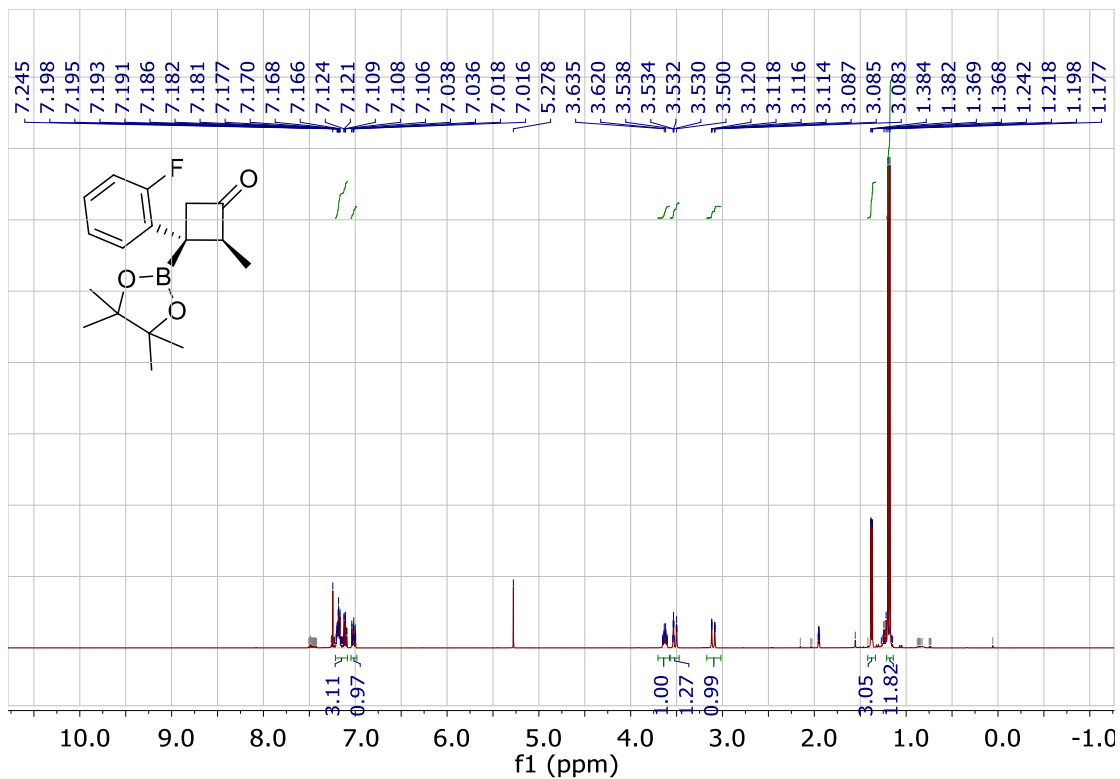


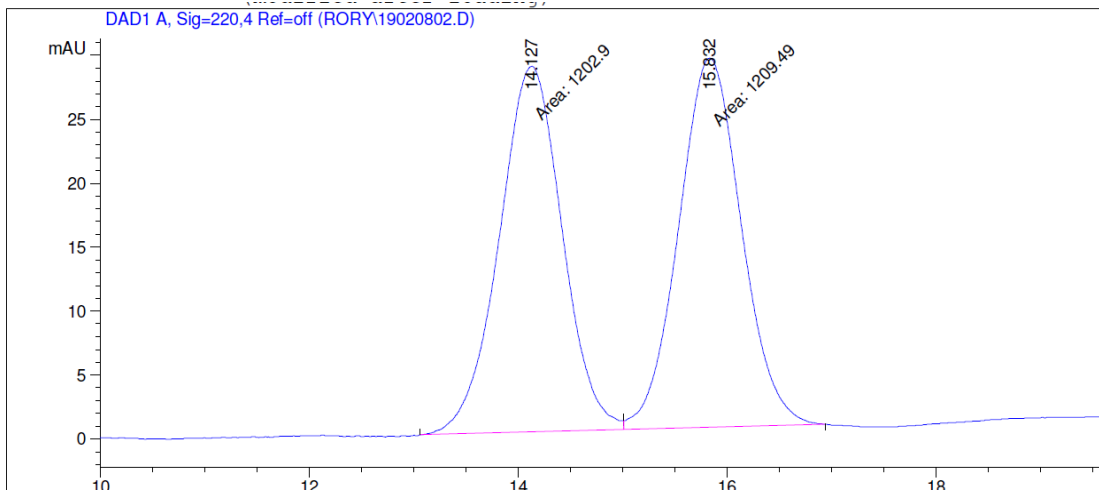
Peak #	RetTime [min]	Type	Width [min]	Area [mAU*s]	Height [mAU]	Area %
1	7.469	MM	0.2082	240.39522	19.24120	49.9348
2	8.799	FM	0.2925	241.02281	13.73247	50.0652
Totals :				481.41803	32.97367	



Peak #	RetTime [min]	Type	Width [min]	Area [mAU*s]	Height [mAU]	Area %
1	7.508	MM	0.1866	60.03654	5.36166	7.2676
2	8.838	MM	0.2250	766.04535	56.74189	92.7324
Totals :				826.08189	62.10354	

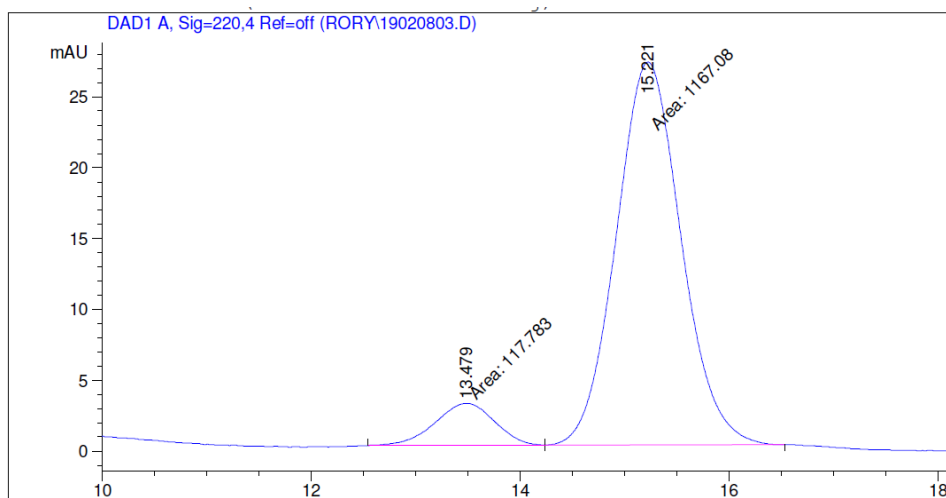
(2*S*,3*R*)-3-(2-fluorophenyl)-2-methyl-3-(4,4,5,5-tetramethyl-1,3,2-dioxaborolan-2-yl)cyclobutanone





Signal 1: DAD1 A, Sig=220,4 Ref=off

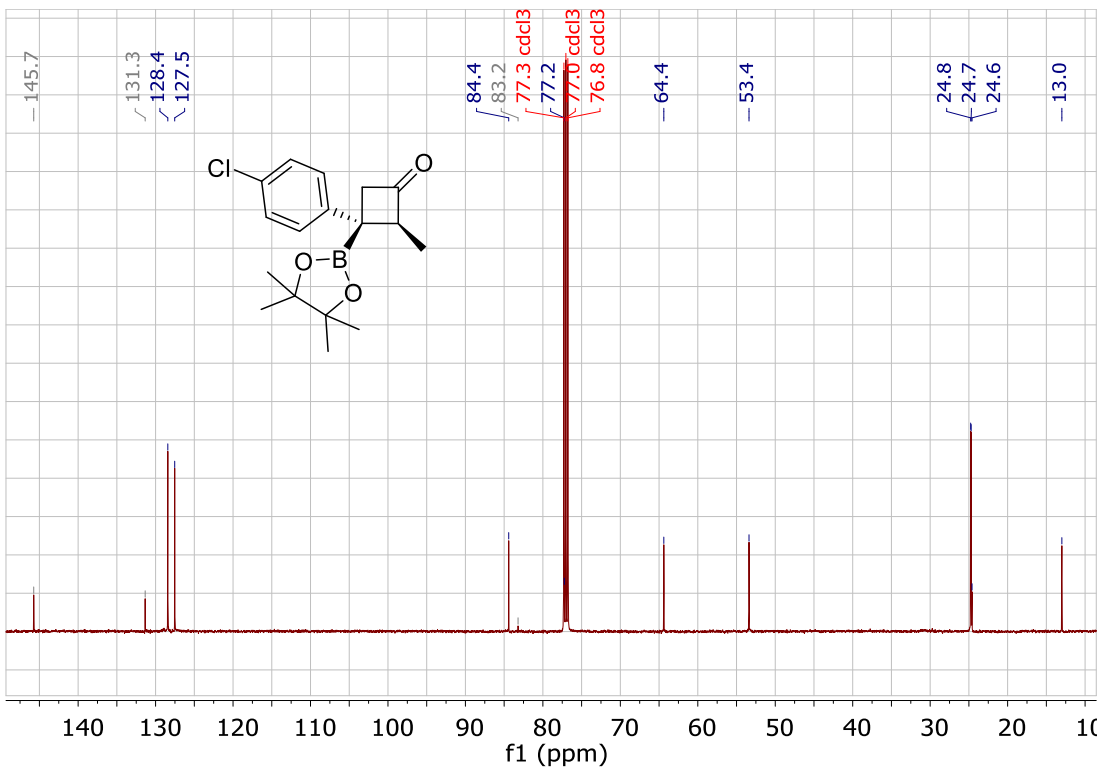
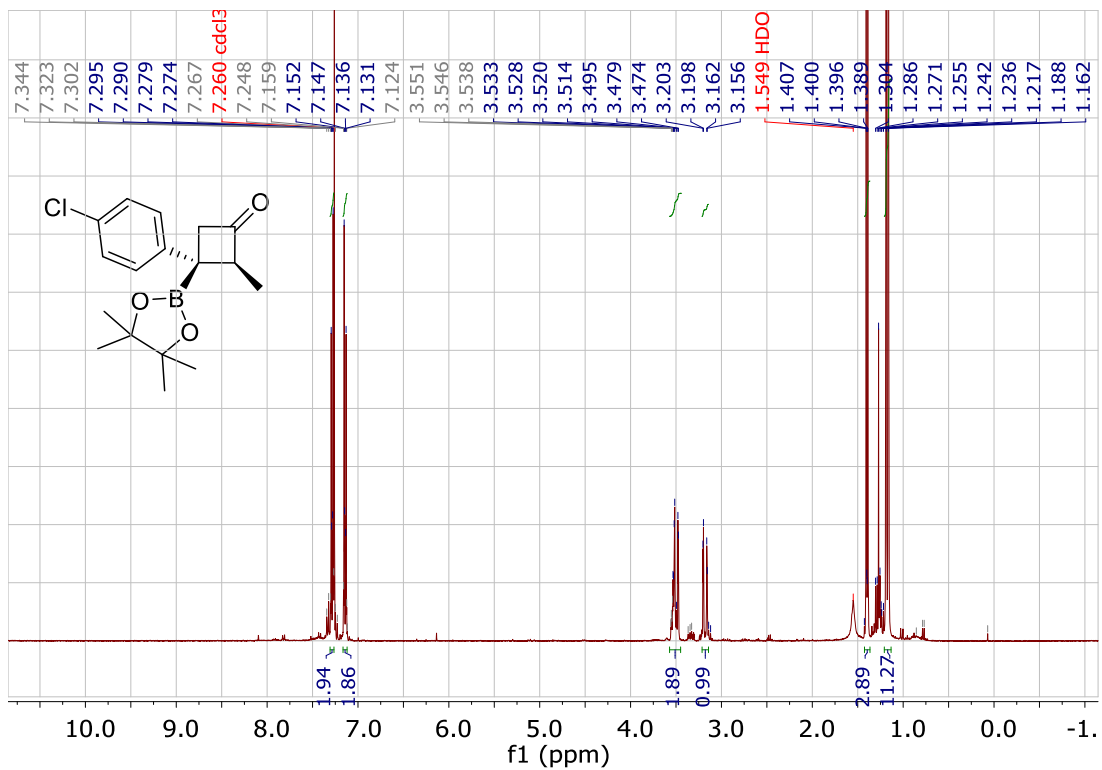
Peak #	RetTime [min]	Type	Width [min]	Area [mAU*s]	Height [mAU]	Area %
1	14.127	MF	0.7002	1202.89966	28.63406	49.8635
2	15.832	FM	0.6970	1209.48621	28.91993	50.1365



Signal 1: DAD1 A, Sig=220,4 Ref=off

Peak #	RetTime [min]	Type	Width [min]	Area [mAU*s]	Height [mAU]	Area %
1	13.479	MF	0.6594	117.78329	2.97692	9.1670
2	15.221	FM	0.7197	1167.08289	27.02705	90.8330

(2*S*,3*R*)-3-(4-chlorophenyl)-2-methyl-3-(4,4,5,5-tetramethyl-1,3,2-dioxaborolan-2-yl)cyclobutanone



(1*R*,2*S*,3*R*)-2-methyl-3-(4,4,5,5-tetramethyl-1,3,2-dioxaborolan-2-yl)-3-(p-tolyl)cyclobutanol

